AFCRL-70-0415

Flow of Radiation in the Earth's Atmosphere

Walter J. Williams, Frank H. Murcray,

David G. Murcray, and Thomas G. Kyle

Department of Physics

University of Denver

Denver, Colorado 80210

Contract No. AF19(628)-5706

Project No. 4076, LIRF

Task No. 407604, LIRF54

Work Unit No. 40760401, LIRF 5401

Final Report

1 December 1965 - 31 May 1969

January 1970

This research was partially supported by the Air Force

In-House Laboratory Independent Research Fund

Contract Monitor: Charles V. Cunniff

Optical Physics Laboratory

Prepared for

Air Force Cambridge Research Laboratories

United States Air Force

Bedford, Massachusetts 01730

259

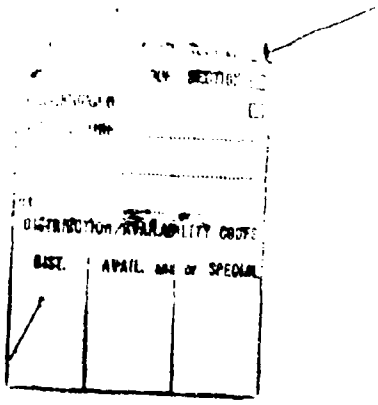

Qualified requestors may obtain additional copies from the Defense Documentation Center. All others should apply to the Clearinghouse for Federal Scientific and Technical Information.

AFCRL-70-0415

Flow of Radiation in the Earth's Atmosphere

Walter J. Williams, Frank H. Murcray,

David G. Murcray, and Thomas G. Kyle

Department o Physics

University oi Denver

Denver, Colorado 80210

Contract No. AF19(628)-5706

Project No. 4076, LIRF

Task No. 407604, LIRF54

Work Unit No. 40760401, LIRF 5401

Final Report

1 December 1965 - 31 May 1969

January 1970

This research was partially supported by the Air Force

In-House Laboratory Independent Research Fund

Contract Monitor. Charles V. Cunniff

Optical Physics Laboratory

Prepared for

Air Force Cambridge Research Laboratories

United States Air Force

Bedford, Massachusetts 01730

ABSTRACT

Four grating spectral radiometers and a filter radiometer were designed, constructed and flown on a balloon vehicle five times to measure atmospheric radiance from 5 to 20 microns. Measurements were made at twelve different angles between zenith and nadir and at altitudes up to 100,000 feet. The equipment and calibration procedures are described. Numerous sample spectra are presented showing the change in radiance with both angle and altitude.

A program is developed for theoretically calculating atmospheric radiance. This program combines a line by line calculation of atmospheric transmittance with a sixteen layer model of the atmosphere to calculate emission spectra at various angles and altitudes.

TABLE OF CONTENTS

LIST OF FIGURES

LIST OF TABLES

I. INTRODUCTION

Radiation plays a dominant role in the thermodynamics of the earth's atmospheric system. An understanding of the flow of radiation within and through the earth's atmosphere is important from a meteorological standpoint. The flow of radiation within the atmosphere has not received much experimental attention. Few experimental observations concerned with this flow have been made, particularly concerning the spectral distribution of such radiation. The radiation emerging from the top of the atmosphere has been more extensively studied, partly because satellites make an ideal vehicle for such measurements. Considerable attention has been given to the problem of using such data to infer the characteristics (particularly the temperature profile) of the atmosphere below the satellite. The success of these techniques depends ultimately on how accurately the flow of radiation through the atmosphere can be predicted. The objective of this study was to measure the intensity and spectral distribution of the radiation emitted by the earth and its atmosphere at various altitudes above the earth's surface, and to compare these measurements with those predicted theoretically. Accordingly, a spectral radiometer system was constructed to record data of this type automatically while it was carried aloft by a large balloon. This system was flown five times.

Large computers have made it possible to predict the results of radiometric measurements, given sufficient information on the distribution of the various atmospheric constituents that have strong absorption bands in the infrared, and the variation of temperature with altitude and geographic location. As part of the effort of this study a computer program has been developed for performing such calculations. The cost of these calculations may become prohibitive unless criteria are placed on the theoretical calculations which limit the computation time. These criteria are based on an understanding of the molecular physics involved and are designed to reduce the computer time required without sacrificing physically significant accuracy. The results of these investigations are discussed in detail below.

II. INSTRUMENTATION

The object of the program was to study the variation of the spectral radiance with altitude and elevation angle. To accomplish this instrumentation was designed and constructed consisting of four Czerny-Turner 1/2 meter spectrometers, a filter radiometer, and on-board digital recorder, FM-FM telemetry and associated batteries and power supplies. The spectrometers scanned from 5 to 20μ at discrete angles while the filter radiometer scanned all angles with two filters.

The signals from the infrared detectors are amplified and synchronously rectified. The output signals, which consist of voltages between 0 and 5 vdc, are recorded by means of the on-board digital magnetic tape recording system. Parallel outputs are telemetered to the ground via the FM/FM telemetry system. The telemetered data are used as backup for the on-board recording and to monitor the system performance during flight. All mechanical rotations are accomplished by means of 400-cycle, synchronous motors powered by transistorized inverters. Primary power for operating all units is obtained from a 28 vdc silver-zinc battery pack. The voltages required for the electronics are supplied from small nickel cadmium battery packs or mercury cells. The various units are mounted in a gondola system constructed of brazed electrical conduit, which serves to protect the instrument. The complete system without the Air Force command and control package weighed 350 kgs.

A. Spectrometers

Four Czerny-Turner 1/2 meter spectrometers were employed in pairs in the balloon system. The pairs of spectrometers were set so that one pair viewed an elevation angle of $+\theta^{\circ}$ while the other pair viewed an elevation angle of $-\theta^{\circ}$. Thus both incoming and outgoing data were obtained simultaneously at complementary angles. This also has the effect of reducing by a factor of two the time required to obtain information from all the angles being viewed and therefore the altitude change between data at the same look

angle is reduced by a factor of two. If only one spectrometer is used the balloon will normally ascend about 5 km during the time required to make a spectral scan at each of the 13 angles employed.

Each pair of spectrometers is designed to scan from 5 to 20μ. One spectrometer scans from 5 to 10μ while the other scans from 10 to 20μ. All spectrometers employ Bausch and Lomb replica gratings, 100mm x 125mm in size. The gratings used for the 5 to 10μ scan are blazed at 8μ and those used for the 10 to 20μ scan are blazed at 16μ. Order separation is accomplished by using long wavelength pass filters which cut on at 4.8μ and 9.8μ, respectively.

The optical schematic of one of the spectrometers is shown in Figure 1. One of the previously mentioned gratings along with two 15cm diameter 1/2m focal length spherical mirrors form the basic instrument. Fore-optics consisting of a plane mirror and a 10cm diameter 25cm focal length spherical mirror reduce the angular field of view of the instrument. The incoming radiation is interrupted by an optically reflecting chopper. Radiation from a conical black body source is reflected from the chopper to the spectrometer entrance slit. Thus the output voltage from the detector is proportional to the difference in radiance between the "target" and that of a black body of known temperature. The black body consists of a series of conical cavities machined in a block of aluminum with thermistor beads embedded in the wall. The temperature of the black body is not controlled but is allowed to vary with its thermal environment.

A plane mirror is placed at a 45° angle in front of each spectrometer. These mirrors are rotated at the end of each spectral scan so that each spectrometer can receive and measure the spectral radiance from different angles. The positions of these mirrors are controlled by a series of cams and microswitches. A microswitch activated at the end of each spectral scan causes the mirrors to rotate to the next position. The elevation angles at which data were taken were chosen so that the secant of the zenith angle was

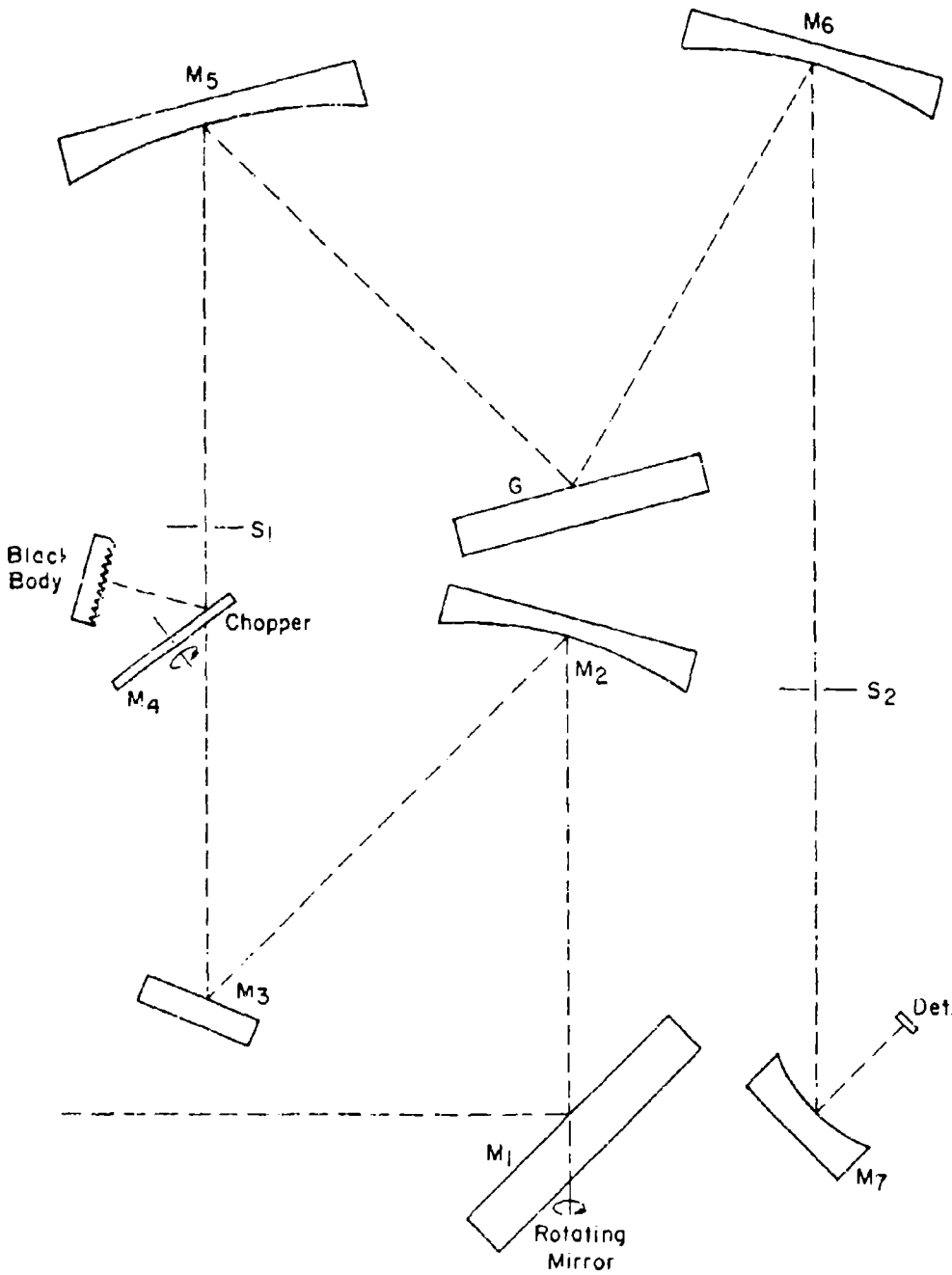

Figure 1. The Optical System of the Spectrometers

doubled; thus: the nadir (180°), 132°, 120°, 104.5°, 97°, 93.5°, 90°, 86.5°, 83°, 75.5°, 60°, 30° and the zenith. A black body is placed on each spectrometer so that it is viewed when the spectrometer is viewing the zenith, which serves as an in-flight calibration.

The time required to scan the spectrum can be varied by changing a set of gears in the grating drive system. For all flights made under this program the spectral scan was 2.7 minutes.

Reeder thermocouples were used as detectors on all four spectrometers for the first four flights. The thermocouples are low impedance devices. Therefore, the preamplifiers used with the units had to be carefully designed to make sure the system was detector-noise limited. For the 24 February 1969 flight two spectrometers were modified to accept liquid helium cooled Ge:Cu detectors which increased the overall sensitivity of the units.

B. Filter Radiometer

The filter radiometer was designed to complement the grating radiometer system. The object was to obtain emission data at all angles during the time it takes the grating instrument to make a single spectral scan at one angle. Thus at each altitude the variation of radiance with wavelength would be measured at one angle and the variation of radiance with angle would be measured over a wavelength region. If an amplitude anomaly occurred on one instrument it would be checked against the other instrument to determine whether the anomaly is spectral or spatial.

During each scan of 360° two different filters were used. One of these transmitted only the emission from the 15 micron region, which was totally dominated by carbon dioxide (See Figure 2). The other transmitted radiation from five to twenty-five microns in wavelength. The transmittance of the wide-band filter falls off at the longer wavelengths. The two filters were alternately placed in the optical path after each 180° scan. Figure 3 shows the partly disassembled radiometer, the cylinder at the lower right (5) contains

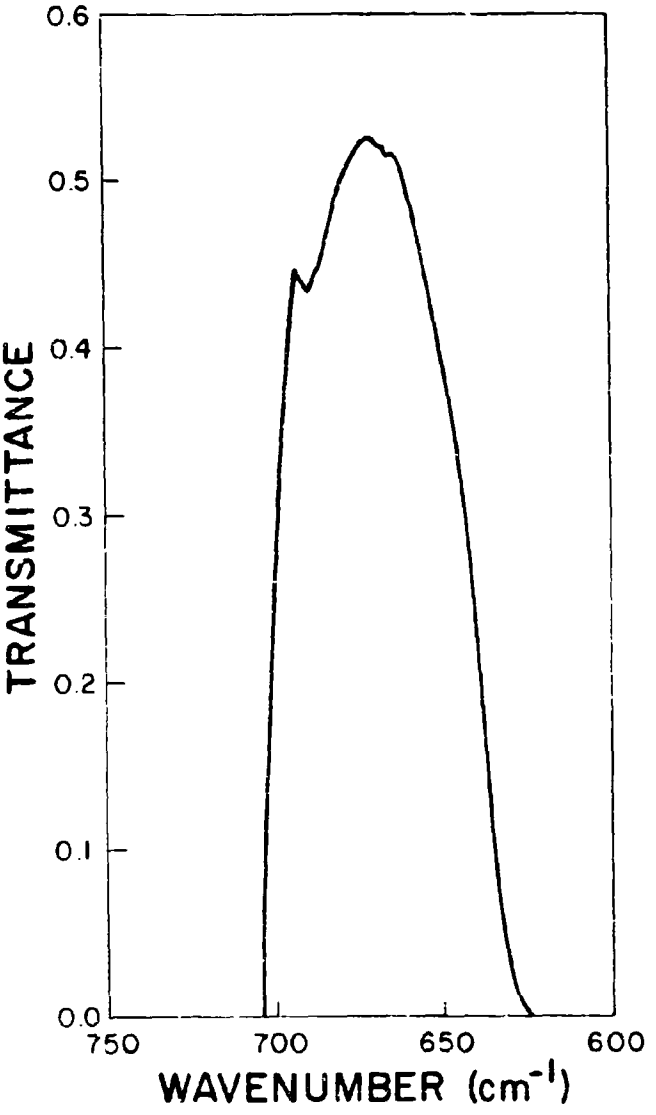

Figure 2. Transmittance Curve for the Filter Radiometer (15μ Band Filter).

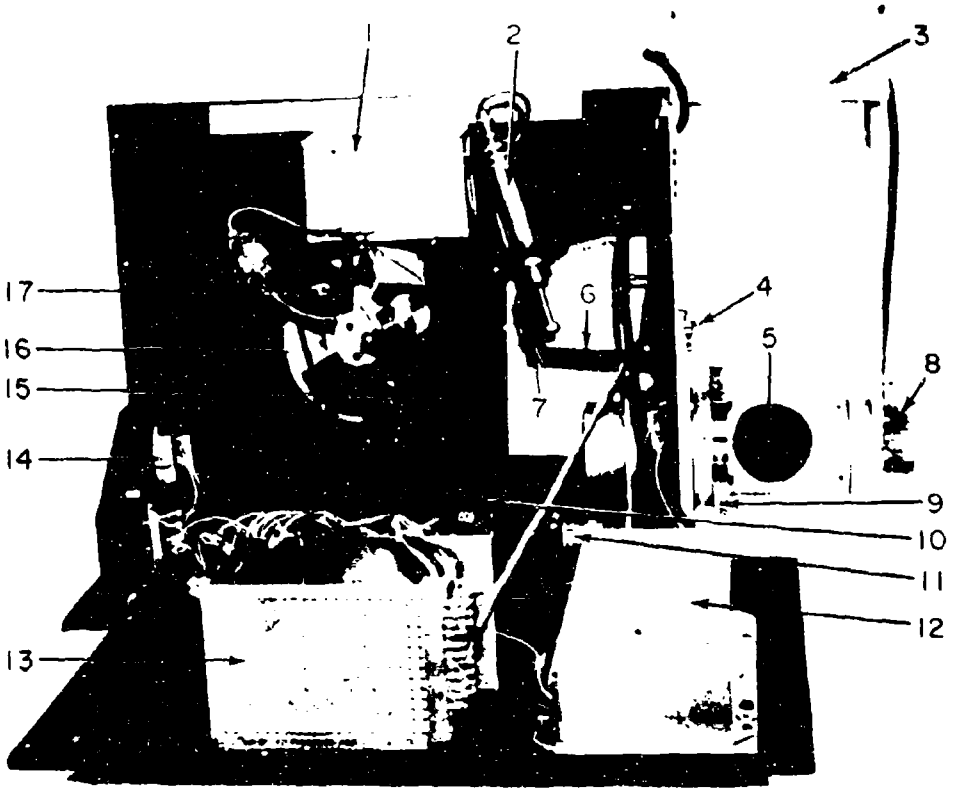

1. Geoformer
2. Radiation Thermocouple
3. Calibrating Blackbody
4. Gain Change Switch
5. Diagonal Scanning Mirror
6. Filter Lever
7. Filters
8. Scan Position Pot
9. Cam
10. Reference Blackbody
11. Scanning Motor and Gearbox
12. Battery Pack
13. Amplifier and Rectifier
14. Spherical Mirror
15. Aperture
16. Reflective Chopper Blade
17. Chop Frequency Pickup

Figure 3. Filter Radiometer

a plane diagonal mirror. The rotation of this cylinder provided the angular scan. The filters were mechanically changed by a cam (9) mounted on the rotating cylinder, when the viewing angle was either upward (zenith) or downward (nadir). The cam also actuated a switch that changed the gain of the amplifier to compensate for the difference in the spectral bandpass of the two filters.

Just before and just after the filter change at the zenith, the radiometer viewed a calibrating black body (3). Thus a calibration for each of the filters was obtained during each 360° of scan. The black body obscured approximately the field of view blocked by the balloon. In the downward direction 10° of scan were also lost during the change of filters. Since the variation of the radiance with angle is very slow at angles near vertical, the loss of these angles in the zenith and nadir directions is not significant.

The angular scan was driven by a synchronous motor and gear train at a rate of 220 seconds per scan. The angular position of the diagonal mirror was continuously monitored by measuring the resistance of a direct coupled potentiometer.

The radiation detector was a Reeder thermocouple with a 1mm square target, the field of view was restricted by an aperture (15) to 9°. Just in front of the aperture is a motor-driven reflective chopper blade (16) that interrupted the incoming atmospheric emission and reflected the radiance of a reference black body cone (10). The atmospheric emission was focused onto the thermocouple by the 2 inch-diameter spherical mirror (14) mounted at the rear of the radiometer. The radiation passing through the filter from this mirror is converging, but the convergence does not significantly affect the bandpass of the filters.

The output of the radiation thermocouple was fed into a geoformer, then into a solid state amplifier, and finally into a syncroverter for synchronous rectification. An offset voltage was also provided at the output to insure that the output would not go below the 0-5 volt range when the radiance viewed became greater than that of the reference black body.

C. Magnetic Tape Recording System

The data to be recorded consists of five radiometric channels, the outputs of pressure transducers, thermistor outputs, mirror angle indicators and voltage standards. The digital recorder, designed and built by project personnel, provides for time-sharing recording of this data with sampling rates as required by each data input.

Time sharing is provided for by an eight step commutator with a basic sampling rate of 200 samples per second, giving 25 samples per second for each input. In addition a subcommutator with 16 steps is used as an input to the main commutator and operated in synchronism with it to provide 16 inputs with a sampling rate of 1.56 samples per second. By connecting inputs in parallel, other sampling rates can be obtained, such as 50 or 100.

Analog to digital conversion is accomplished at the output of the commutator by a linear ramp, a crystal oscillator and two comparators. The result is a 12-place binary number for each data point, adjusted so that 5 volts at the input is represented by 4000 increments. Tests have shown that the recorder is reproducible to a single increment (1.25 m.v.) providing a dynamic range of 4000.

The 12-bit binary number is translated by microcircuits into an I.B.M. format and recorded on 1/2 inch tape with standard 7 track heads. The recorder uses 10-inch computer reels mounted coaxially to save space. The overall volume of the unit is less than $0.03 m^3$.

III. CALIBRATION

Three major problems were encountered in calibrating the spectral radiometers. The first was acquiring a known source (known emissivity and temperature) with an adequate aperture. The second was determining how the radiation from this source was affected by the subsequent optical path. The third was ascertaining whether the calibration varies when the instruments were subjected to the operational environment.

The radiometers use a rotating mechanical chopper with a mirror surface to pass radiation alternately from the target and a reference through the grating spectrometer and onto the detector. Thus the calibration process seeks to define the absolute response of the radiometer to the difference in the spectral radiance between a "known" target and a "known" reference. It is necessary to consider both attenuation and emission from all optical components preceding and including the chopper. The radiation from optical components behind the chopper does not enter into the calibration, although attenuation due to these components is significant.

The accuracy of the radiance measurement is potentially greatest when the radiance emitted by the optical components is minimal, constant or both. This can be accomplished by using a small number of mirrors of high reflectivity at a low temperature in a sheltered or insulated environment, preferably at the same temperature as the reference source. Therefore the instrument, mirrors and reference black body were operated as near atmospheric ambient temperature as possible, and most of the components were partially shielded from exposure to the direct flow of atmospheric wind and direct exposure to solar radiation.

A minimum number of mirrors was used in front of the chopper. Only the chopper mirror is in the reference path, three mirrors are in the target path, two mirrors constitute a small telescope to limit the field of view to less than 1° in elevation and a third mirror is used to scan through 13 elevation angles from zenith to nadir.

The relation between these mirrors and the incoming radiance is expressed in the following equation:

$$N_T\varepsilon_1\rho_2\rho_3 + M_1(1-\rho_1)\rho_2\rho_3 + M_2(1-\rho_2)\rho_3 + M_3(1-\rho_3)$$

$$- N_R\rho_4 - M_4(1-\rho_4) = Kd \qquad \text{(Eq.1)}$$

where

N_T = Spectral radiance of the target or calibrating source

N_R = Spectral radiance of reference black body

$M_{1,2,3,4,}$ = Spectral radiance of mirrors 1,2,3,4

$\rho_{1,2,3,4,}$ = Reflectivity of mirrors 1,2,3,4

d = Recorder units (digital counts)

K = Calibration factor.

The attenuation due to the remaining optical path is included in K. This attenuation varies with wavelength and may vary with the gaseous content along the path. A small correction was applied to K for the absorption due to instrumental CO_2 in the lower atmosphere. Any non-linearities, either in the detector or electronics, would also be included in an expression for K, unless the parameter d had been adjusted to compensate.

To a fair approximation all the mirror radiances (temperatures) except the rotating mirror can be equated to the reference black body radiance. The reflectivities are also nearly equal. These assumptions simplify Equation 1. Since the data reduction was handled by computer, at least one of the sets of data was reduced using Equation 1 with the only modification, $N_R = M_4$. Because the chopper mirror temperature could not be measured and is in close proximity to the black body this appeared to be a good approximation.

The emissivity of the reference black body is assumed to be 1. It is in a semi-enclosed area and any reflective component would represent radiances of nearly the same level, so the equivalent emissivity is 1.

The spectral radiometers were calibrated in the lab before they were flown. A large black body with a known emissivity of better than .99 was used. Absorptions due to CO_2 and H_2O precluded obtaining a good calibration at some wavelengths. This problem

persisted but to a lesser extent when the black body and instrument were sealed in plastic and flushed with dry N_2.

The preflight calibration was supplemented with two in-flight calibrations. The zenith position of the rotating mirror was used for one of these calibrations. The rotating mirror would normally see the balloon in this position. A wide aperture black body was mounted such that it filled the field of view of the radiometer when the rotating mirror was in the zenith position. For the other in-flight calibration, the "window" regions were used as a source of near zero radiance at the higher altitudes with small zenith angles. This data usually represents the maximum signal level attained, and is therefore the most sensitive calibration in terms of signal to noise. Also, these spectral scans were made just before and just after the scan of the in-flight black body and the temperature of the mirrors and instrument remained nearly constant during this interval. It was therefore possible to obtain a two temperature calibration for at least some wavelengths with all other parameters remaining fixed.

IV. ACCURACY OF DATA

The absolute accuracy of the data is difficult to assess. It is certainly not greater than the equivalent noise level. However, at some wavelengths it may be nearly equal to the equivalent noise. This is particularly true near the beginning and the end of the spectral scans, where the cutoff filters and the blaze efficient of the grating reduce the apparent sensitivity of the radiometer. Within the central part of the scan the greatest errors appear to be due to systematic sources. When identified, they are removed in the data reduction. Based on in-flight calibrations and some physical interpretation of the data, they seldom exceed 10 to 15μ cm^{-2} sr^{-1} μ^{-1} One such error is due to the CO_2 attenuation within the spectrometers. Since the instruments operate at ambient pressure, the attenuation due to CO_2 falls off with increased altitude. The resulting error approximated 10μw cm^{-2} sr^{-1} μ^{-1} in the center of the band at low altitudes. A correction was applied to the calibration coefficient in the form

$K(1 + \alpha P)$. P is the local pressure, α is similar to an absorption coefficient and is a function of wavelength.

One point should be stressed regarding systematic errors. The relative accuracy between records, close in time, is greater than the absolute accuracy implied by these errors. In particular, when working with the differences between two such records, the systematic errors are significantly reduced.

On the flight of 25 February 1969 the detectors were changed to Ge:Cu cooled to liquid helium temperature. The noise was reduced more than an order of magnitude and the resolution improved. Details can be observed in the data below the microwatt level. However, these detectors change sensitivity with altitude, (probably due to their temperature environment). The sensitivity change was greatest through the lower atmosphere, approaching 3% per spectral scan, however, above the tropopause the change in sensitivity was less than 1/2% per spectral scan, introducing an uncertainty above the noise level. Knowledge of the parameters of the calibrating sources place the accuracy limit slightly above the microwatt level. At 15μ the reference black body varies in radiance by $5\mu w/1^{\circ}C$. The calibration black body has a similar variation with temperature and in addition varies above $3\mu w/.01$ in emissivity. When comparing the 15μ region with the atmospheric radiance for horizontal paths, similar uncertainties occur due to discrepancies in measuring the atmospheric temperature. To take fullest advantage of the data the differences between successive records should be considered along with the absolute level of each record.

V. FLIGHT RESULTS

A flight program was planned which would obtain data from a variety of conditions and utilize all available time on each flight. Flights were planned for both day and night ascents and at various times of the year. The first three flights were launched about sunrise. This is generally the best time for launching large balloons in the Holloman area and because daytime flights generally present better temperature environment for balloon borne instruments. After

the instrumentation was proven in the daytime environment, two night ascents were made. On all flights the balloon was valved after reaching a floating altitude of about 31 km to establish a descent rate near 100 m/min. This allowed additional data to be taken and compared with the ascent data. The ascent rate on all flights was about 150 m/min. On all flights recovery was accomplished without incident and the instrumentation suffered no damage on impact. Details of the flights and pertinent meteorological data are presented below and in Table I through V.

1 June 1967

The instrumentation was flown for the first time on 1 June 1967. Everything operated properly throughout the flight and data were obtained at all altitudes. The spectrometer slits and overall system gain had been chosen on the assumption that the spectrometer black body source would follow the ambient temperature fairly closely. This did not prove to be the case. The black body stayed considerably above ambient. Part of the data obtained when the spectrometer system was looking up (measuring the atmospheric radiance) were off scale, and this was particularly true of the "window" regions at the higher altitudes where the difference between the radiance of the black body and the atmosphere was large. Data were obtained when the spectrometer was looking below the horizon and in the major absorption bands where the radiance differences were less. Samples of the data obtained during this flight are given in Figures 4 through 6 with the auxiliary information listed in Table I. Sample data from the filter radiometer are shown in Figures 7 and 8.

A frost point hygrometer supplied by the aerospace instrumentation laboratory of AFCRL was flown along with the instrumentation. The data obtained with this unit are included in Figure 9. The results indicate that the unit may have been contaminated at the higher altitudes however the data obtained up to the tropopause are probably valid. The emission from water vapor at the higher altitudes is below the noise level of the instrumentation, therefore the frost point hygrometer was not flown on subsequent flights.

30 November 1967

On the 30 November 1967 flight the spectrometer slits were closed in order to reduce the signal levels and to keep the data on scale at the higher altitudes. Closing the slits increased the resolution of the data obtained and reduced the sensitivity, thus the data obtained had a greater absolute uncertainty than that obtained on the first flight. Spectra representative of those obtained during this flight are presented in Figures 10 through 33, with the auxiliary information listed in Table II. With the change in slits the data remained on scale and were obtained at all wavelengths, at all altitudes, and at all angles. Sample data from the filter radiometer are shown in Figures 34 and 35.

On the basis of the data obtained during the first two flights it was possible to adjust the spectrometer slit and overall system gain so that the peak signals fully utilized the dynamic range of the recording system without saturating the system.

25 June 1968

The instrumentation was flown the third time on 25 June 1968. Everything operated properly and data were obtained throughout the flight. These data are presented in Figures 36 through 127 with the auxiliary information listed in Table III.

1 July 1968

The flight of 1 July was launched at 0205 MDT and data were obtained at night. The on-board magnetic tape recording system malfunctioned because it got too cold. The telemetry system operated properly and data were obtained via this link. However, this required a number of auxiliary steps which delayed data reduction. Data from this flight are presented in Figures 128 to 151 with the auxiliary information listed in Table IV.

25 February 1969

Thermocouple detectors were used in the spectrometers during the first four flights. These detectors had sufficient sensitivity in the regions of strong absorption, however little information was obtained in the regions where the atmosphere transmits fairly well. In order to attain more sensitivity two of the spectrometers were modified to accept Ge:Cu photoconductors as detectors. This change resulted in at least an order of magnitude increase in sensitivity. The absolute accuracy was still limited by the knowledge of temperature of the black bodies. These spectrometers were flown on the February 25, 1969 flight. For this flight the units were set to look at zenith angles of 48.2, 70.5, 80.2, 85.2, 90.0 and 93.6°. Everything operated properly and data were obtained at all altitudes. The spectra obtained during this flight are given in Figures 152 through 166 with auxiliary information listed in Table V.

A number of interesting atmospheric emissions were noted during this flight. Of special interest was the atmospheric emission at 11.3μ due to HNO_3. The data indicates that this constituent occurs only at the higher altitudes. Additional emissions due to HNO_3 are noted at 5.8μ, and overlapping the methane at 7.5μ.

VI. CALCULATIONS OF ATMOSPHERIC EMISSIONS

The calculations of atmospheric emissions are designed to permit a reasonable comparison to be made between the predicted and observed results. The model used for the calculation is described below, the physical and experimental parameters of the model are explained, and finally a partial examination of the possible errors is given. A complete examination is not possible due to a lack of knowledge of quantities related to the concentration of aerosols, lack of thermal equilibrium, and the accuracy of the line parameters used in the calculations. The calculations are divided into two parts. First the absorption coefficients were calculated for a

zenith path through each of 16 layers (see below) of the atmosphere. Second, each of these layers was divided into two parts and, after appropriate slit functions and secants were applied, atmospheric emission was calculated based on the temperature profile for the flight date.

A. Absorption Calculations

For the purpose of the absorption calculations, the atmosphere was divided into sixteen layers. Each of the first 15 layers, which commence at sea level, was two kilometers thick. The sixteenth layer includes the portion of the atmosphere above 30 kilometers. Each layer is treated as having a constant pressure, temperature, and mixing ratio of the various gases. The temperature and pressure were determined by the average of the values listed in the Handbook of Geophysics for Air Force Designers[1] at the boundaries of the different layers. In the case of the sixteenth layer, a temperature of 227°K and a pressure of 5.95 millibars were used. This corresponds to the Curtis-Godson approximation for uniformly mixed gases in a constant temperature atmosphere. The above mentioned temperatures were only used for the purpose of calculating absorption coefficients. The temperatures measured by sondes flown at the same time as the emission measurements were used for the Planck function in the radiative emission integrals.

The optical thicknesses of the different molecules were also taken from the Handbook of Geophysics, with the exception of H_2O and O_3 for which values of 2.5 gm/cm^2 and 0.35 atmosphere cm, respectively, were used. With the exception of CH_4, H_2O, and O_3, the different absorbers were considered uniformly mixed. The percentage of total of the absorbers which were used are given in Table VI. The source of the mixing ratios for these molecules is as follows: The ozone concentration and distribution are the result of smoothing and averaging of several rocket-borne measurements[2] over White Sands, New Mexico. The decrease in the concentration of methane at the upper

altitudes is based on recently reported infrared absorption measurements.[3] The upper altitude water vapor values are also obtained from infrared absorption measurements,[4] while the lower altitude values are taken from a particular sonde measurement which corresponds to one of the emission measurements flights.

The absorption coefficient was calculated on a line by line basis. The line parameters were primarily those collected as a part of the AFCRL Atmospheric Transmission program. The 15 micron band of carbon dioxide line parameters was based on a compilation by Drayson and Young.[5]

The monochromatic absorption coefficients were calculated at different frequency separations, or net intervals, in the different layers.[6] The smallest net interval 0.001 cm^{-1}, was used in the upper two layers, as required by the low pressures in these layers. A net interval of 0.002 cm^{-1} could be used in layers 11 through 14, while a 0.01 cm^{-1} net interval was sufficient for the lowest 10 layers. In all layers but the first 10, a Voigt profile, which is a convolution of the Lorentz and Doppler shapes, was the shape function used.[7] The ground was taken as totally absorbing.

B. Emission Calculations

The above description concerns the assumptions and approximations made about the atmosphere itself. It was also necessary to restrict the computations to some degree. One very effective restriction was to compute the emission only once for each kilometer above sea level. The previously calculated absorption coefficients can thus be converted to transmissions once, and then used for the computations of emission at any number of altitudes. The absorption coefficients are valid for any angle of observation in the atmosphere if the proper slant path factor is used, so they need be calculated only once, provided the distribution of the various absorbers is not altered.

Each two kilometer layer must be broken down into two sublayers to properly account for the thermal structure of the atmosphere. In order to cut by a factor of two the number of exponentials which are required and also to alleviate a storage problem, it is advantageous to consider these two sublayers as having the same transmittance. Thus only one exponentiation is required for each layer. The square of this transmittance is the transmittance for each layer as a whole. The lower sublayer can be thought of as being only 0.88 kilometers thick, while the upper portion is 1.12 kilometers thick. This approximation is not exact, and it will be discussed again later. It should be emphasized that this approximation does not affect the transmission of the layer as a whole. The transmissions calculated are at altitudes corresponding to even numbers of kilometers above sea level and to those even numbers plus 0.88 kilometers. It will be seen that this distinction from calculations at integral numbers of kilometers is primarily a pedantic point in the actual comparisons of calculations with observations, since the altitude is not known this closely.

C. Choice of Model

The experimental reasons for the choice of this model will now be considered. The large number of different conditions was the most important experimental consideration. The experimental values to which the calculated values were to correspond were to be taken during a number of balloon flights, not only during the time at float altitude, but primarily during the balloon ascent. Had the object been to predict the emission spectra which would be observed from a single altitude, then a different approach would have been followed.

The instrumentation consisted of four spectral radiometers, each scanning a different wavelength region or looking through the atmosphere at a different angle. Each spectral scan would require slightly more than two minutes of time. At the ascent rate of the balloon, each radiometer should complete a spectral scan during an altitude change of about one-half kilometer. Thus, in rising to

30 kilometers altitude, a total of over two hundred spectral scans would be recorded. If each radiometer looked in a fixed direction, then some of the repeated scans could be neglected, but the angle in which the radiometer is pointed is changed after each spectral scan. That particular angle would not be repeated for a few kilometers.

The need for an efficient means of carrying out the computation for a large variety of altitudes, angles and different atmospheric temperature profiles, can be seen to have been quite essential. This was the reason for adopting a procedure that only calculated transmissions a single time, and then used these transmissions for different altitudes as well as different flights.

The effect of the balloon ascending during the data acquisition should be pointed out. During each spectral scan, the balloon would always be within 0.25 km of an integral number of kilometers, however, the actual altitude was not known to an accuracy significantly better than this. Unless the altitude is adjusted as a function of wavelength for each scan, the altitude steps need not occur at smaller increments than one kilometer.

There are some other experimental points which should be mentioned, but which do not deal directly with the present experiment. In completely different computations by persons here and at other locations, differences in the transmittance observed and calculated are often as large as 5%. It is unusual for band strengths or halfwidths to be known to an accuracy of 5%. The line shapes are known to often differ from the Lorentz shape which is used. In addition, little work has been done concerning temperature dependence of the halfwidth. The halfwidth is usually assumed to vary as $T^{\frac{1}{2}}$, but in a recent report,[8] the CO_2 halfwidth was found to vary nearly as $T^{3/2}$.

The above considerations are not mentioned to suggest a crude calculation is all that is justified. Quite the contrary, a very careful calculation is required to even reach these limitations.

Many effects can cause a disagreement between the computed and observed emissions. The basic philosophy in the calculations has been to carry out calculations which are accurate enough so that deviations from the experimental values can be ascribed to either the theoretical inputs, or to the experimental errors, but not to the computational procedures or the model used.

D. Mathematical Model

The mathematical form of the problem for the emission observed at altitude X_1 and wavelength λ is

$$R(\lambda,X_2) = \int_{X_1}^{X_2} B_\lambda (X) \frac{dT}{dX} (\lambda,X) dX \qquad (1)$$

Before comparing the result of this integral to experimental data, it is necessary to degrade $R(\lambda,X_2)$ by application of an instrument or slit function. The transmittance is expressed here as a function of wavelength, not wavenumber, but this only involves a trivial change of variables. The value used for the geometric coordinate X_2 is either zero or infinity, depending on whether the angle involved results in an optical path terminating at the ground or at a point outside the atmosphere. The transmittance $T(\lambda,X)$ is given by

$$T(\lambda,X) = \exp\left(-\sum_{\substack{i = \text{all} \\ \text{lines}}} \int_{X_1}^{X_2} \frac{S_i U_i}{\pi} g(\lambda,\alpha_i,\alpha_i',\nu_i X) dX \right) \qquad (2)$$

The Doppler and Lorentz halfwidths, α_i and α_i', the line strengths, S_i, and quantity of absorber, U_i, are functions of the pressure and temperature along the integration path. The function g is the line shape function. The quantity of absorber has been given the same subscript at the lines to indicate that its value will be different for the lines belonging to the different absorbers. The line positions are ν_i.

The form of (1), when it is specialized to the previously described model, is

$$R(\lambda,N) = \sum_{m=N}^{M} B_{\lambda}(m) \left[T_{N,m} - T_{N,m+1} \right] \qquad (3A)$$

where

$$T_{N,m} = \prod_{j=N}^{m} T_j \ , \qquad (3B)$$

with

$$T_{2j} = T_{2j+1} = \exp \left(- \sum_{\substack{i=A_{11} \\ \text{Lines}}}^{S.U_i} g(\lambda,\alpha_i,\alpha_i',\nu_i) \right) \qquad (3C)$$

Using equation 3A emission spectra have been calculated for three flights. For each flight spectra are calculated for 2 km intervals from 2 to 32 km and for secants of 1, 2, 4, 8 and 16 in the upward and downward directions. There are 160 spectra for each flight calculated for geometric situations similar to the observed data. The 1 June 1967 data are presented in Figures 167 to 176. The 30 November 1967 data in Figures 177 to 186, and the 1 July 1968 data in Figures 187 to 196.

E. Accuracy of Model

For the purpose of seeing the effect of the one kilometer thick layers of isothermal atmosphere, it is convenient to choose an example which does not precisely correspond to the atmospheric problem, but which is not too different.

Let the Planck function at altitude X be

$$B_{\lambda} = B_{o} \exp(-bX) \qquad (4)$$

A value of b=0.28 results in a decrease in the Planck function of 25% per kilometer. This is approximately the case encountered at 5 microns wavelength, when the temperature is decreasing at 5° per kilometer from -40°C. The transmission is taken to be

$$T = \exp(-aX) \qquad (5)$$

This would be true for the exact center of a Lorentz line with no Doppler or temperature effects and for uniformly mixed atmosphere. These conditions permit (1) to be integrated and (3) to be summed exactly. Equation (1) becomes

$$R(\lambda,o) = \int_o^\infty B_o \exp(-bX)\, d(\exp(-aX)) = B_o \frac{a}{a+b} \qquad (6)$$

Equation (3A) will use one kilometer thick layer in this case, and has the form

$$R(\lambda,o) = \sum_{m=o}^{\infty} B_{\lambda,m} \left[\exp(-am) - \exp(-a(m+1))\right] \qquad (7)$$

The point within the layer by which the temperature of the layer is determined has not yet been specified. The method used will be given below, at the end of this example, but for now assume it is at a distance Z from the lower boundary of the layer. Then

$$B_{\lambda,m} = B_o \exp(-b(m+Z)) \quad . \qquad (8)$$

The value of Z will be determined so that (6) and (7) give the same result. Since (7) is evaluated to be

$$R(\lambda,o) = B_o \exp(-bZ) \left[\frac{(1 - \exp(-a))}{(1 - \exp(-b-a))}\right] \qquad (9)$$

the equality of (6) and (7) requires Z to be

$$Z = -\ln \left(\frac{a}{a+b}\right) \left(\frac{1 - \exp(-b-a)}{1 - \exp(-a)}\right) \qquad (10)$$

It can be seen that as $a \to \infty$, $Z \to 0$. It is not so obvious from the form, but by evaluation one finds $Z \to 0.5$ as $a \to 0$. The value of Z determined by (10) is plotted as a function of the transmission, T, through a 1 kilometer thick layer. That is, $T = \exp(-a)$.

If only a single layer had been considered, and the Planck function had been considered to vary linearly with altitude in the single layer, then the value of Z would have been found to be -

$$Z = \frac{1}{a} - \frac{e^{-a}}{1-e^{-a}} \qquad (11)$$

The results (10) and (11) may be taken as equivalent for cases encountered in the atmosphere, in particular they have the same limits for large and small values of a. Strictly, they are only equivalent for small values of b. With the possible exception of the shortest wavelengths at the lowest temperatures in the atmosphere, b can be considered to be small. In the calculations of atmospheric emission, the value of Z was determined by equation (11).

The transmittance of each two kilometer thick layer should have been quite accurate, provided the line parameters and mixing ratios were correct. The pressure was taken to be the mean of the boundary values. The quantity of absorber in the upper and lower sublayers was taken to be the same, and equal to one-half the quantity of absorber in the layer. This resulted in the transmittance of the layer as a whole, (that is, the square of the transmittance for either of the sublayers), being correct to the accuracy of the Curtis-Godson approximation, which is quite reliable for layers as thin as two kilometers. If the two sublayers had been considered to have the same thickness, then the transmittance of the upper sublayer would have been too small, while that of the lower layer would have been too large.

The approximation for the sublayers was improved by considering thw two sublayers to have a different geometric thickness. The only actual effect of this thickness interpretation was the change of the input temperatures for the Planck functions. The change in these temperatures was less than one degree, and so the improvement was of doubtful use. Since no additional computation was involved, however, it was used.

There is an ambiguity in what the thickness of the layers should be. It could have been picked so that the quantity of the absorber in the two layers was the same. This would have resulted in almost exact results for weakly absorbing regions. The thickness could have also been picked so that the integral of pressure with

respect to the absorber thickness, $\int p du$ was the same for each sublayer. This value would have resulted in a good approximation for strongly absorbing regions. The division of levels for the weak absorption case would have been at 0.93 kilometers from the lower boundary, and at 0.84 kilometers for the strongly absorbing case. These values assume a uniformly mixed exponential atmosphere. The average of the above two values, 0.88 kilometers, was used in the calculations. The error in thickness could have thus been as much as 6%, but assuming a temperature gradient of $5^{\circ}C$ per kilometer, this is only a temperature difference at the boundaries of $0.03^{\circ}C$.

There are two cases in which the effects of an error in the transmittance will be considered. The first is the case when the observations are made at the lower boundary of the two kilometer layer, and the second at the intermediate position in the layer. The first of these cases is the more important since it can be considered to be the total emission of the layer. Even if the effects of the layers are to be measured at a lower altitude, the remaining portion of the calculation only involves the calculation of a transmittance through the intermediate layers. As stated above, the transmittance of complete layers involves almost no approximation.

Let the emission at the lower boundary of the two sublayers having transmittance T_1 and T_2, and Planck functions B_1 and B_2 be R. The nearest of the sublayers is denoted by the symbols T_1 and B_1. The value of R is

$$R = B_2(1-T_2)T_1 + B_1(1-T_1) \qquad (12)$$

It will be assumed that $B_2 = kB_1$. The above value of R is the value obtained when T_1 and T_2 are correct. If values in error by amounts Δ_1 and Δ_2 are used, while the value of $T_1 T_2$ (which is the transmittance of the layer) is correct, the difference in R is

$$\Delta R = B_1[k\Delta_1 - \Delta_1] = B_1\Delta_1(k-1) \qquad (13)$$

For example if k equals 1.25 and Δ is 6%, (notice that this value is an absolute error of 6%, which would correspond to a 12% fractional error if T_1 were 50%) the error in emission would be 1.5% of the value which would have been observed if the lower sublayer had been black. This is the error in radiance that would be expected under the most adverse condition of B_1 and B_2 differing by 25%. In the case of the longer wavelengths, the error would be considerably less. A better perspective is to consider it as a temperature error, which would be approximately $0.3^{\circ}C$.

It is interesting that (12) also applied to the case of the emission calculated at the intermediate position of the layer. That is, there is an amount of radiance $B_2(T-T_2)$ reaching the upper boundary of the layer, of which an amount T_1 is transmitted through the upper sublayer, having an emission $B_1(1-T_1)$ itself. In this case the error in T_2 is considered zero, while that of T_1 is still Δ_1. The total error in the calculated emission is

$$\Delta R = B_2(1-T_2)\Delta_1 - B_1\Delta_1 \qquad (14)$$

Again, let $B_2 = 1.25\ B_1$. In order to see what size error this represents, it is important to consider the cases which can actually arise. Take Δ to be $0.1(1-T_1)$ (i.e., a 10% fractional error in the absorption of the sublayer). It is not reasonable to expect T_2 to be greater than T_1. This is an important observation in the evaluation, but its physical basis is obvious. The only point at which it could be in doubt is where there is a large sudden decrease in absorber concentration, and although there are such large sudden decreases, the above observation appears to remain valid.

If $T_1=T_2=0.5$ the temperature error is only $0.00625B_1$. It is often true that $T_2=0$ while $T_1\neq 0$. In this case the error is $\Delta R=(0.25)\ B_1\ \Delta(1-T_1)$. This error could thus be as much as $0.025B_1$, or an equivalent temperature error of $0.5^{\circ}C$ when $T_1=T_2=0$. This is the largest error possible under the restruction $T_2\leq T_1$. The value

of $0.1(1-T_1)$ for Δ_1 is almost twice as large as the previous considerations have indicated the model would yield.

The above considerations indicate that the model used for the atmospheric calculations would not lead to errors, in total, of greater than that which would be caused by an error of $0.5^{\circ}C$ in the measurement of the atmospheric temperature. This is most likely a reasonable accuracy to expect in such temperature values, especially if not only the possible temperature errors of the sondes, but also the differences in time and geographic location are considered.

There are other possible errors in the calculations which could be much larger than those due to the model. These errors concern both the errors in the input parameters for the line and errors in the mixing ratios. In the case of the variable mixing ratio absorbers, some corrections may have been made in the mixing ratios to correct for the errors in the line parameters. In general experience has shown that these errors may be as large as 5% for the atmosphere as a whole. The errors of this type may result in correspondingly large errors in the atmospheric emission calculations.

VII. ACKNOWLEDGMENTS

The launch and recovery of the balloon instrumentation was capably handled by the Air Force Cambridge Research Laboratories Balloon Group at Holloman Air Force Base, New Mexico. The computer programs for data reduction were developed and operated by John Van Allen and Mrs. Nancy L. Covey. Mazood Zaidi contributed to the operation of the equipment and the reduction of the data. Charles Garwood prepared the figures for this report.

VIII. REFERENCES

1. Handbook of Geophysics for Air Force Designers, Geophysics Research Directorate, USAF (1957).

2. Randkawa, Jager S.; Rocket Measurements of Atmospheric Ozone, ECOM-5196, Atmospheric Sciences Laboratory, White Sands Missile Range, New Mexico (1968).

3. Kyle, T. G., D. G. Murcray, F. H. Murcray, and W. J. Williams; Journal of Geophysical Research 74, 3421 (1969).

4. Murcray, D. G., T. G. Kyle, F. H. Murcray, and W. J. Williams, to be published in Journal of Geophysical Research.

5. Drayson, S. R., and C. Young; Technical Report: The Frequencies and Intensities of Carbon Dioxide Lines Between 12 and 18 Microns, University of Michigan, College of Engineering (1967).

6. Kyle, Thomas G.; Journal of the Optical Society of America 58, 192 (1968).

7. Kyle, T. G.; Journal of Quantative Spectroscopy and Radiative Transfer 8, 1455 (1968).

8. McCubbin, T. K., Jr., Patiz, J. G., and R. I. Ely; Temperature Dependence of the Collision-Broadened Widths of the Lines in the 10.4μ CO_2 Band, paper presented at the Spring Meeting of the Optical Society of America, 1969, Journal of the Optical Society of America, 59, 496 (1969), (Abstract).

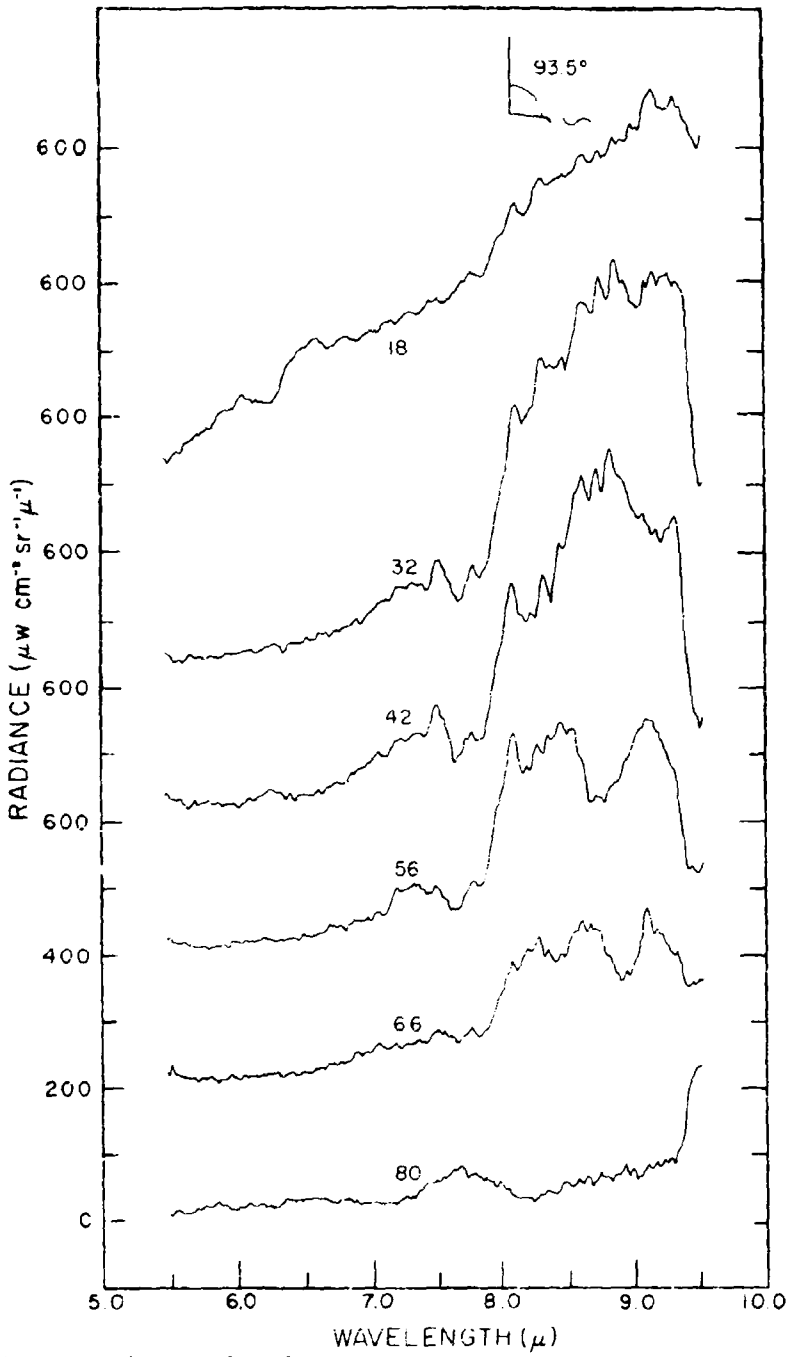

Figure 4 Spectral radiance vs altitude for balloon flight
1 June 1967 (See Table 1)

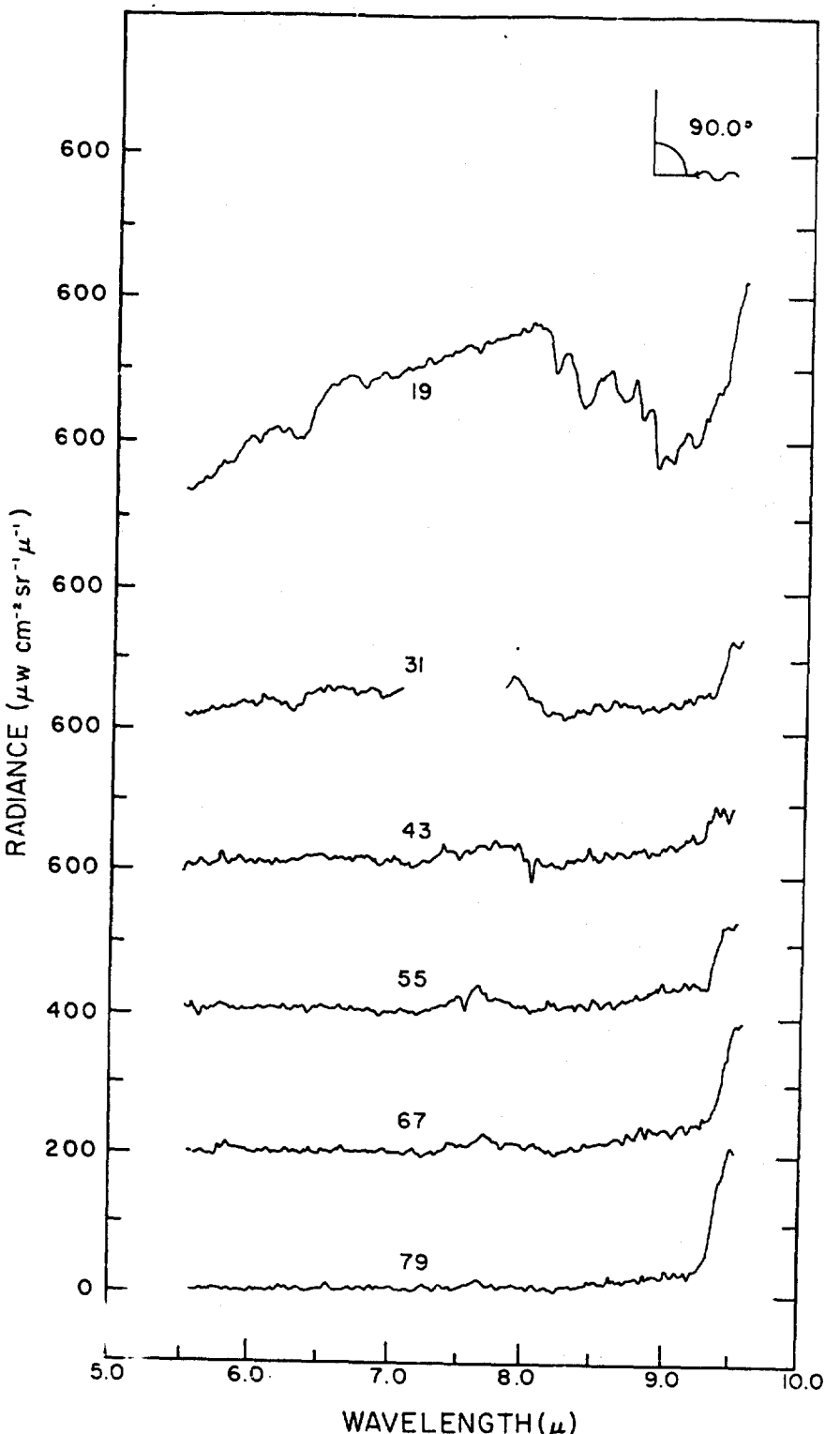

Figure 5 Spectral radiance vs altitude for balloon flight 1 June 1967. (See Table 1).

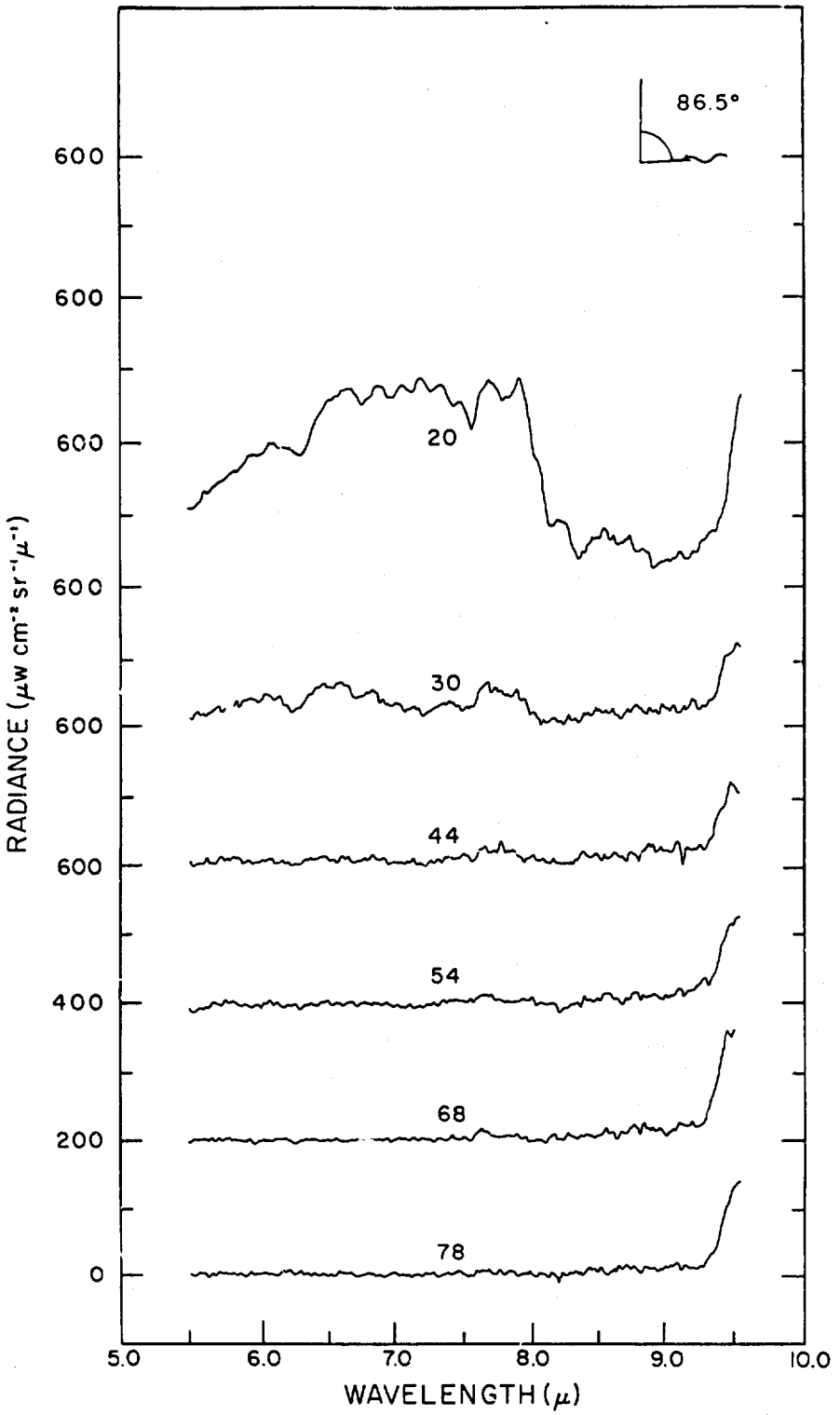

Figure 6 Spectral radiance vs altitude for balloon flight 1 June 1967. (See Table 1)

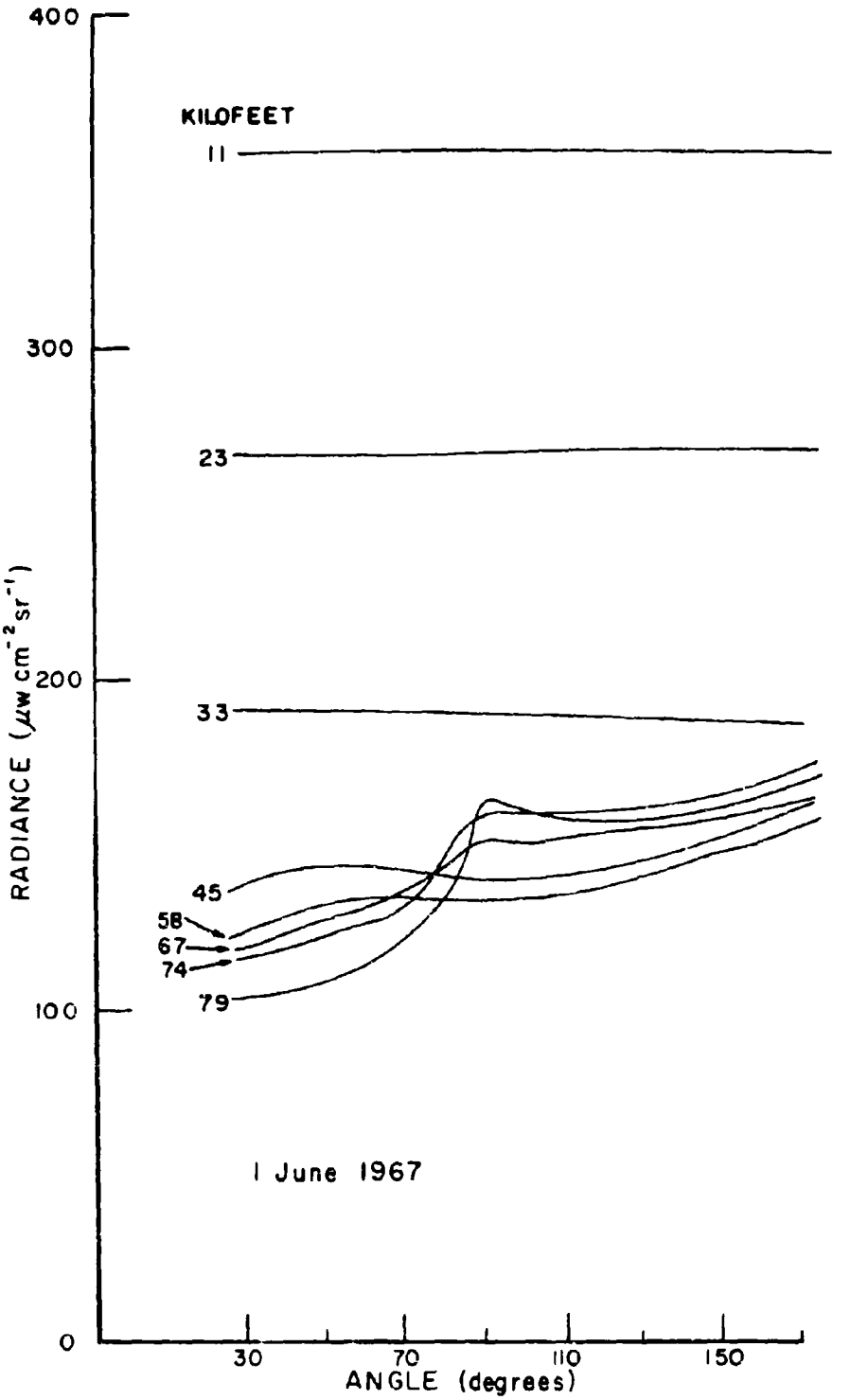

Figure 7. Filter radiance vs scan angle for selected records, 15μ filter. From balloon flight 1 June 1967. Record numbers are identified in Table I.

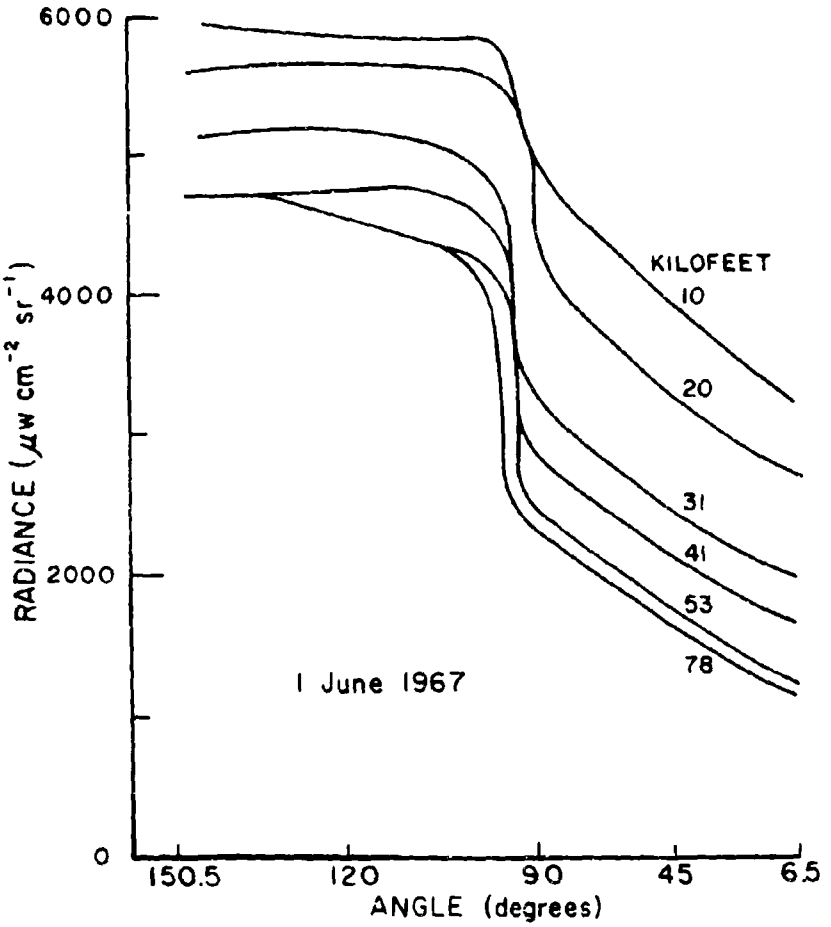

Figure 8. Filter radiance vs scan angle for selected records, wide bandpass filter. From balloon flight 1 June 1967. Record numbers are identified in Table I.

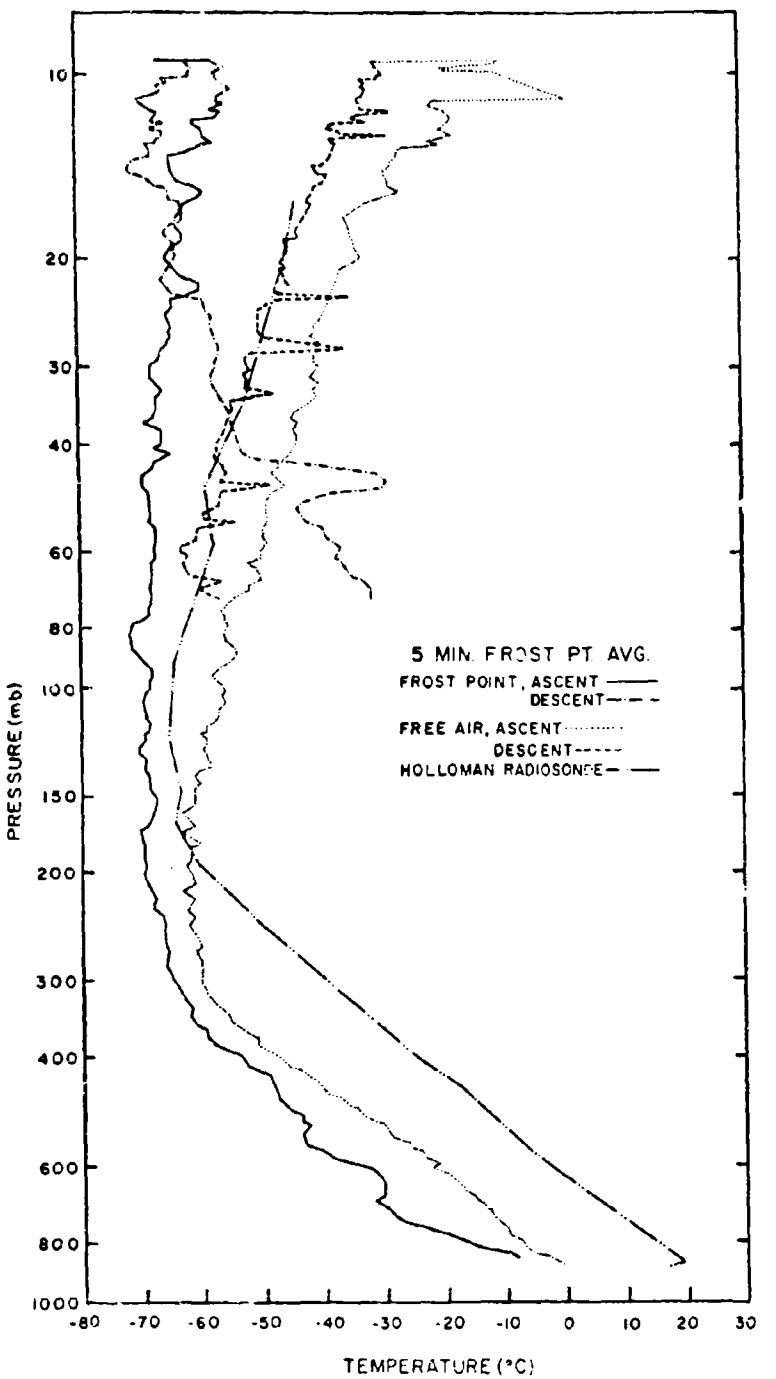

Figure 9 Frost Point Temperature vs Altitude for Balloon Flight 30 Nov. 1967.

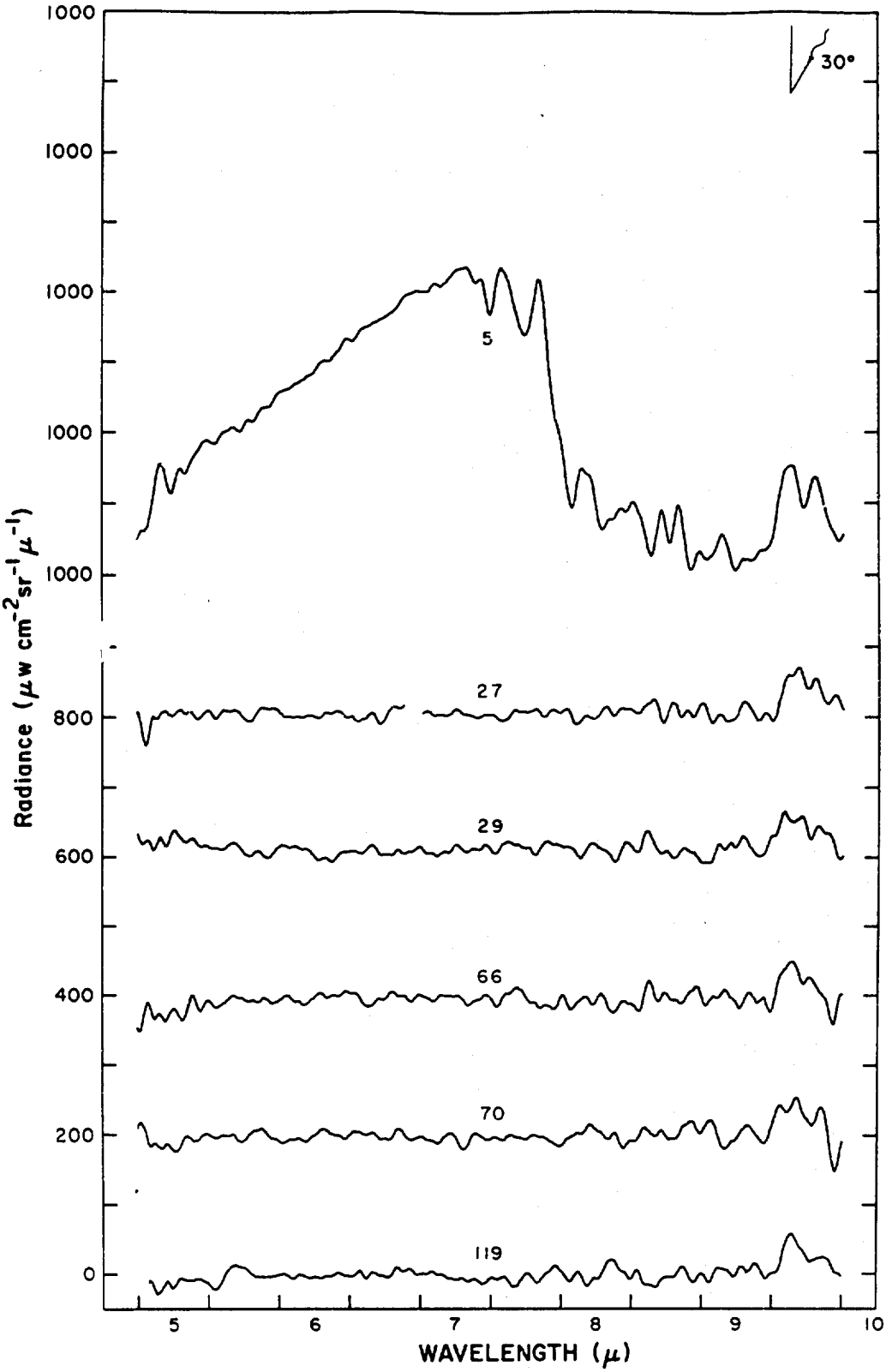

Figure 10 Spectral radiance vs altitude for balloon flight 30 November 1967. (See Table II)

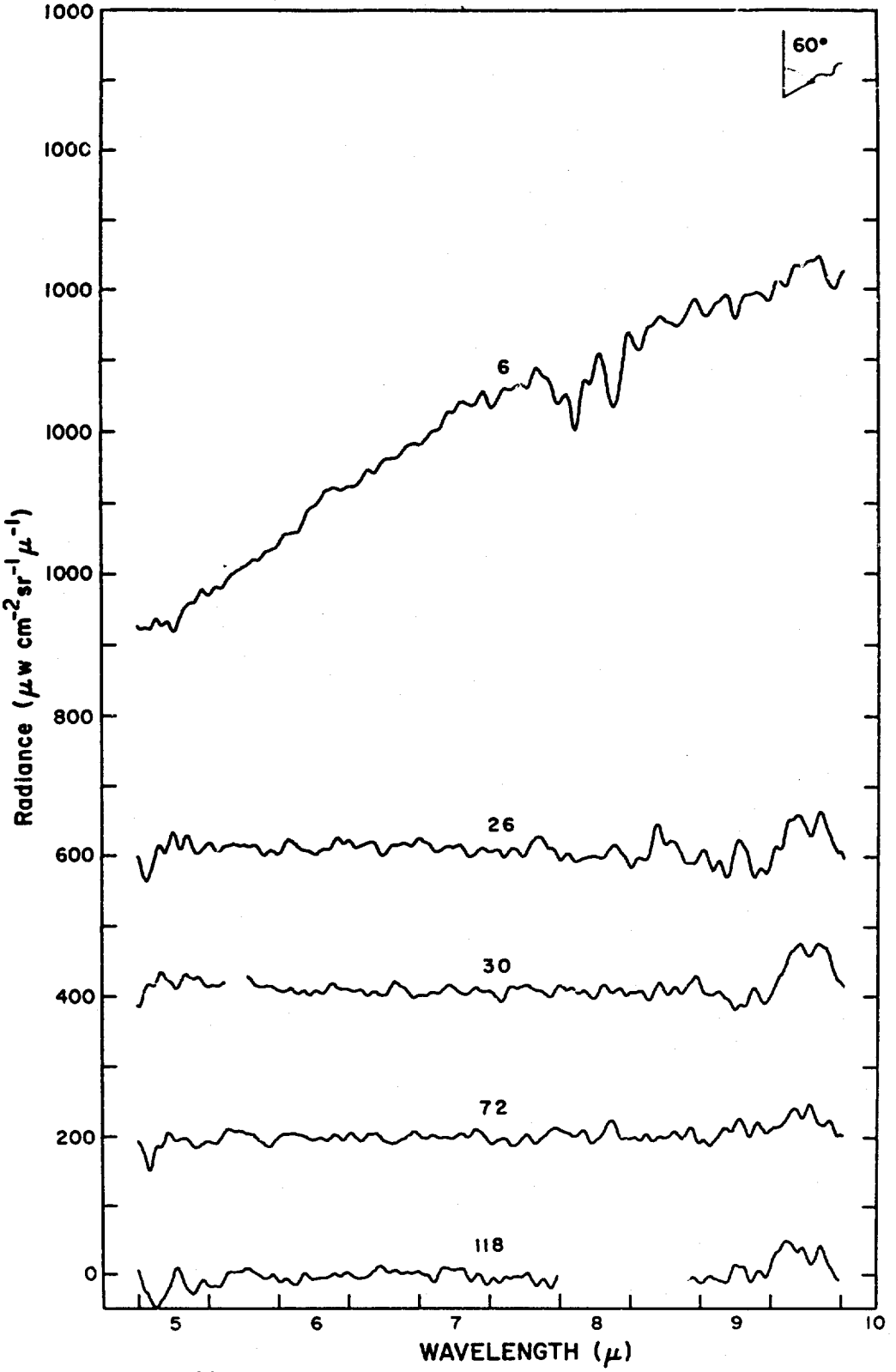

Figure 11 Spectral radiance vs altitude for balloon flight 30 November 1967. (See Table II)

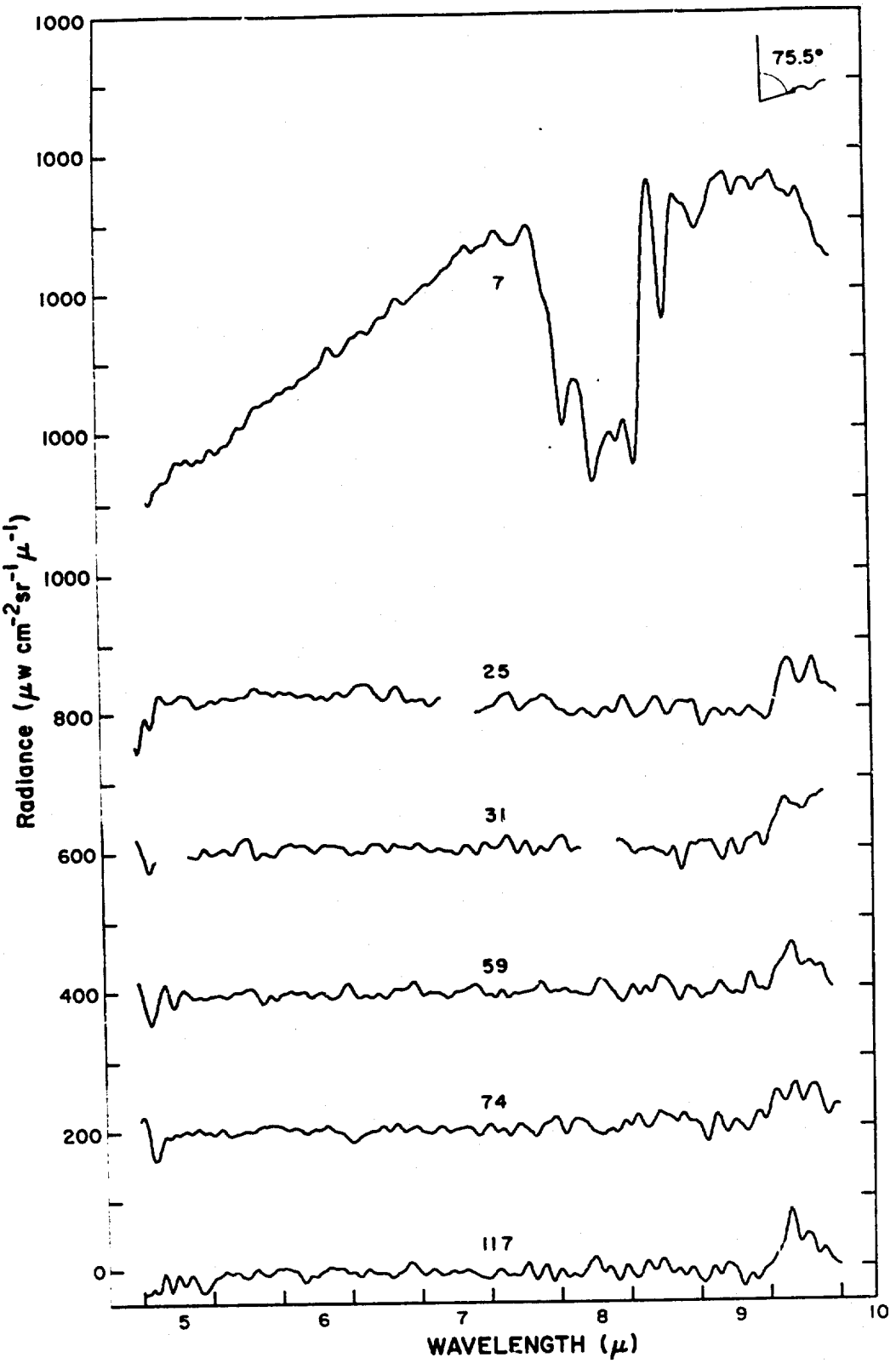

Figure 12 Spectral radiance vs altitude for balloon flight 30 November 1967. (See Table II)

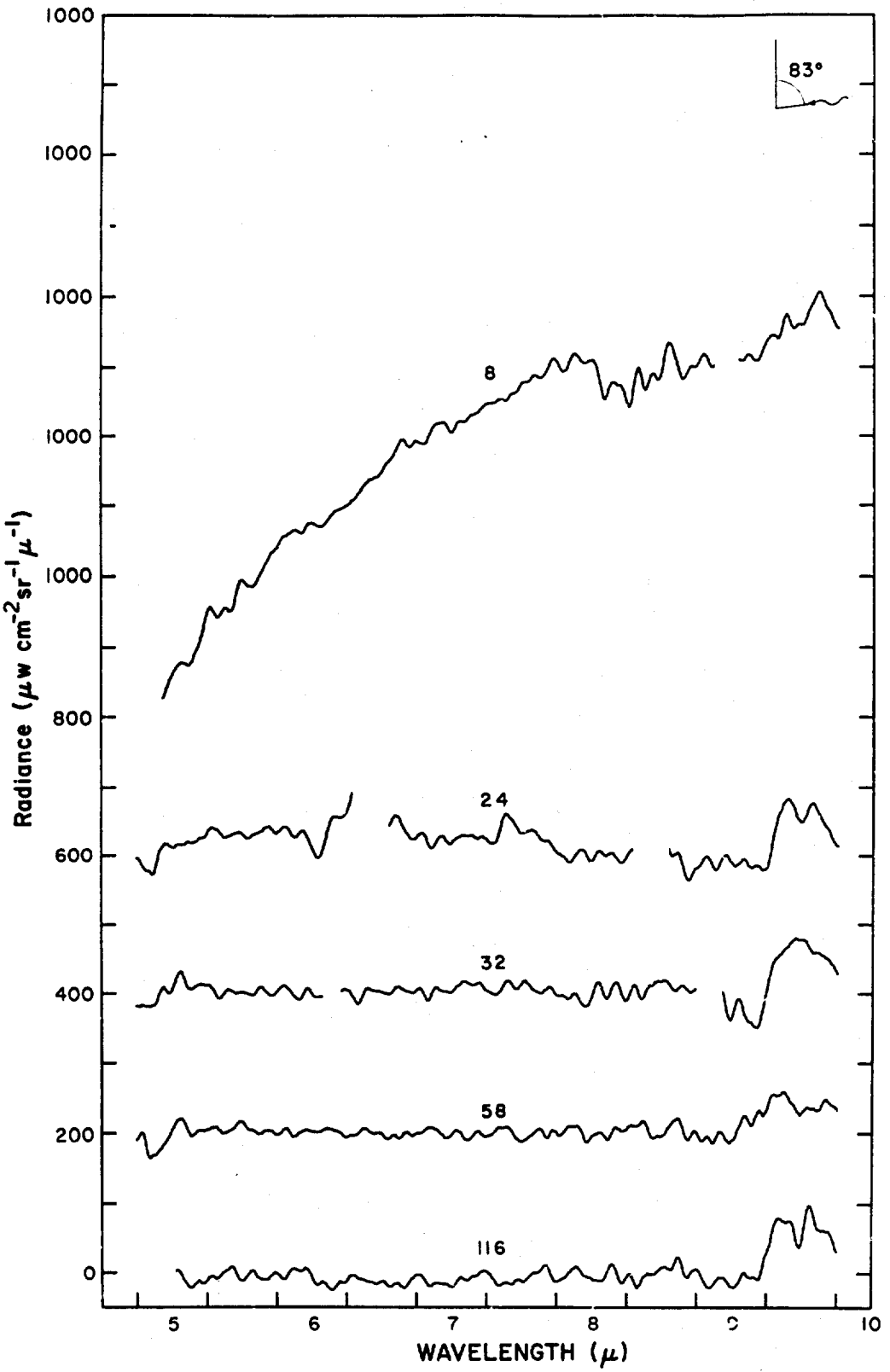

Figure 13 Spectral radiance vs altitude for balloon flight 30 November 1967. (See Table I.)

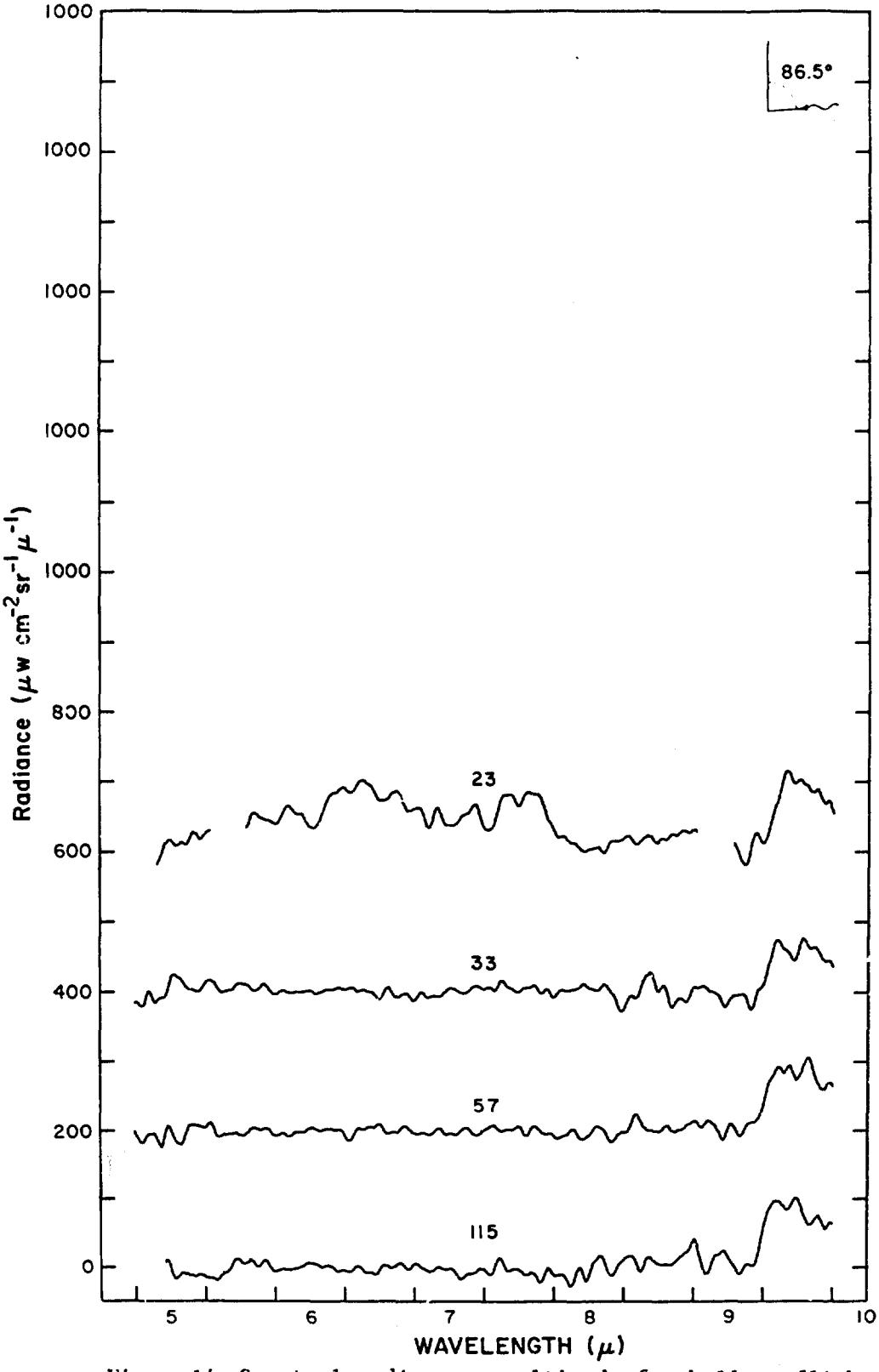

Figure 14 Spectral radiance vs altitude for balloon flight 30 November 1967. (See Table II)

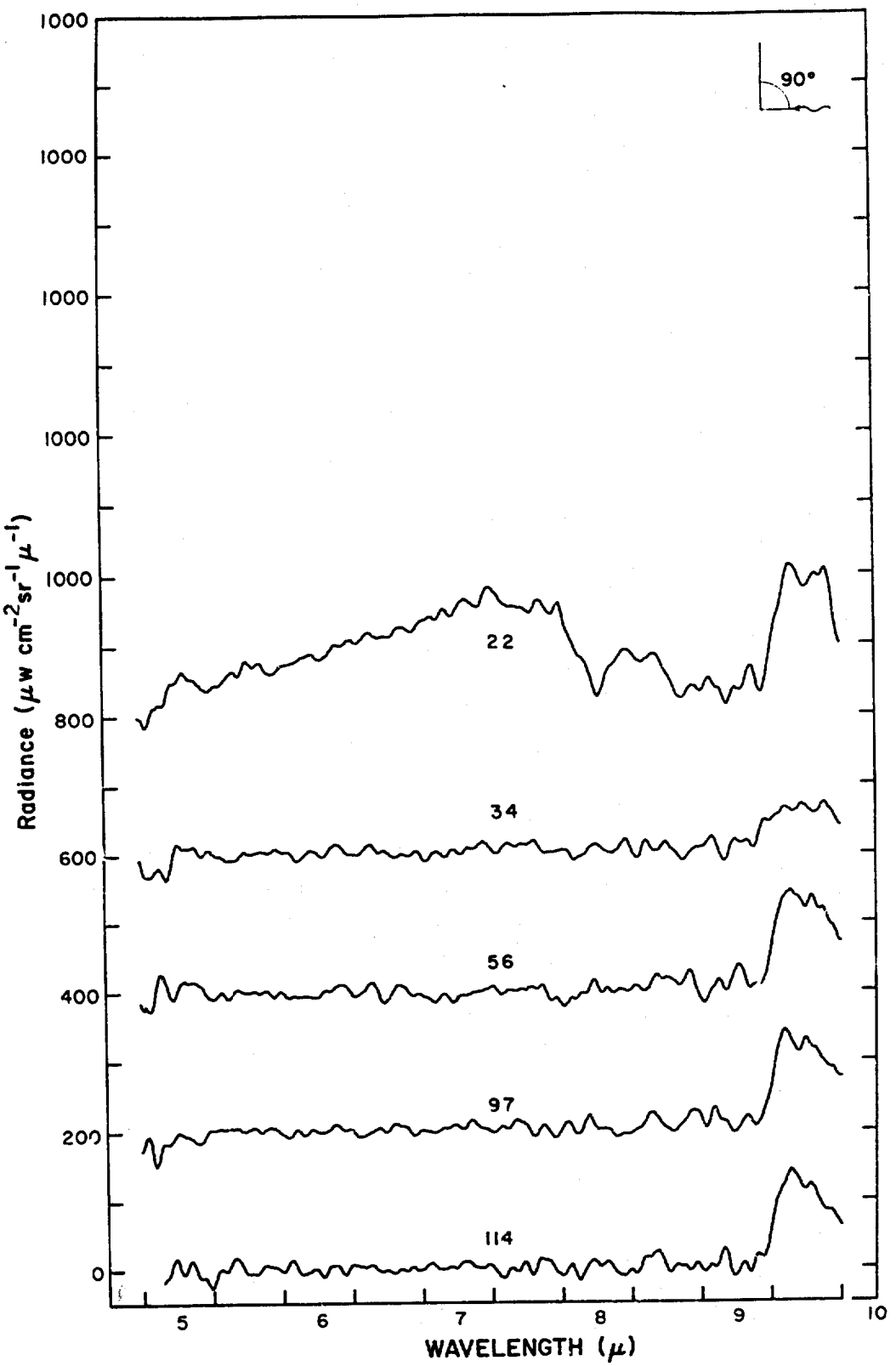

Figure 15 Spectral radiance vs altitude for balloon flight 30 November 1967. (See Table 11)

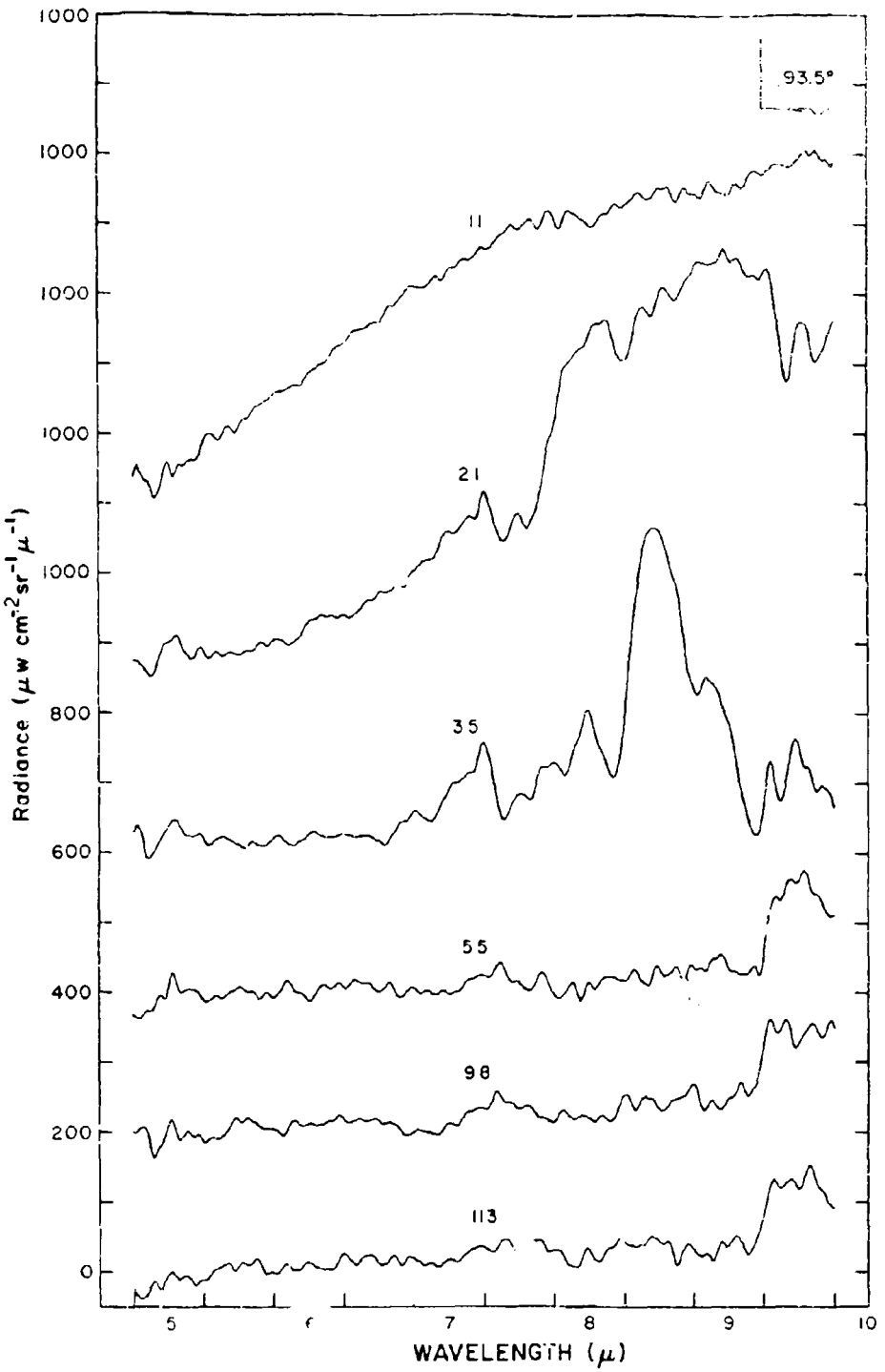

Figure 16 Spectral radiance vs altitude for balloon flight 30 November 1967. (See Table II)

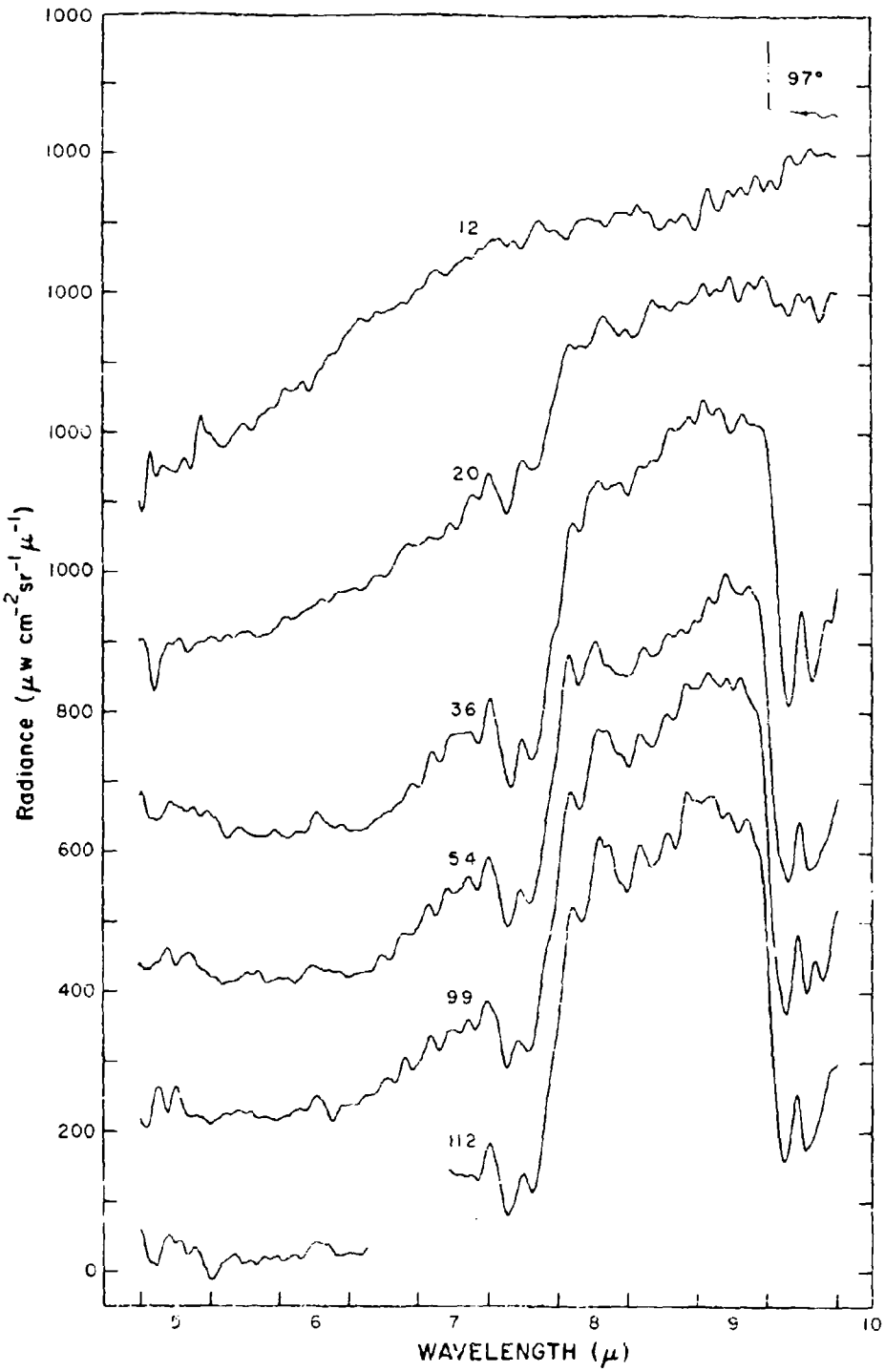

Figure 17 Spectral radiance vs altitude for balloon flight, 30 December 1967. (See Table 11)

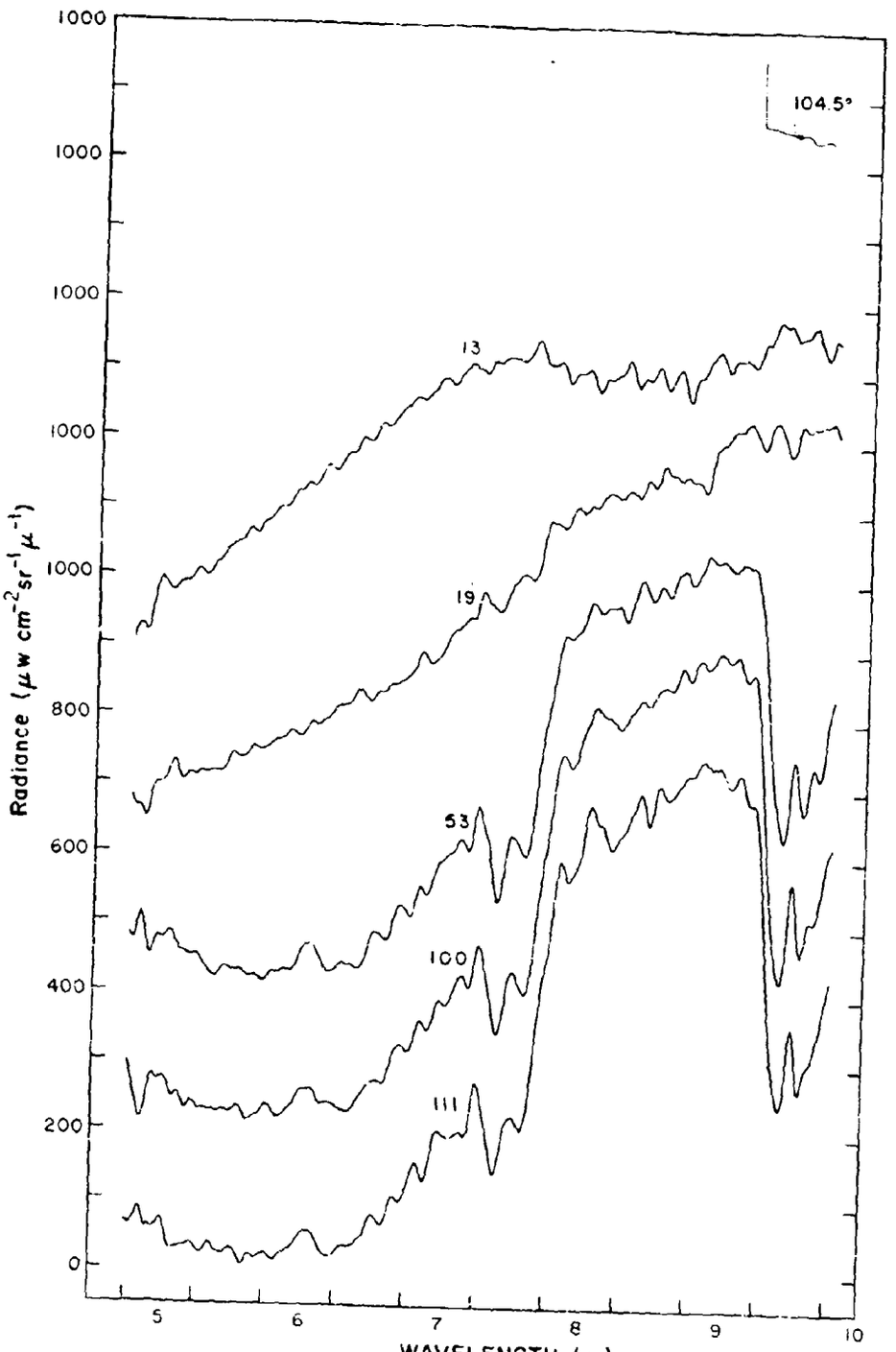

Figure 18 Spectral radiance vs altitude for 1 Nimbus flight 30 November 1967. (See Table 3)

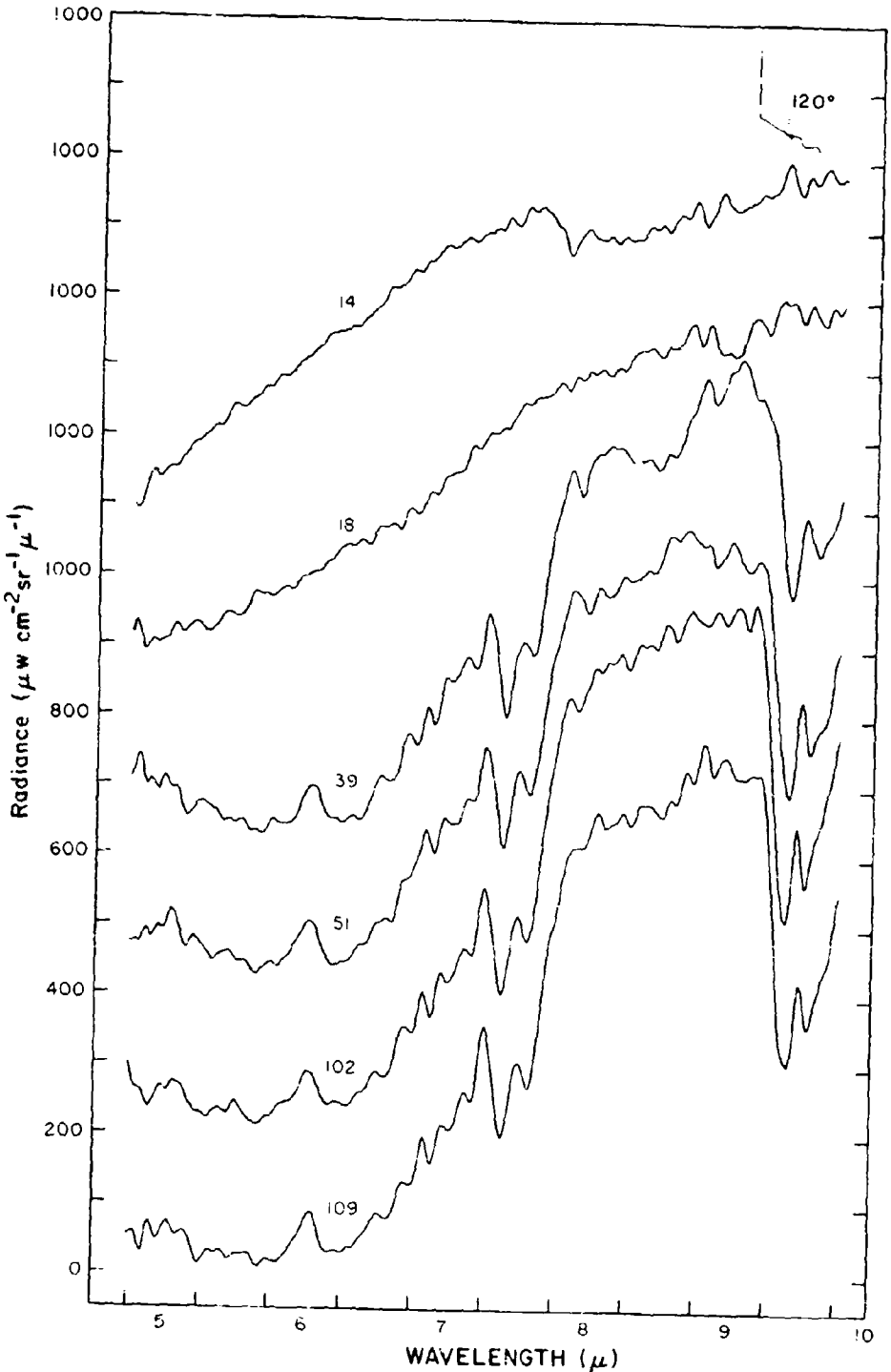

Figure 19 Spectral radiance vs altitude for balloon flight 30 November 1967. (See Table 10)

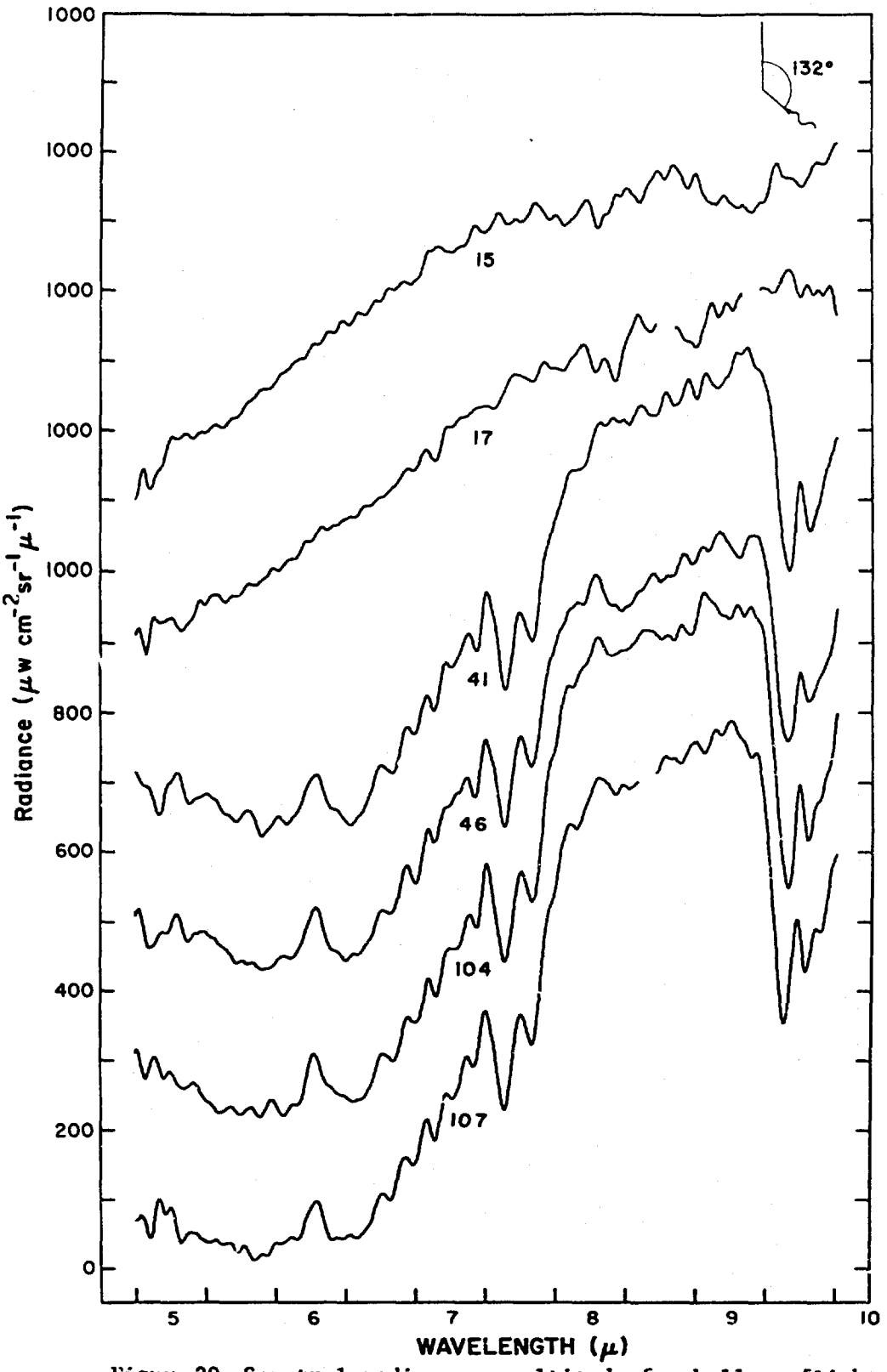

Figure 20 Spectral radiance vs altitude for balloon flight 30 November 1967. (See Table II)

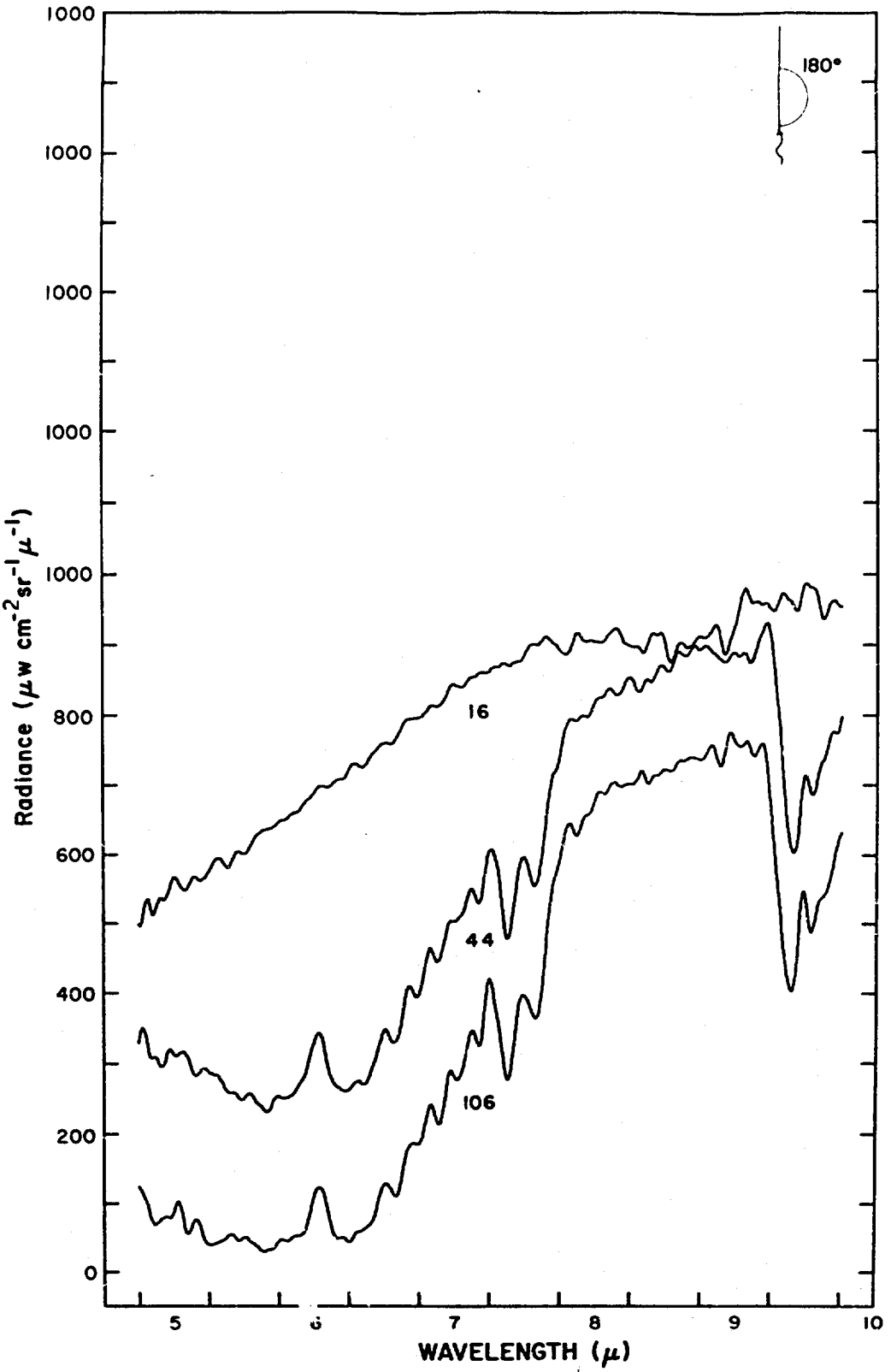

Figure 21 Spectral radiance vs altitude for balloon flight 30 November 1967. (See Table II)

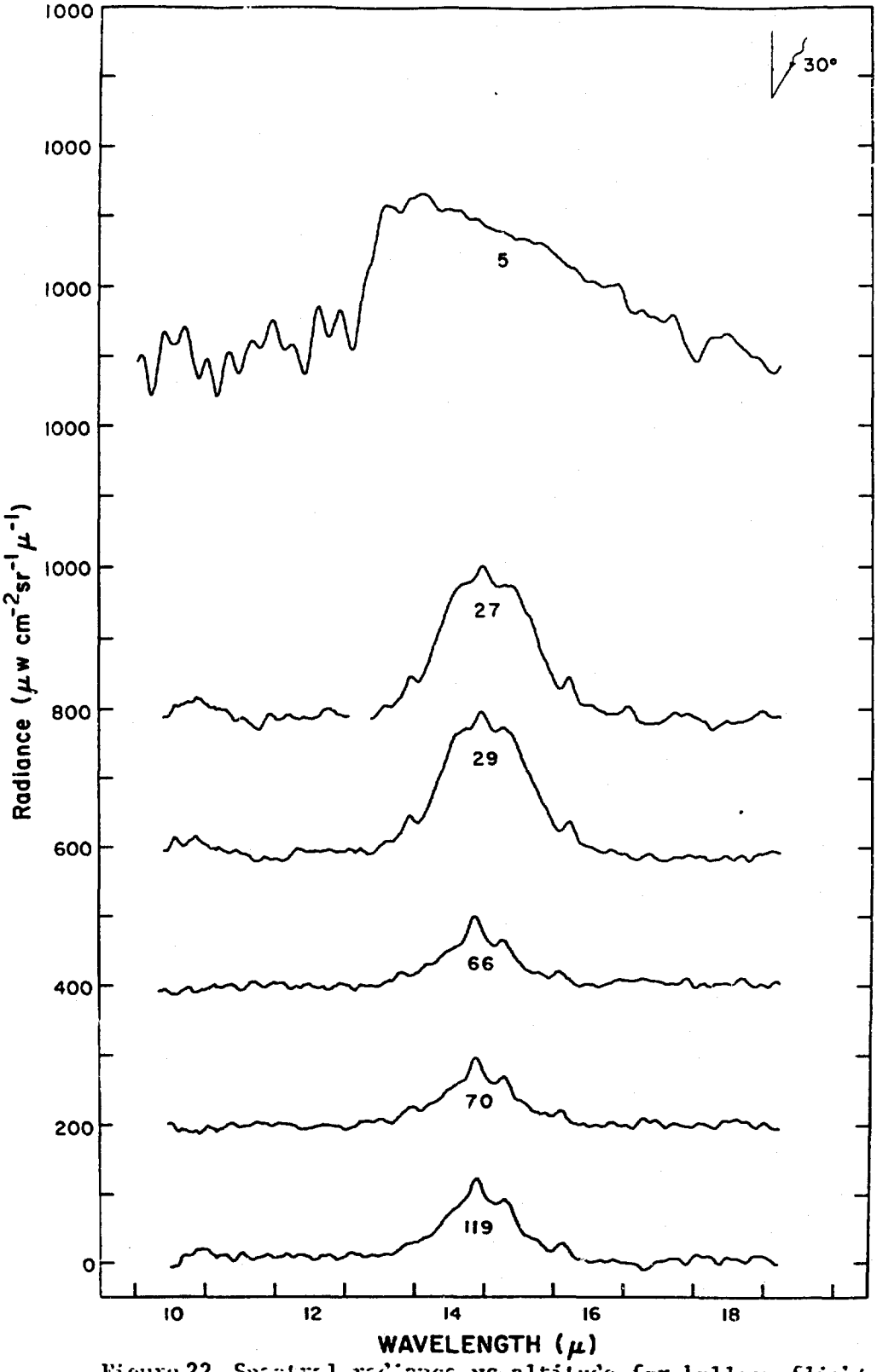

Figure 22 Spectral radiance vs altitude for balloon flight 30 November 1967. (See Table II)

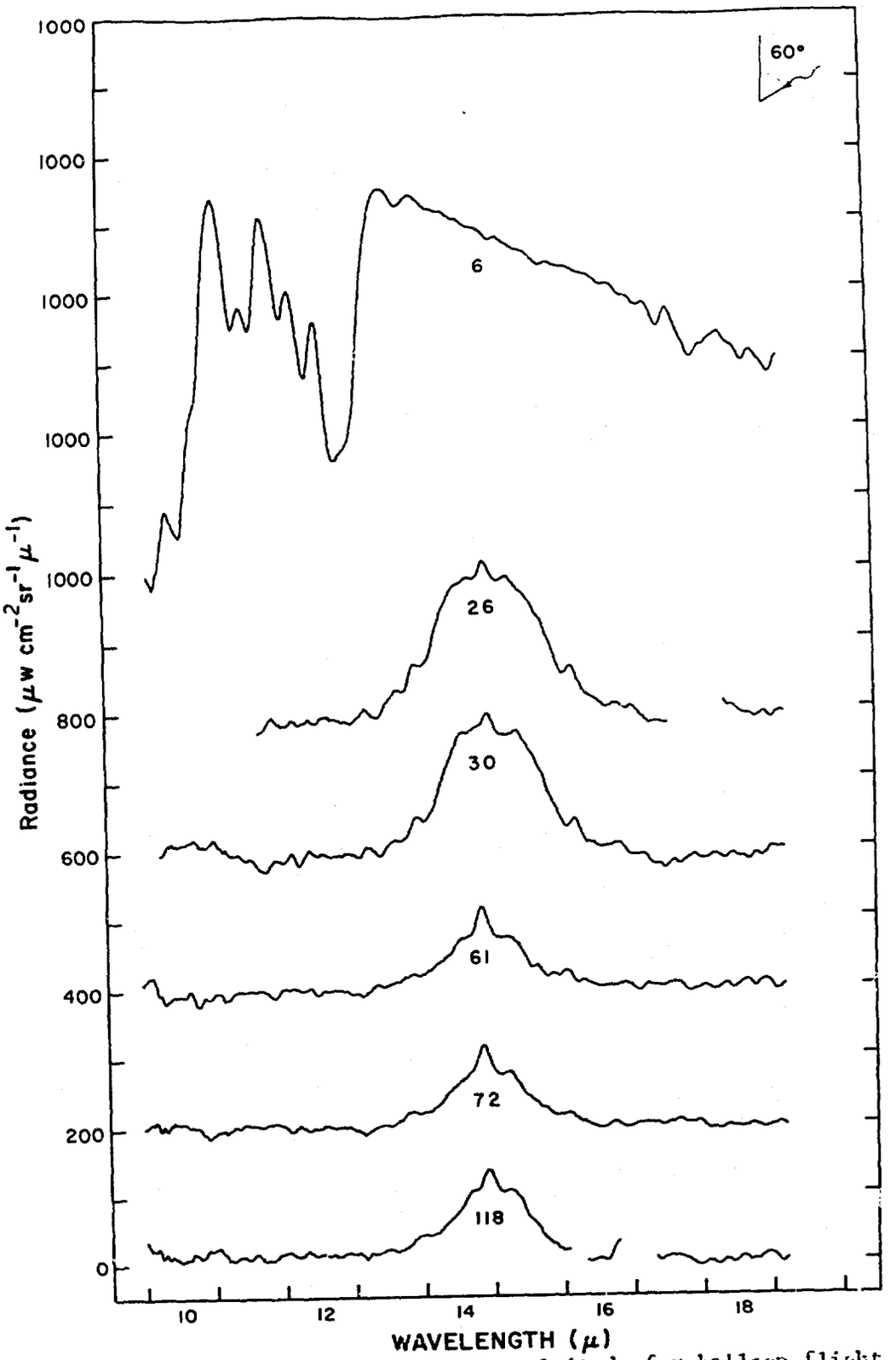

Figure 23 Spectral radiance vs altitude for balloon flight 30 November 1967. (See Table II)

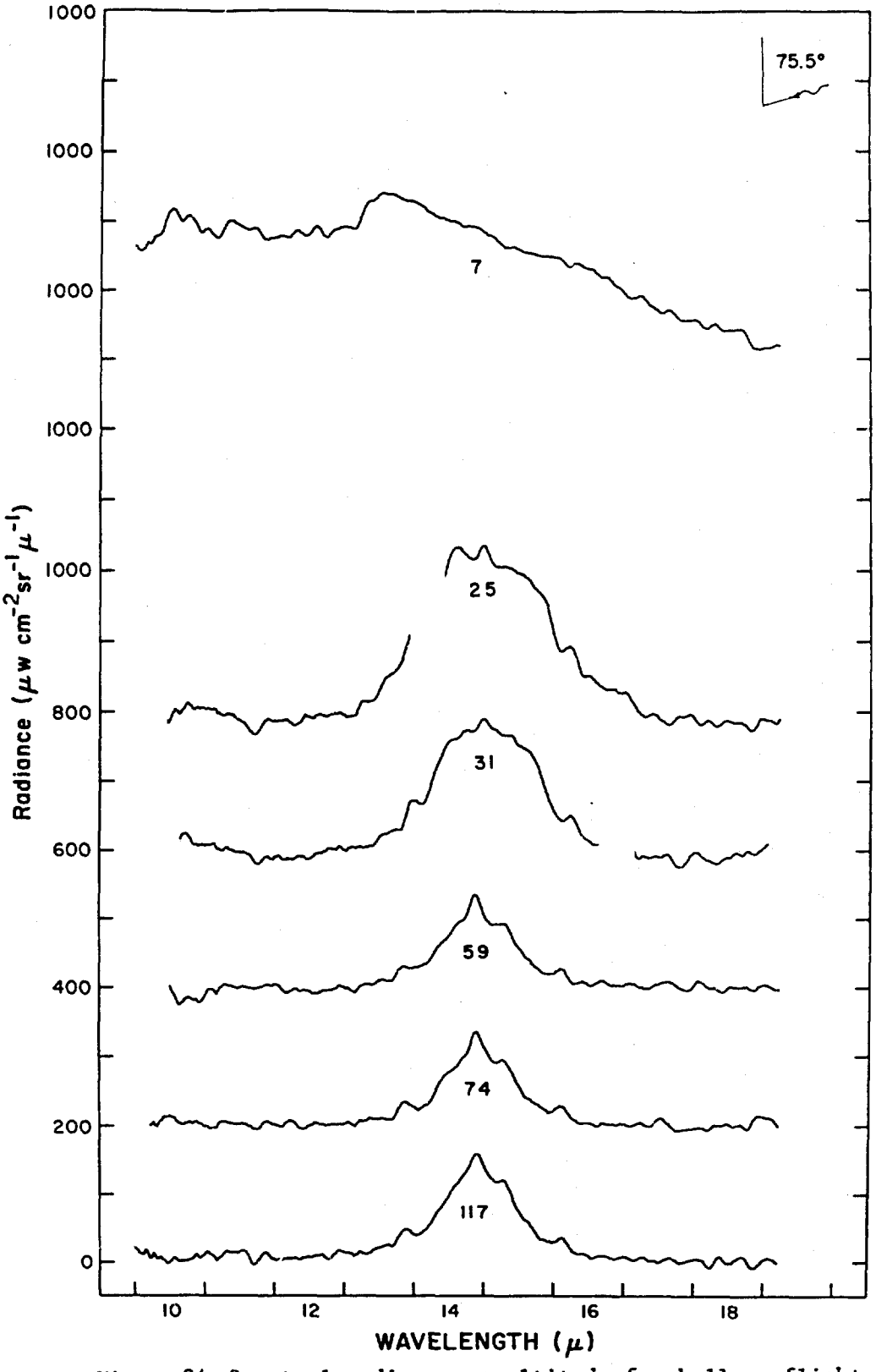

Figure 24 Spectral radiance vs altitude for balloon flight 30 November 1967. (See Table II)

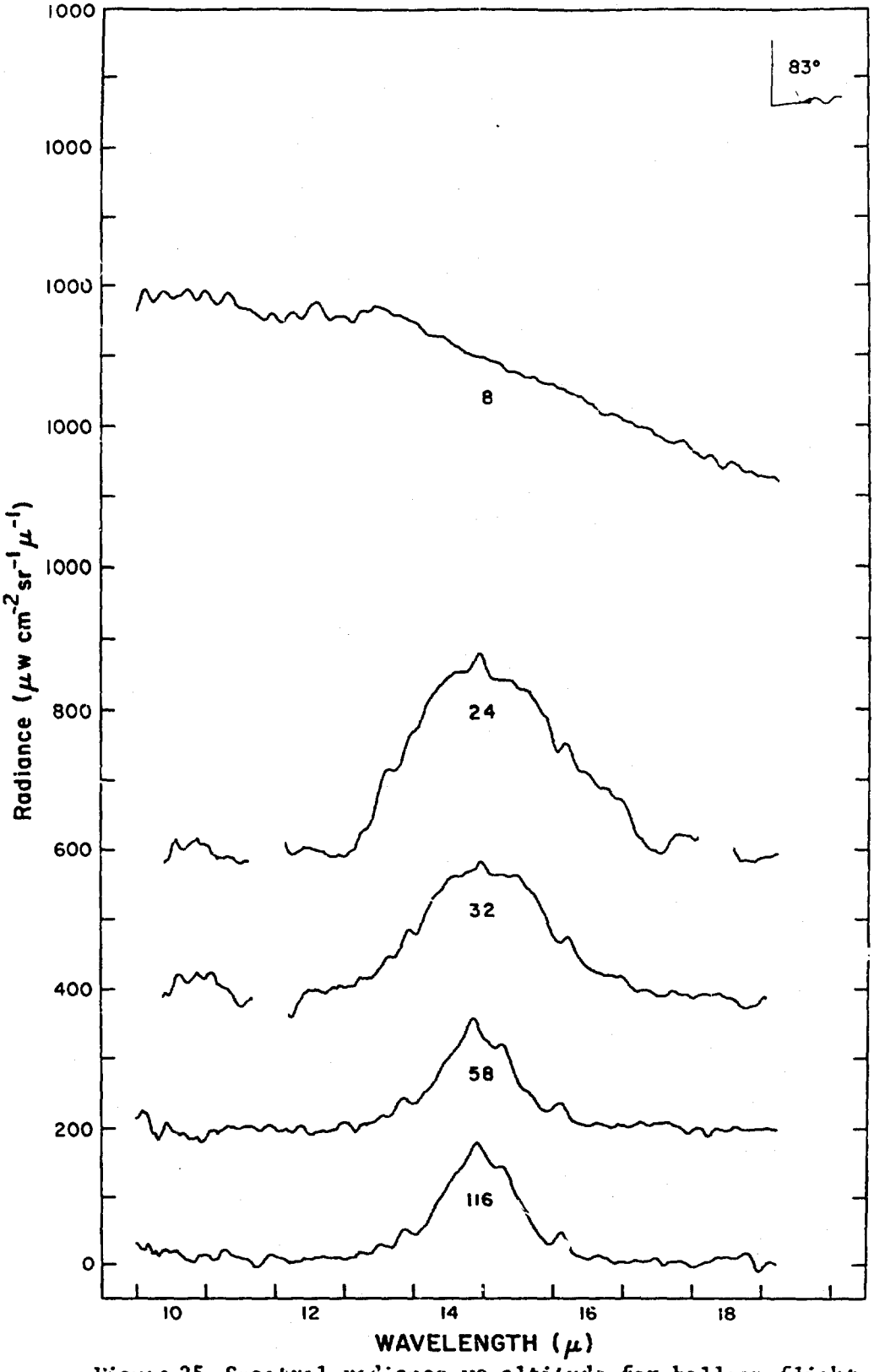

Figure 25 Spectral radiance vs altitude for balloon flight 30 November 1967. (See Table II)

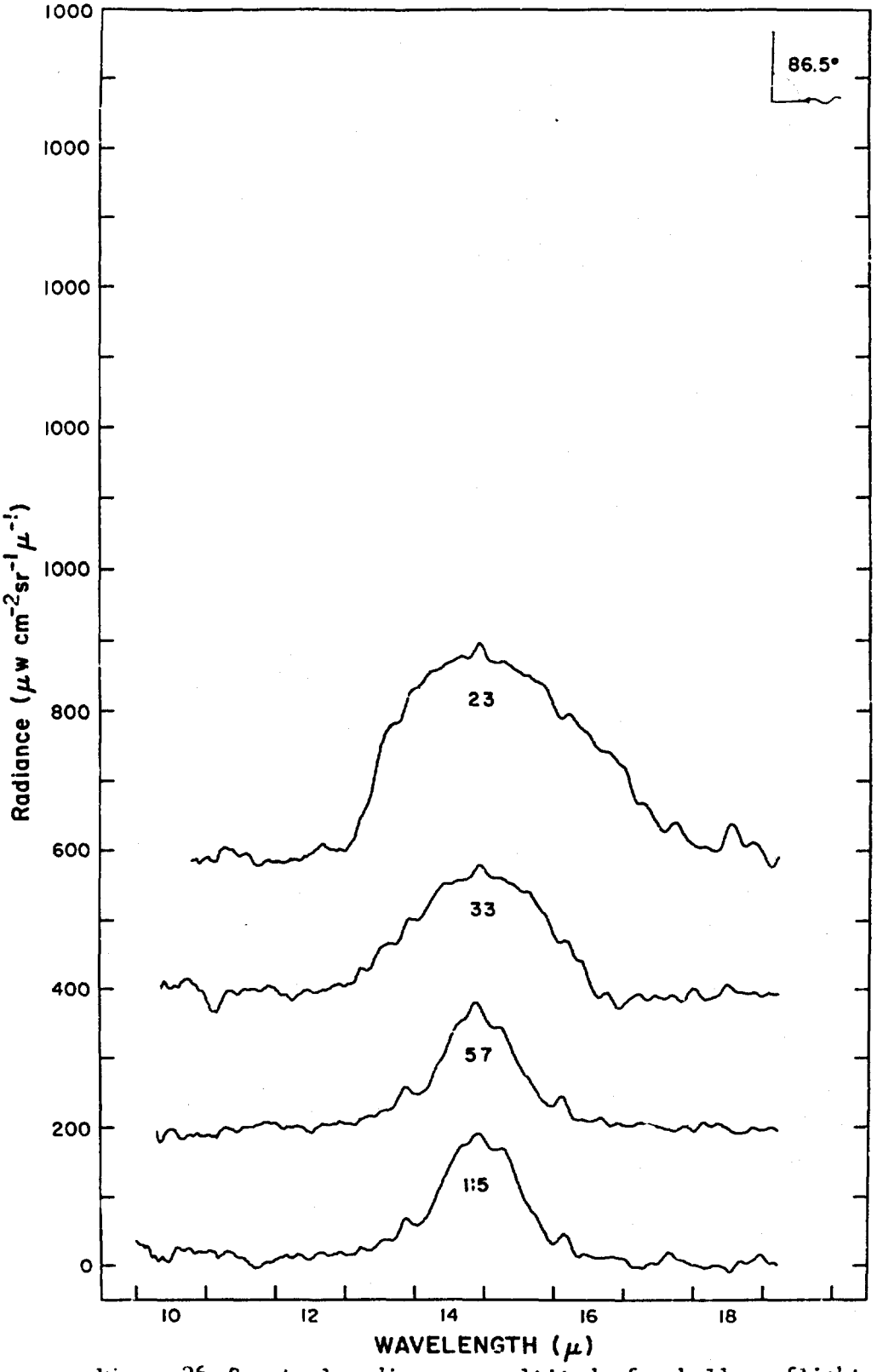

Figure 25 Spectral radiance vs altitude for Lilac flight 30 November 1967. (See Table II)

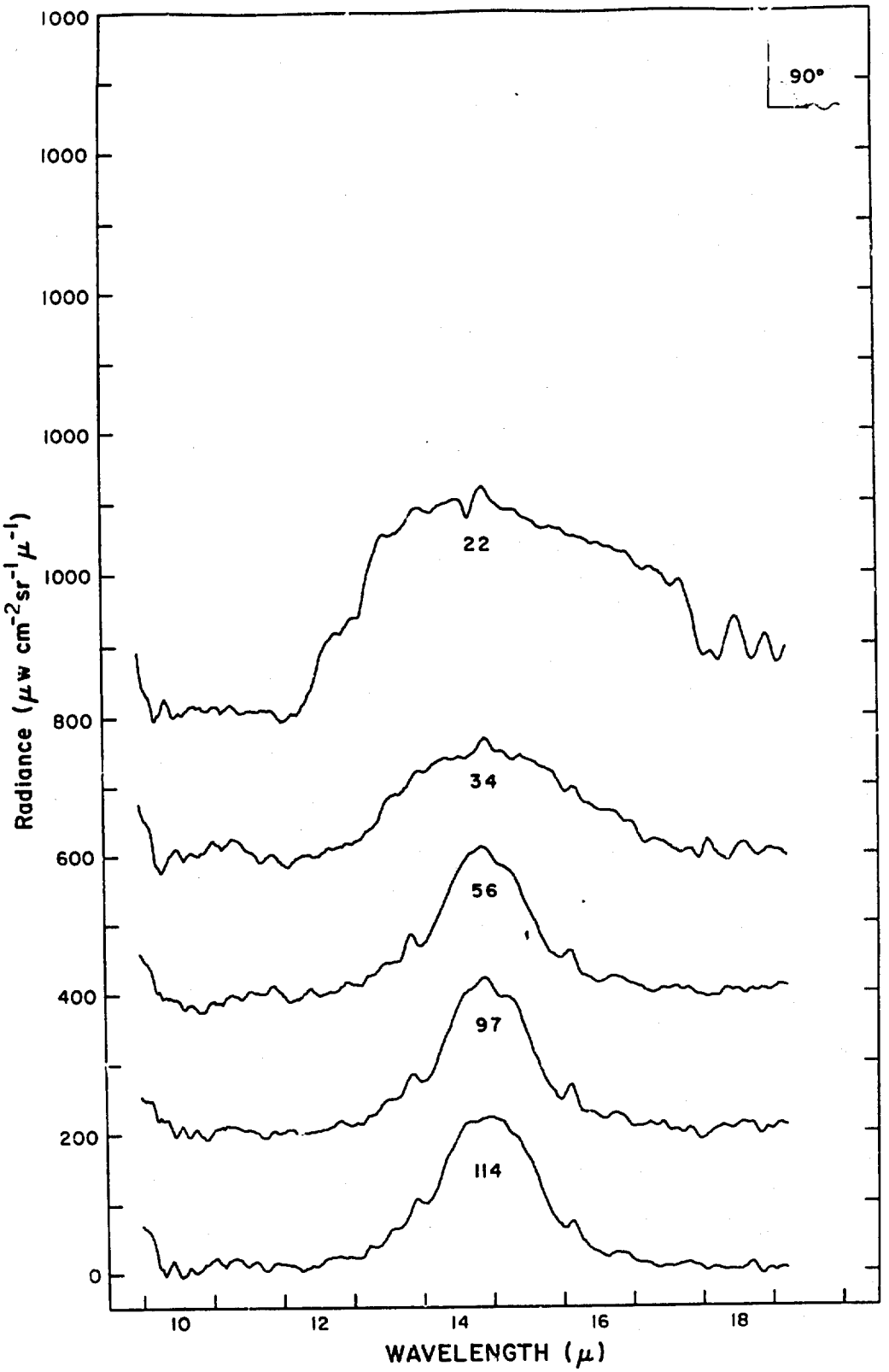

Figure 27 Spectral radiance vs altitude for balloon flight 30 November 1967. (See Table II)

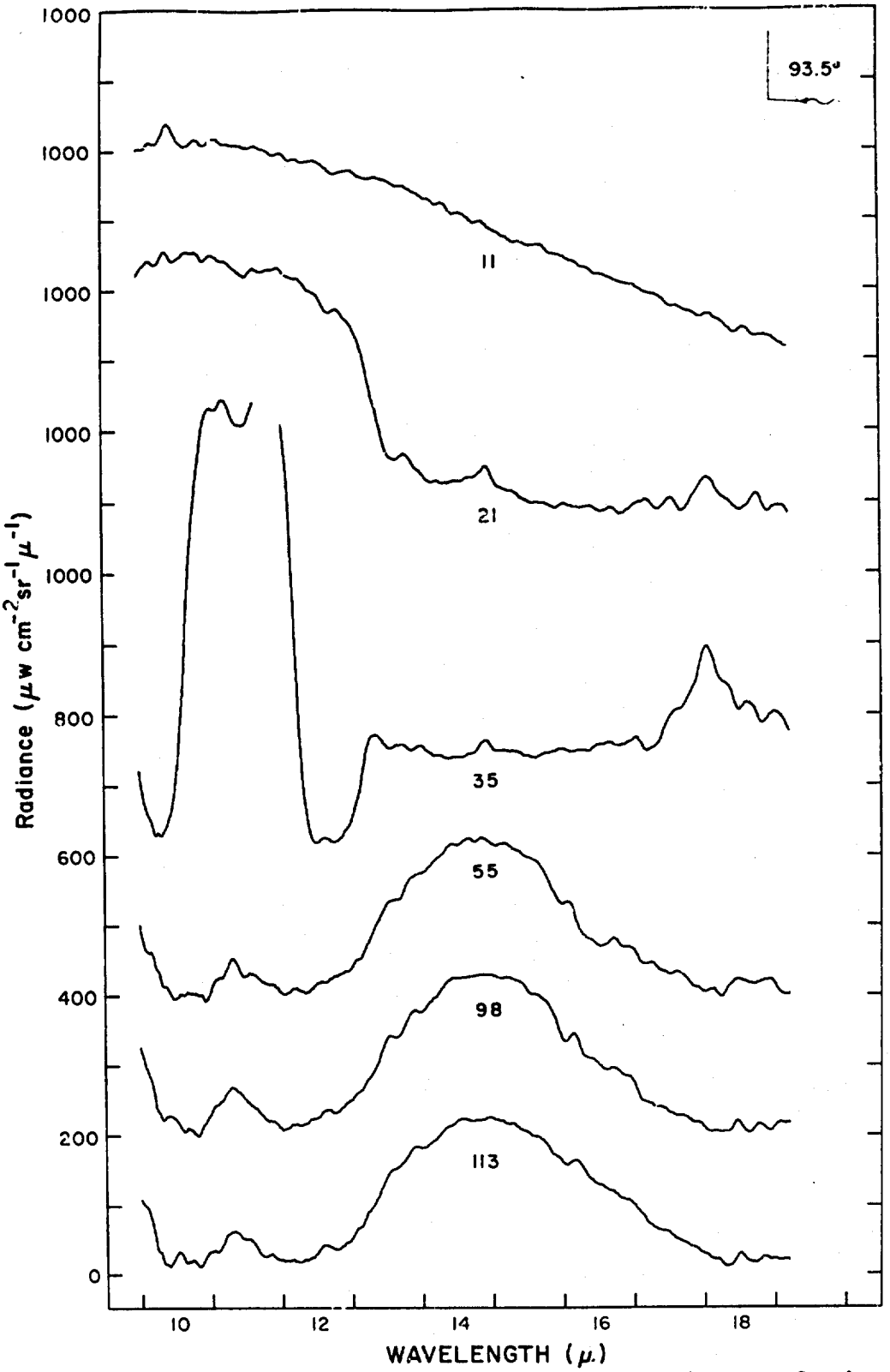

Figure 28 Spectral radiance vs altitude for balloon flight 30 [illegible] Apr 1967. (See Table II)

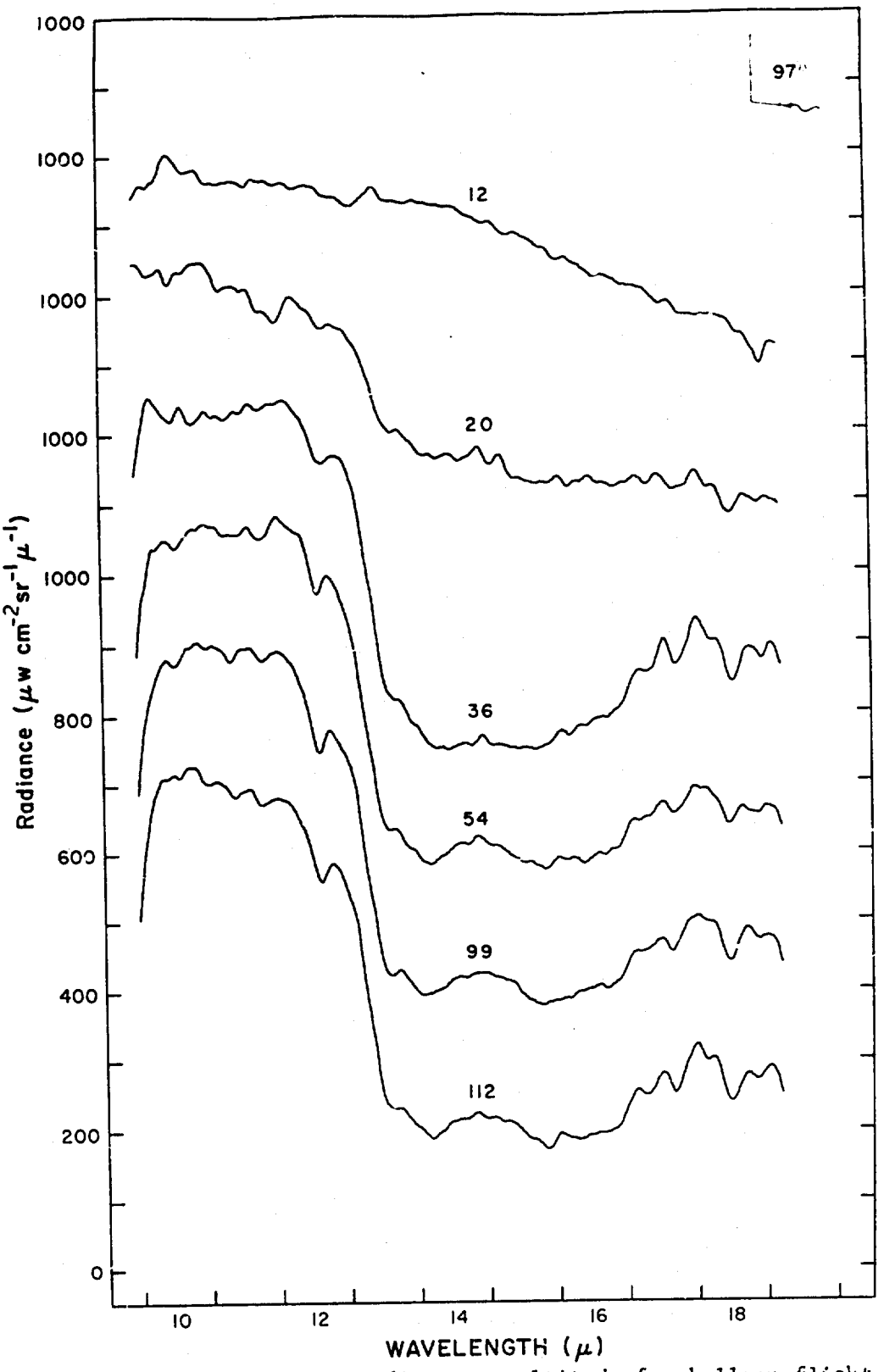

Figure 29 Spectral radiance vs altitude for balloon flight 30 November 1967. (See Table II)

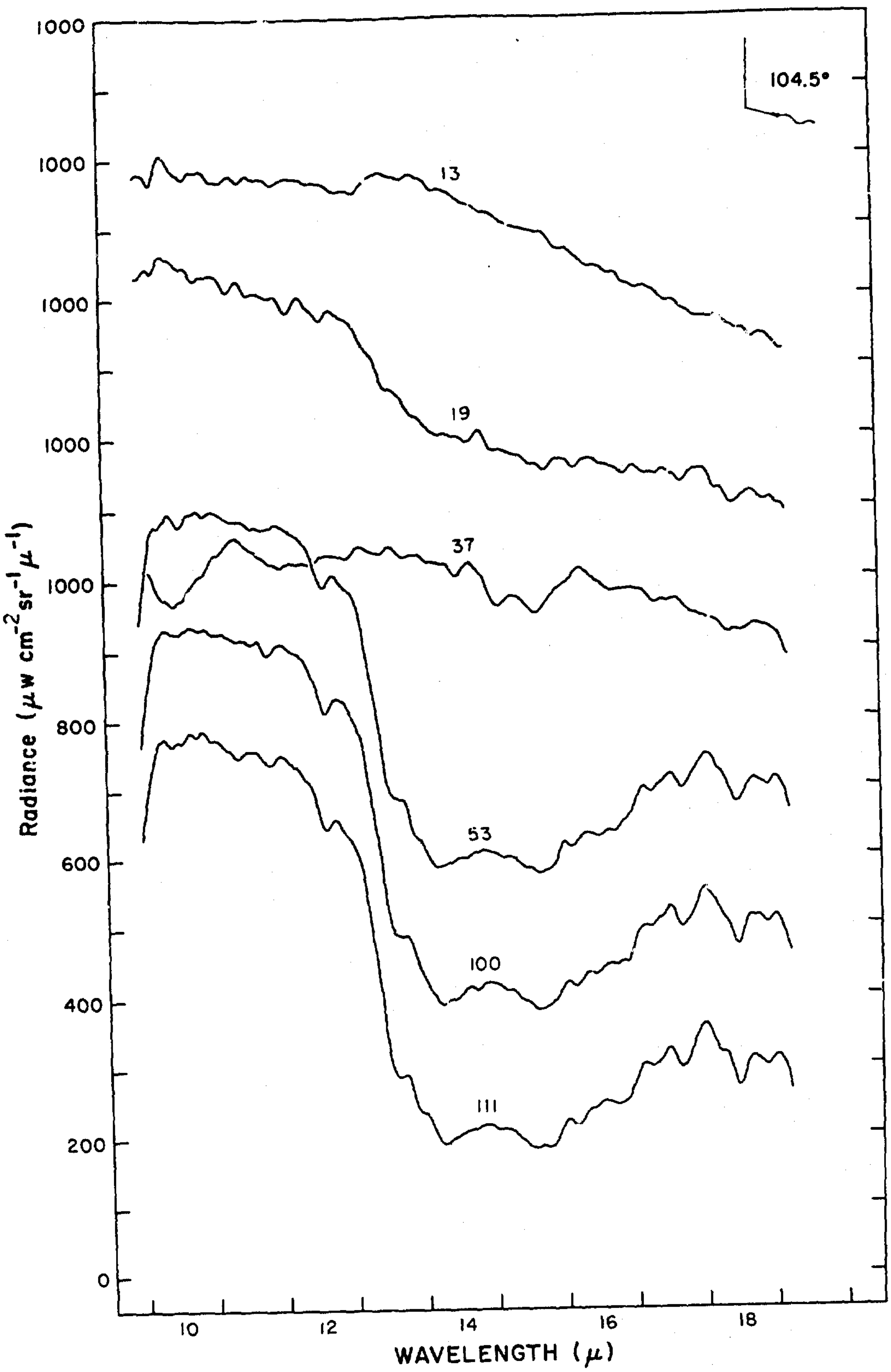

Figure 30 Spectral radiance vs altitude for balloon flight 30 November [illegible]7. (See Table [illegible]).

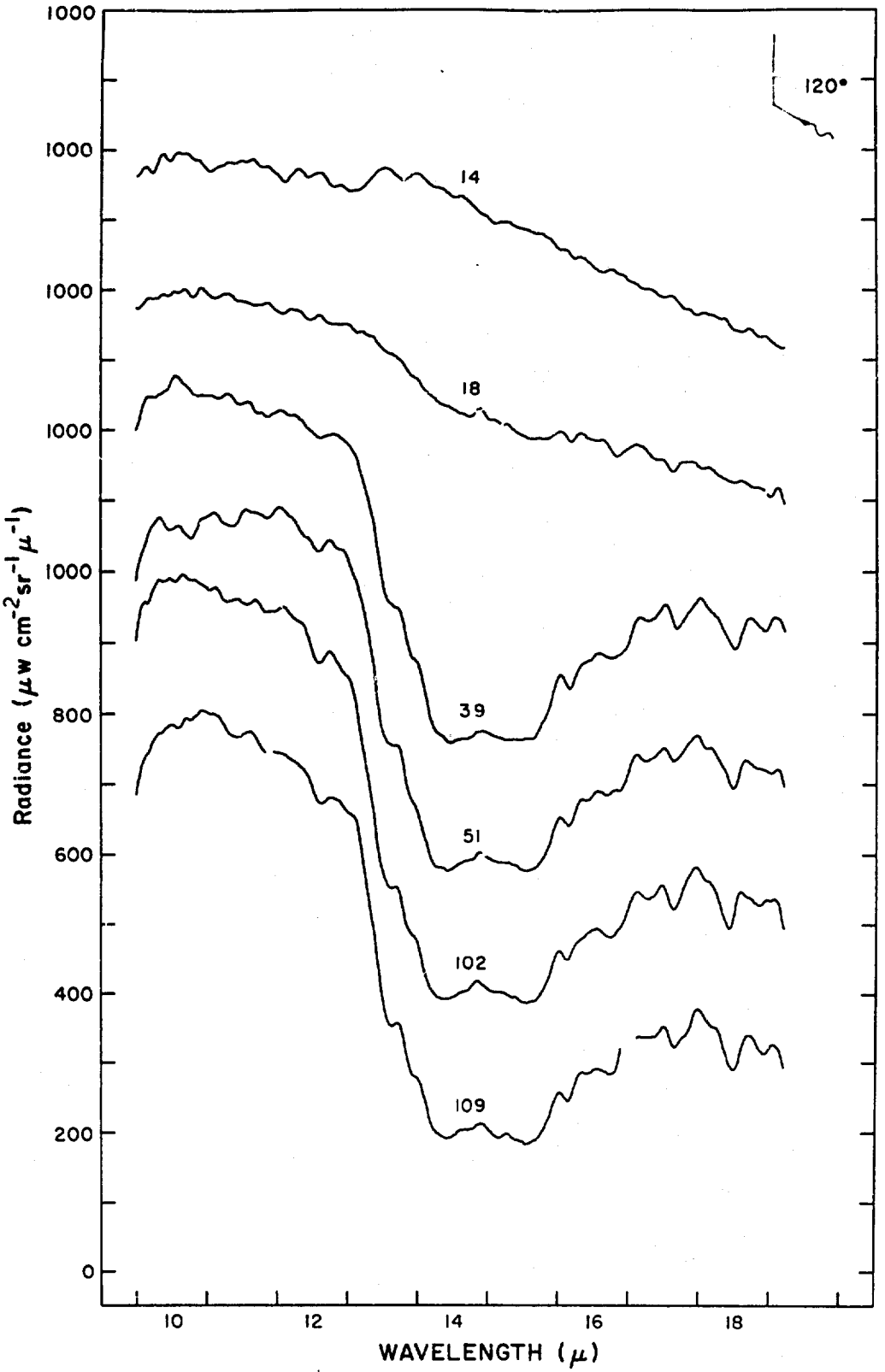

Figure 31 Spectral radiance vs altitude for balloon flight 30 November 1967. (See Table I.)

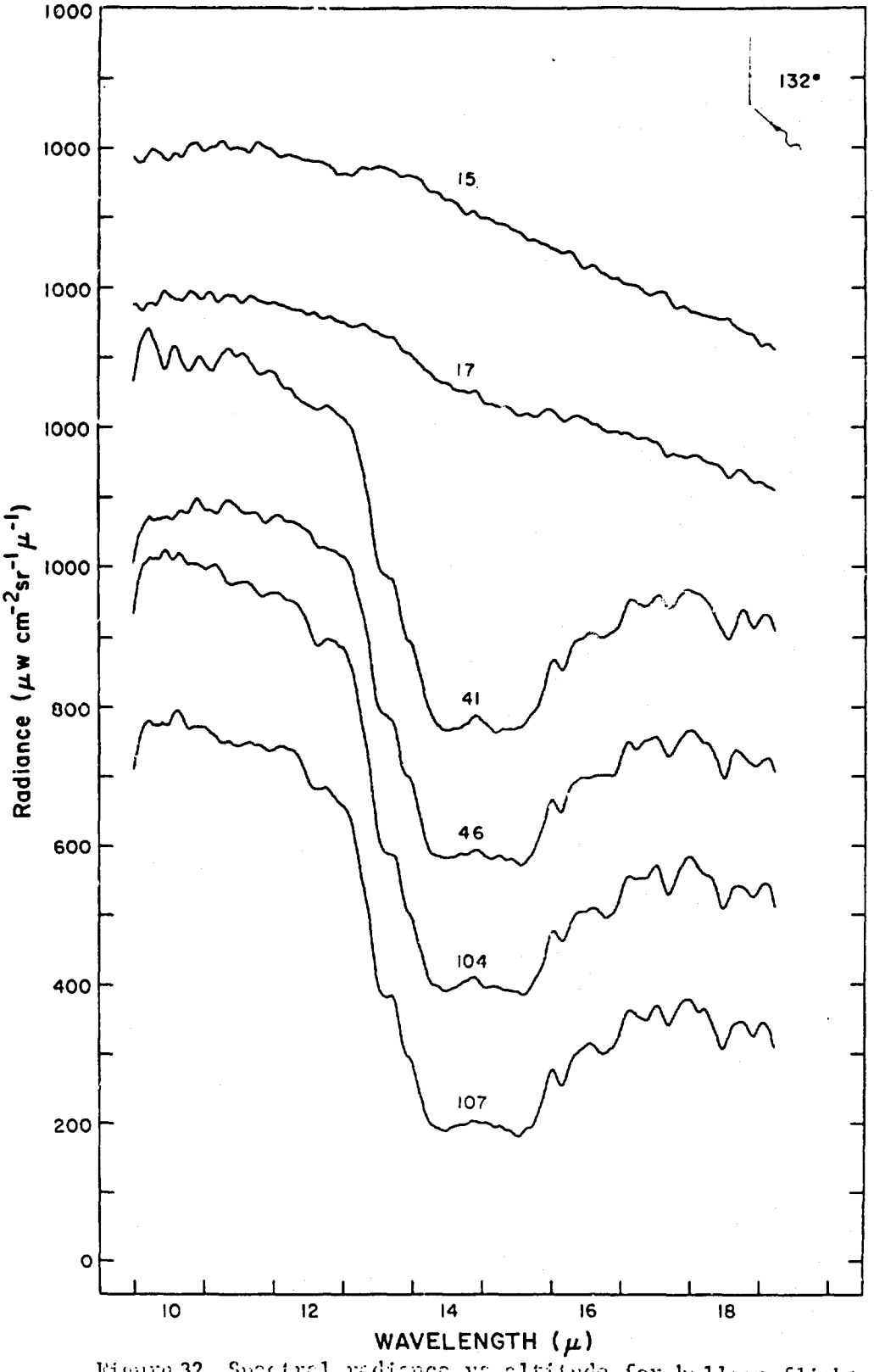

Figure 32 Spectral radiance vs altitude for balloon flight 30 November 1967. (See Table II)

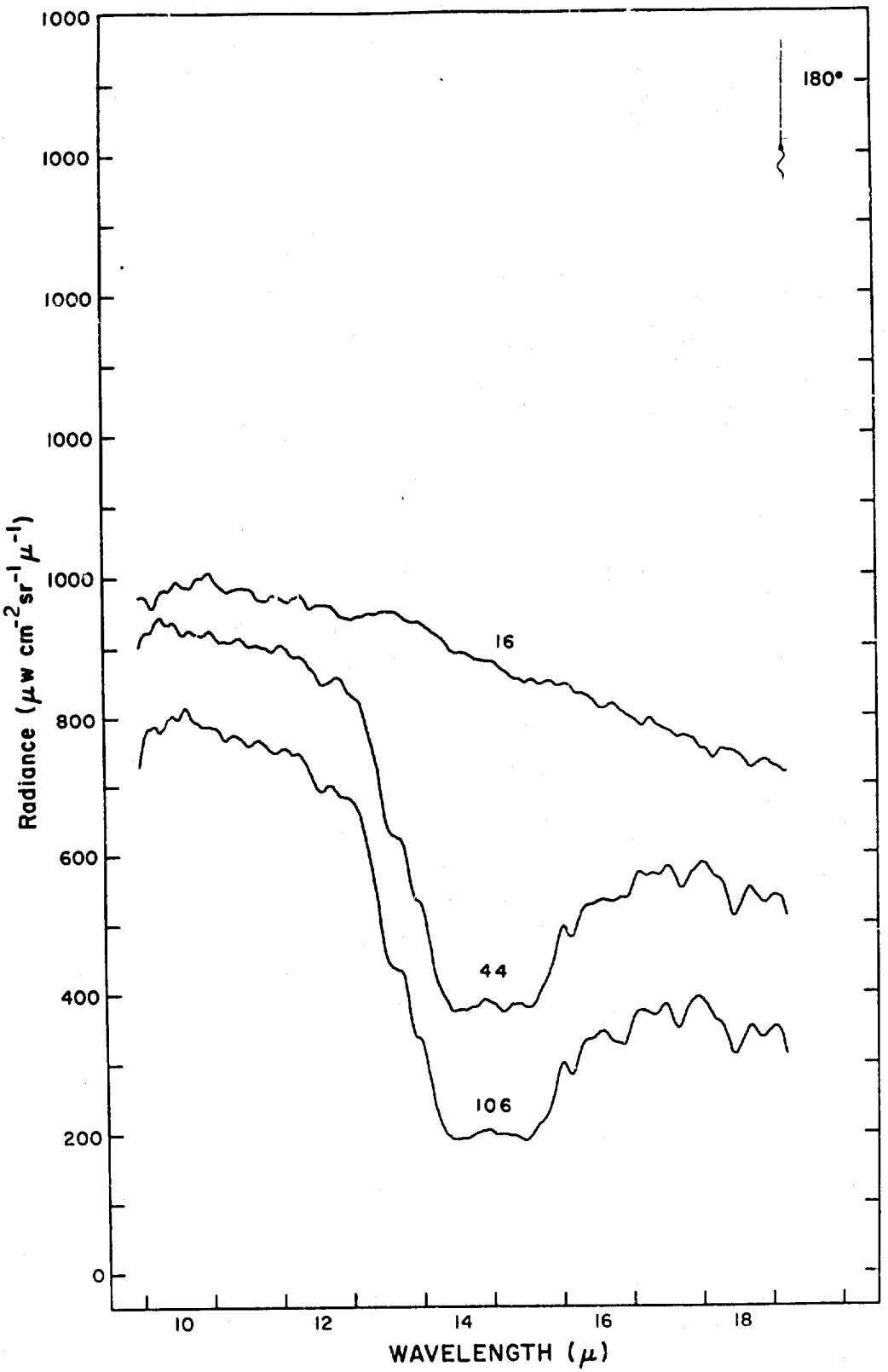

Figure 33 Spectral radiance vs altitude for balloon flight 30 November 1967. (See Table II)

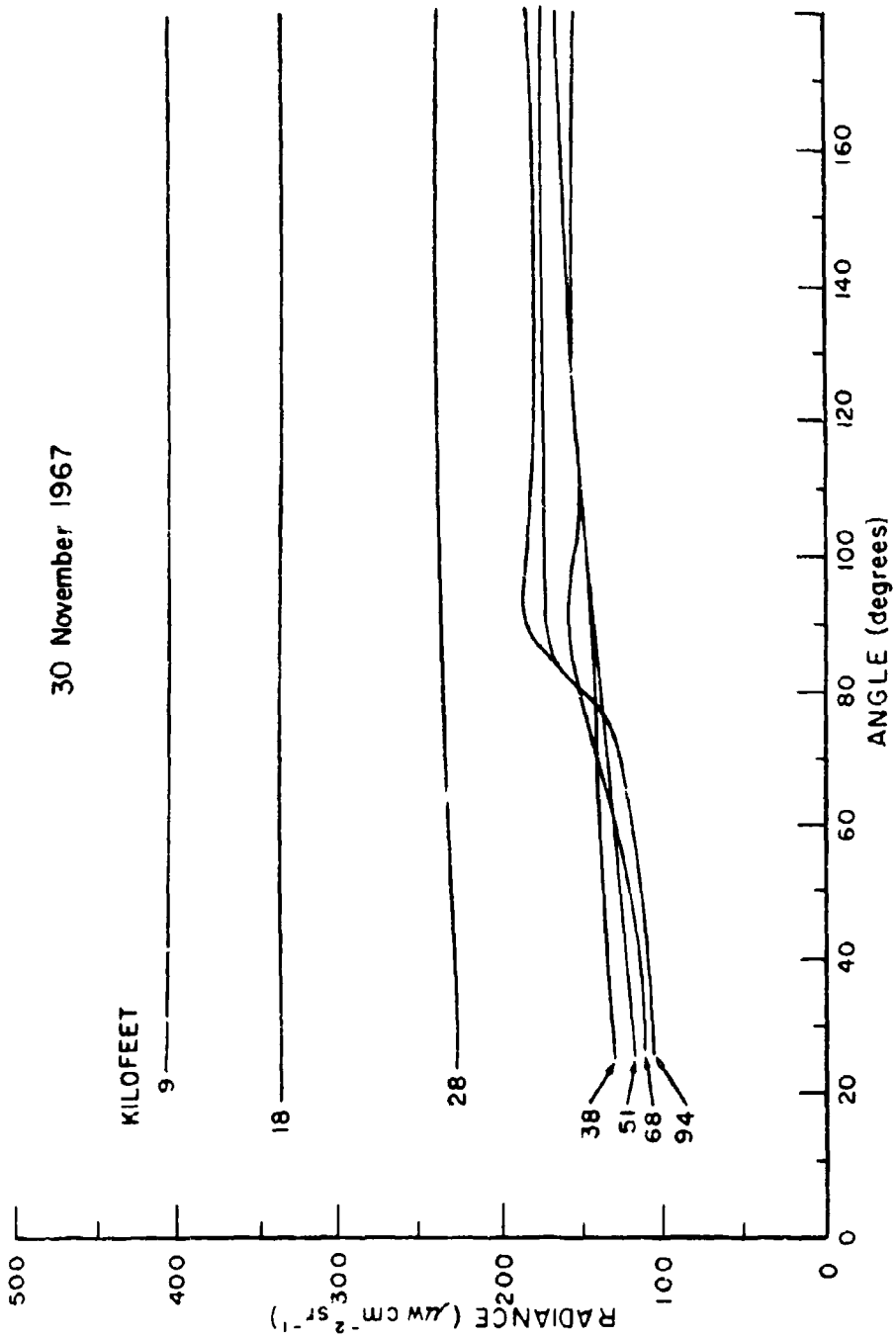

Figure 34. Filter radiance vs scan angle for selected records, wide band filter. From balloon flight 30 November 1967. Record numbers are identified in Table II.

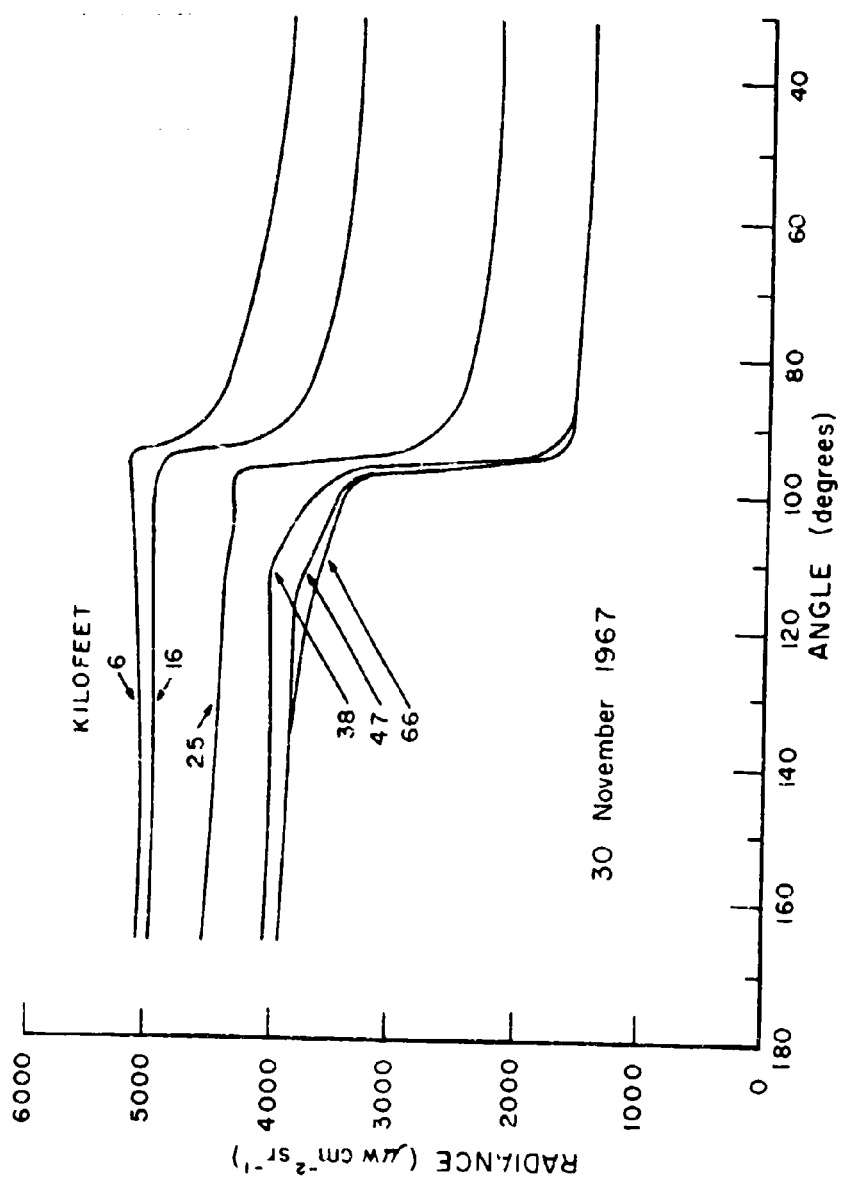

Figure 35. Filter radiance vs scan angle for selected records, 15u filter. From balloon flight 30 November 1967. Record numbers are identified in Table II.

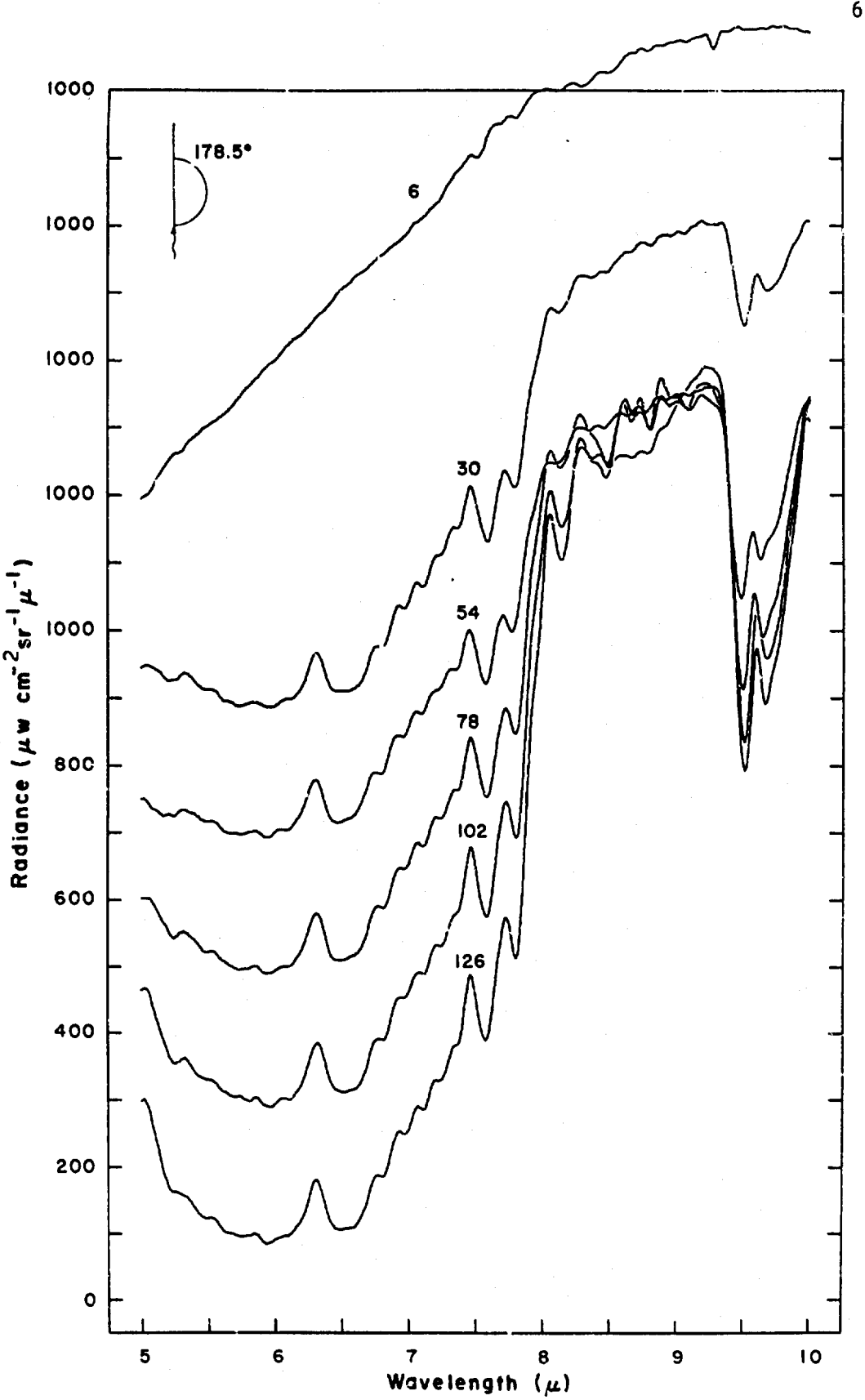

Figure 36 Spectral radiance vs altitude for balloon flight 25 June 1968. (See Table III)

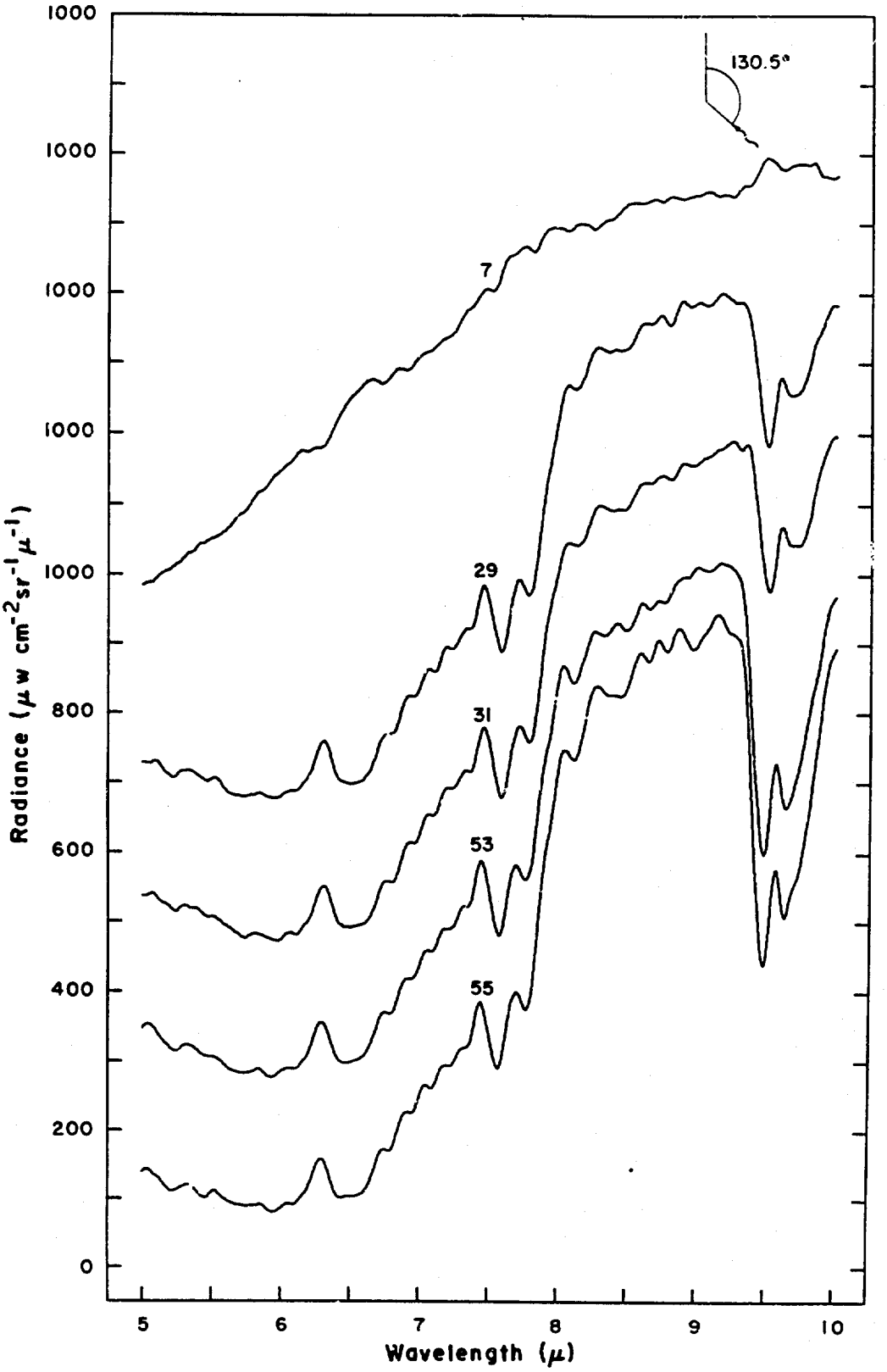

Figure 37 Spectral radiance vs altitude for balloon flight 25 June 1968. (See Table III)

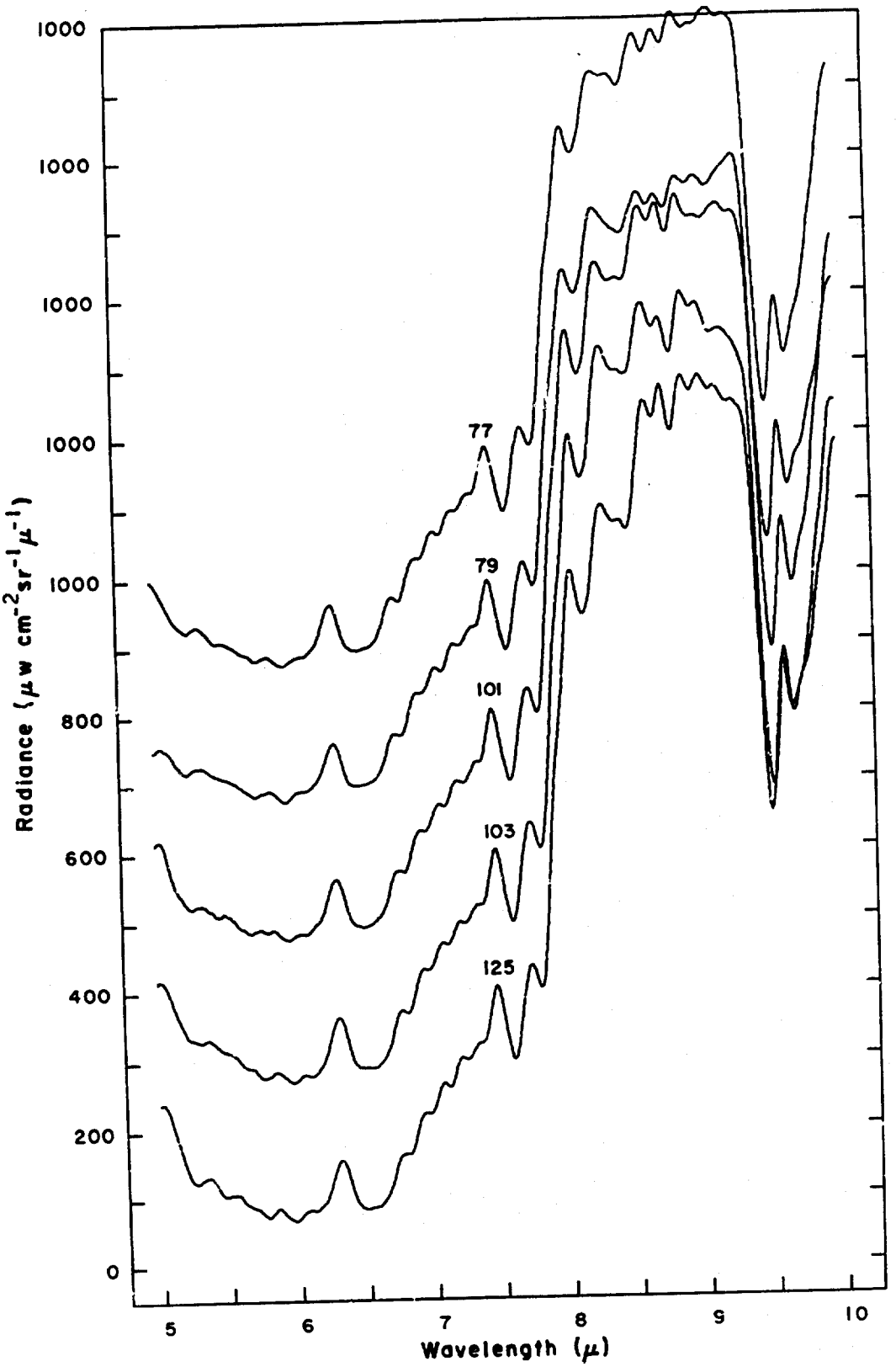

Figure 38 Spectral radiance vs altitude for balloon flight 25 June 1968. (See Table III)

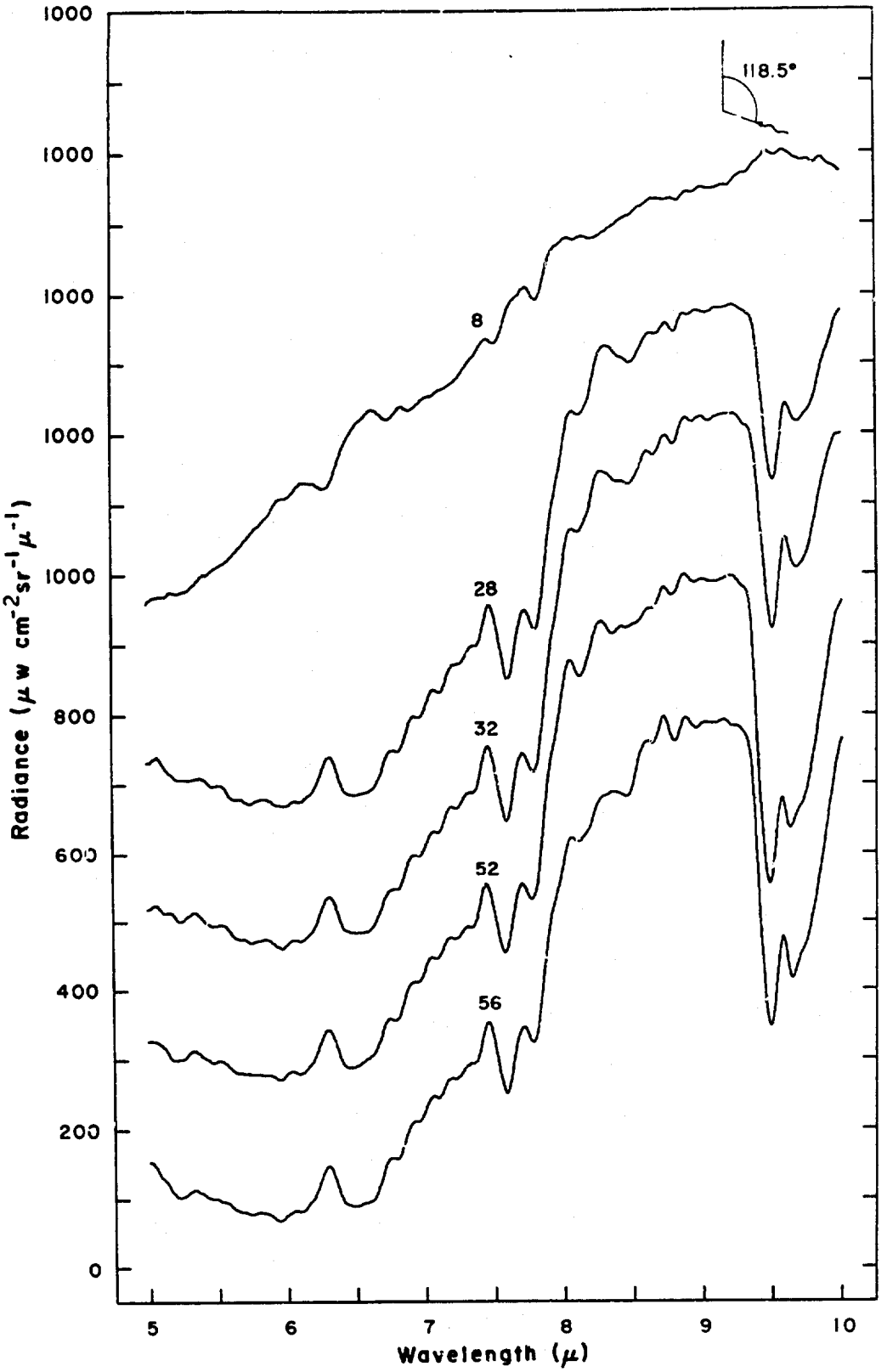

Figure 39 Spectral radiance vs altitude for balloon flight 25 June 1968. (See Table III)

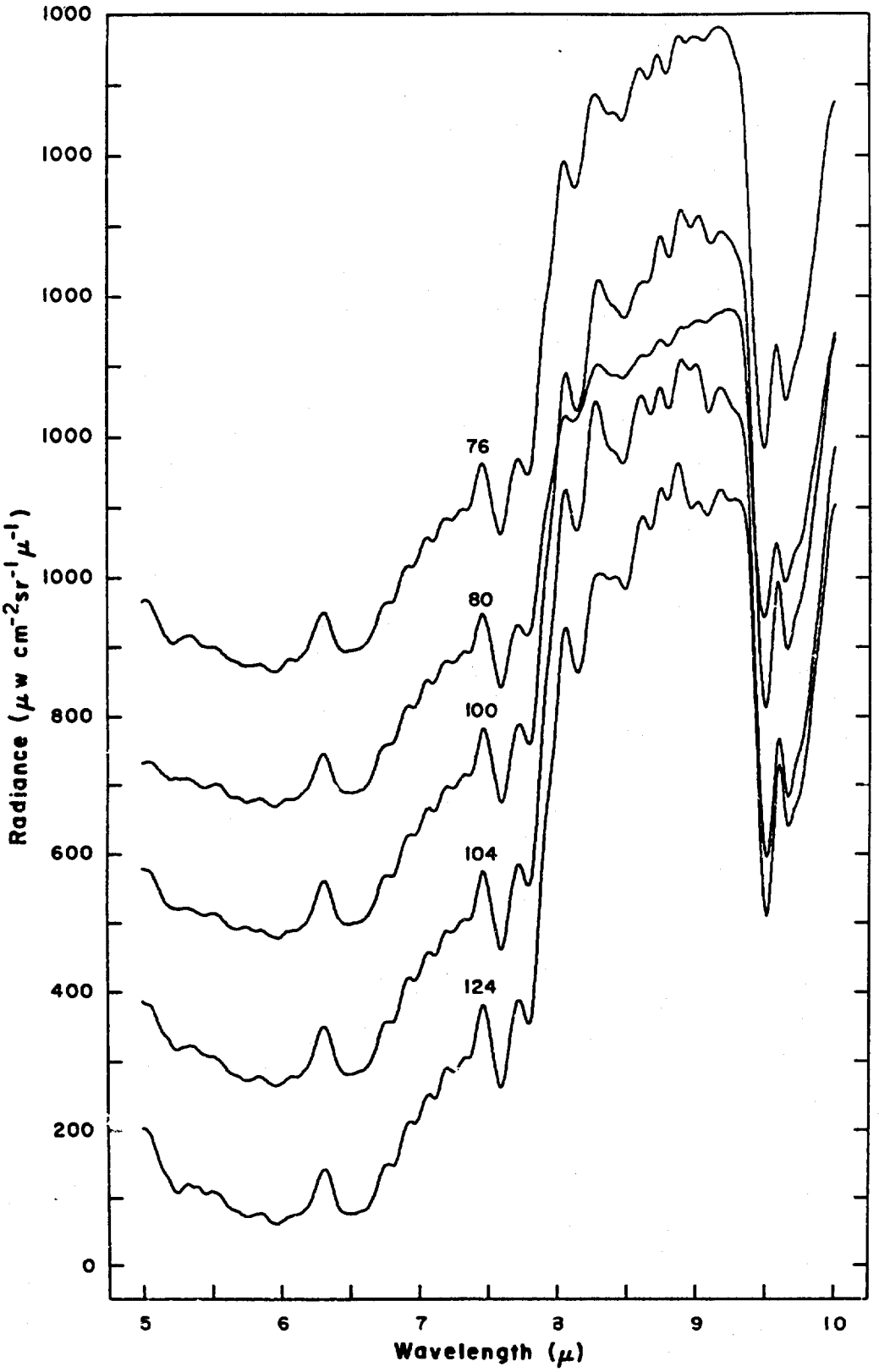

Figure 40 Spectral radiance vs altitude for balloon flight 25 June 1968. (See Table III)

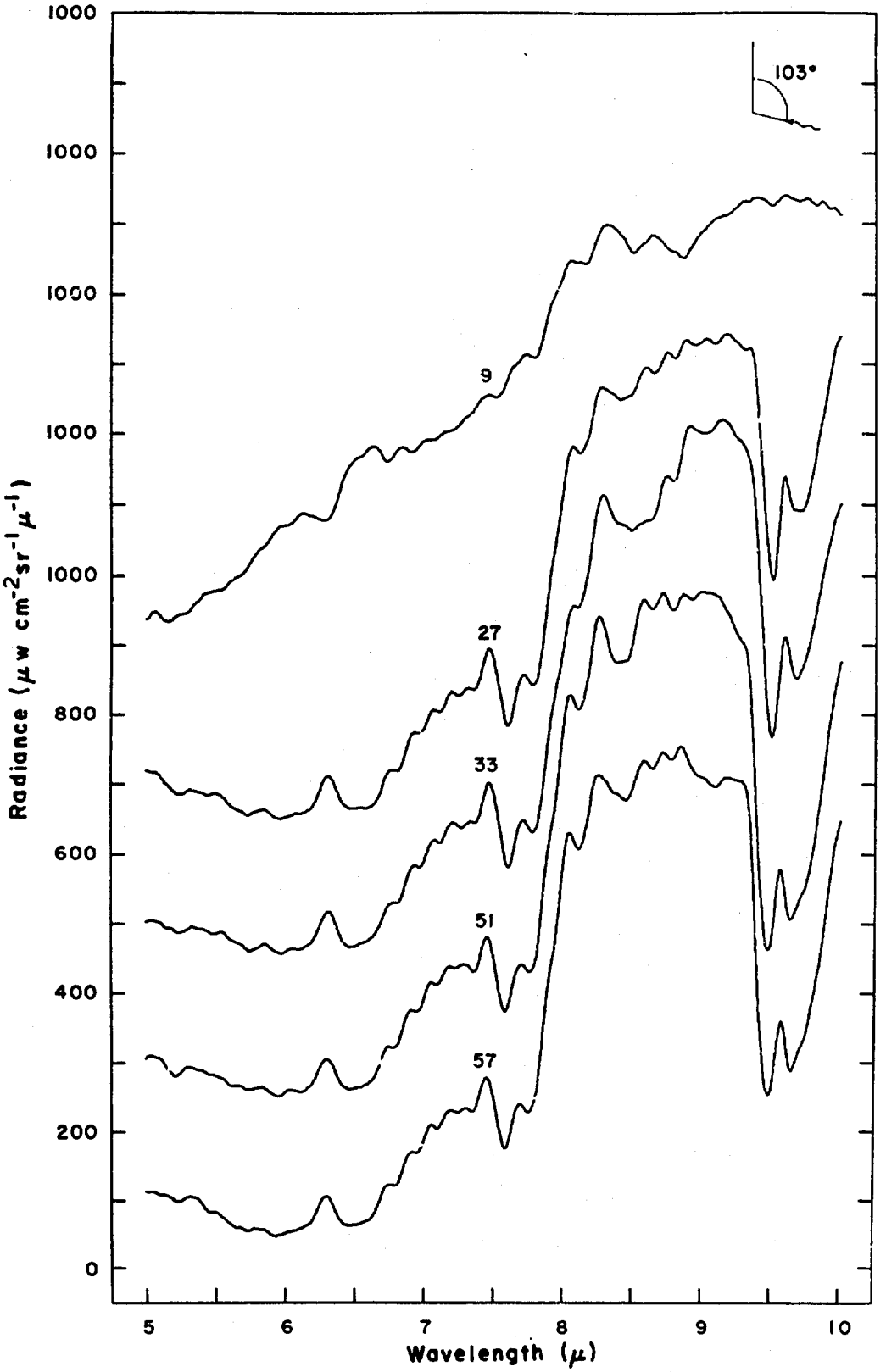

Figure 41 Spectral radiance vs altitude for Moon flight 25 June 1966. (See Table III)

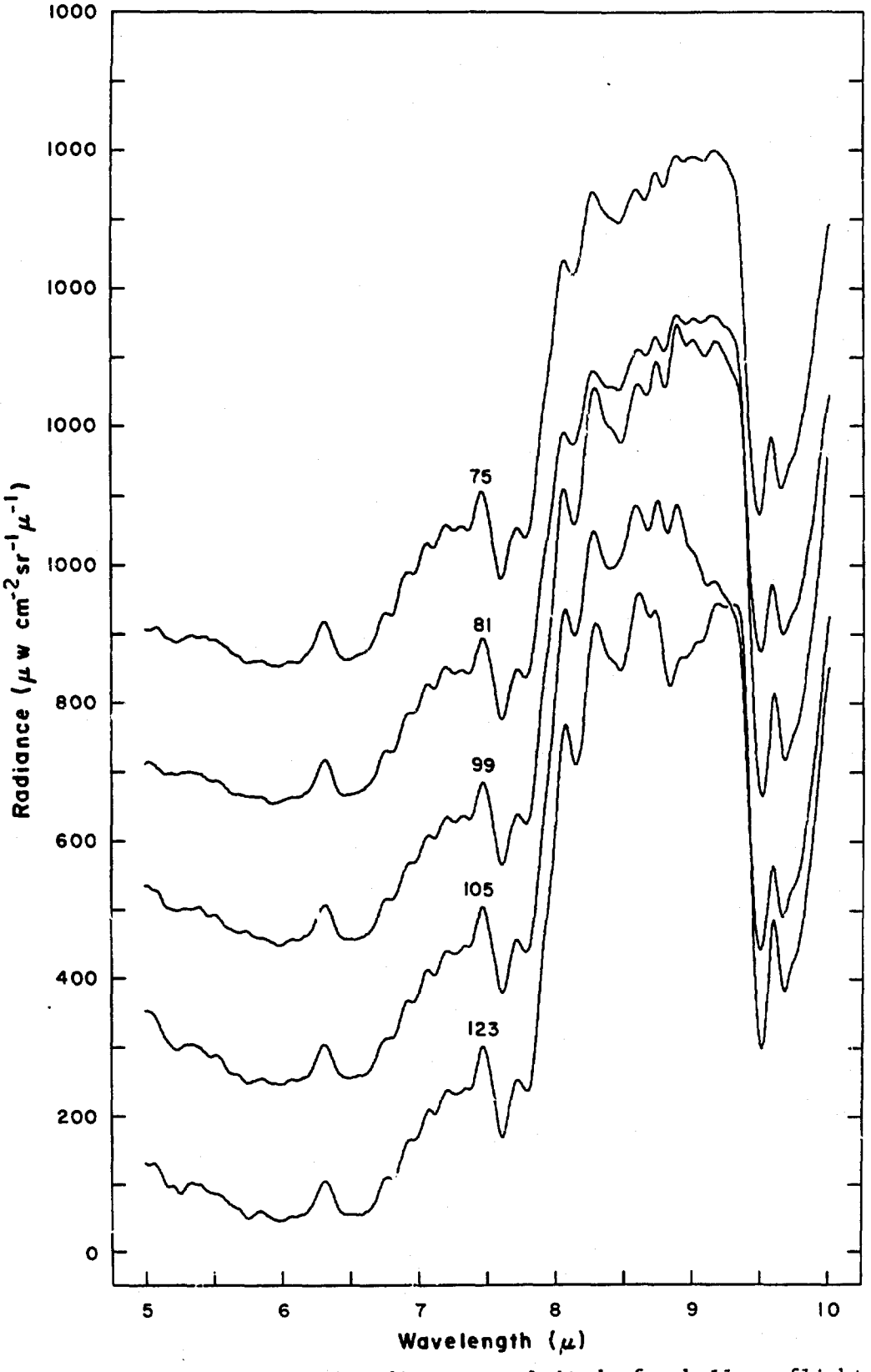

Figure 42 Spectral radiance vs altitude for balloon flight 25 June 1968. (See Table III)

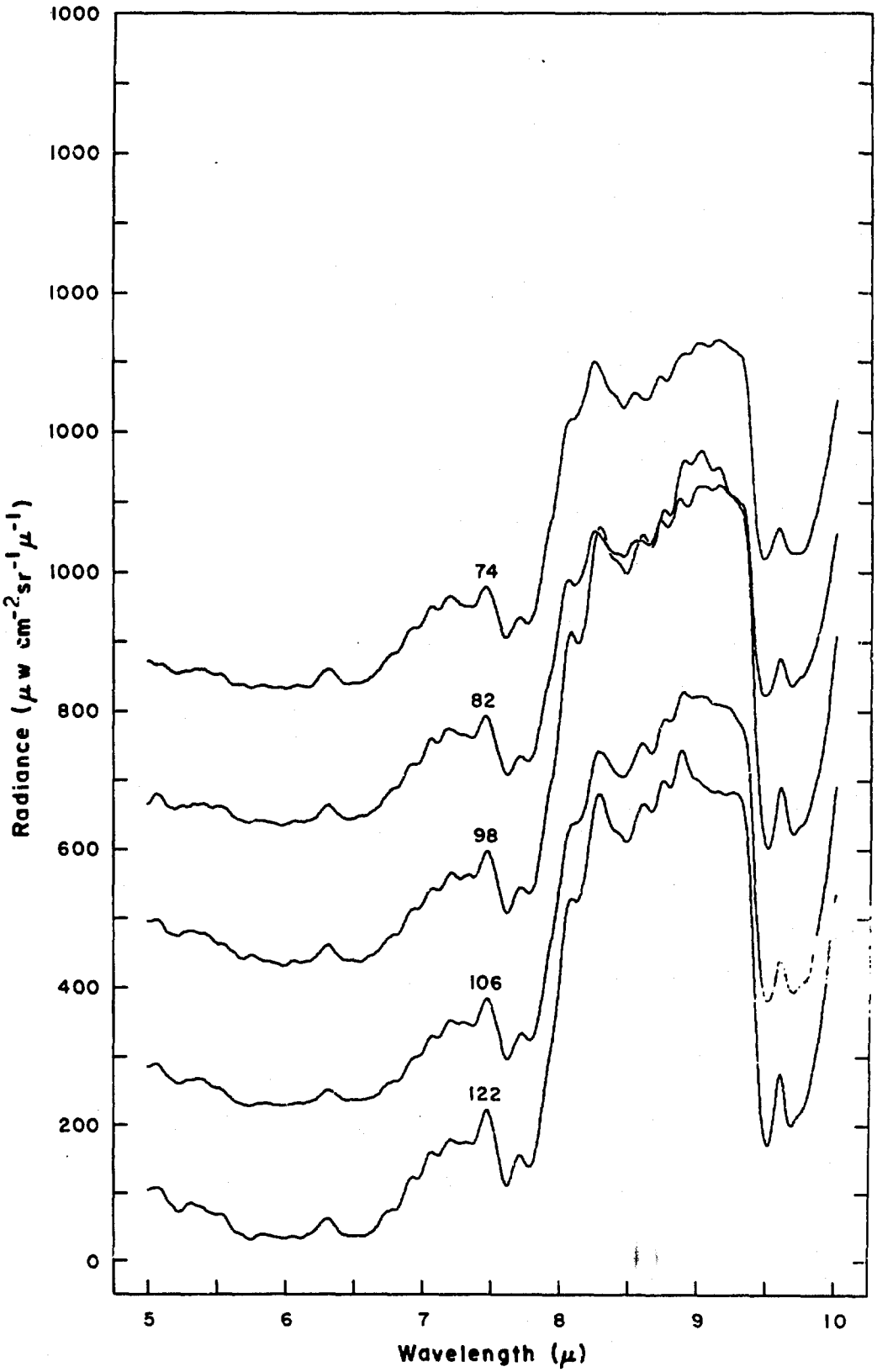

Figure 44 Spectral radiance vs altitude for balloon flight 25 June 1968. (See Table III.)

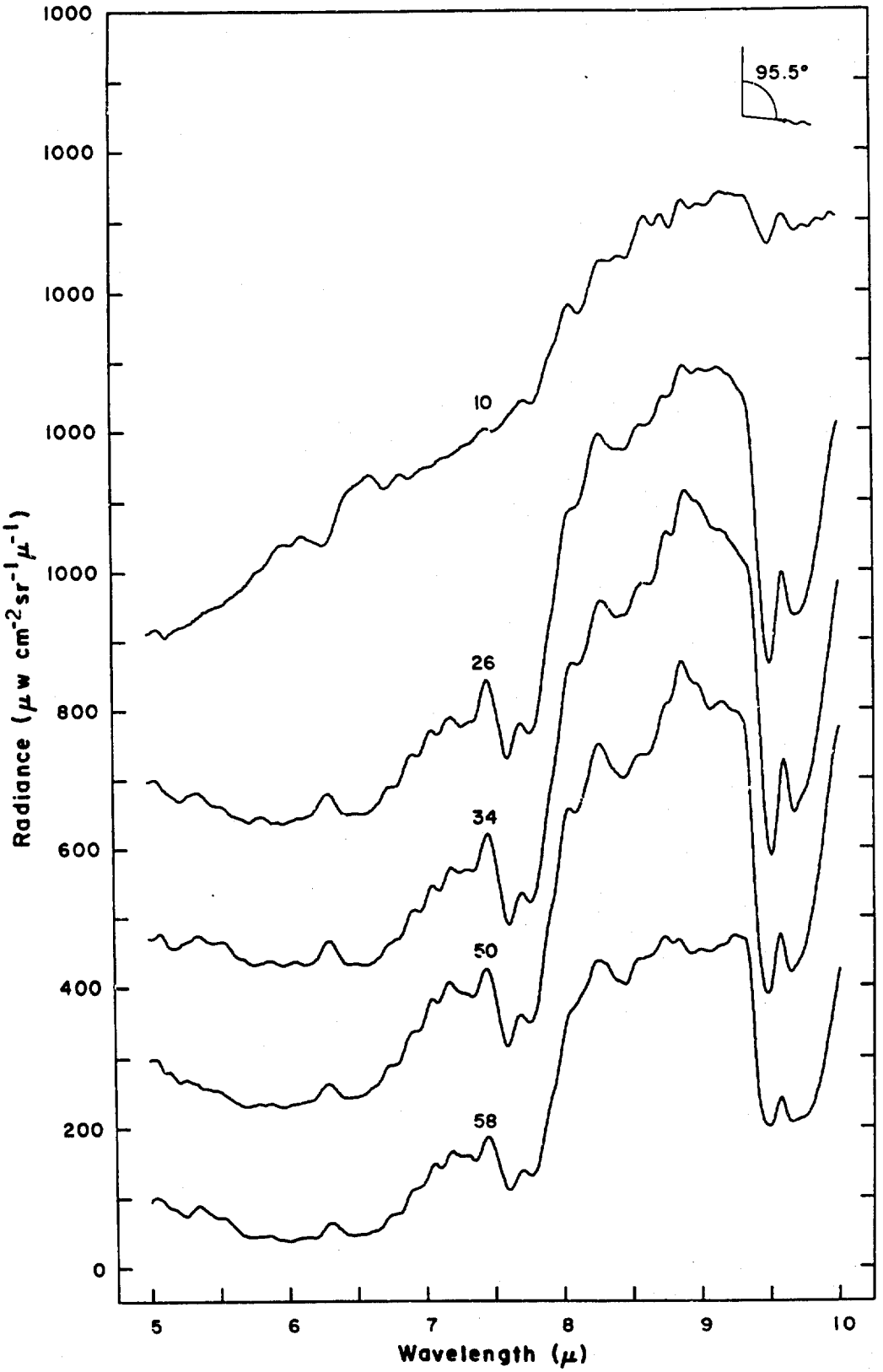

Figure 43 Spectral radiance vs altitude for balloon flight 25 June 1968. (See Table III)

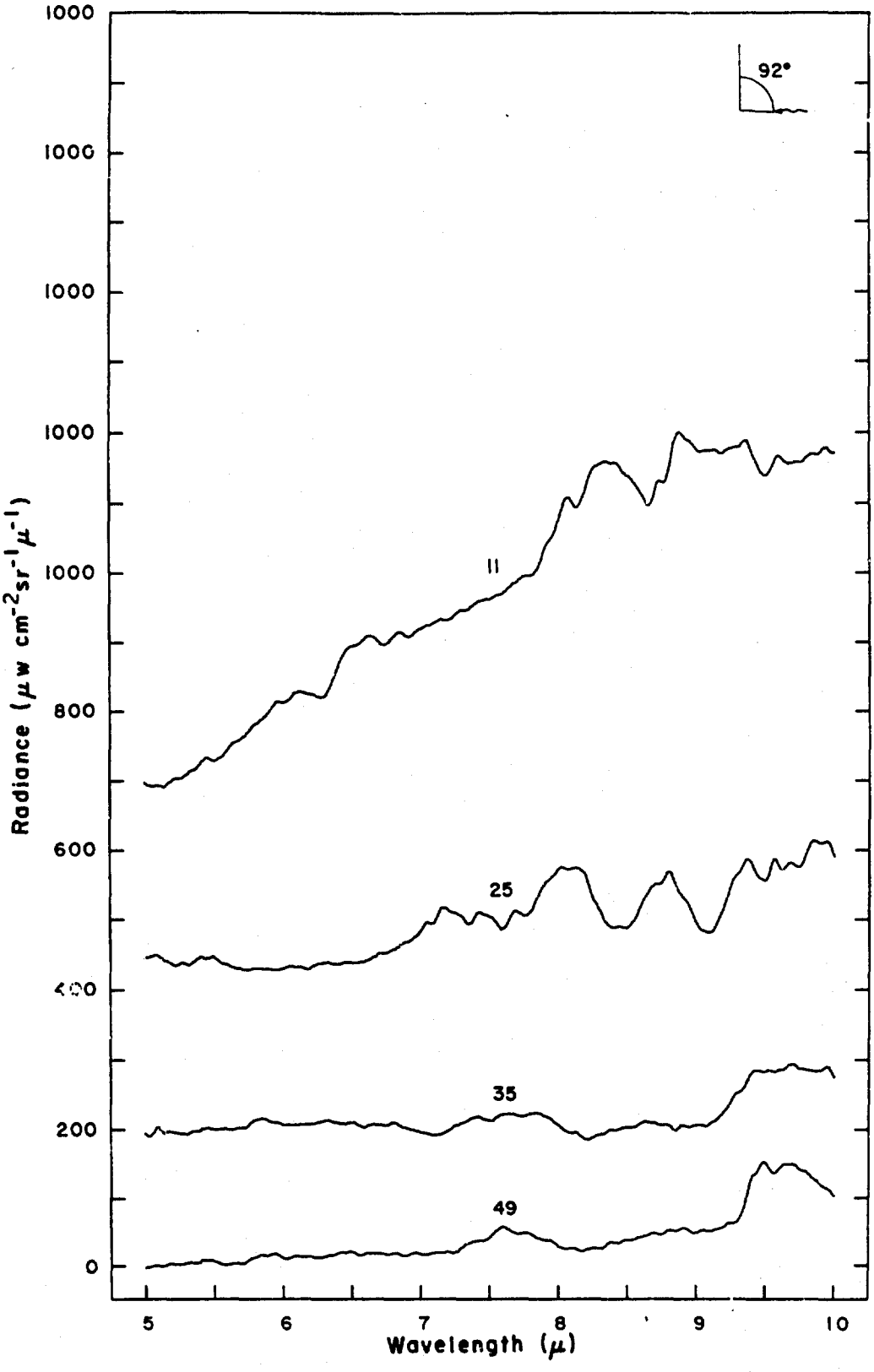

Figure 45 Spectral radiance vs altitude for balloon flight 25 June 1968. (See Table III)

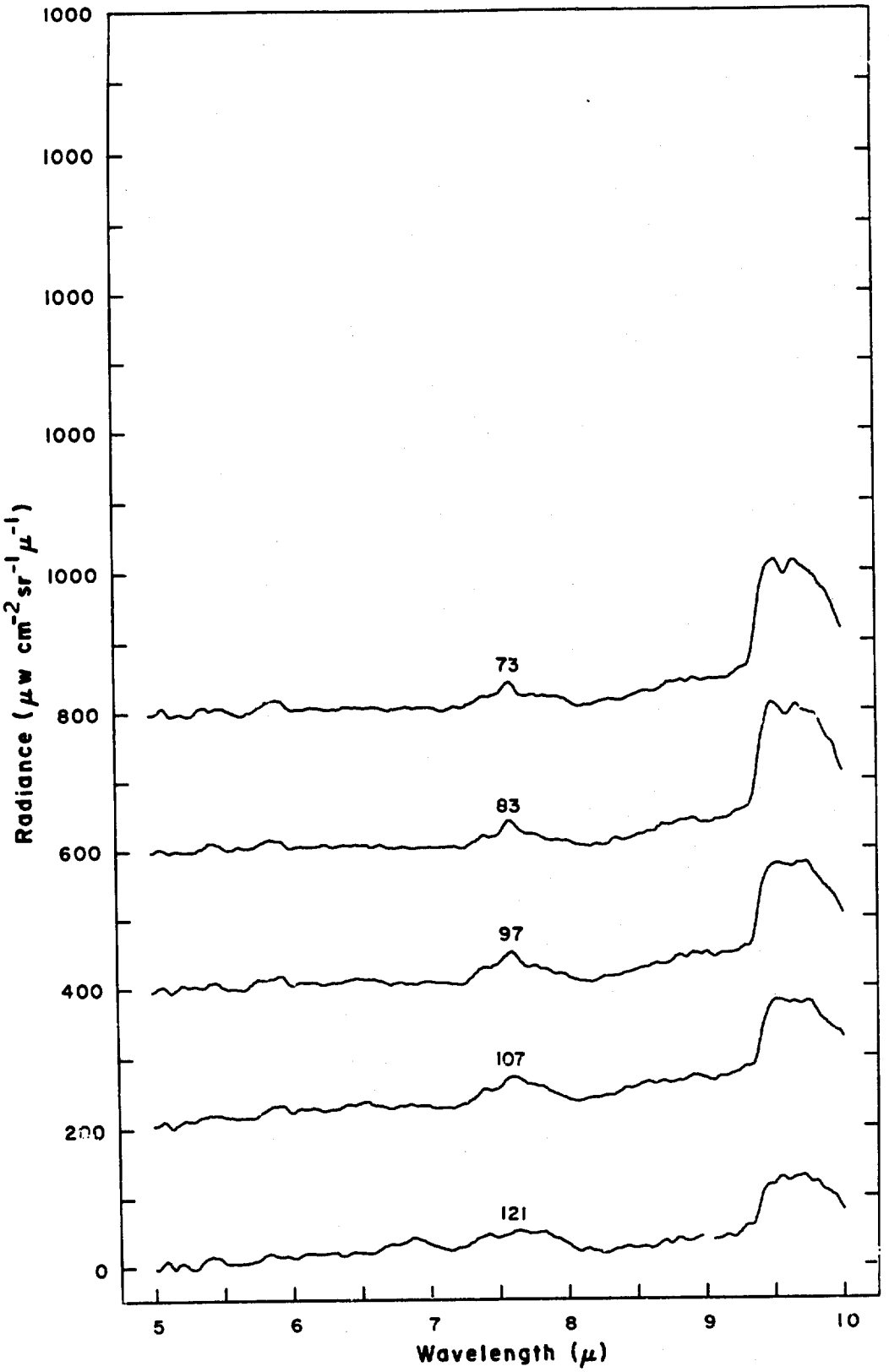

Figure 46 Spectral radiance vs altitude for balloon flight 25 June 1968. (See Table III)

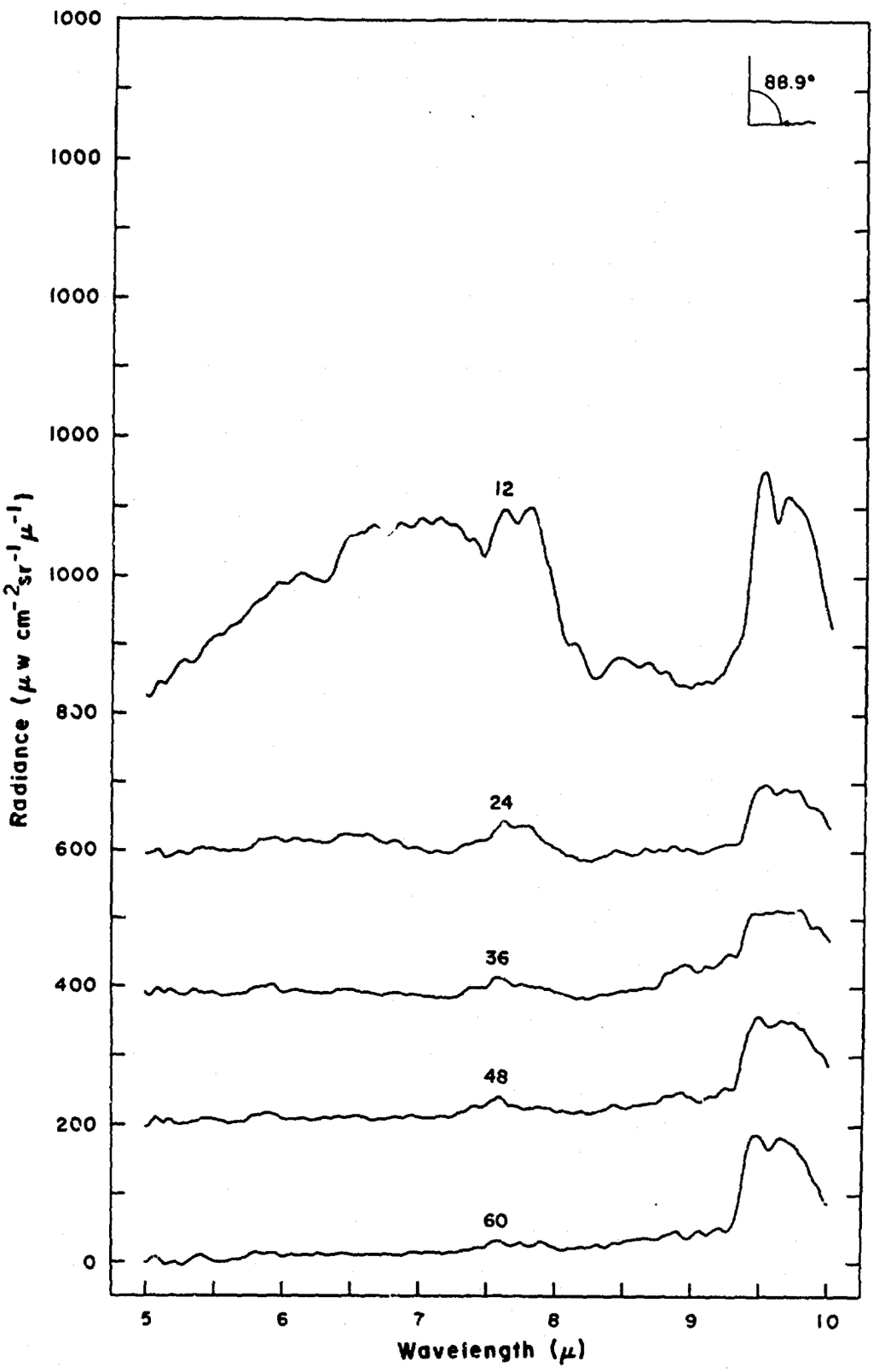

Figure 47 Spectral radiance vs altitude for balloon flight 25 June 1968. (See Table III)

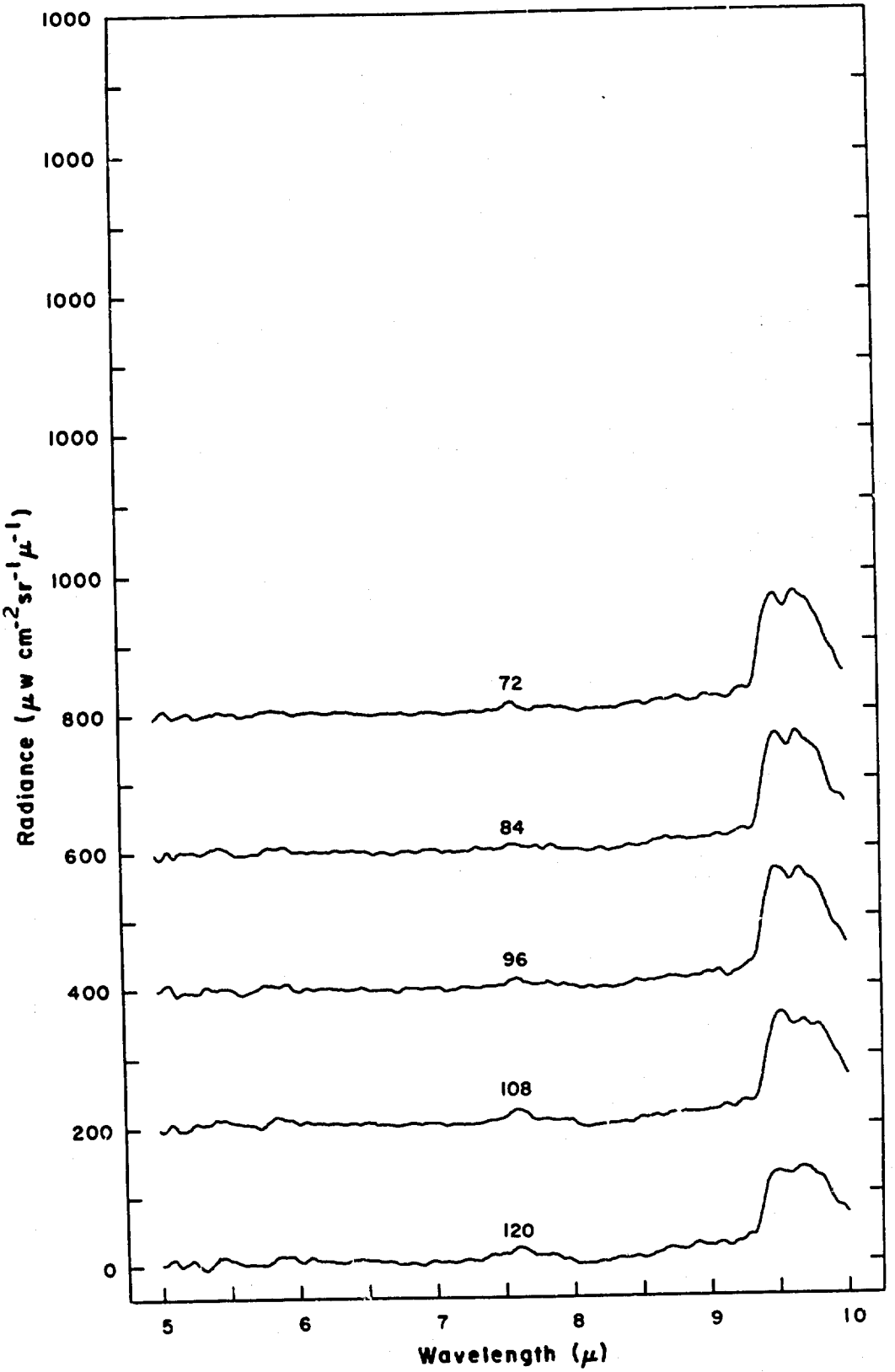

Figure 48 Spectral radiance vs altitude for balloon flight 25 June 1968. (See Table III)

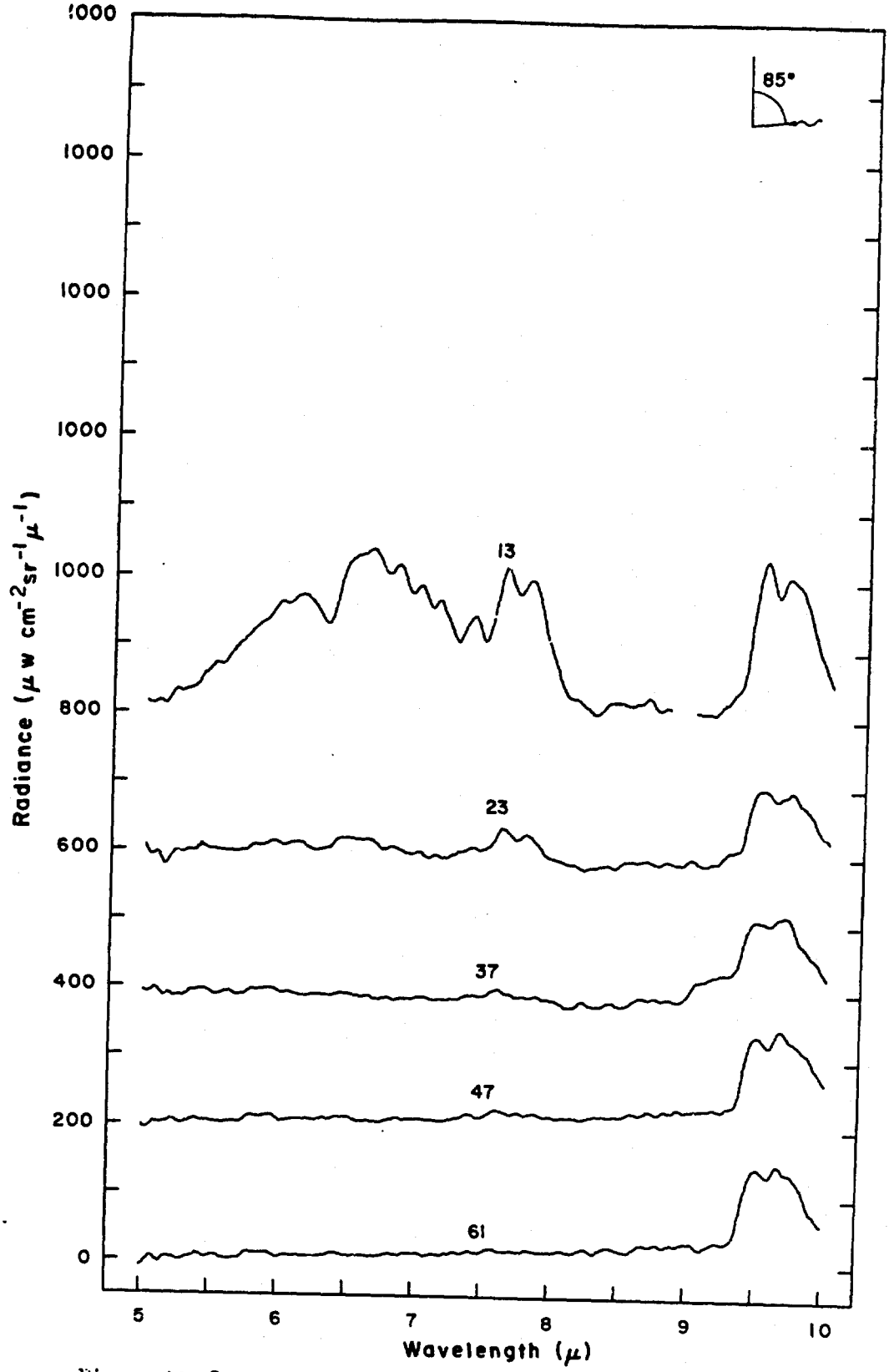

Figure 49 Spectral radiance vs altitude for balloon flight 25 June 1968. (See Table III)

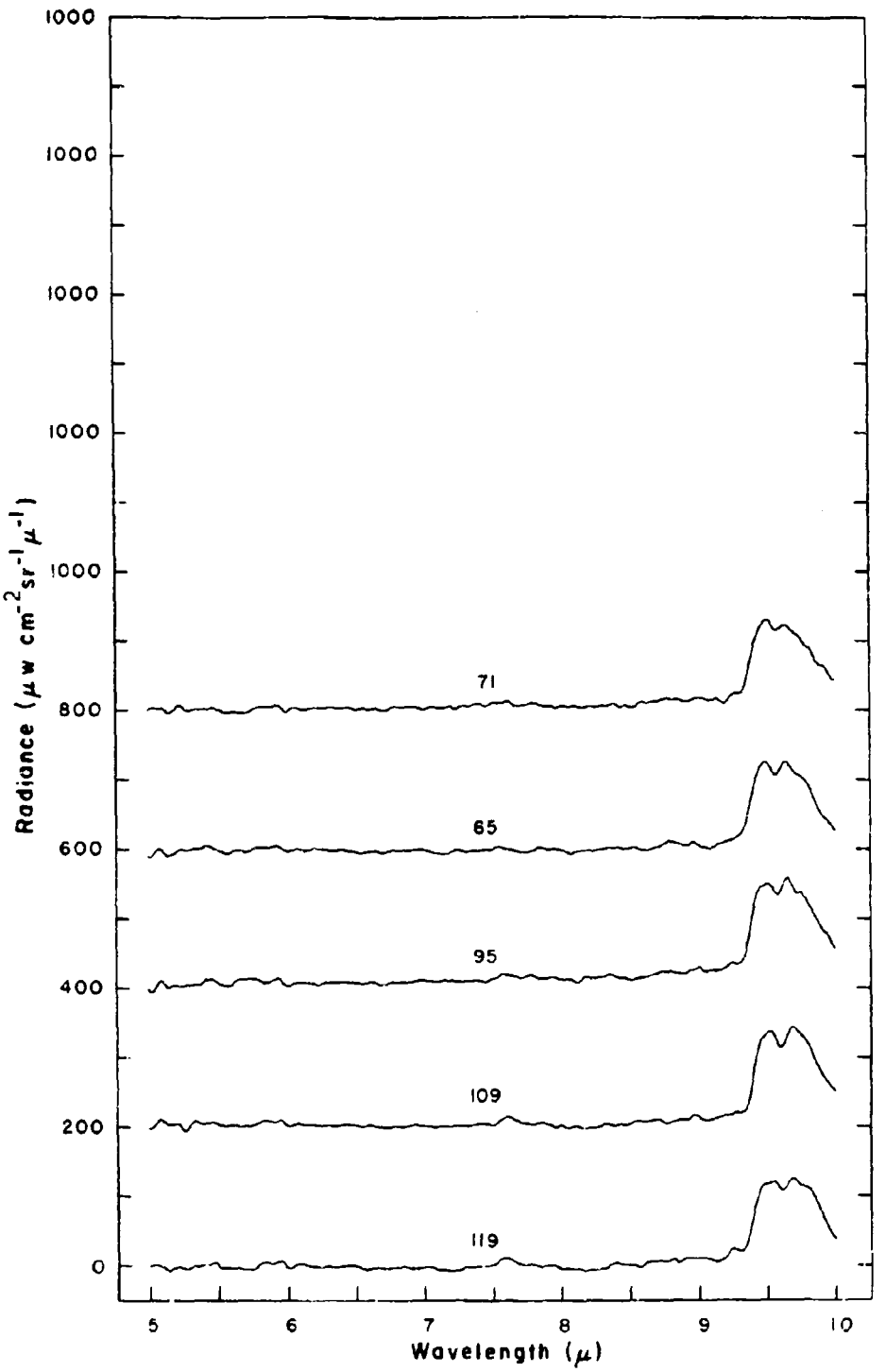

Figure 50 Spectral radiance vs altitude for balloon flight 25 June 19[illegible]. (See Table III)

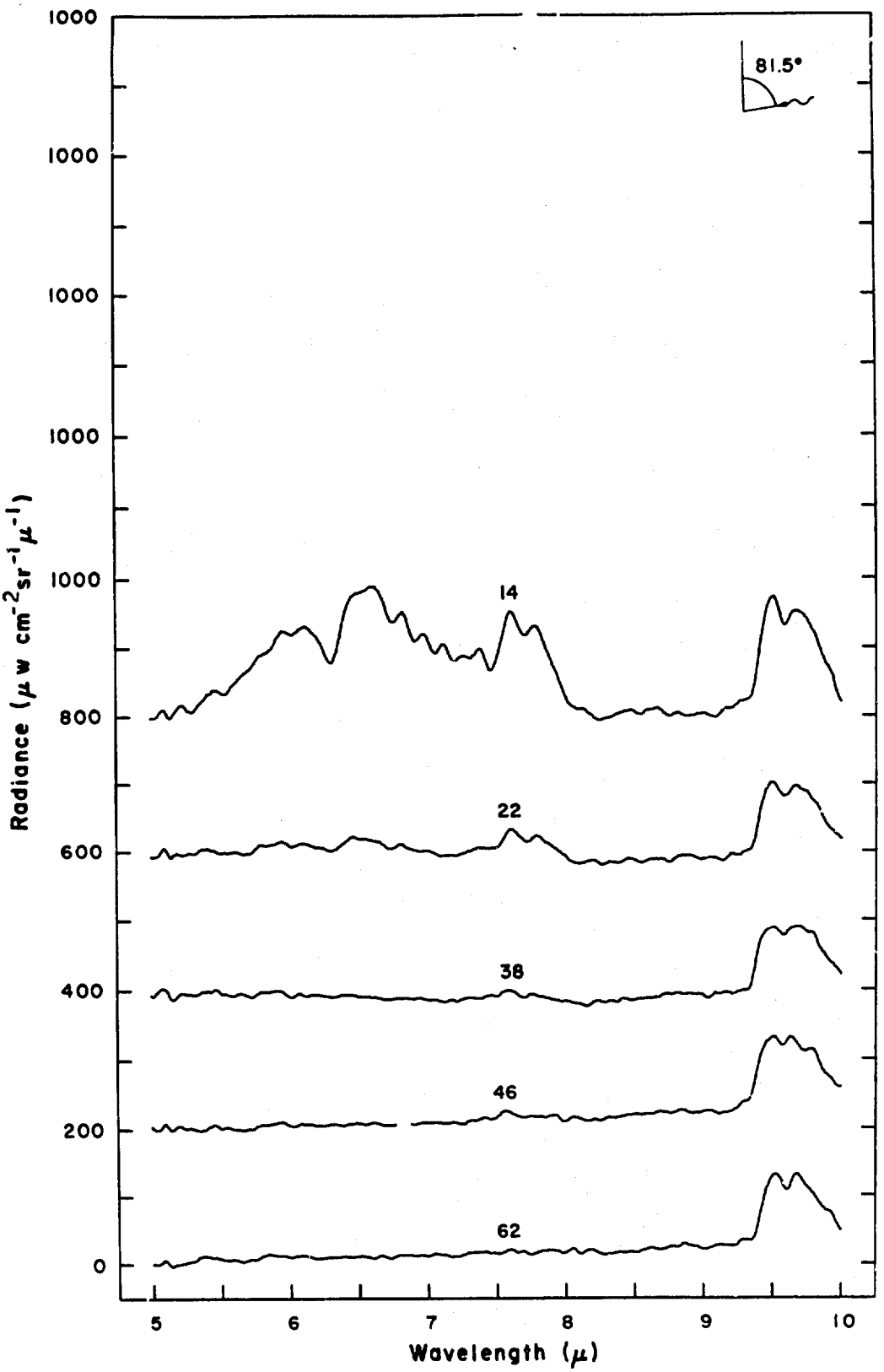

Figure 51 Spectral radiance vs altitude for balloon flight 25 June 1968. (See Table III)

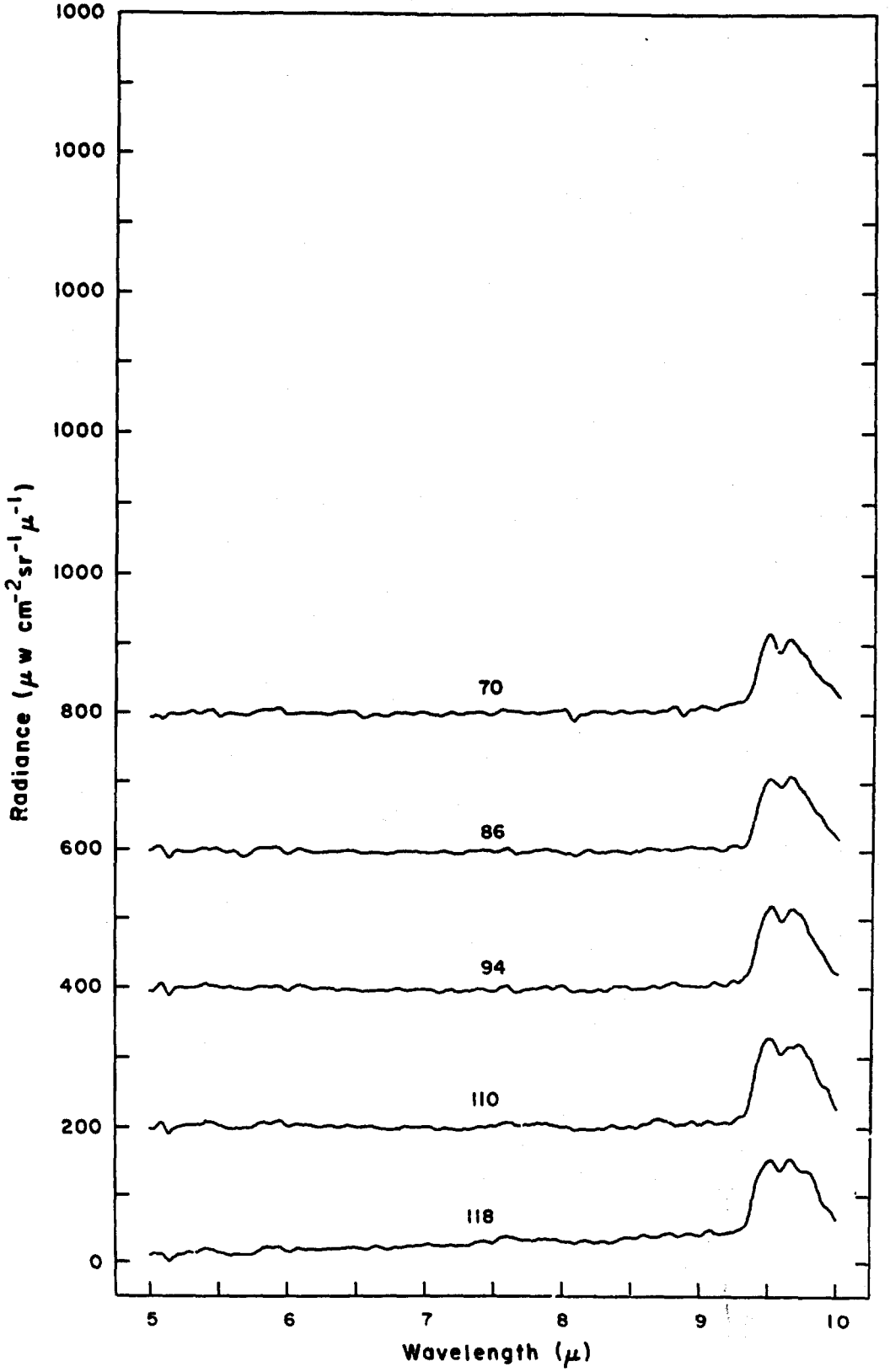

Figure 52 Spectral radiance vs altitude for balloon flight, 25 June 1968. (See Table III)

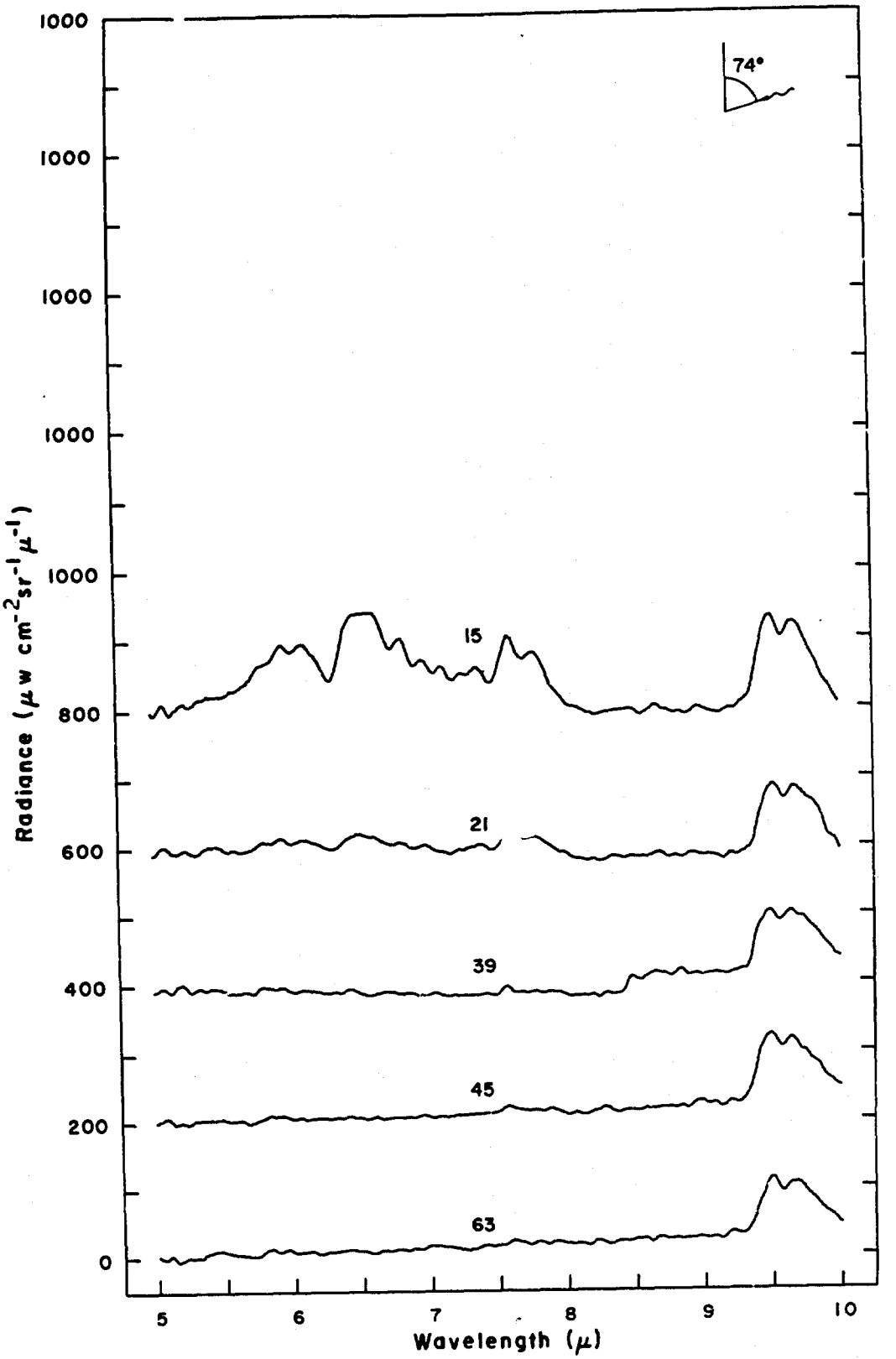

Figure 53 Spectral radiance vs altitude for balloon flight 25 June 1968. (See Table III)

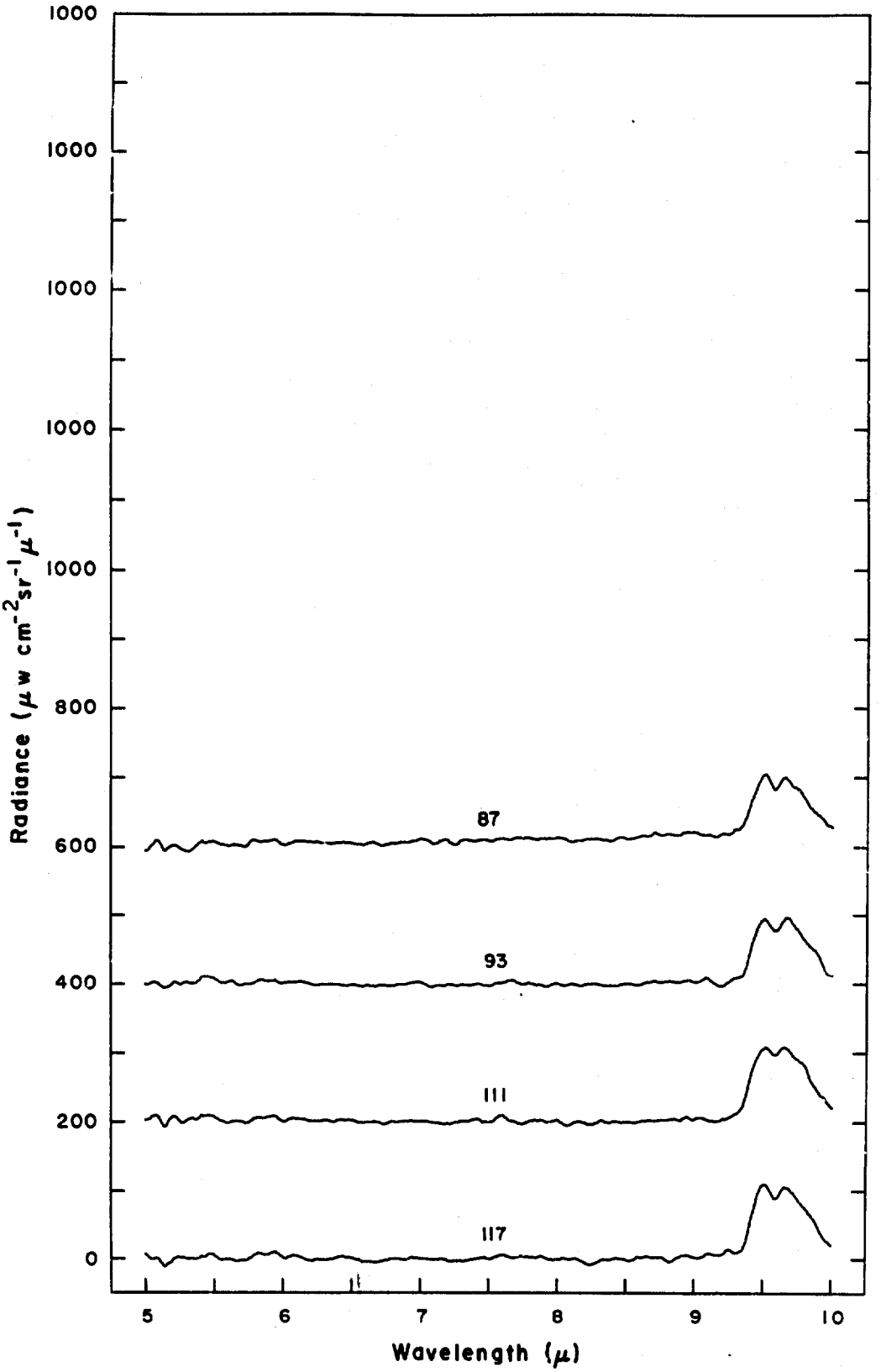

Figure 54 Spectral radiance vs altitude for balloon flight 25 June 1968. (See Table III)

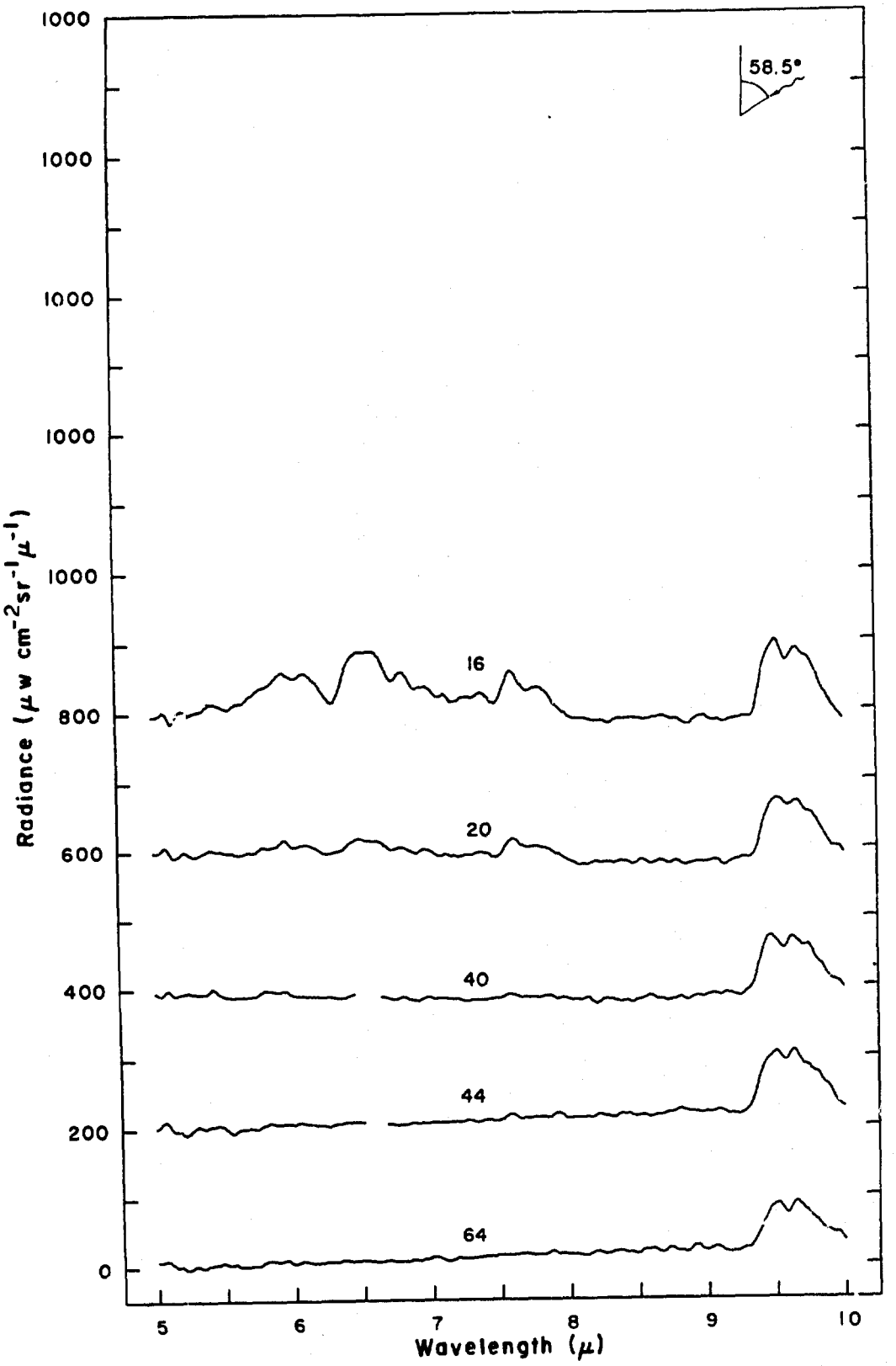

Figure 55 Spectral radiance vs altitude for balloon flight 25 June 1968. (See Table III)

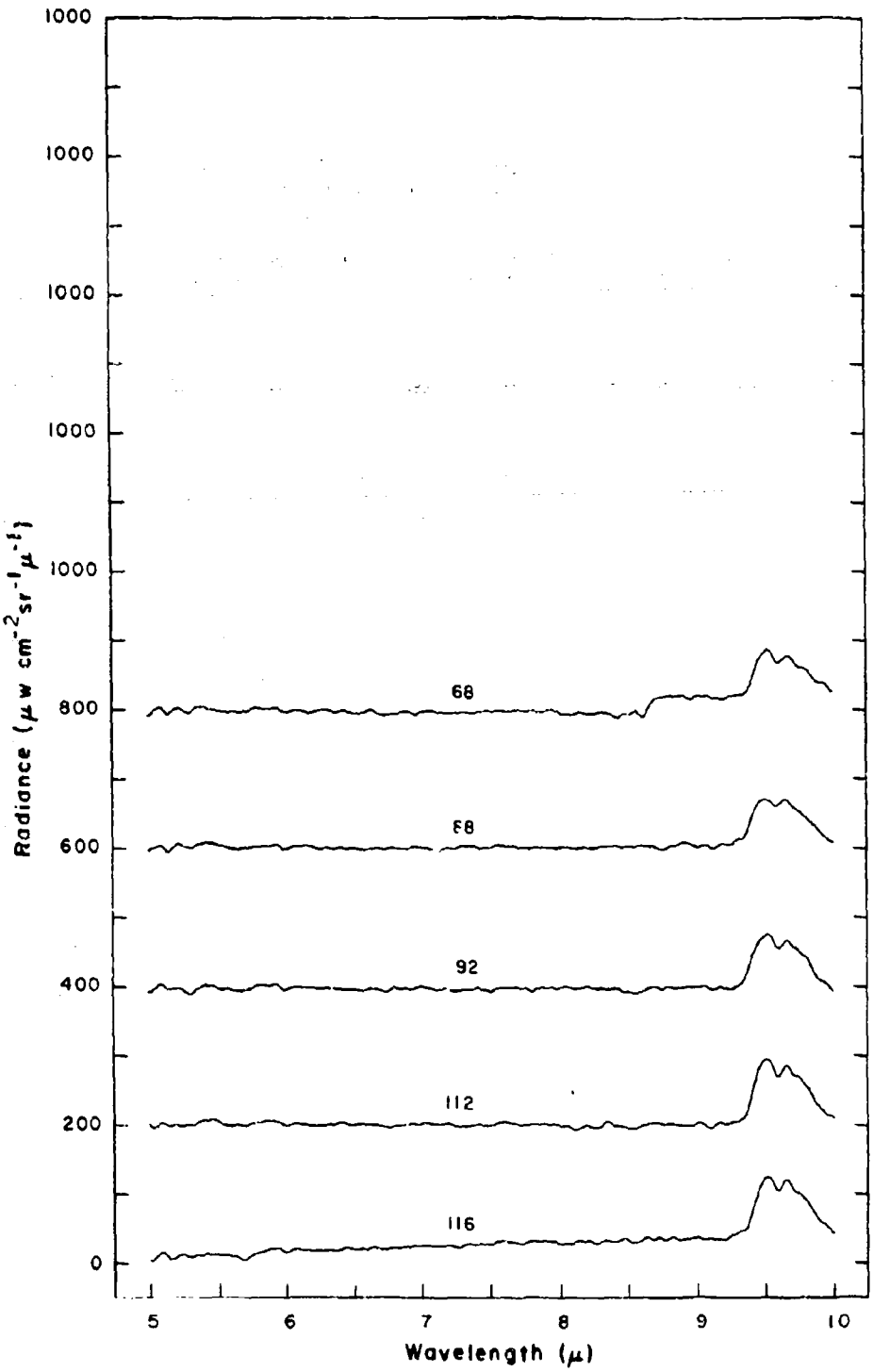

Figure 56 Spectral radiance vs altitude for balloon flight 25 June 1968. (See Table III)

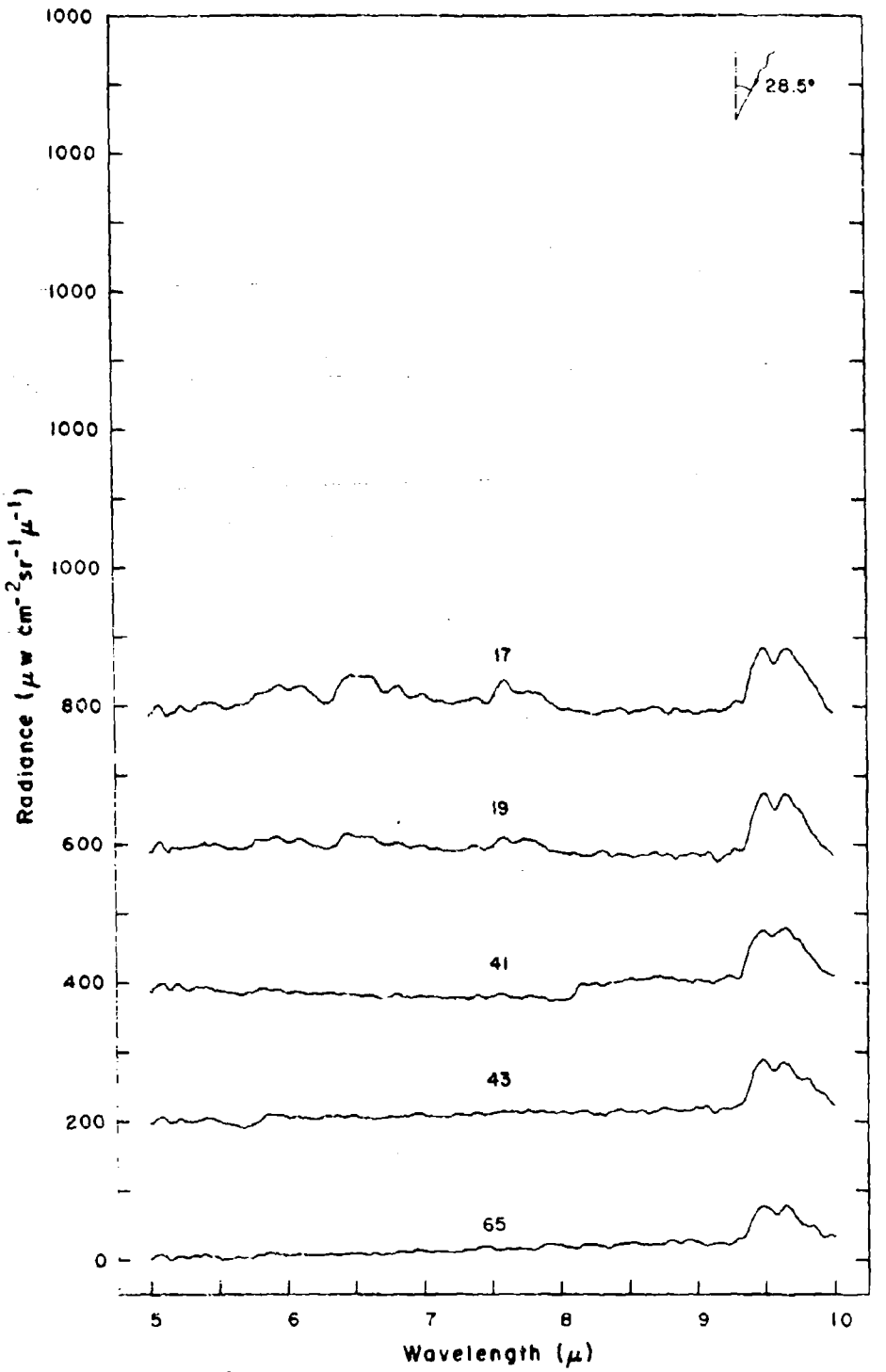

Figure 57 Spectral radiance vs altitude for balloon flight 25 June 1968. (See Table III)

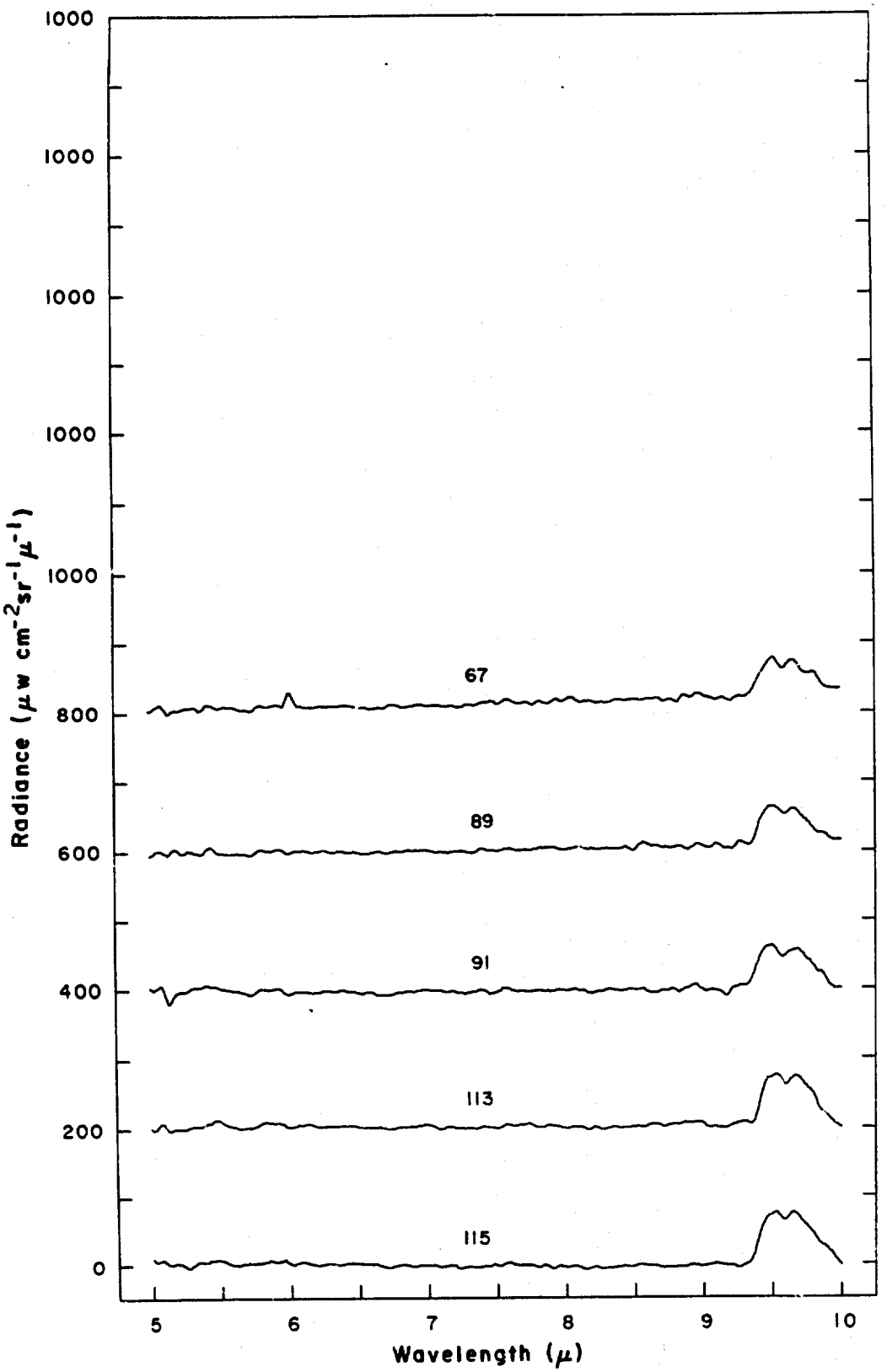

Figure 58 Spectral radiance vs altitude for balloon flight 25 June 1968. (See Table III)

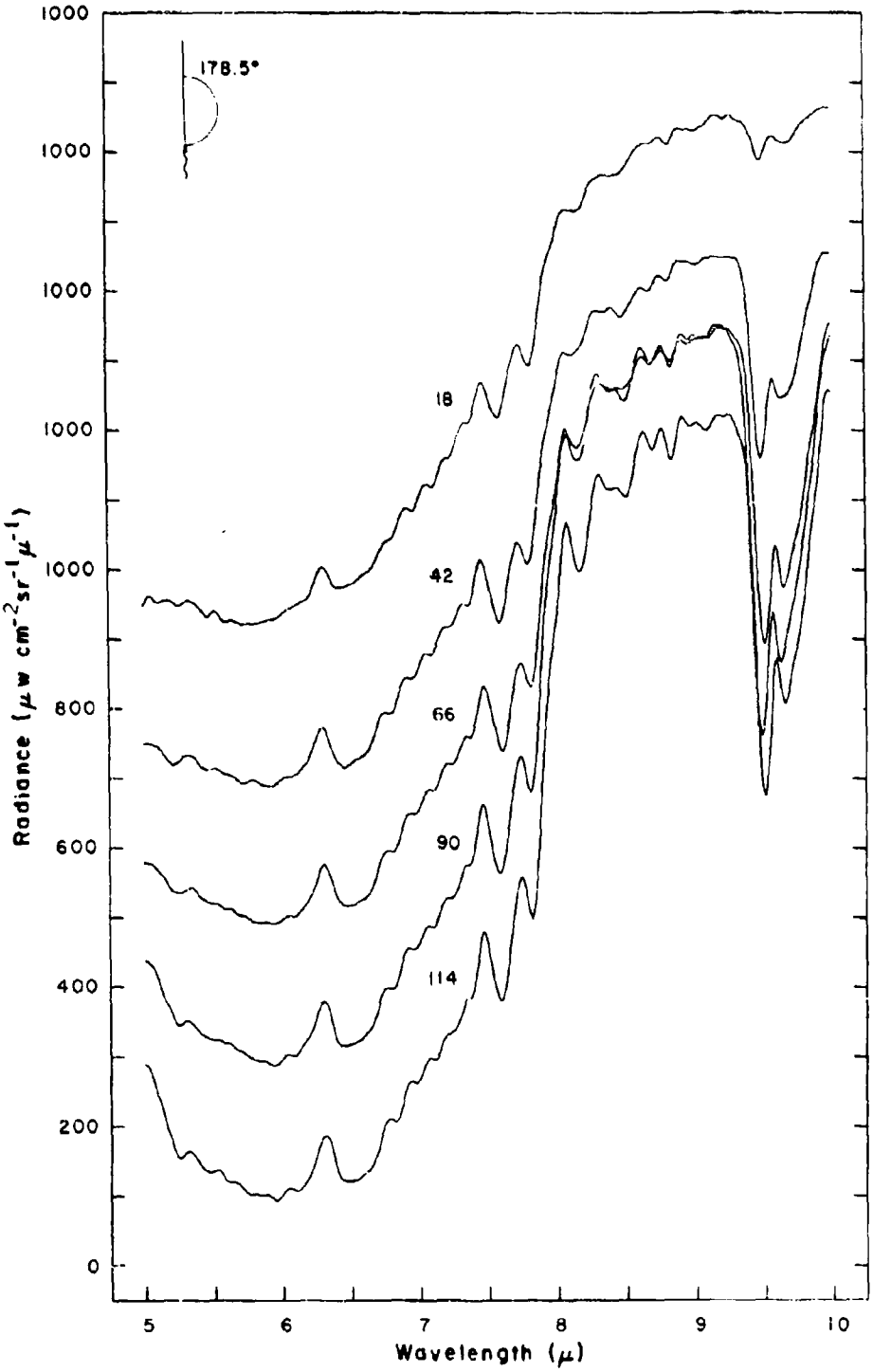

Figure 59 Spectral radiance vs altitude for balloon flight 25 June 1968. (See Table III)

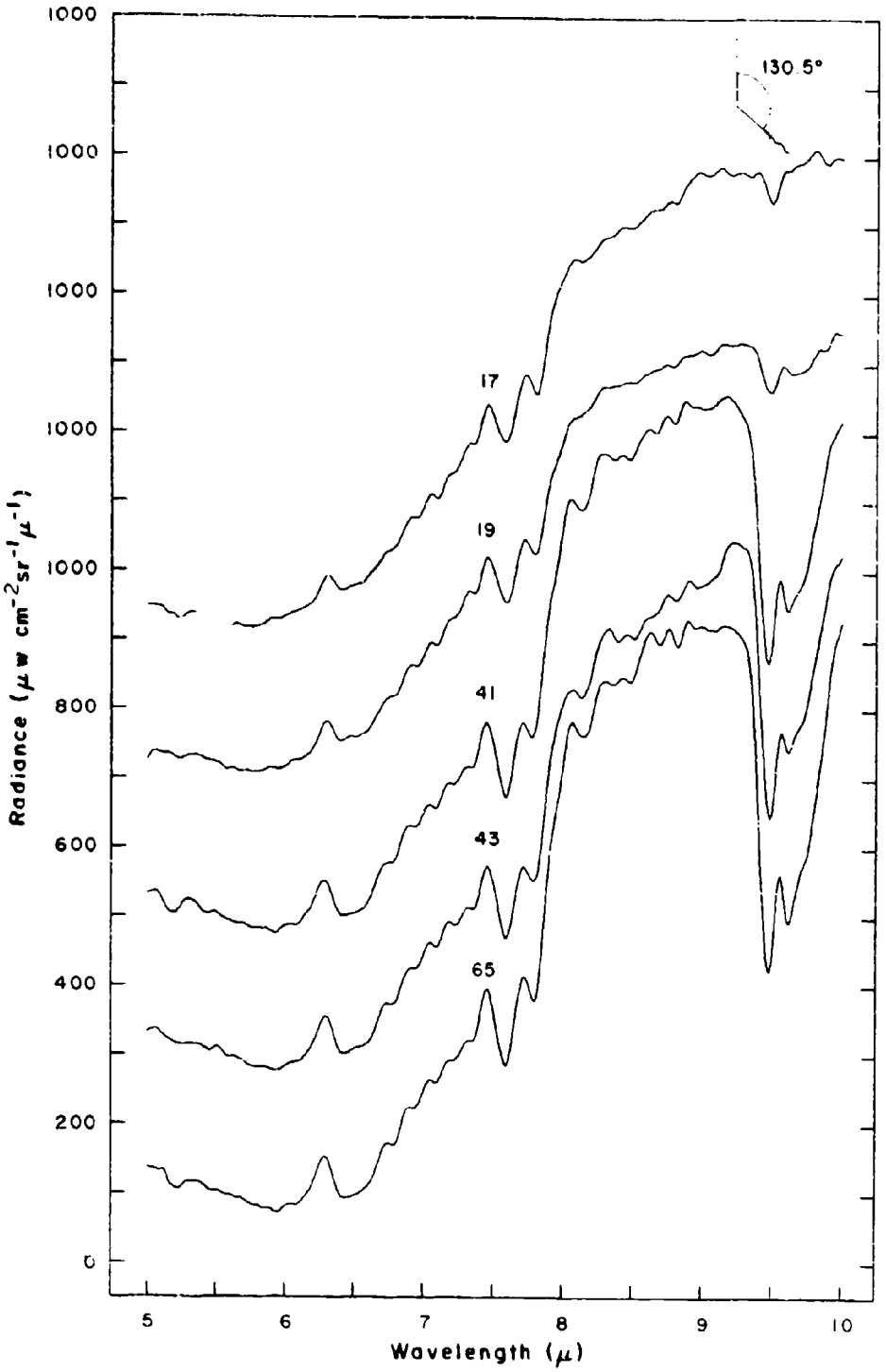

Figure 60 Spectral radiance vs altitude for balloon flight 25 June 1968. (See Table III)

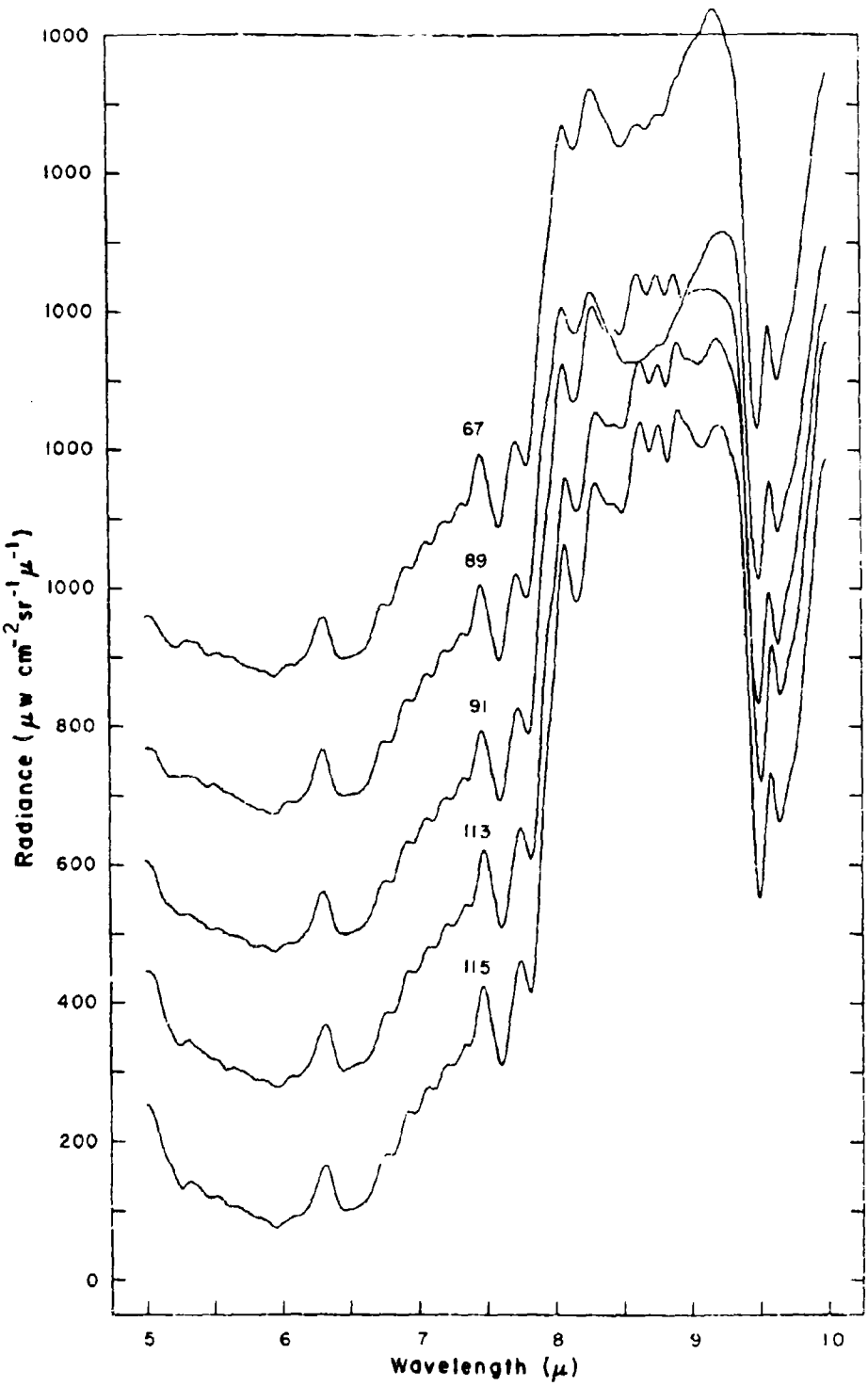

Figure 61 Spectral radiance vs. altitude for balloon flight
25 June 1968. (See Table III)

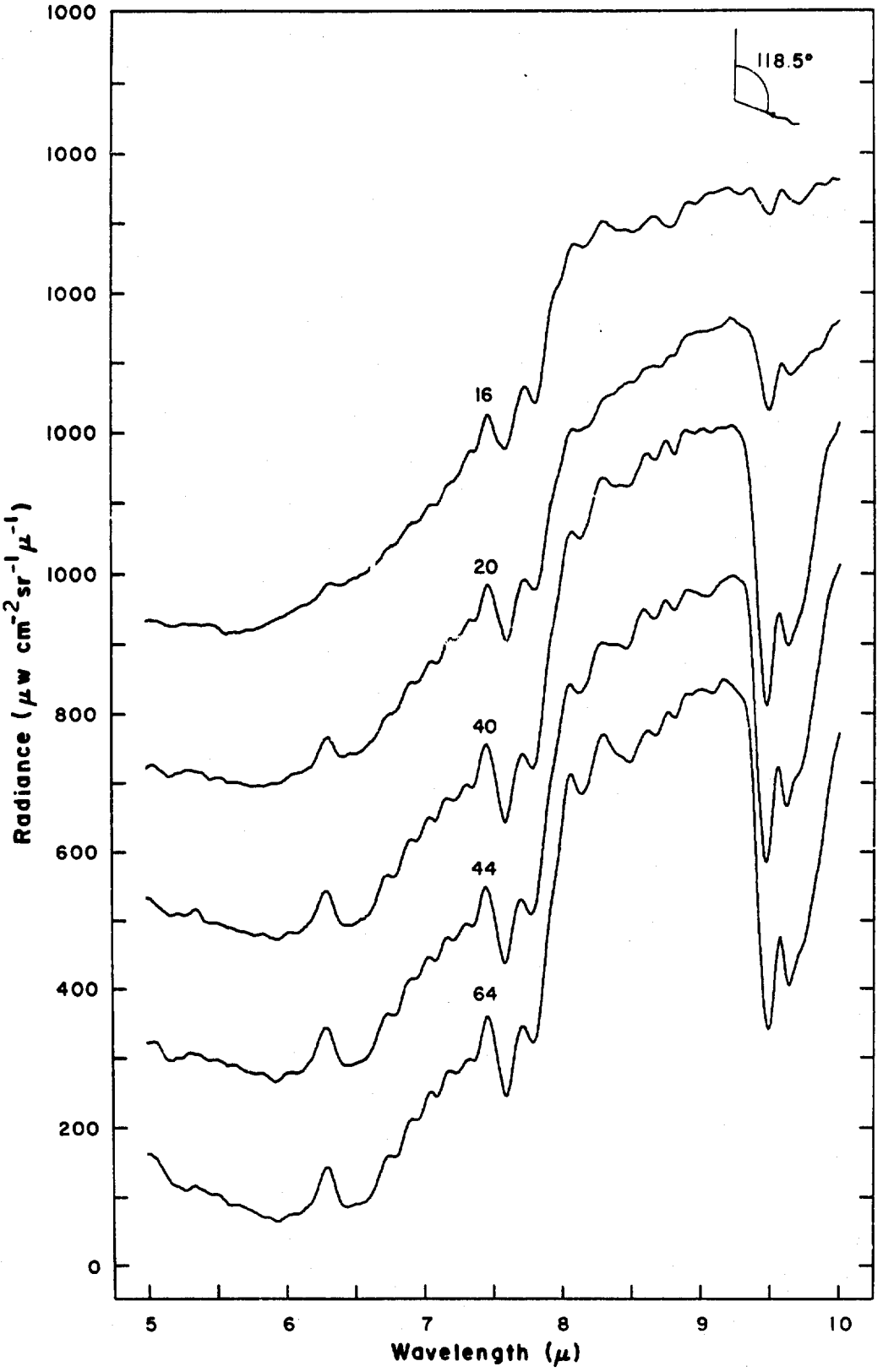

Figure 62 Spectral radiance vs altitude for balloon flight 25 June 1968. (See Table III)

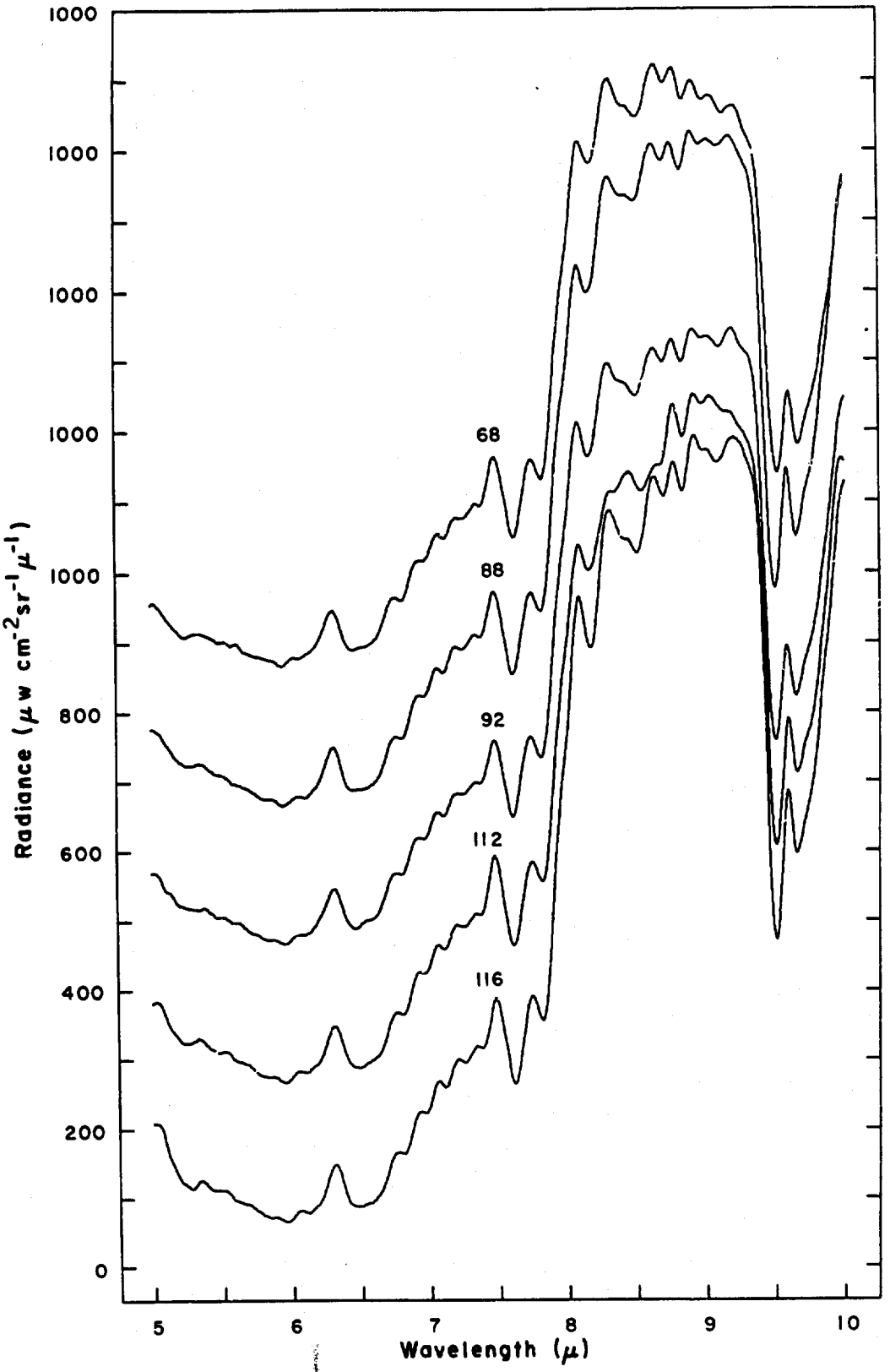

Figure 63 Spectral radiance vs altitude for balloon flight 25 June 1968. (See Table III)

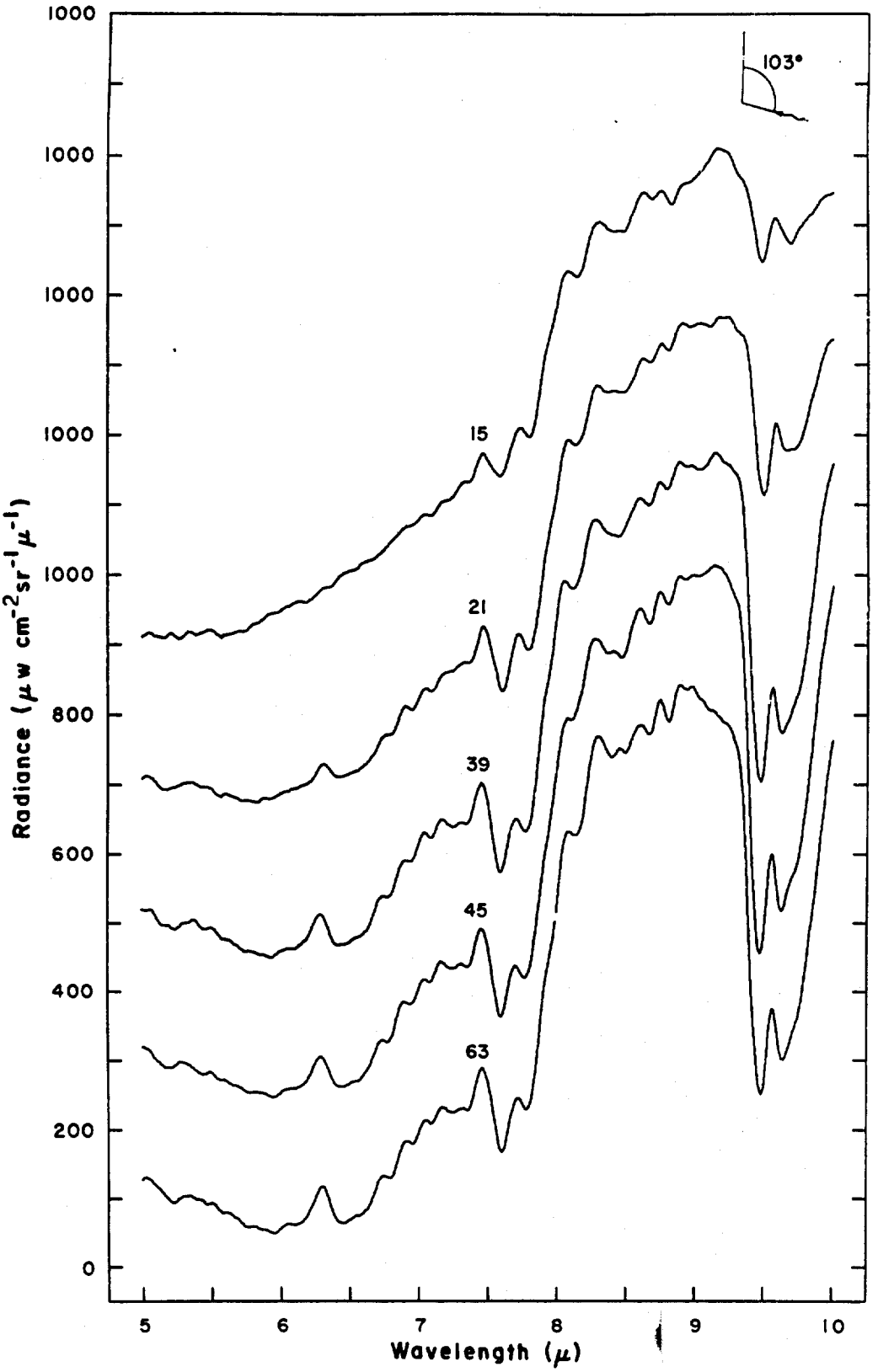

Figure 64 Spectral radiance vs altitude for balloon flight 25 June 1968. (See Table III)

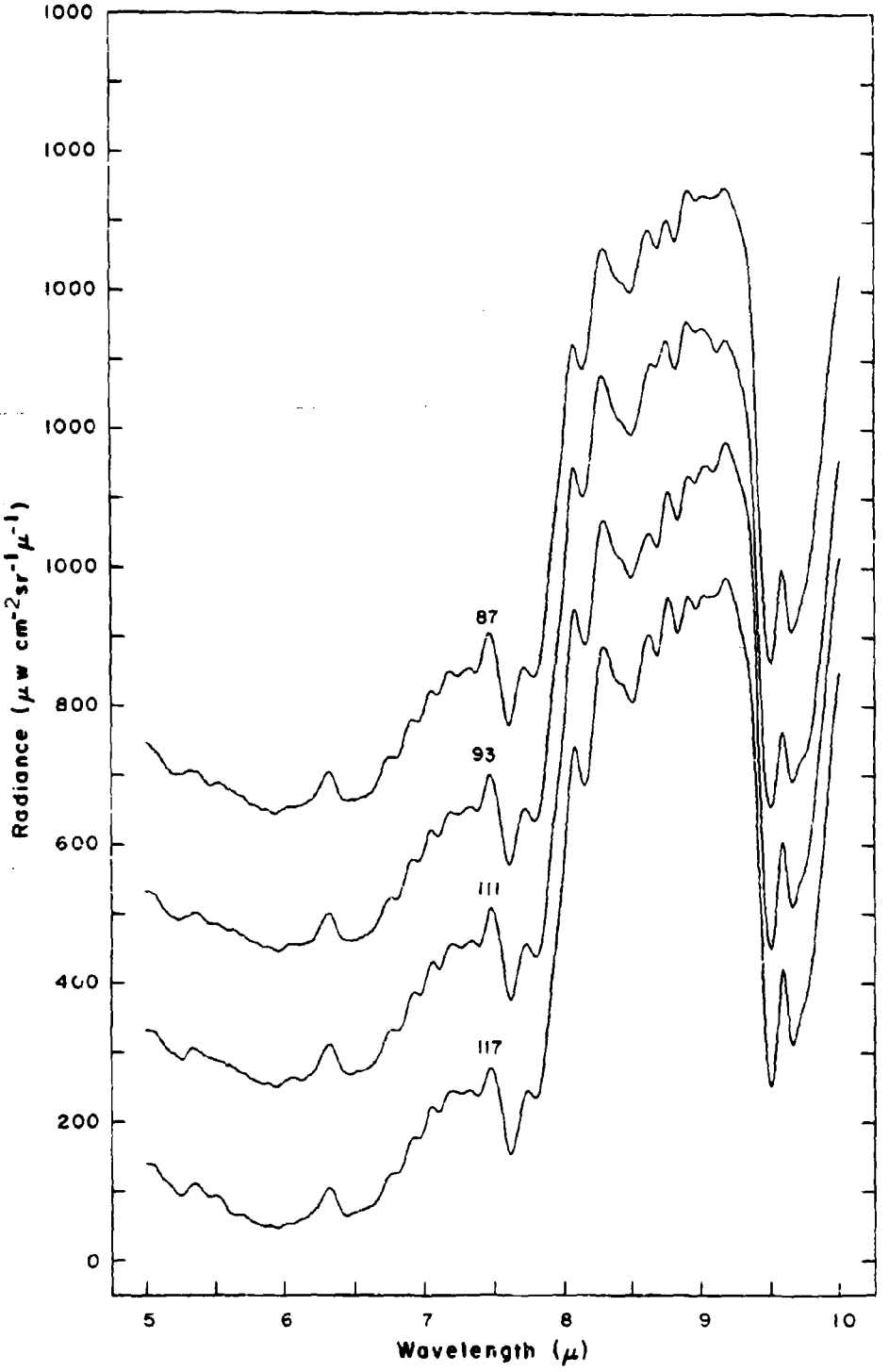

Figure 65 Spectral radiance vs altitude for balloon flight 25 June 1966. (See Table III)

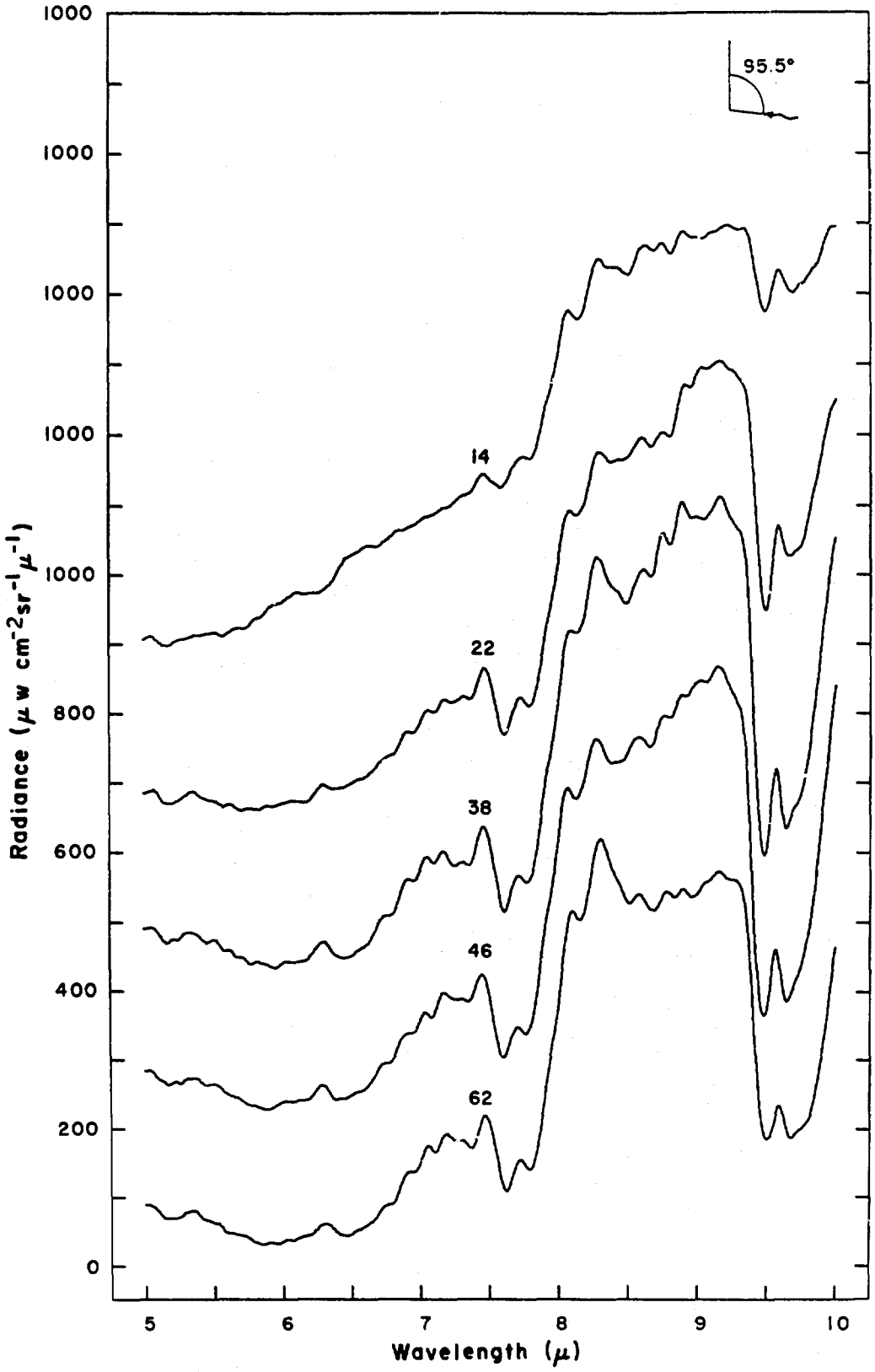

Figure 66 Spectral radiance vs altitude for balloon flight 25 June 1968. (See Table III)

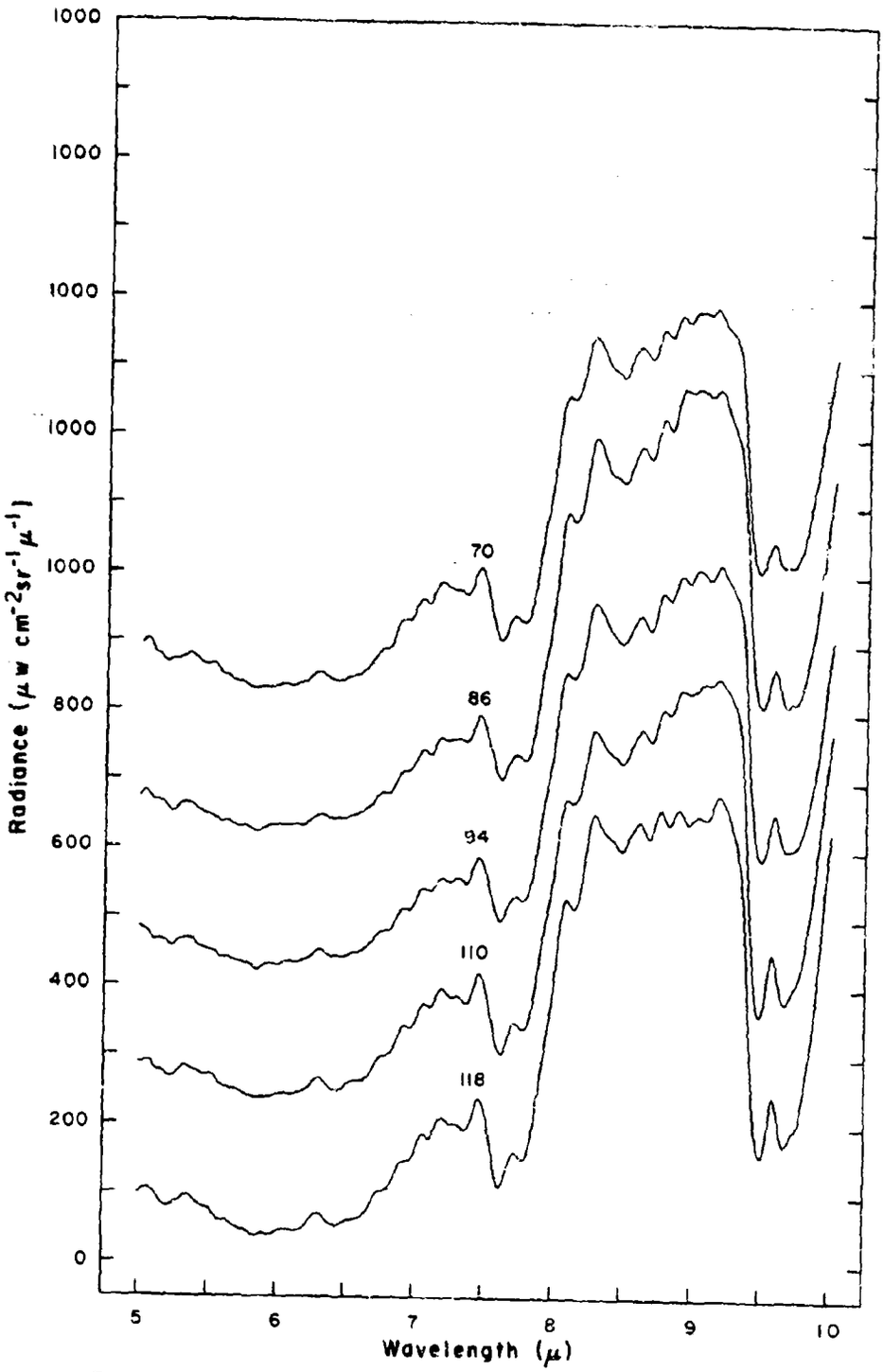

Figure 67 Spectral radiance vs altitude for 1 flight 25 June 1968. (See Table III)

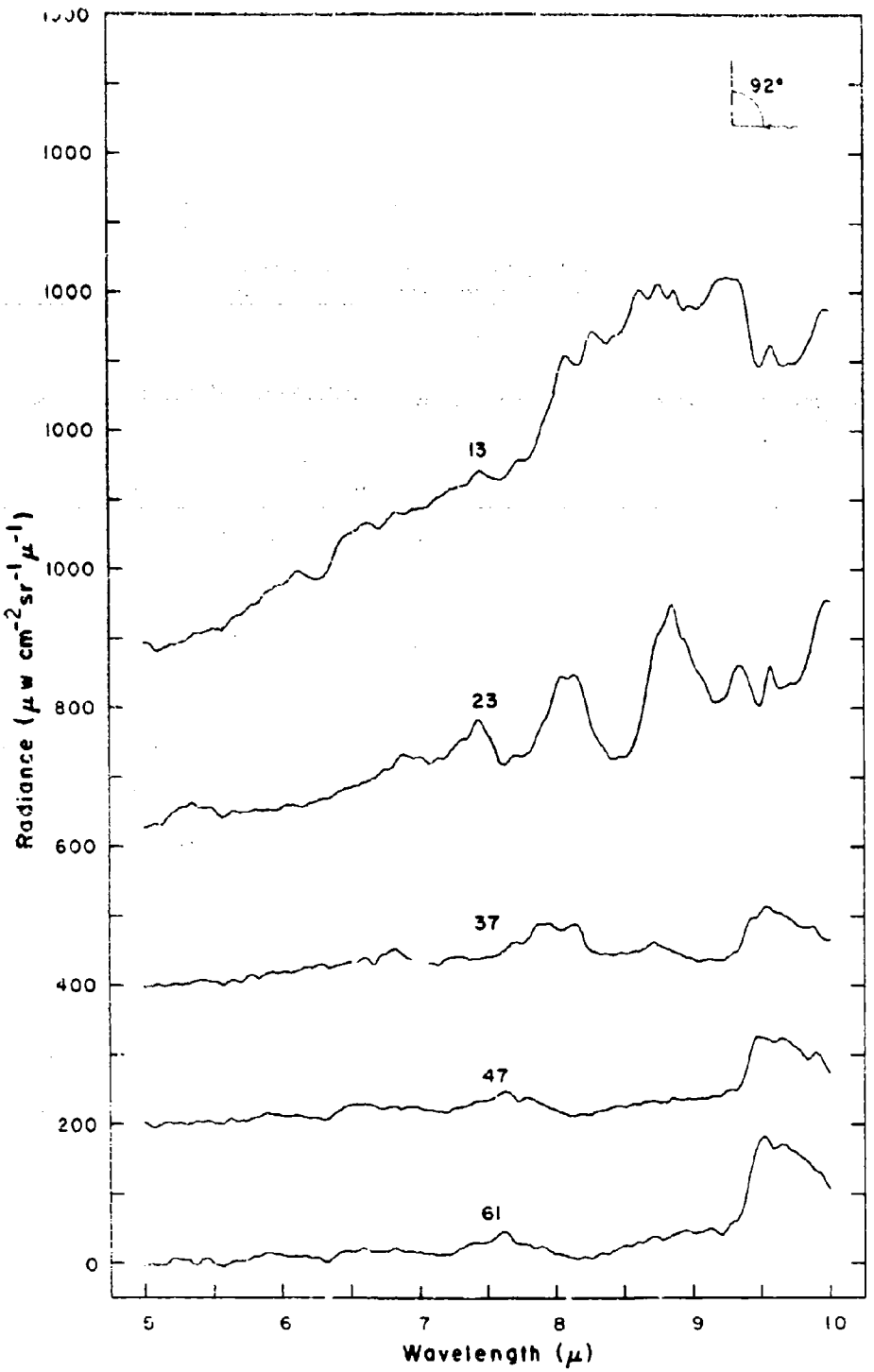

Figure 68 Spectral radiance vs altitude for balloon flight 25 June 1968. (See Table III)

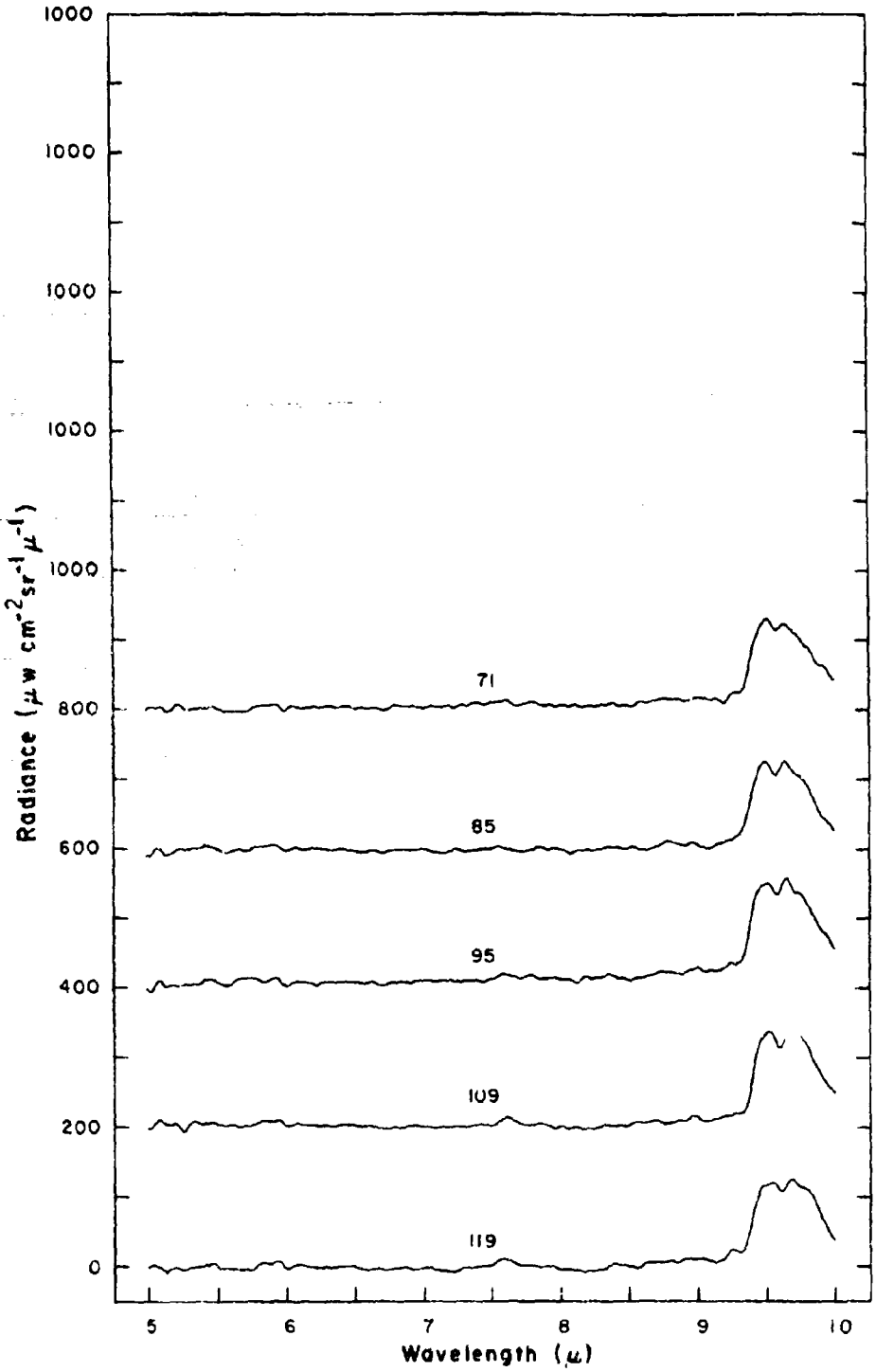

Figure 69 Spectral radiance vs altitude for balloon flight
25 June 1963. (See Table III)

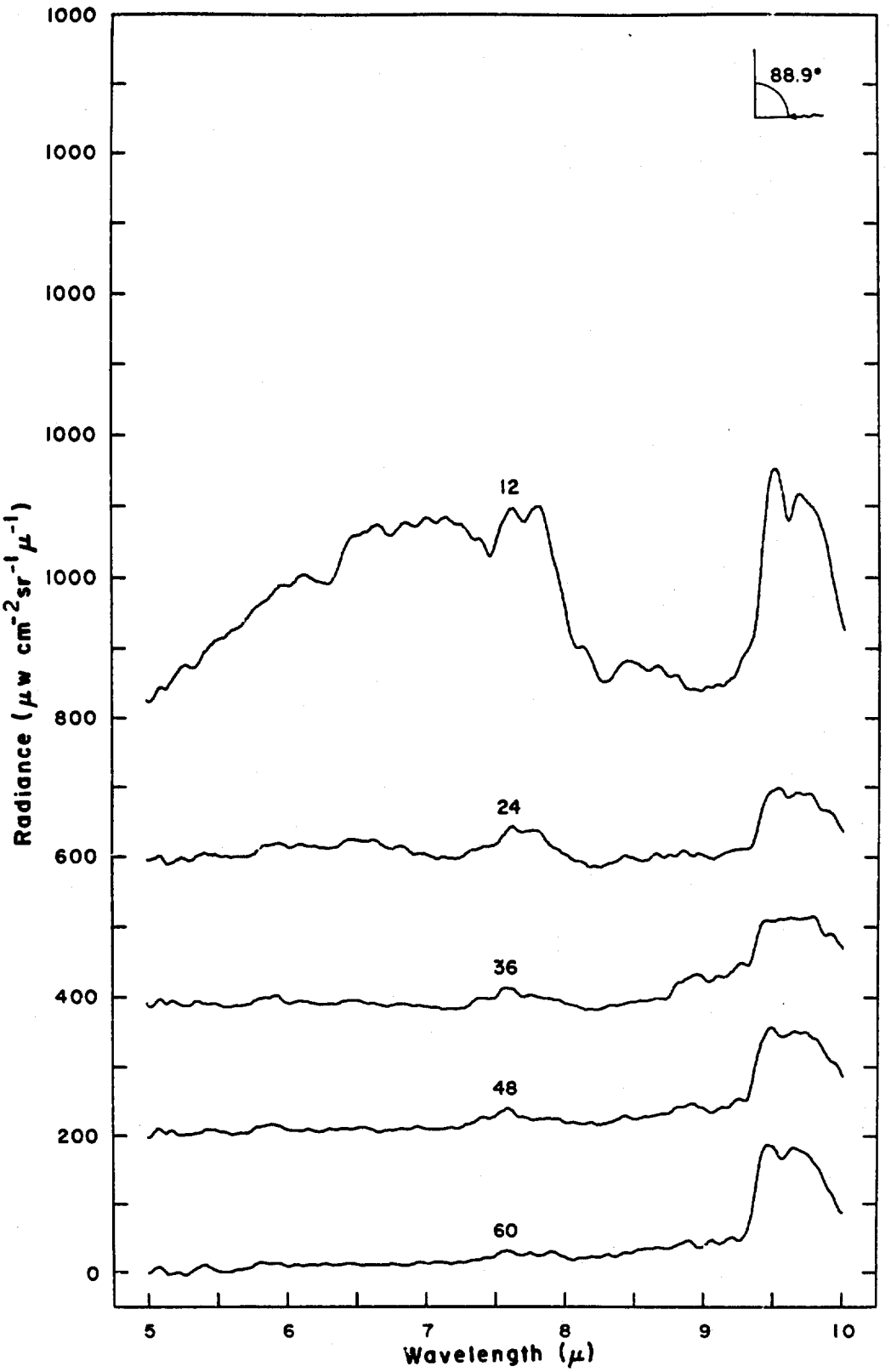

Figure 70 Spectral radiance vs altitude for balloon flight 25 June 1968. (See Table III)

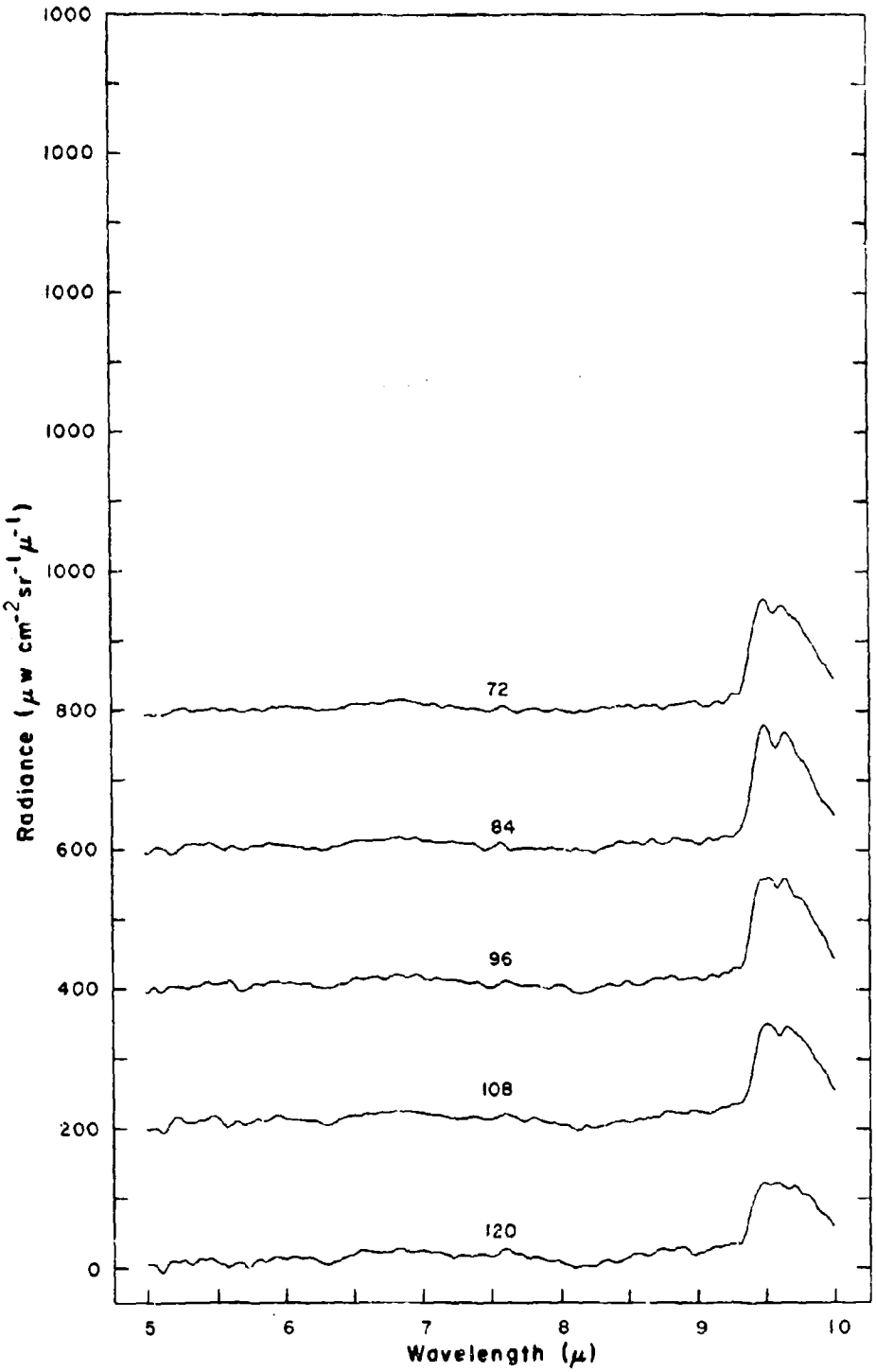

Figure 71 Spectral radiance vs altitude for balloon flight 25 June 1969. (See Table III)

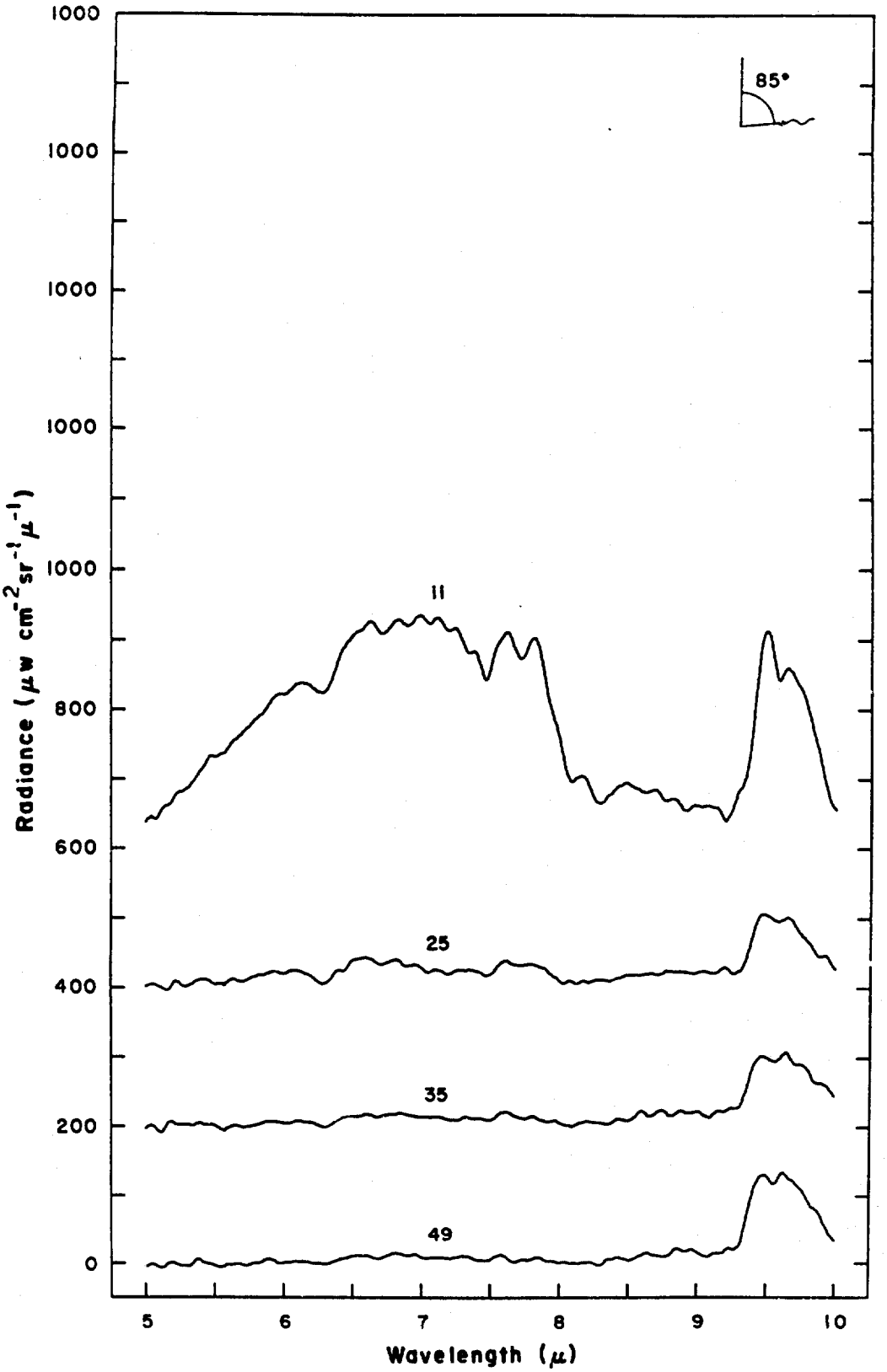

Figure 72 Spectral radiance vs altitude for balloon flight 25 June 1968. (See Table III)

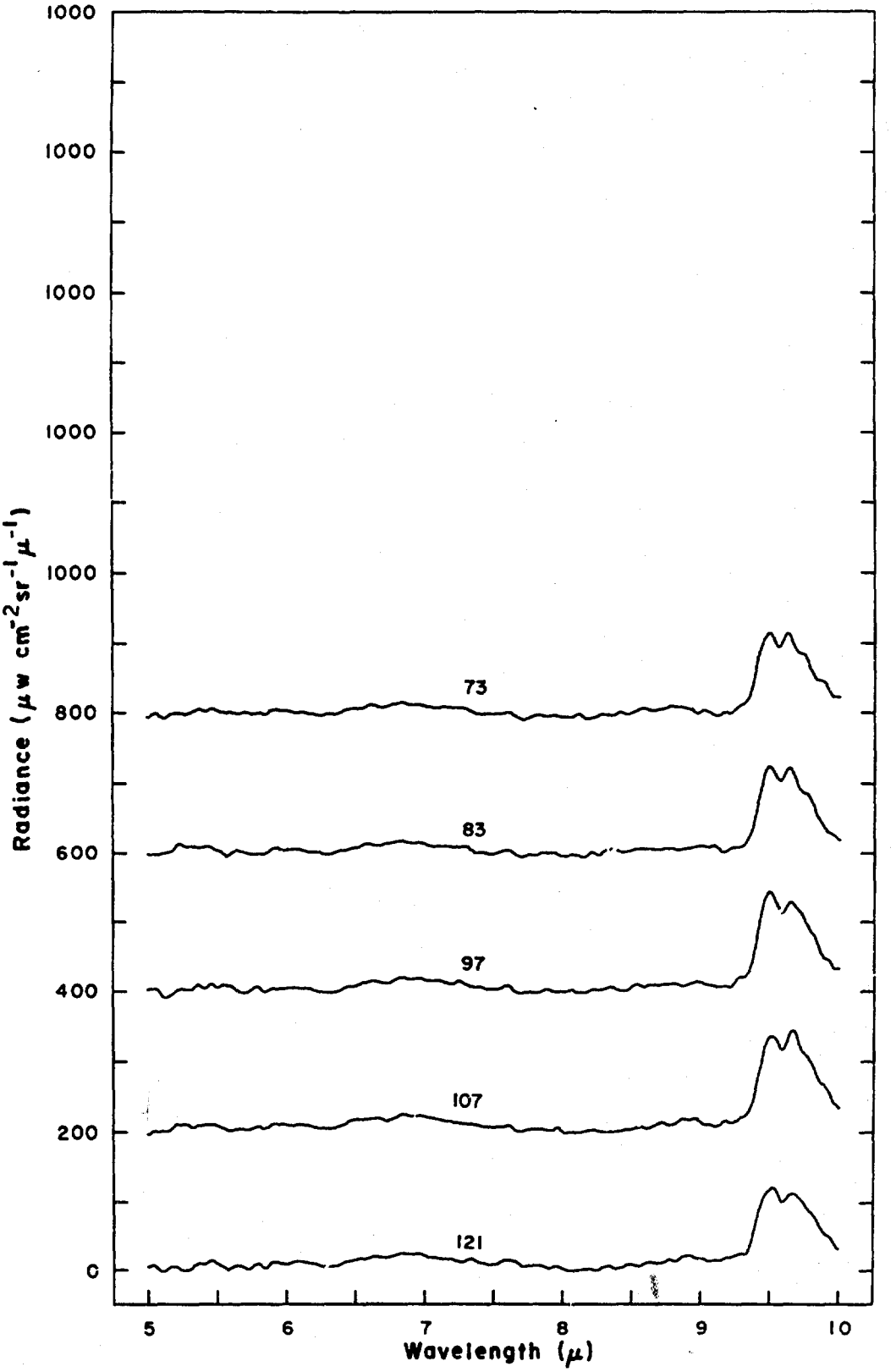

Figure 73 Spectral radiance vs altitude for Mesa flight 25 Jan 1968. (See Table III)

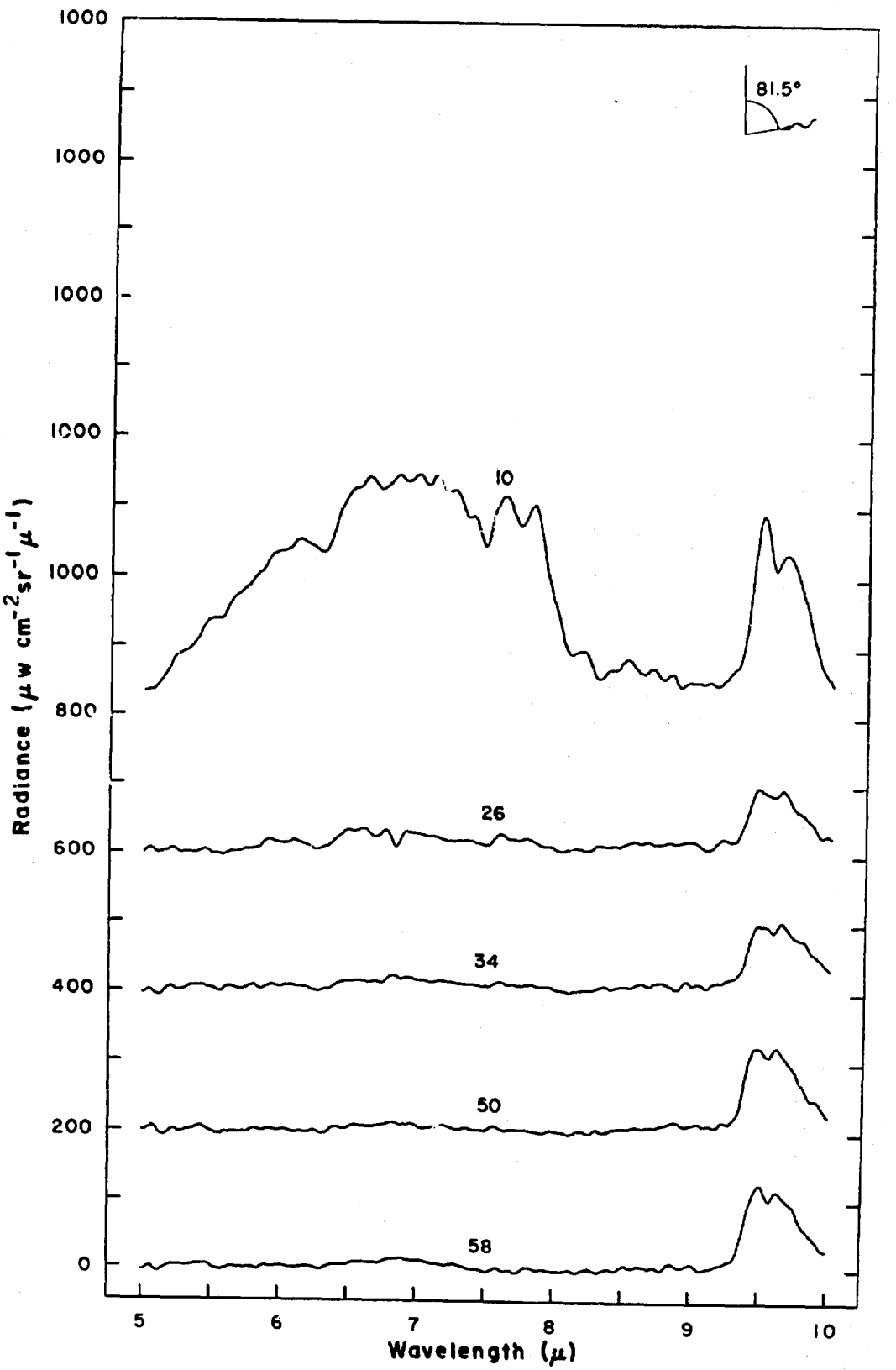

Figure 74 Spectral radiance vs altitude for balloon flight 25 Jun 1963. (See Table III)

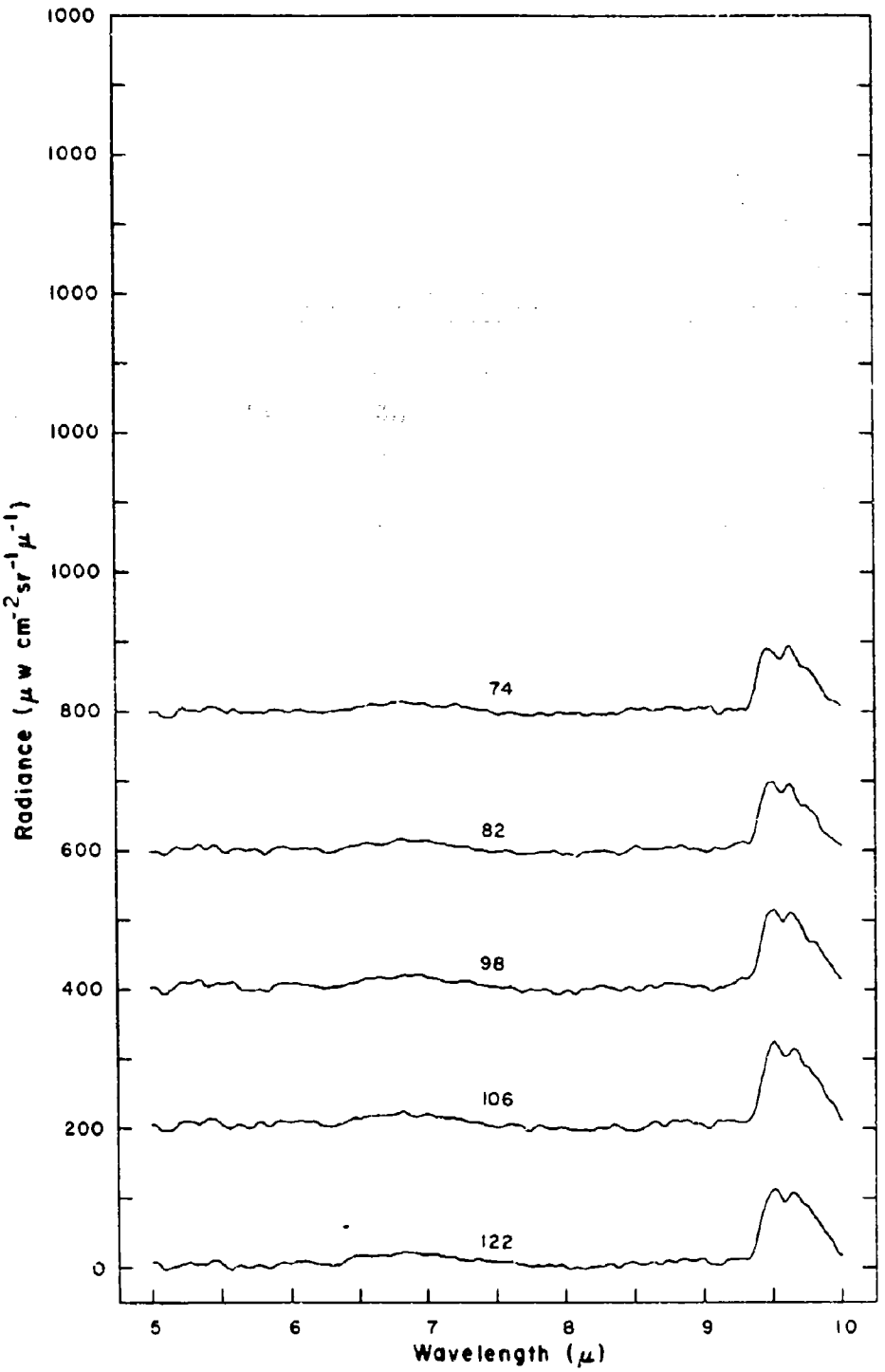

Figure 75 Spectral radiance vs altitude for balloon flight 25 June 1968. (See Table III)

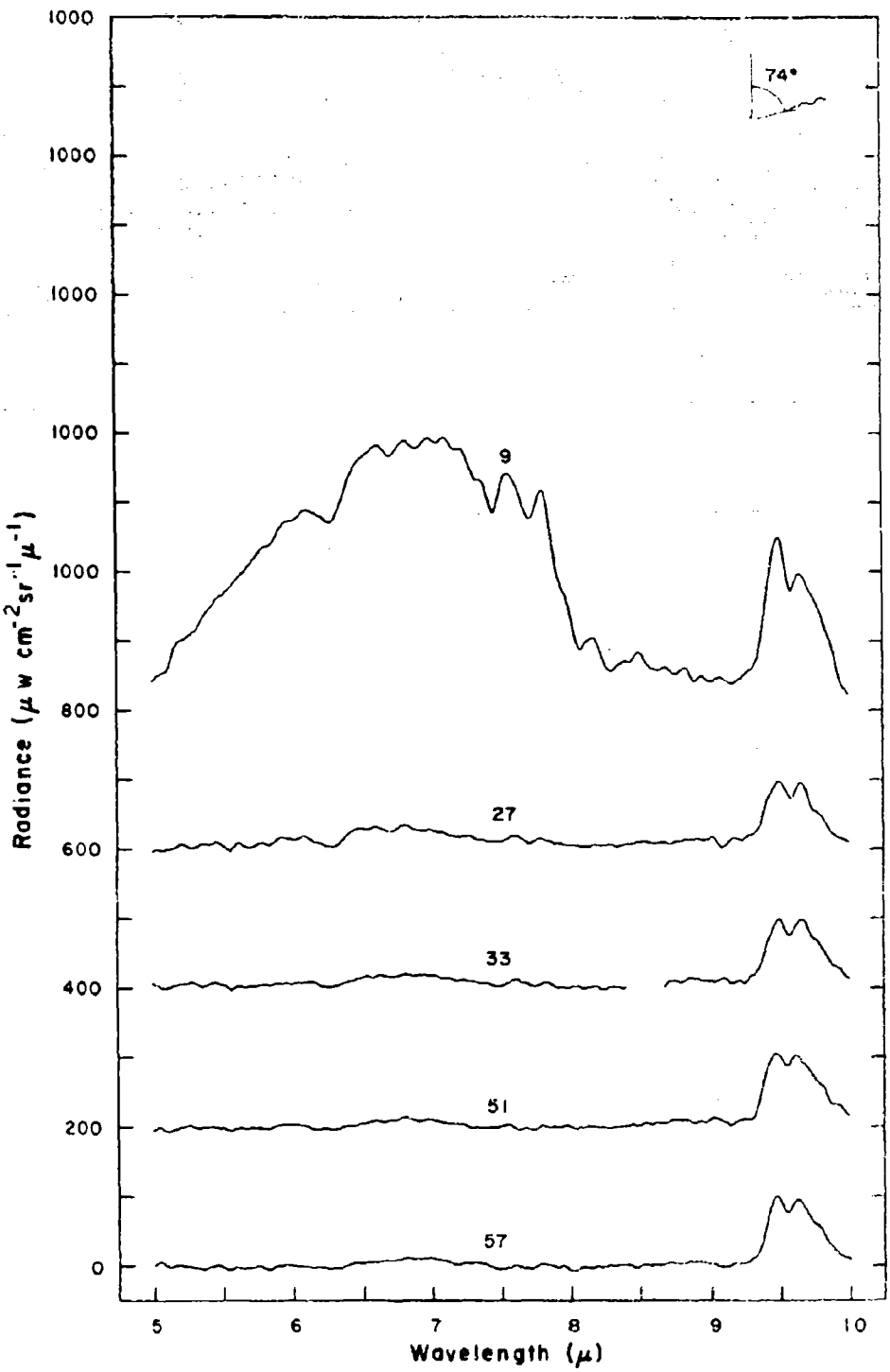

Figure 76 Spectral radiance vs altitude for balloon flight 25 June 1968. (See Table III)

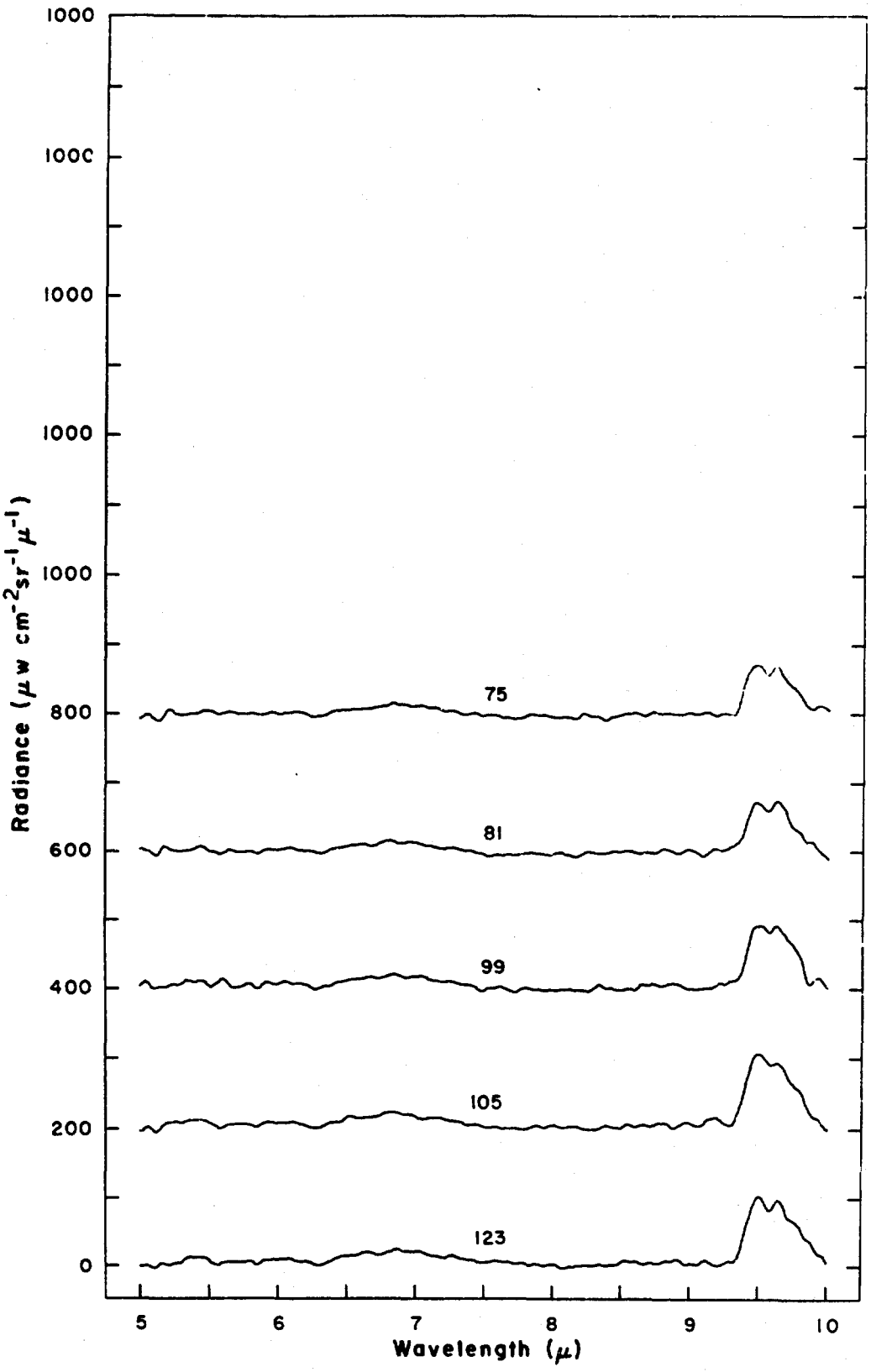

Figure 77 Spectral radiance vs altitude for balloon flight 25 June 1968. (See Table III)

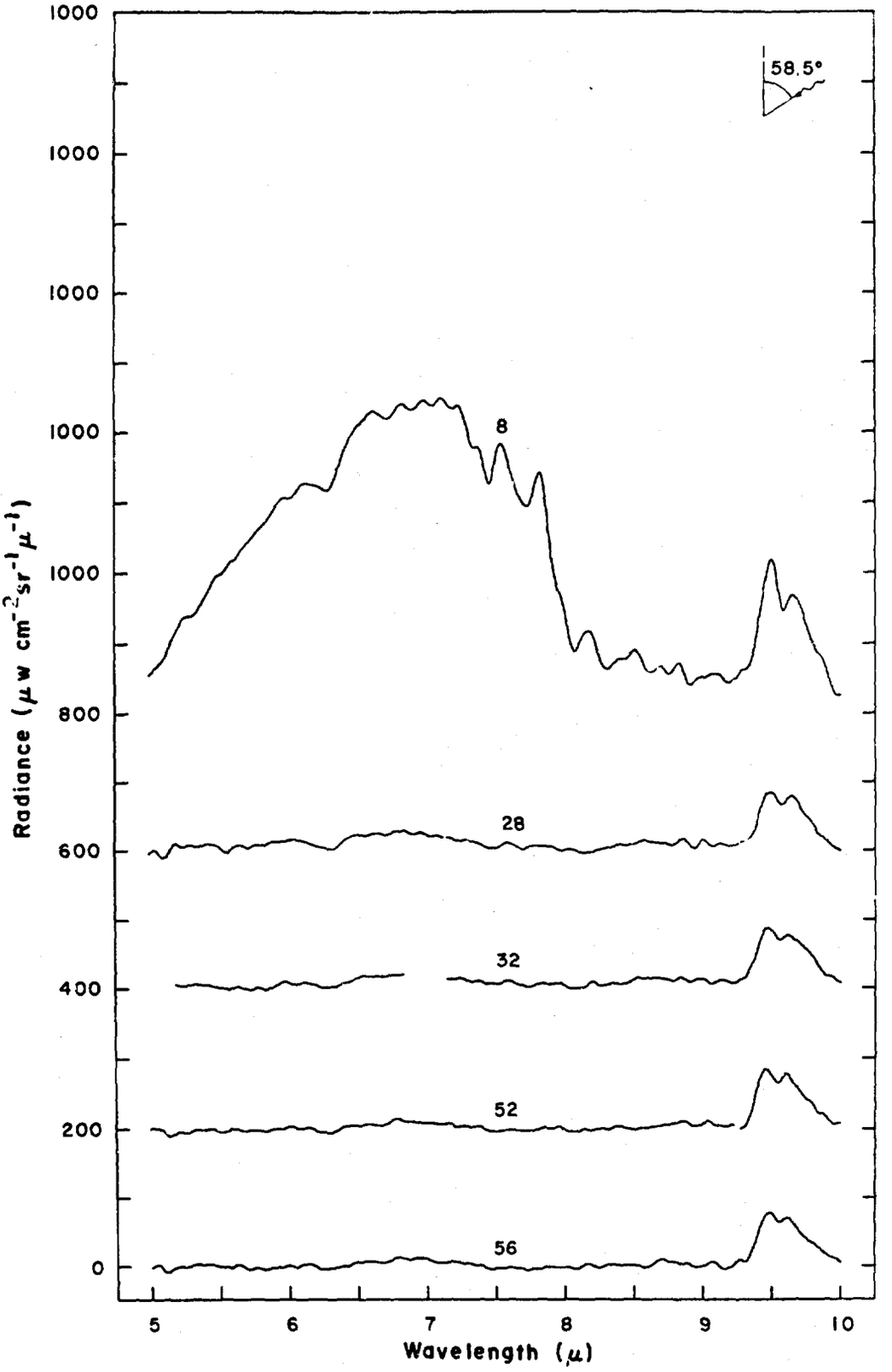

Figure 78 Spectral radiance vs altitude for balloon flight 25 June 1968. (See Table III)

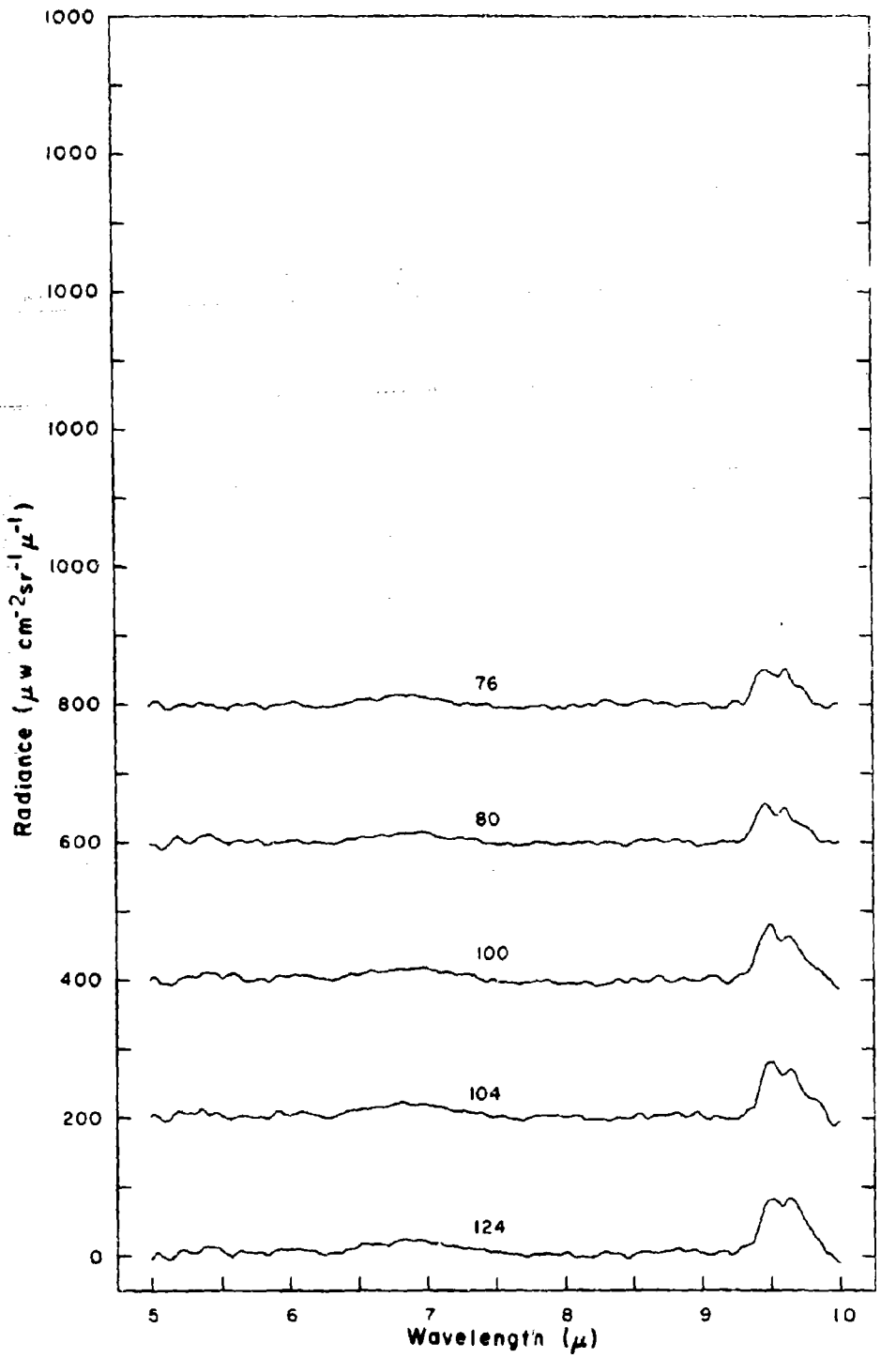

Figure 75 Spectral radiance vs altitude for balloon flight 25 June 1968. (See Table III)

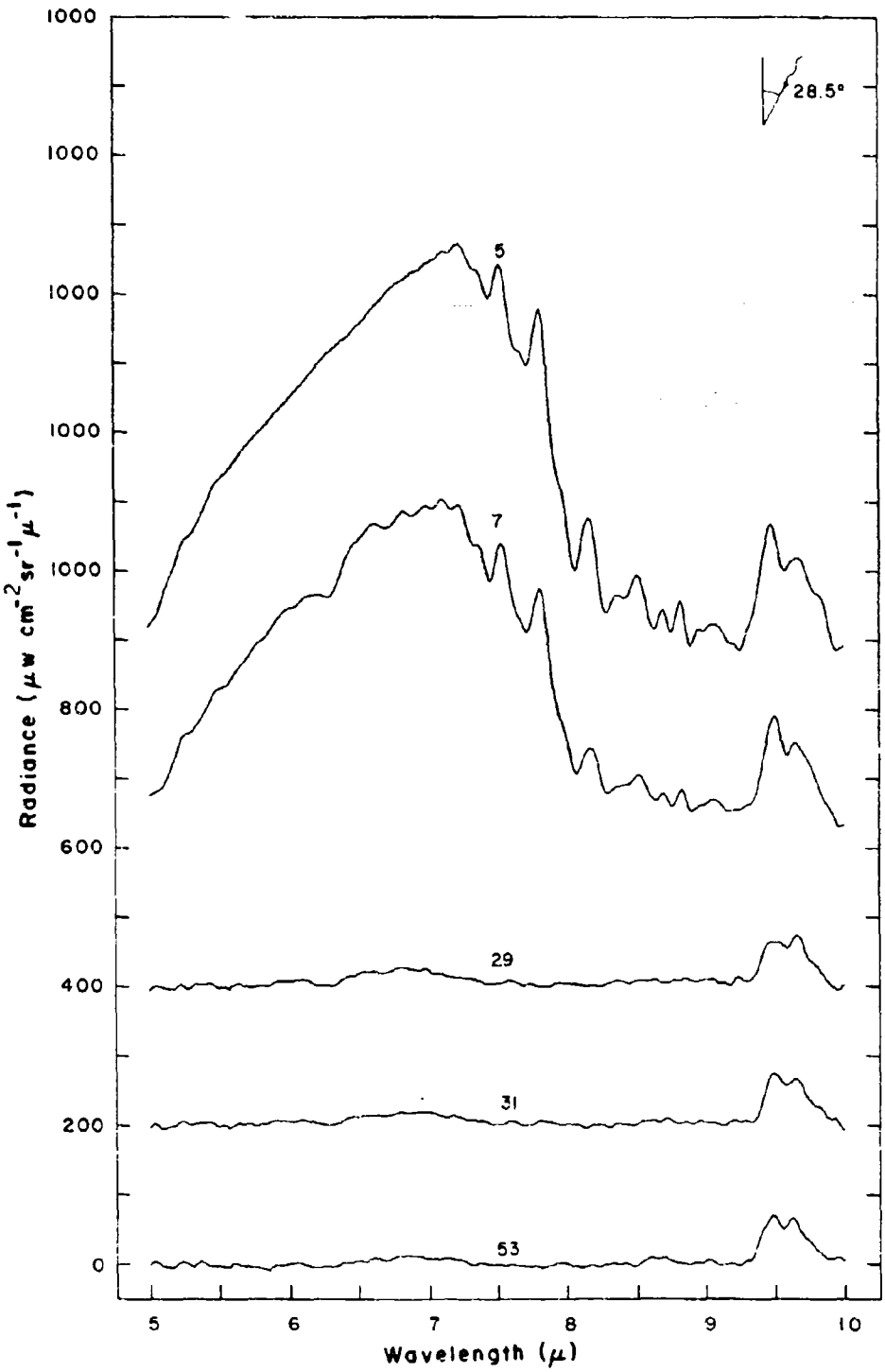

Figure 80 Spectral radiance vs altitude for balloon flight 25 June 1968. (See Table III)

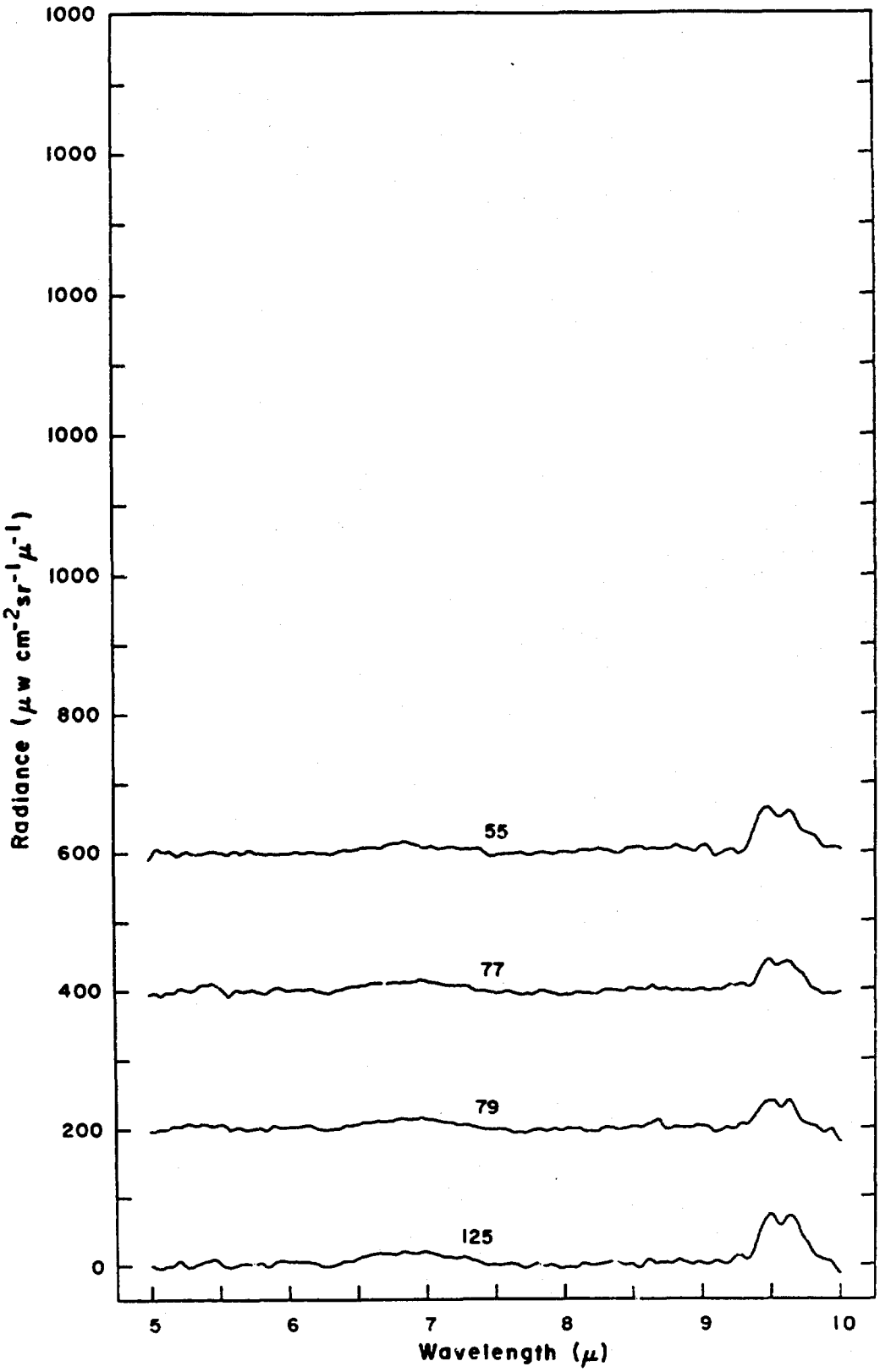

Figure 81 Spectral radiance vs altitude for balloon flight 25 June 1968. (See Table III)

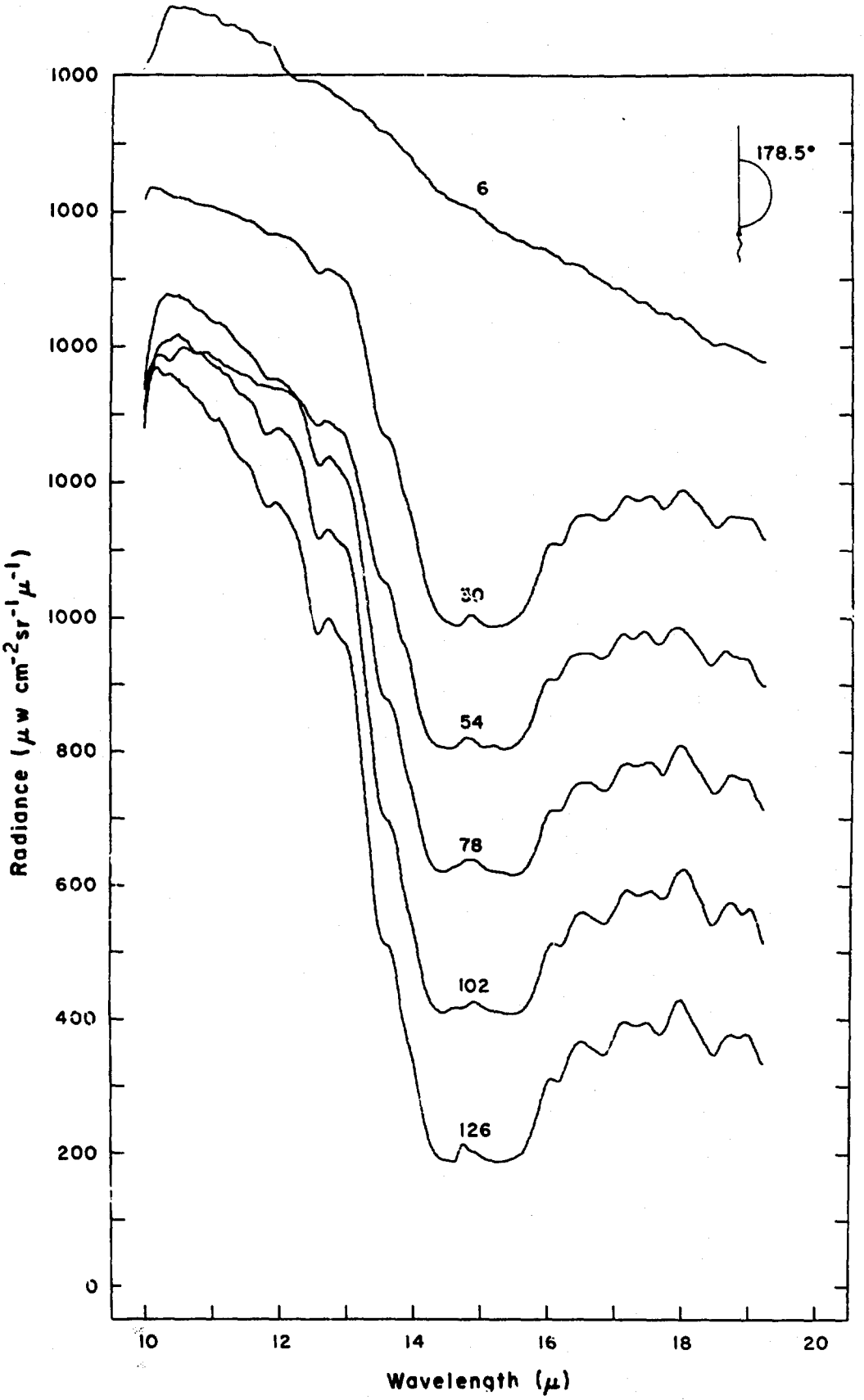

Figure 82 Spectral radiance vs altitude for balloon flight 25 June 1968. (See Table III)

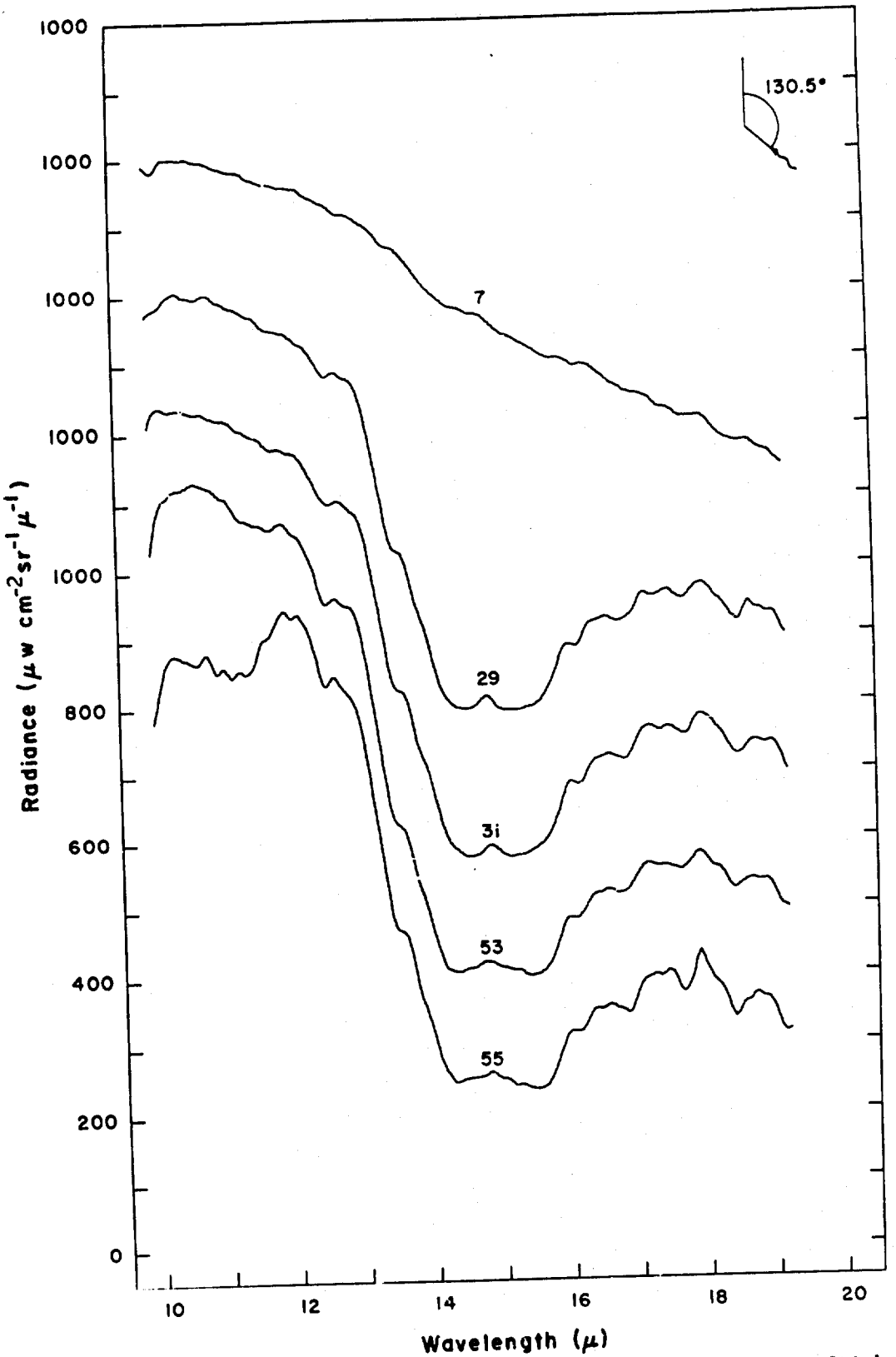

Figure 83 Spectral radiance vs altitude for balloon flight
25 June 1968. (See Table III)

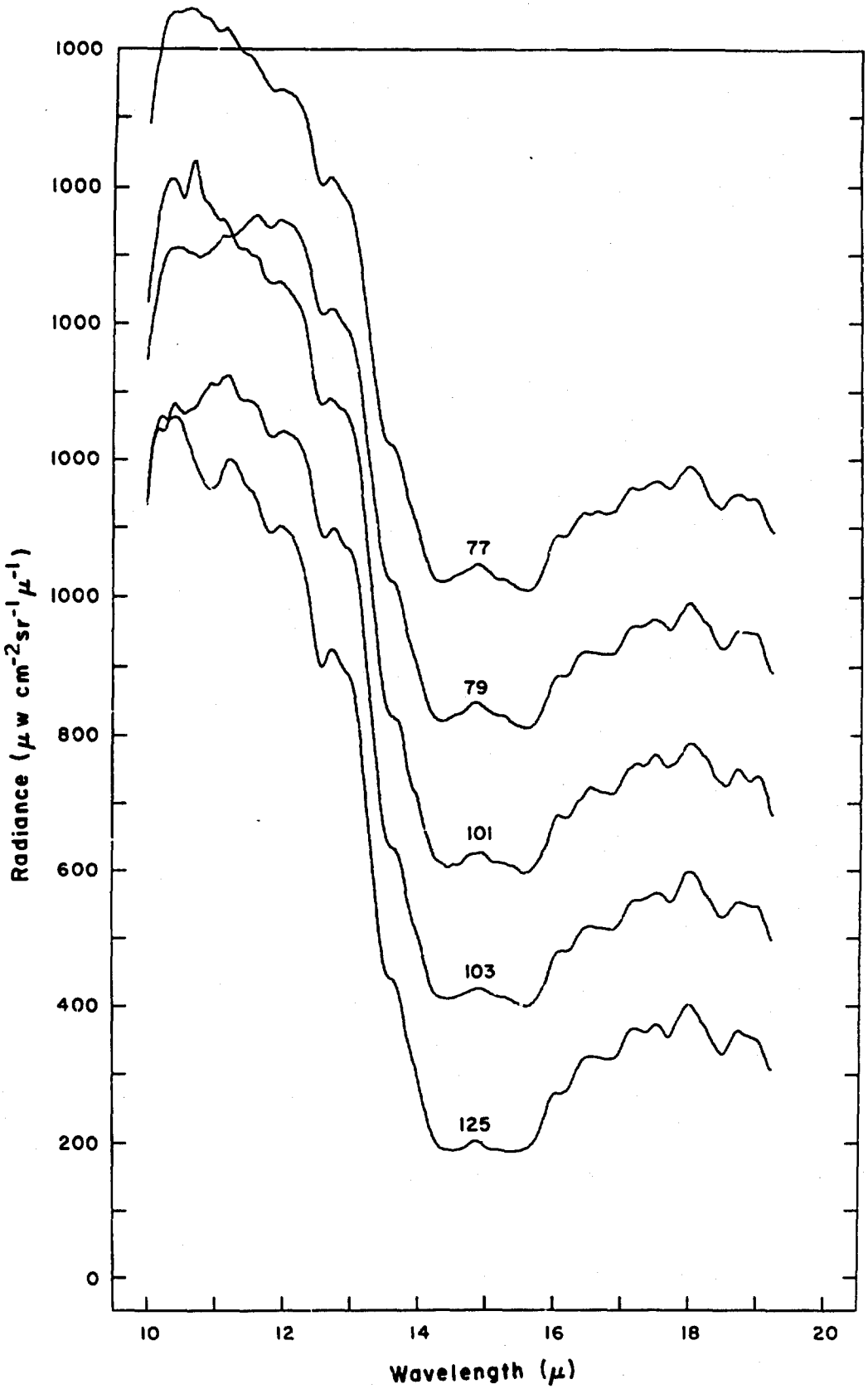

Figure 84 Spectral radiance vs altitude for balloon flight 25 June 1968. (See Table III)

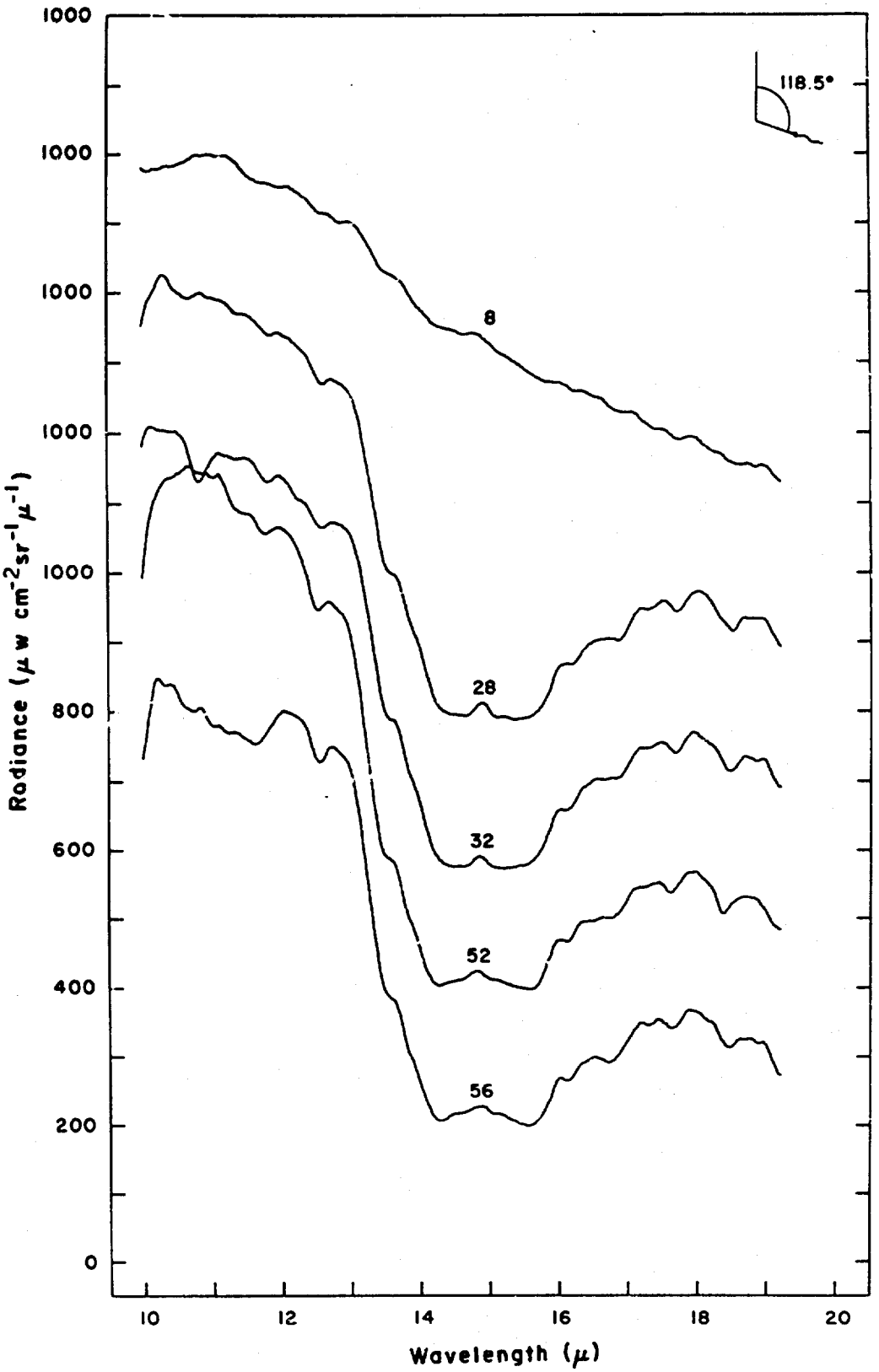

Figure 85 Spectral radiance vs altitude for balloon flight 25 June 1968. (See Table III)

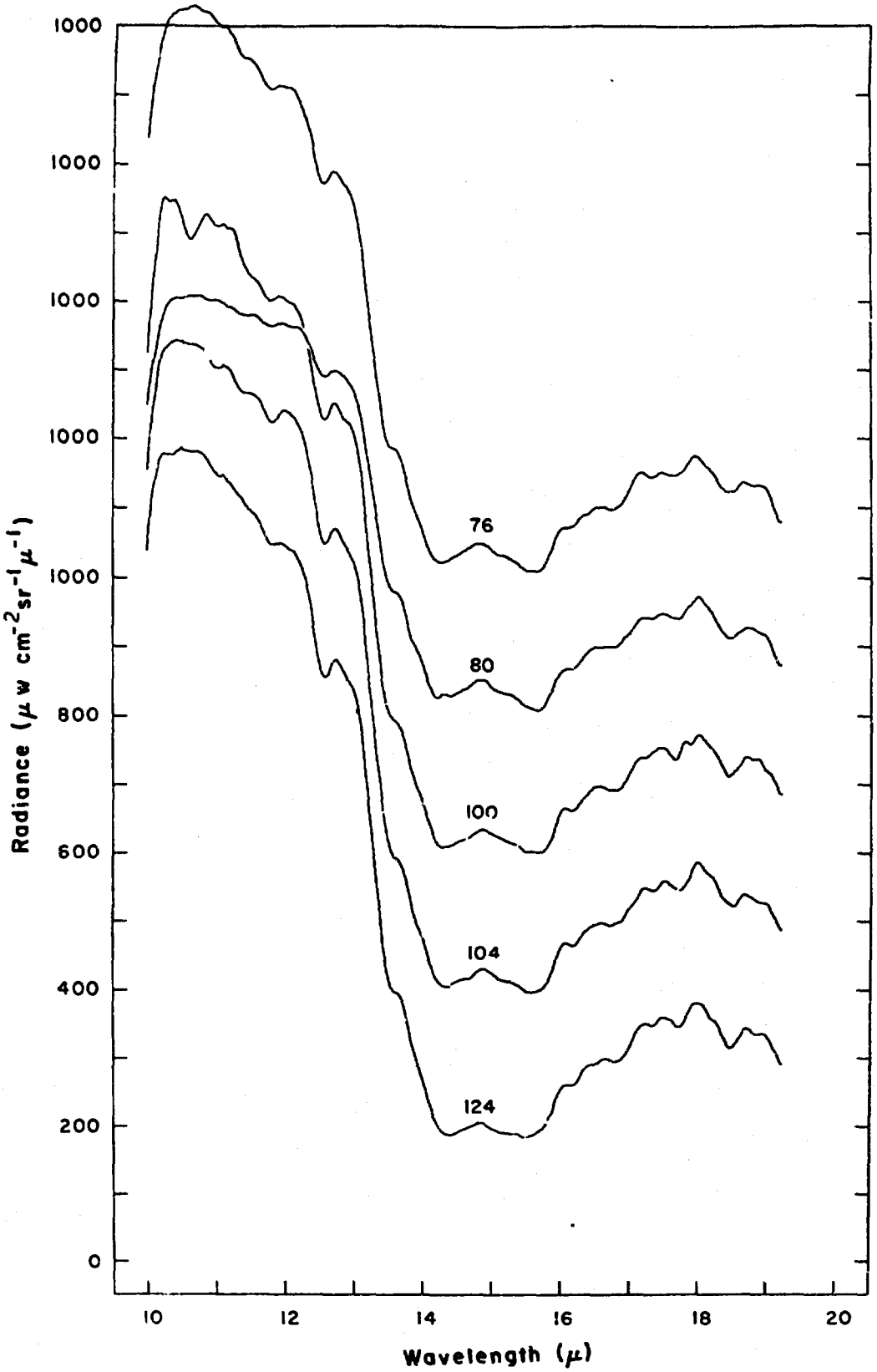

Figure 86 Spectral radiance vs altitude for balloon flight 25 June 1968. (See Table III)

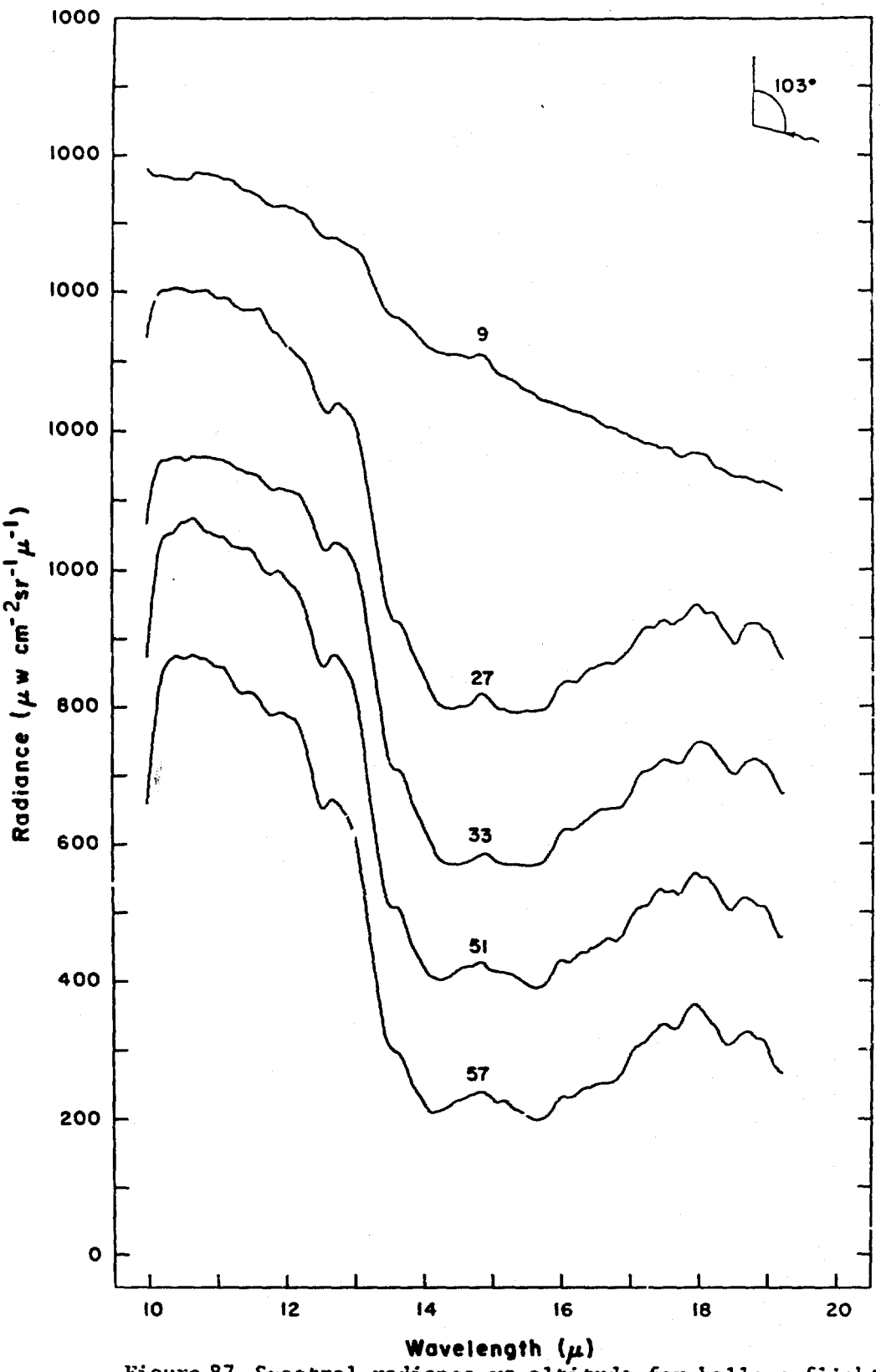

Figure 87 Spectral radiance vs altitude for balloon flight 25 June 1968. (See Table III)

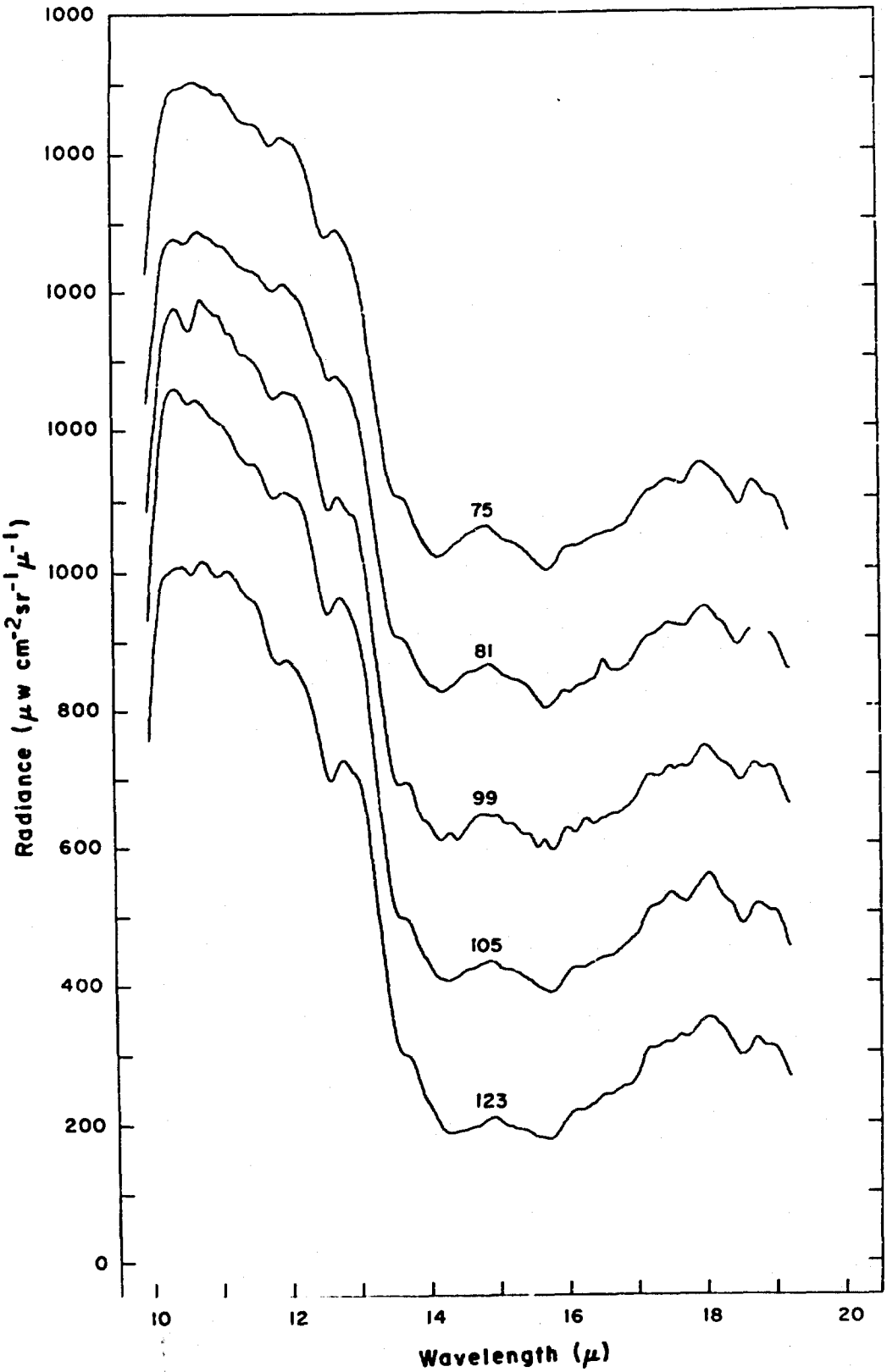

Figure 88 Spectral radiance vs altitude for balloon flight 25 June 1968. (See Table VII)

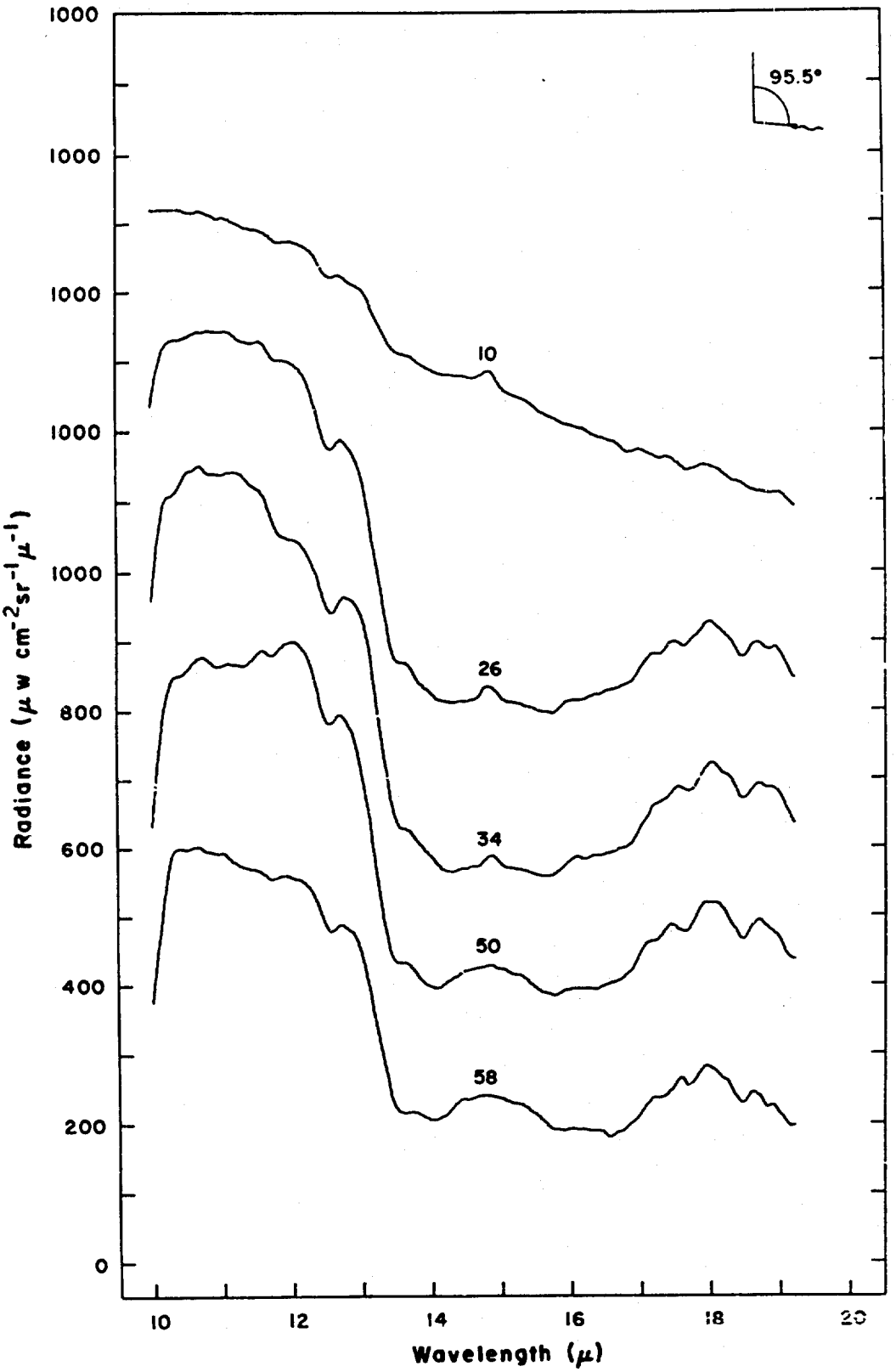

Figure 89 Spectral radiance vs altitude for balloon flight 25 June 1968. (See Table III)

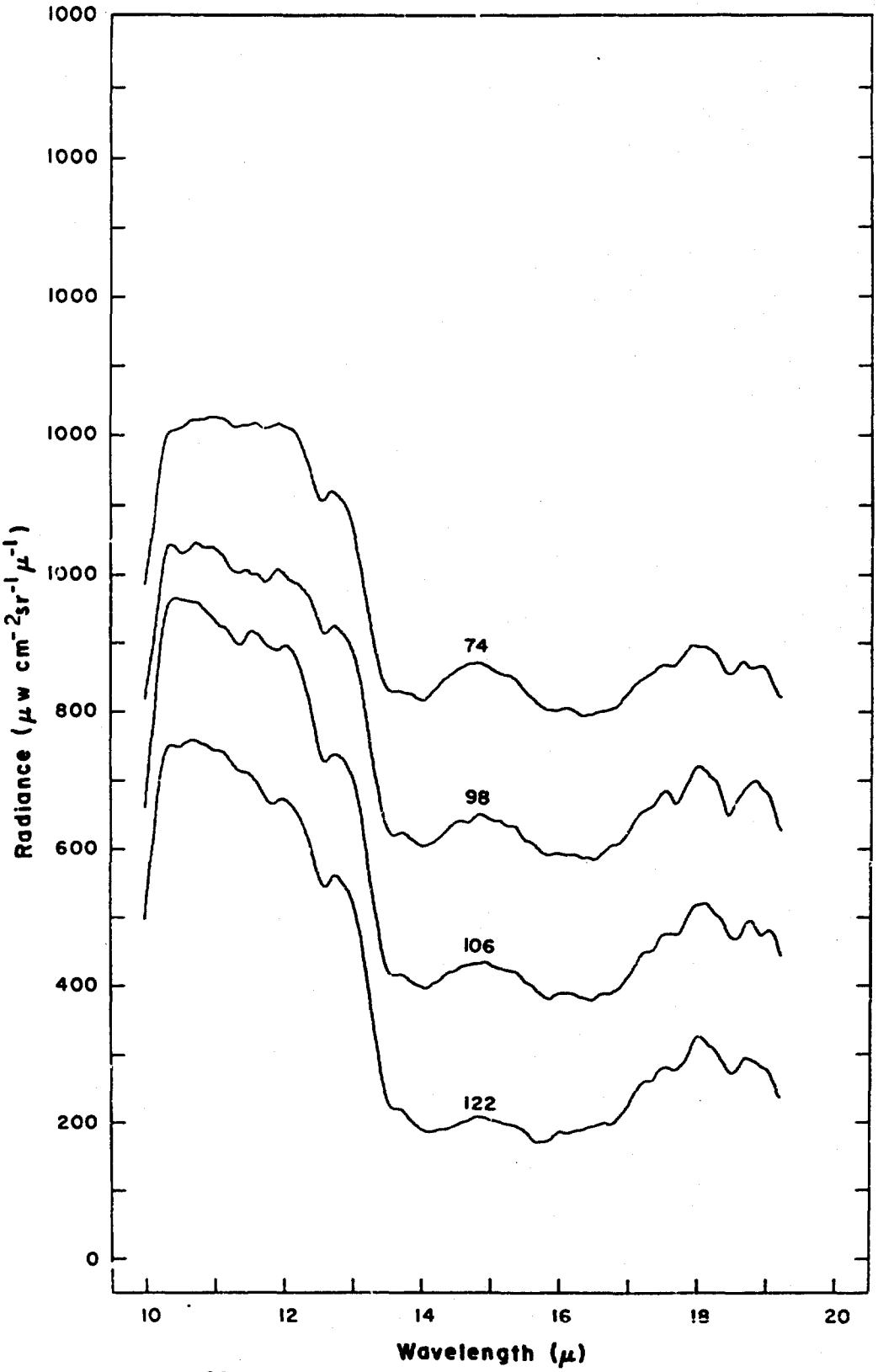

Figure 90 Spectral radiance vs altitude for balloon flight 25 June 1968. (See Table III)

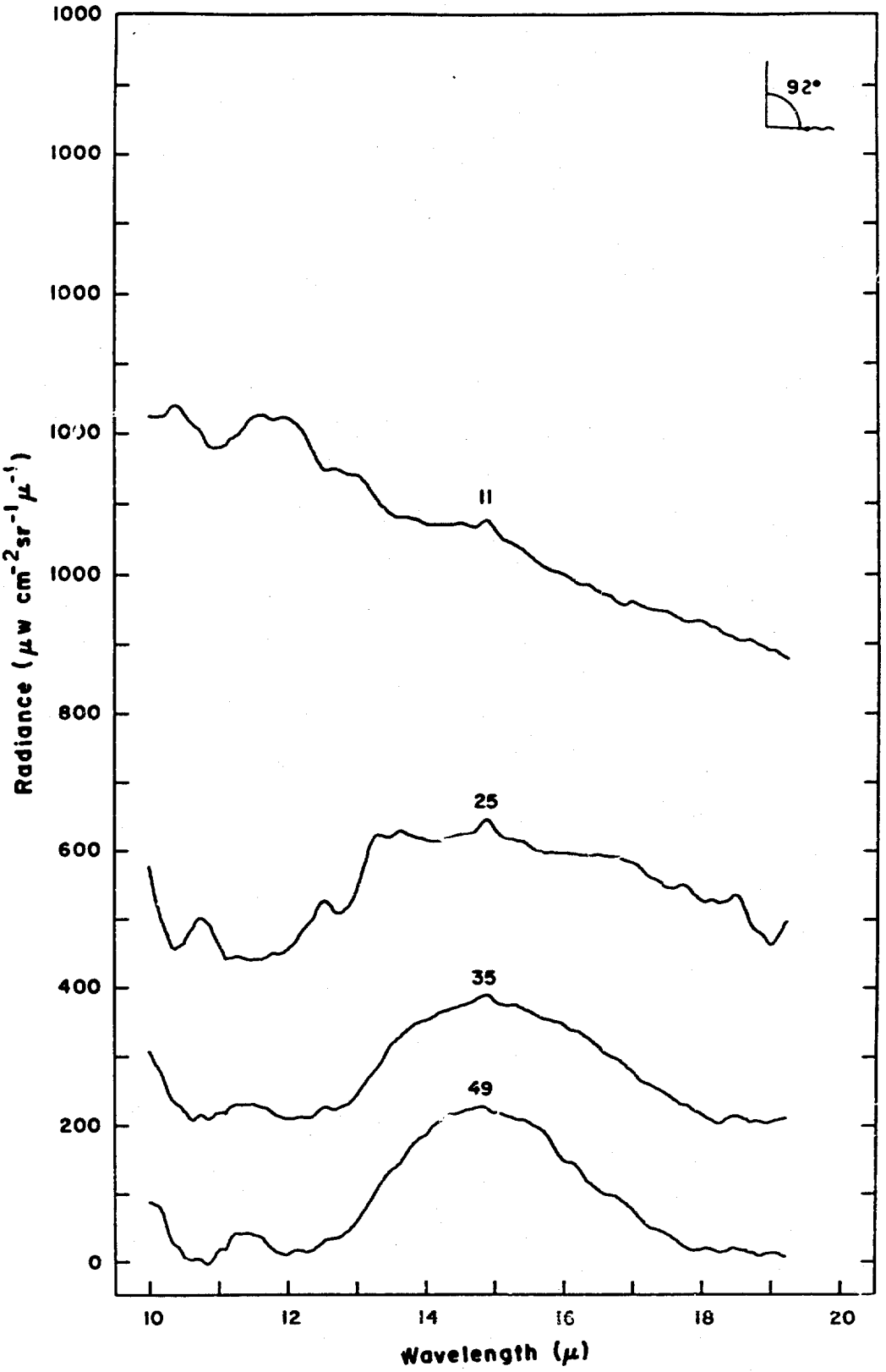

Figure 91 Spectral radiance vs altitude for balloon flight 25 June 1968. (See Table III)

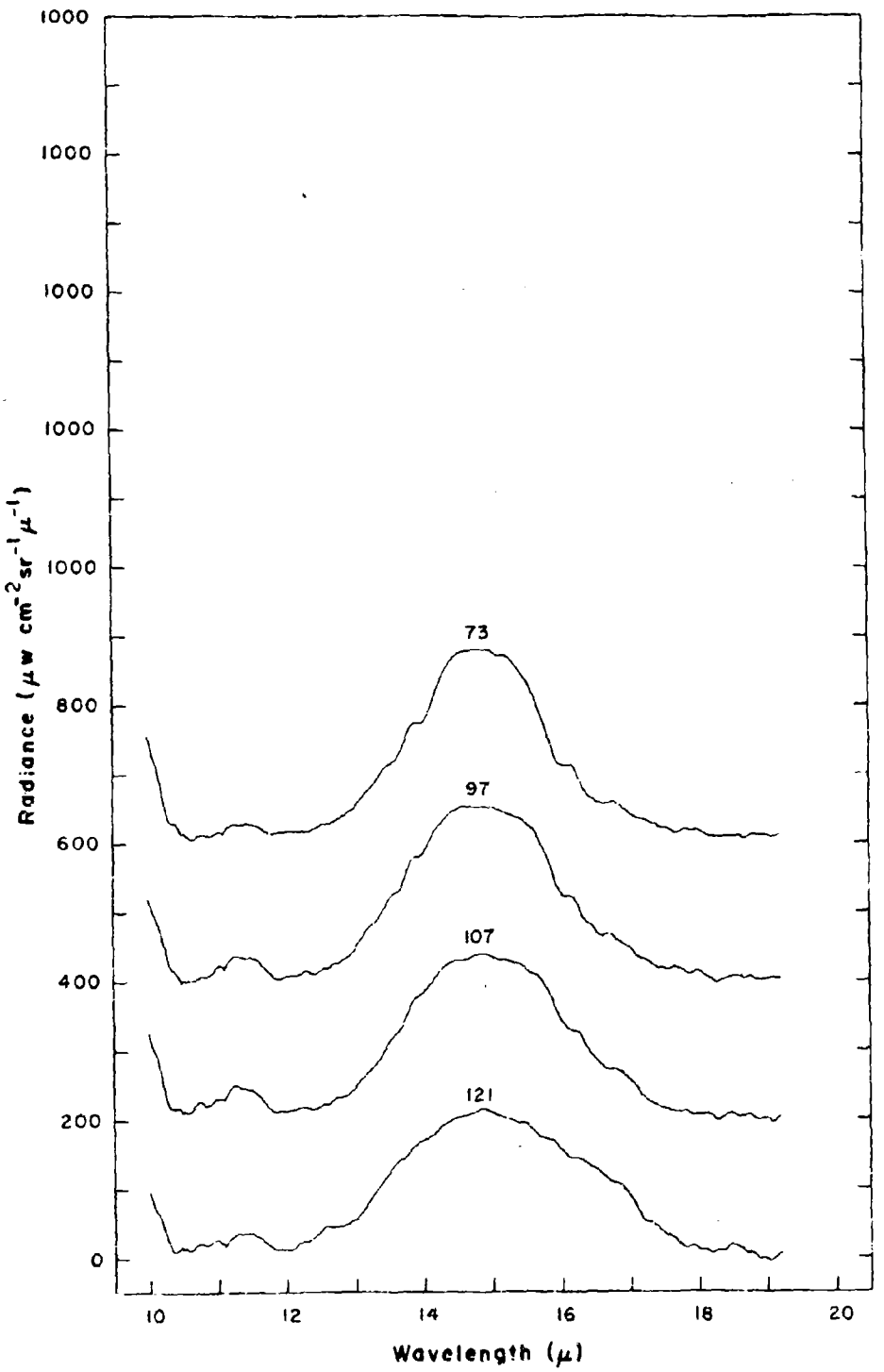

Figure 92 Spectral radiance vs altitude for balloon flight 25 June 1968. (See Table III)

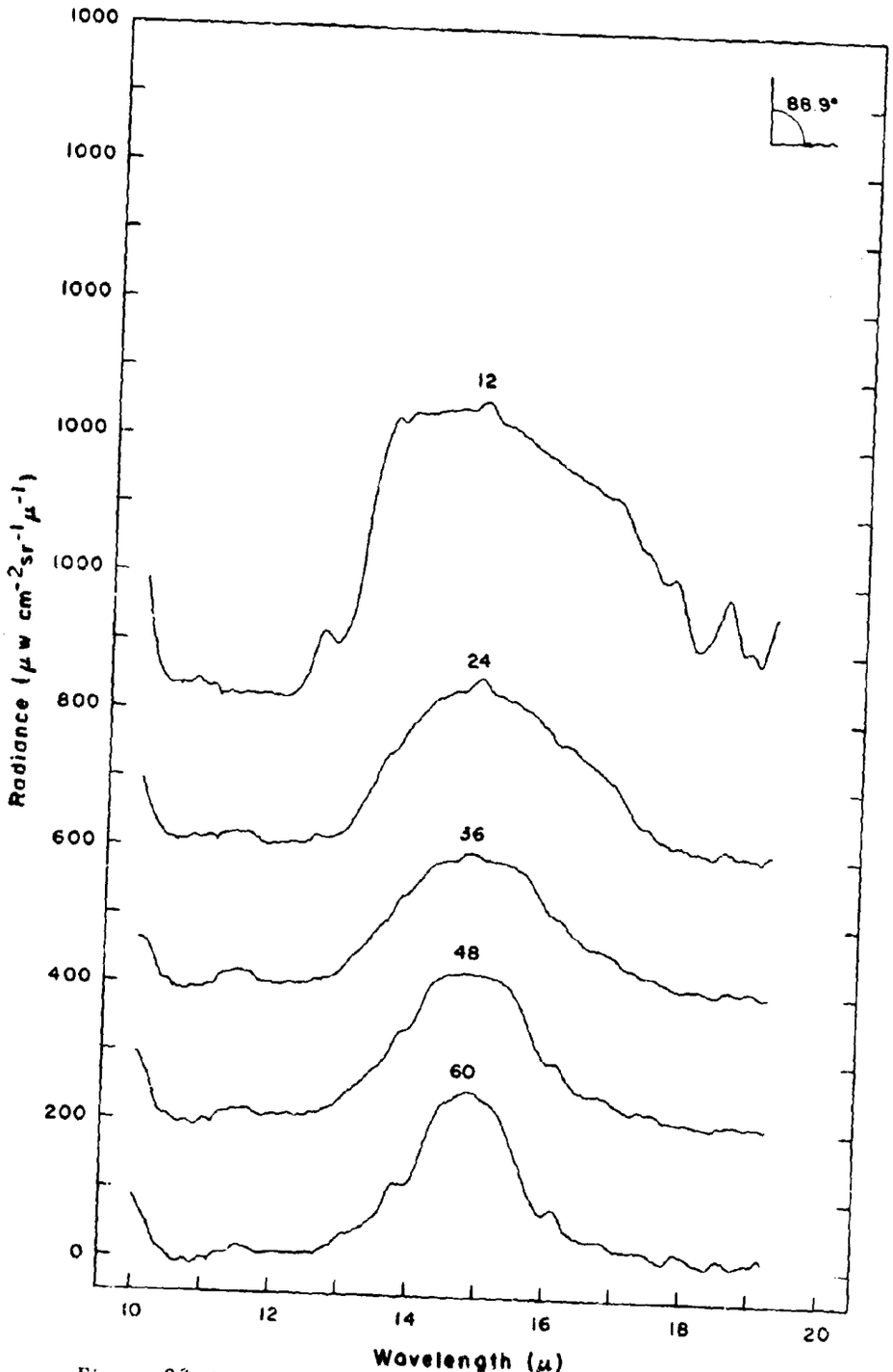

Figure 93 Spectral radiance vs altitude for balloon flight 25 June 1968. (See Table III)

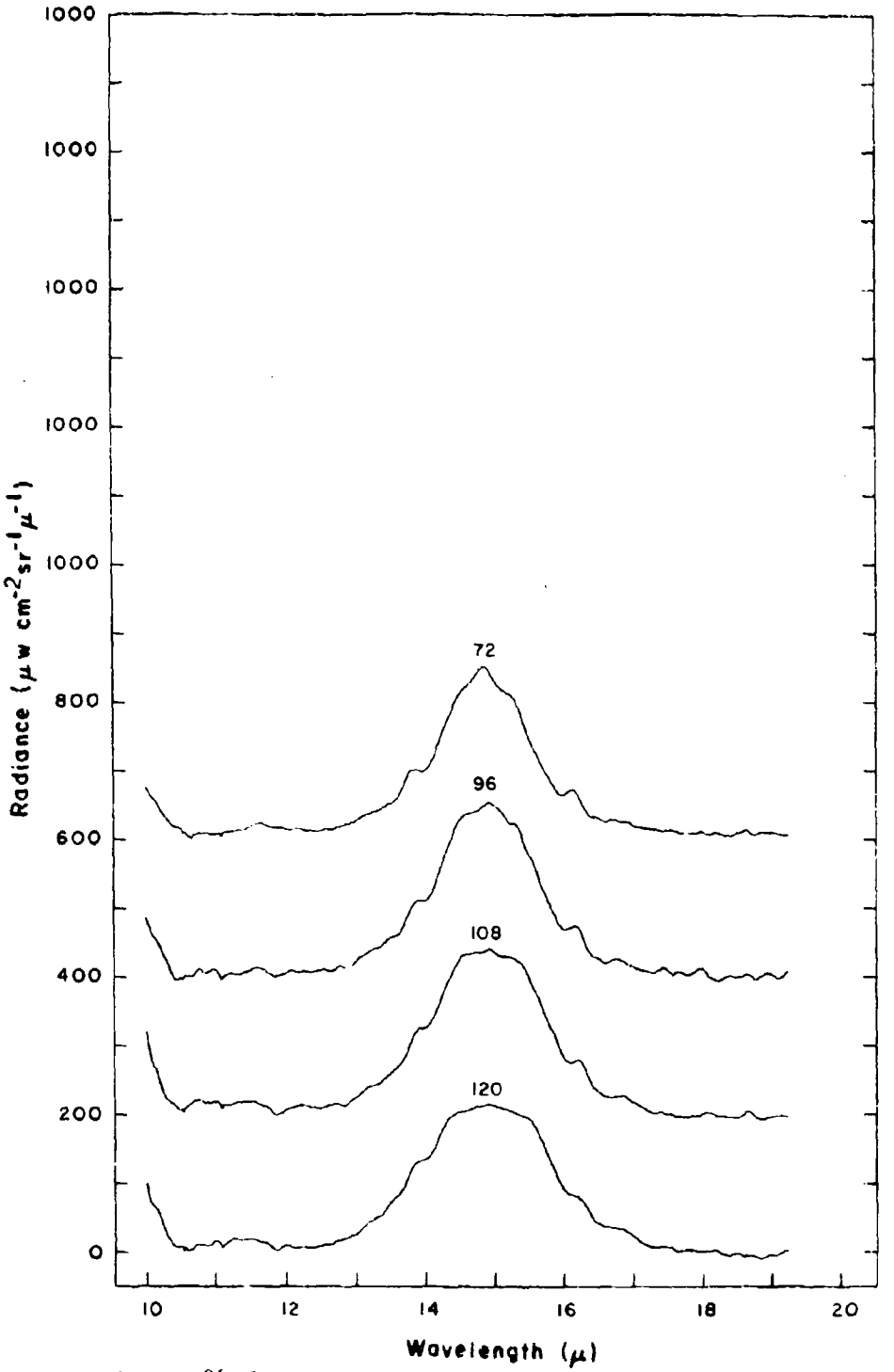

Figure 94 Spectral radiance vs altitude for balloon flight 25 June 1968. (See Table III)

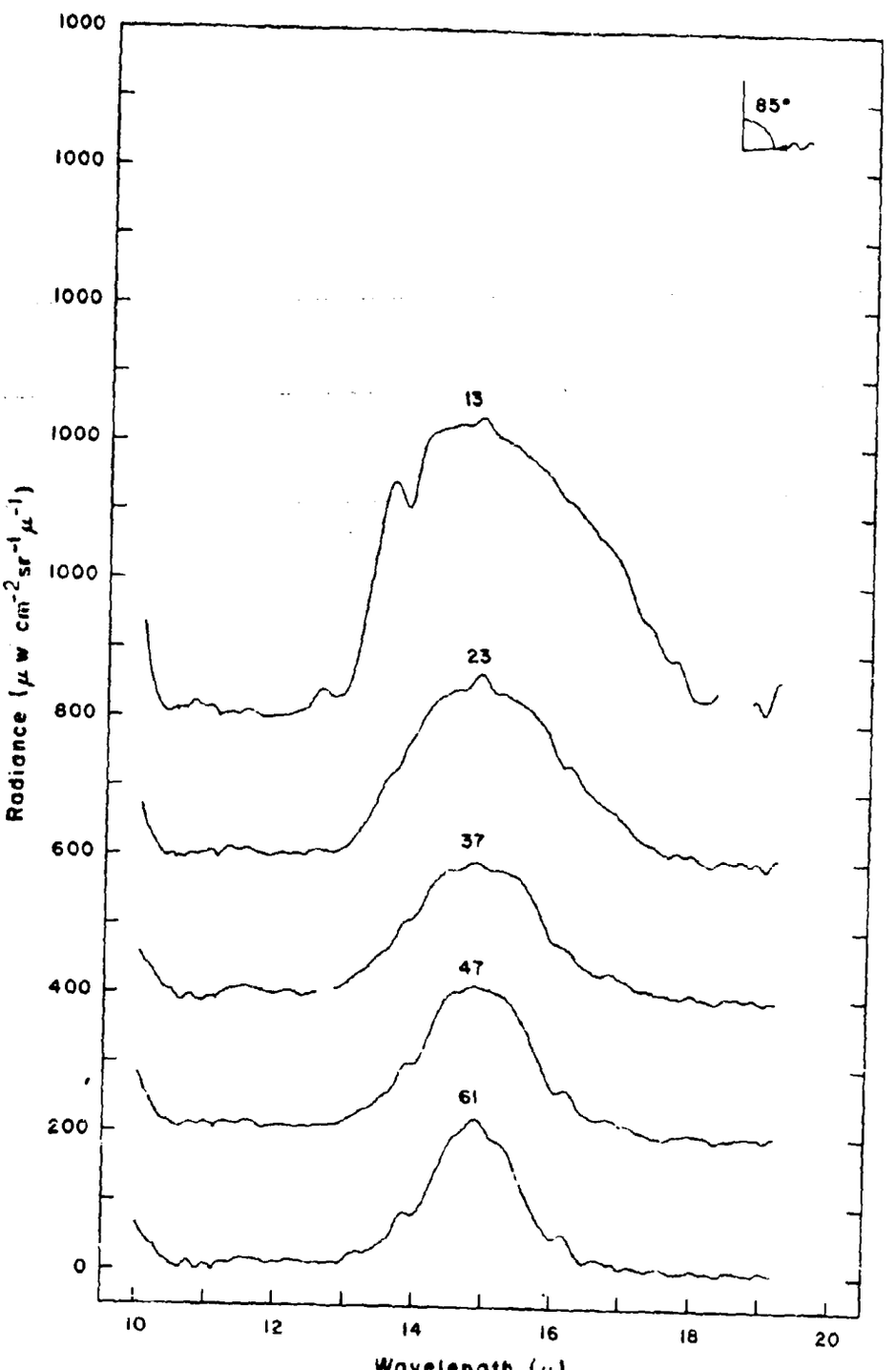

Figure 95 Spectral radiance vs altitude for balloon flight 25 June 1968. (See Table III)

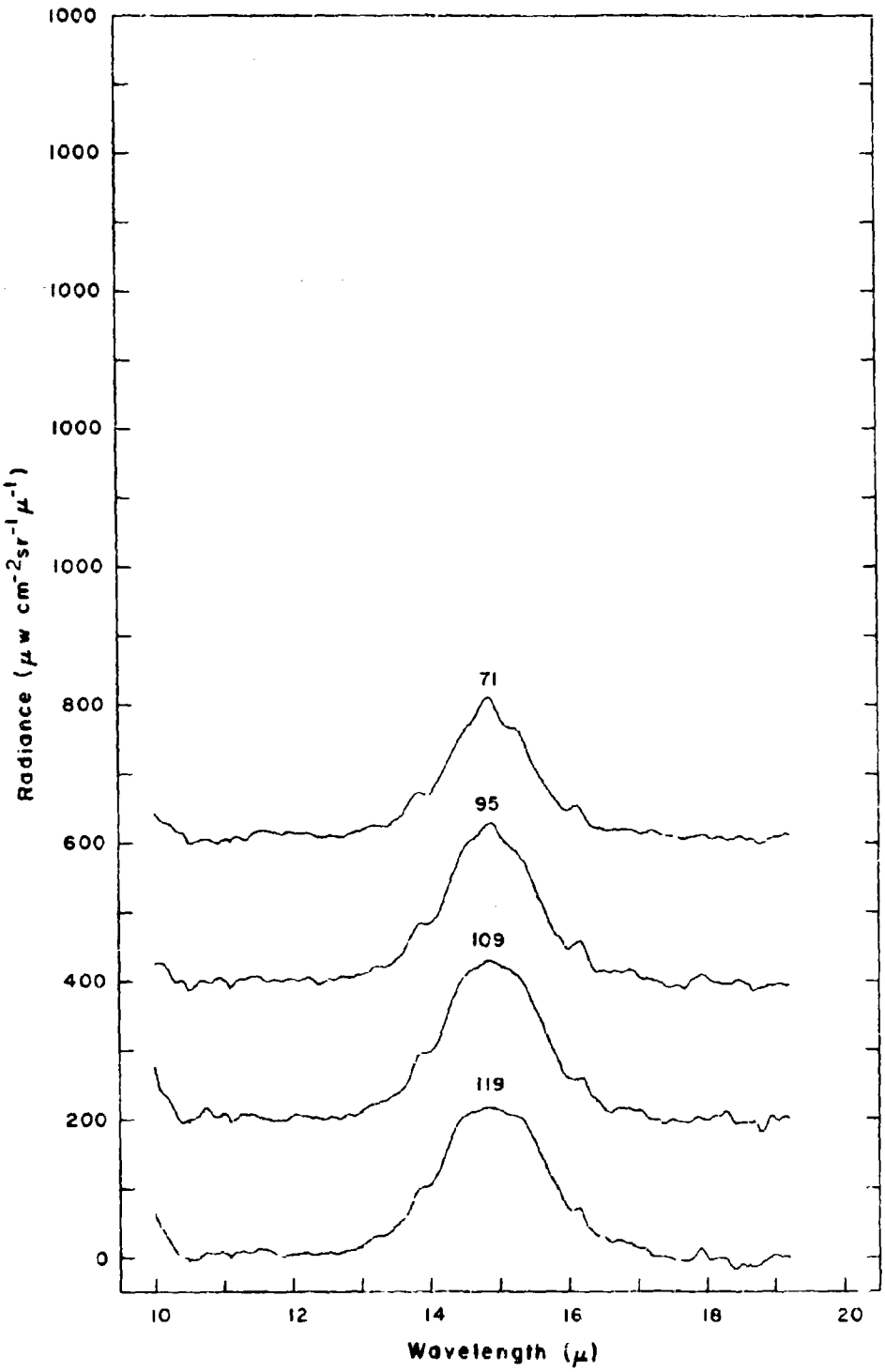

Figure 96 Spectral radiance vs altitude for balloon flight 25 June 1968. (See Table III)

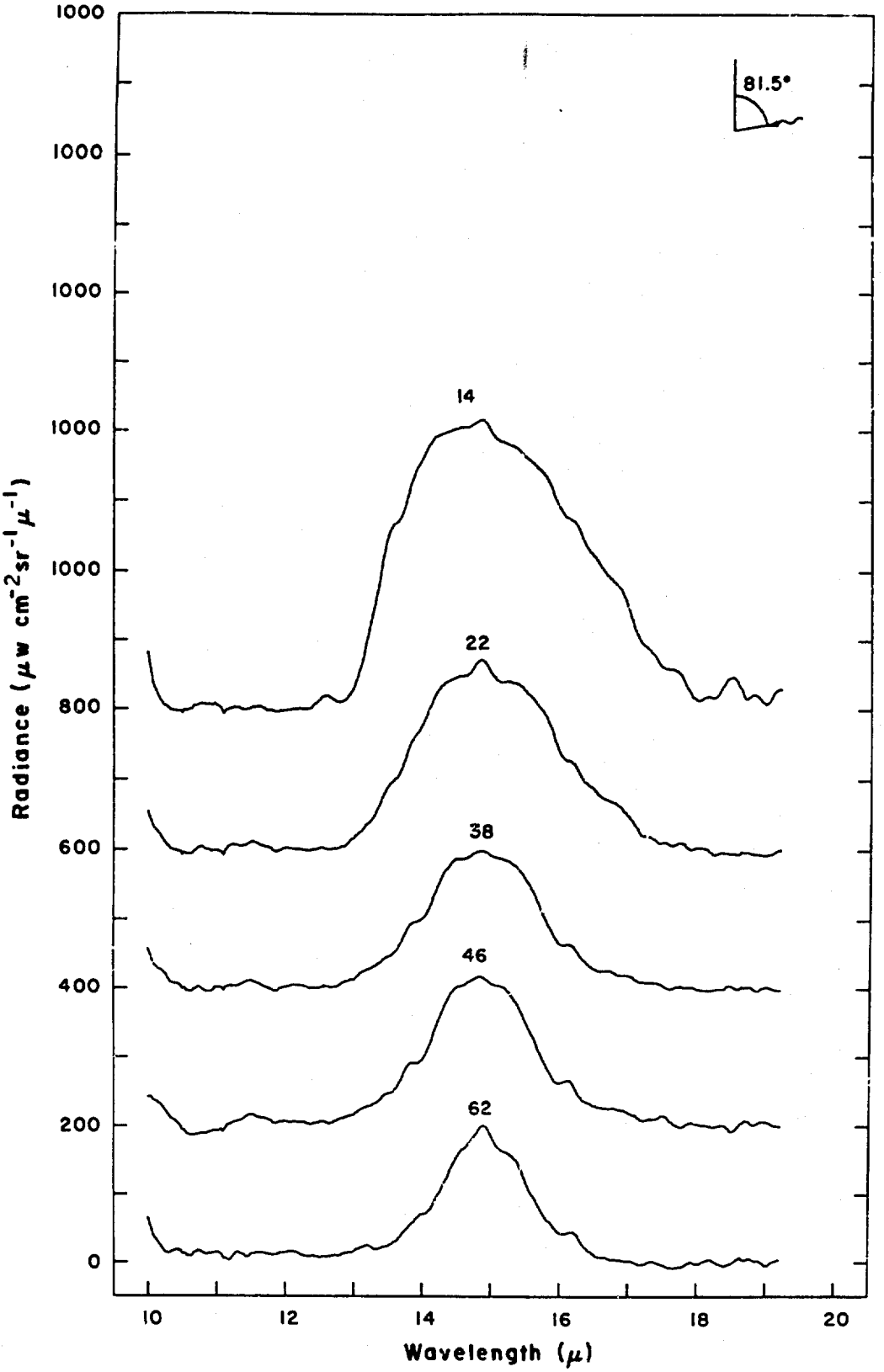

Figure 97 Spectral radiance vs altitude for balloon flight 25 June 1968. (See Table III)

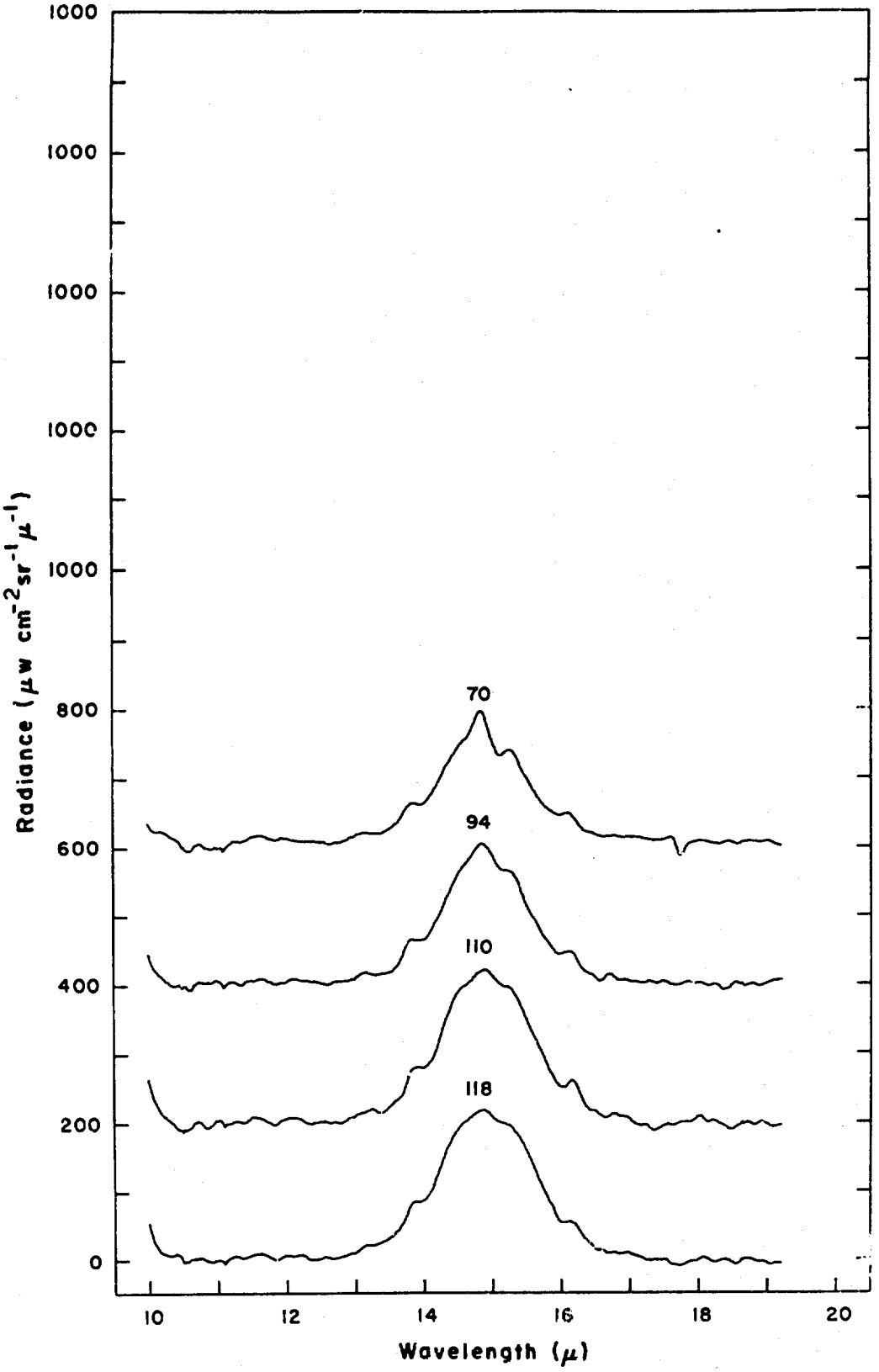

Figure 98 Spectral radiance vs altitude for balloon flight 25 June 1968. (See Table III)

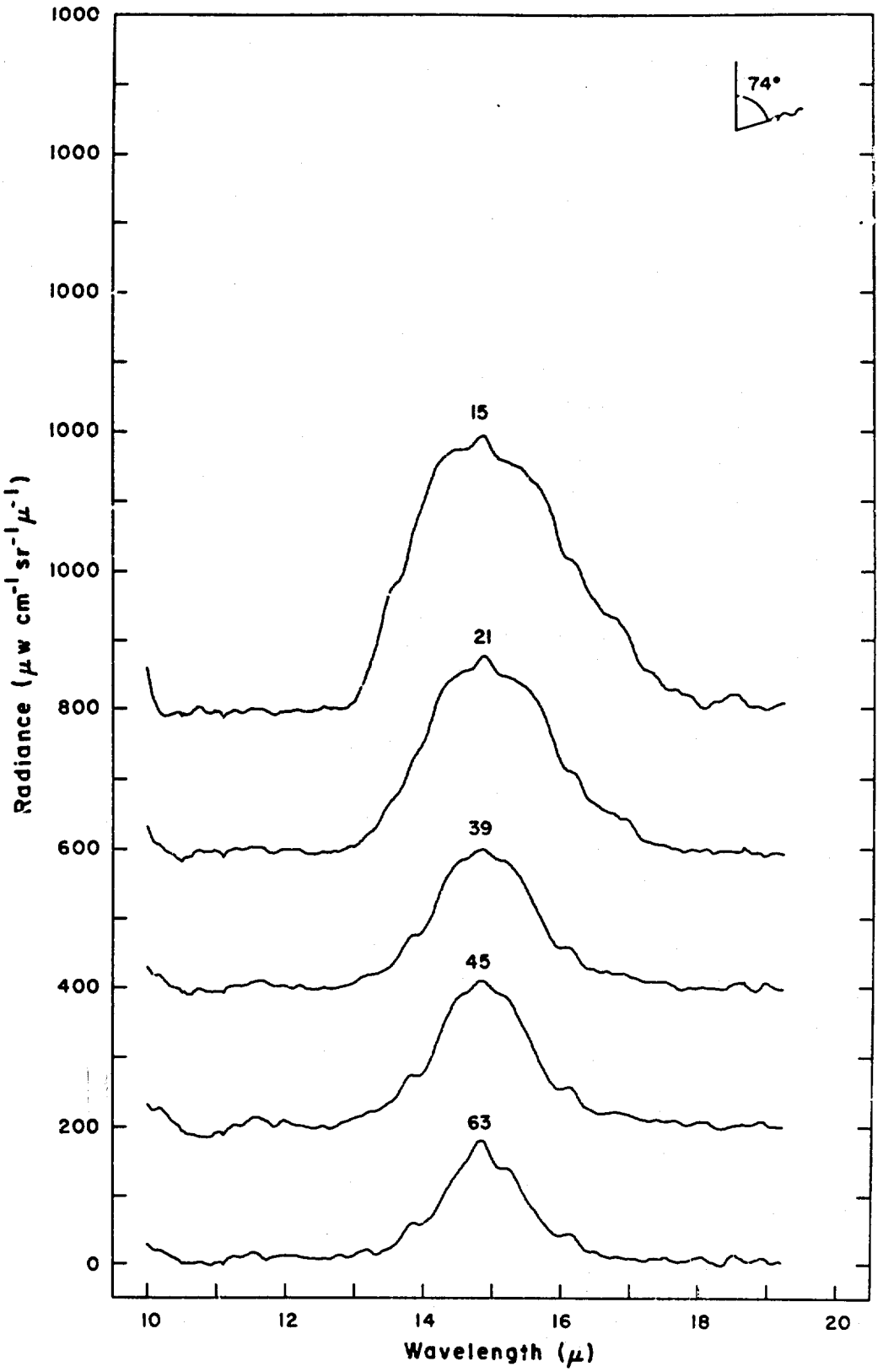

Figure 99 Spectral radiance vs altitude for balloon flight 25 June 1968. (See Table III)

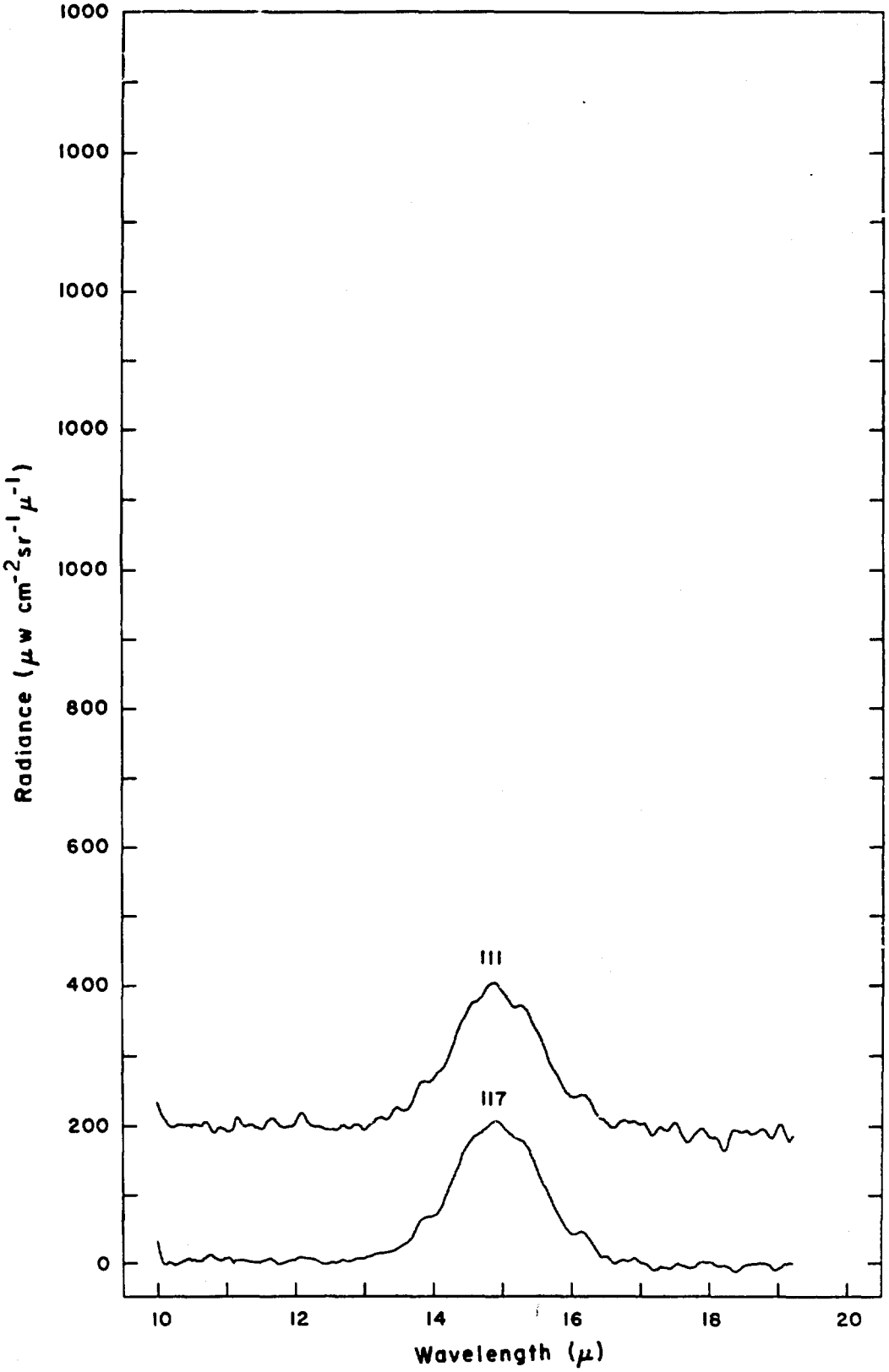

Figure 100 Spectral radiance vs altitude for balloon flight 25 June 1965. (See Table III)

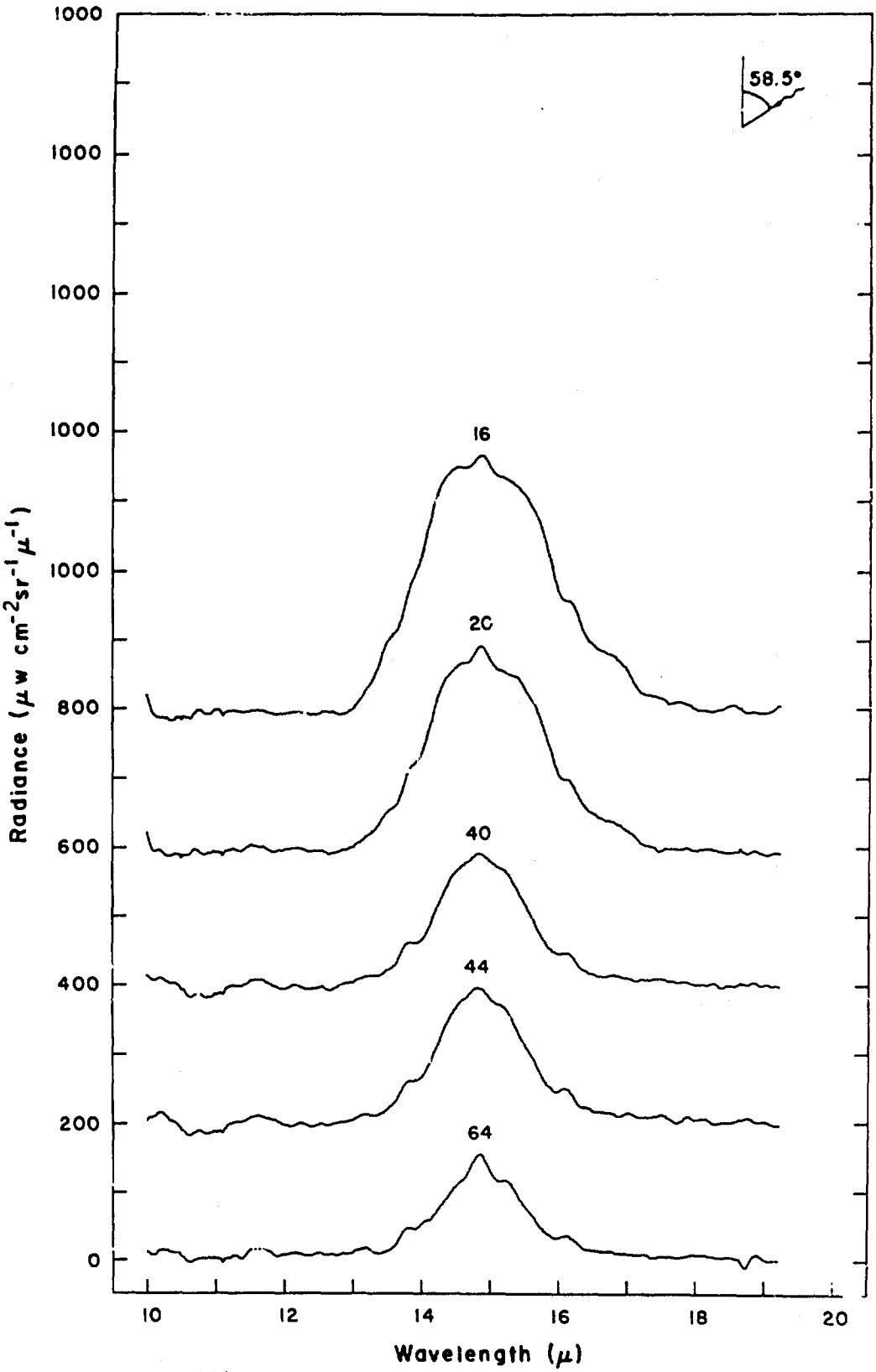

Figure 101 Spectral radiance vs altitude for balloon flight 25 June 1968. (See Table III)

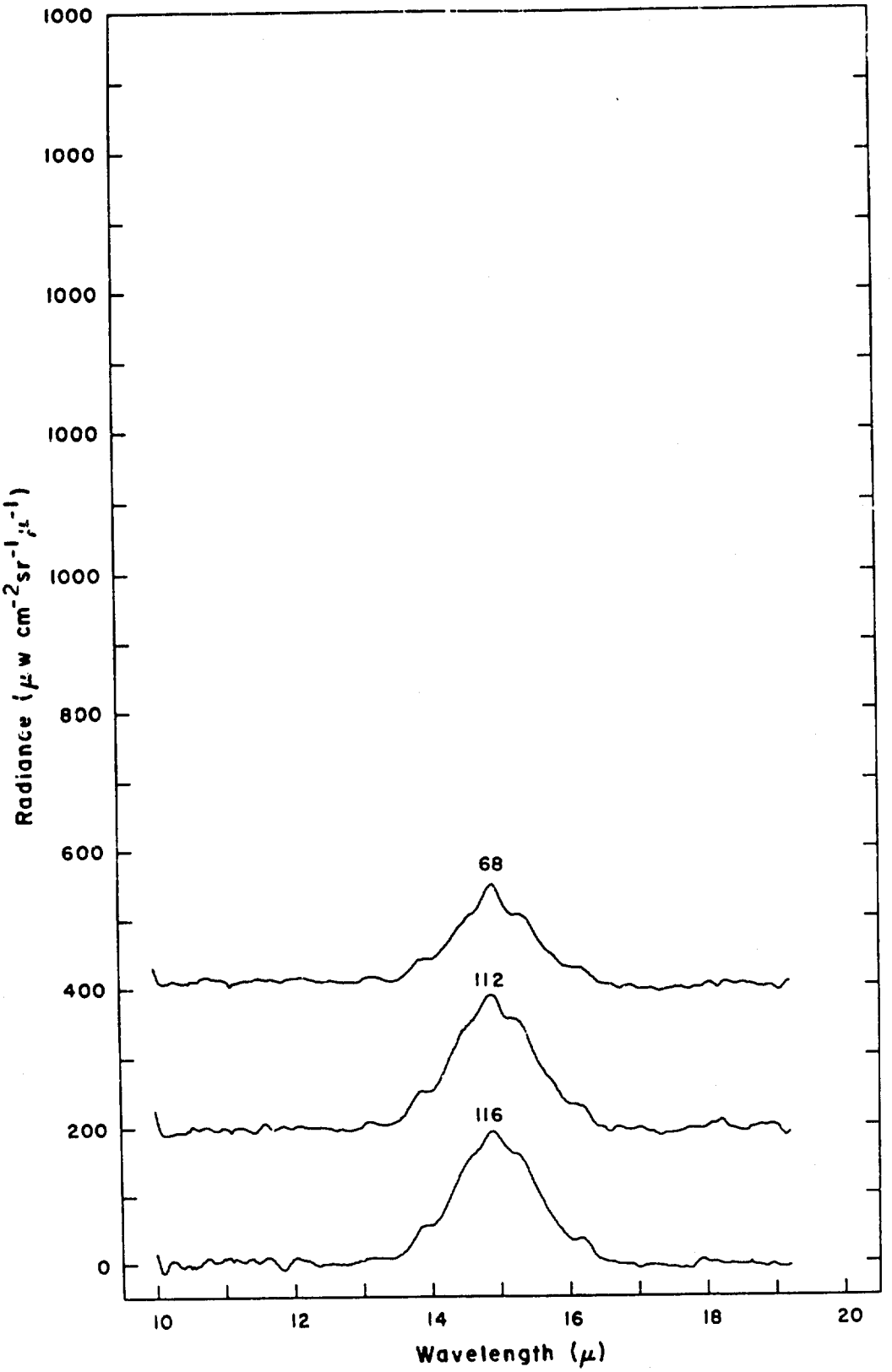

Figure 102 Spectral radiance vs altitude for balloon flight 25 Jun 1968. (See Table III)

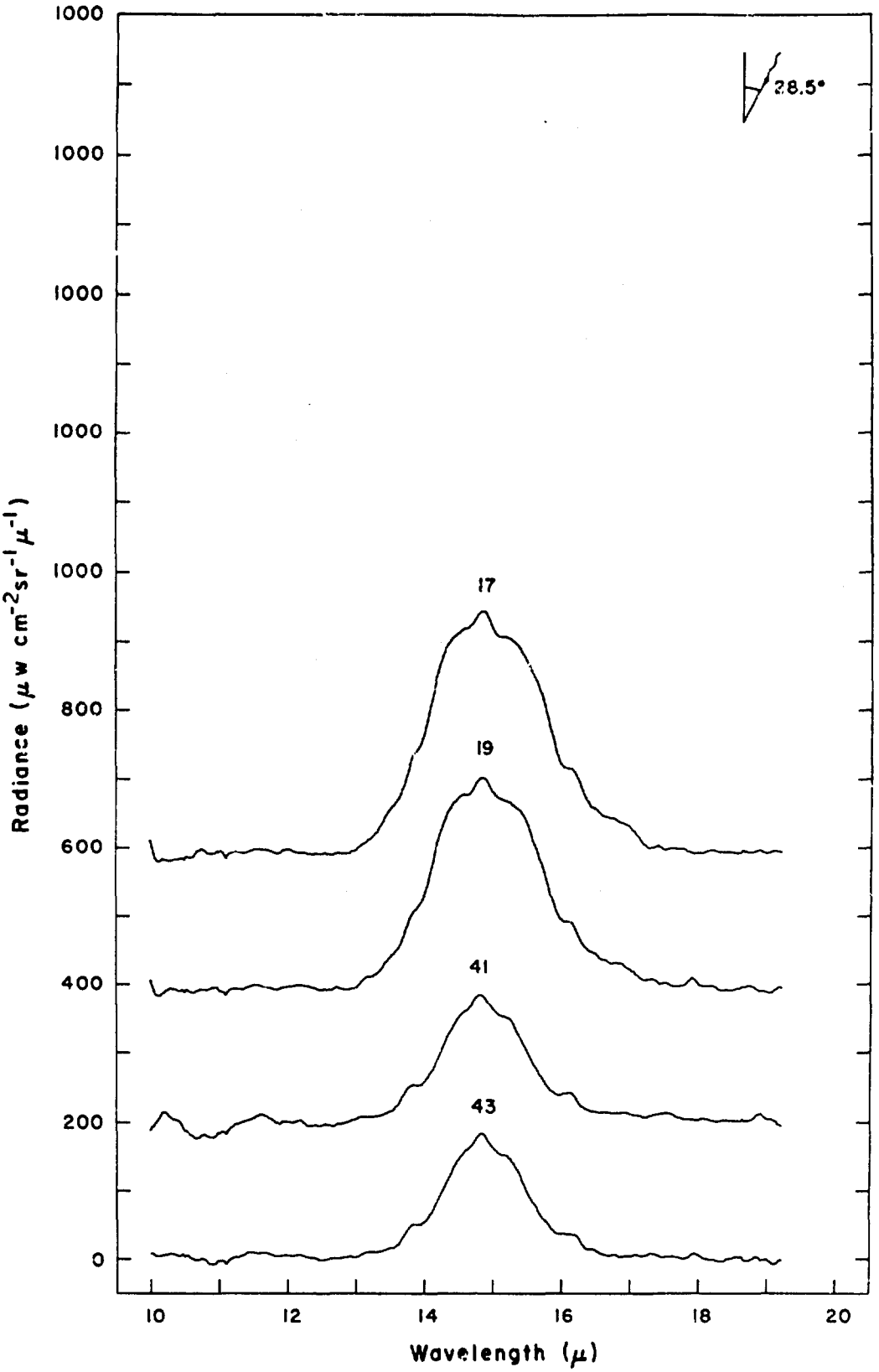

Figure 103 Spectral radiance vs altitude for balloon flight 25 June 1968. (See Table III)

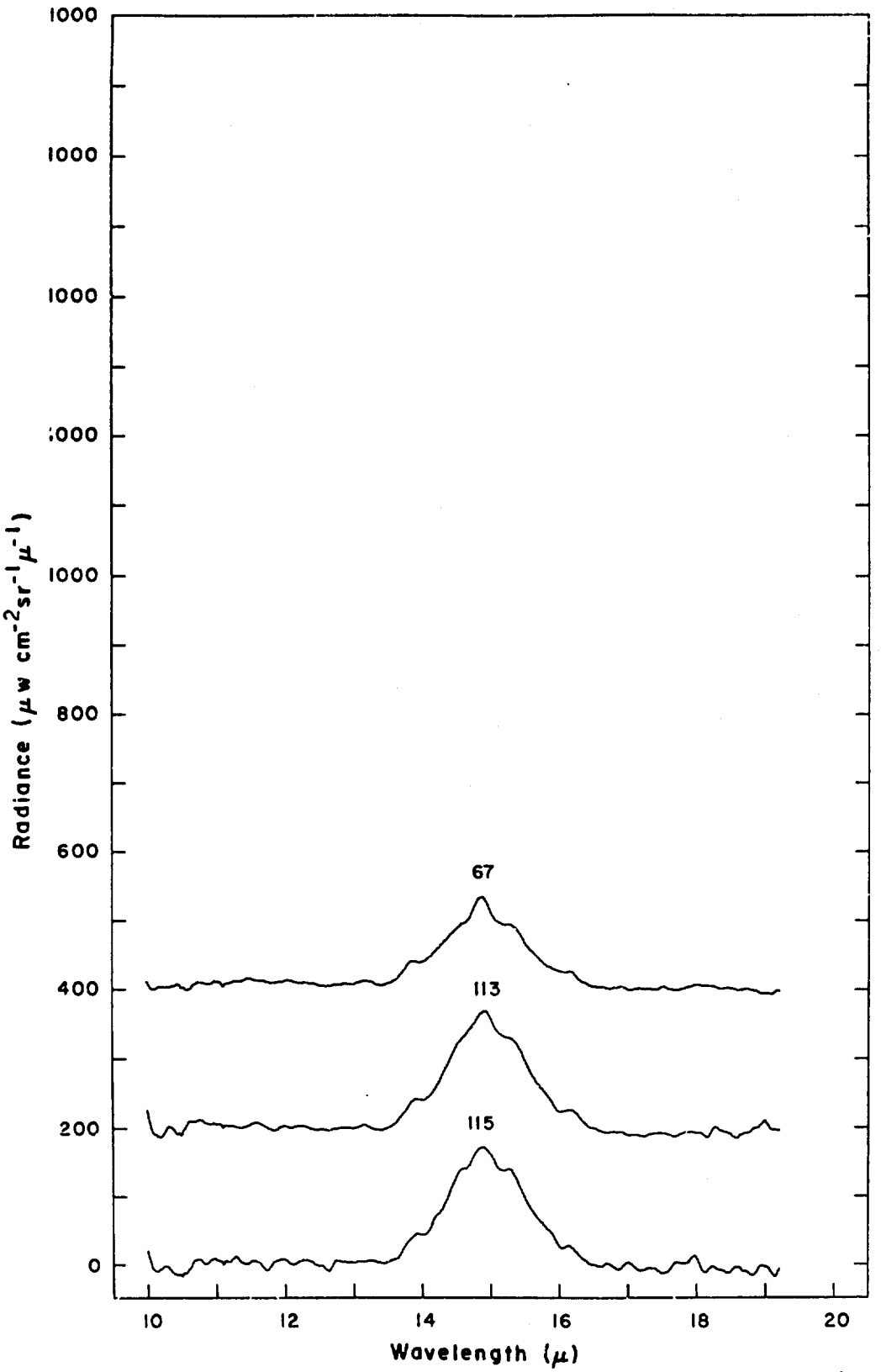

Figure 104 Spectral radiance vs altitude for balloon flight 25 June 1968. (See Table III)

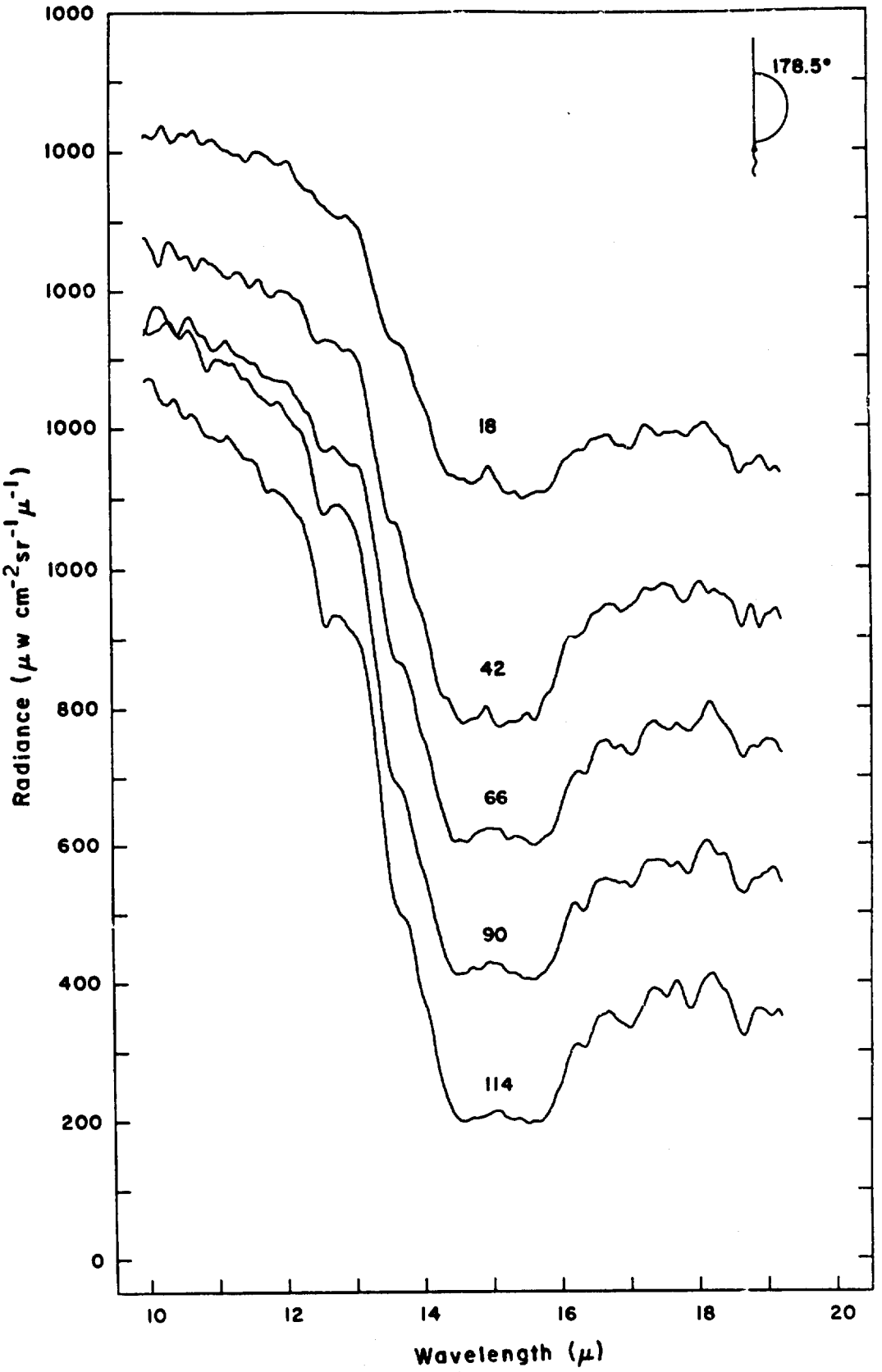

Figure 105 Spectral radiance vs altitude for balloon flight 25 June 1968. (See Table III)

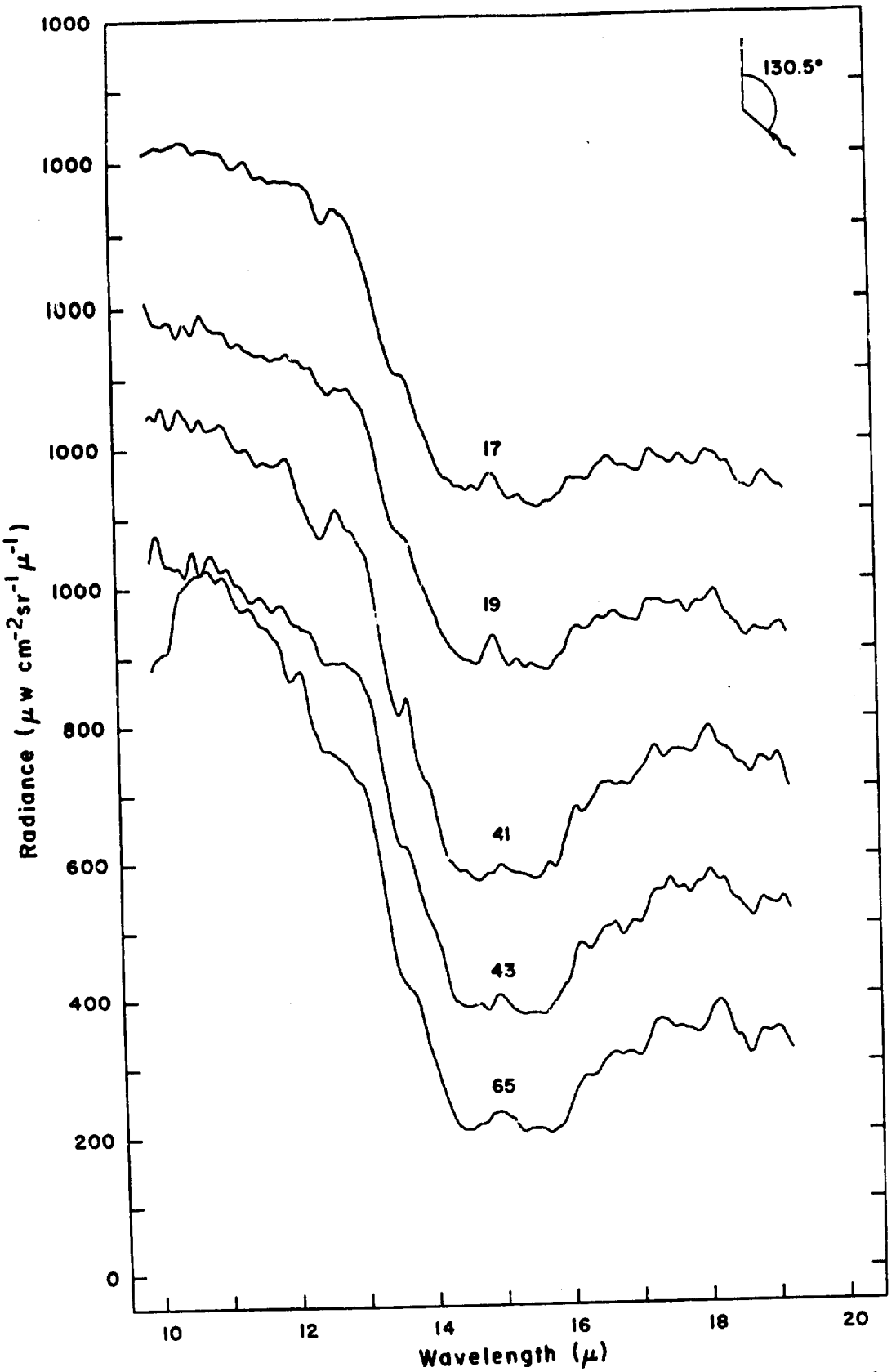

Figure 106 Spectral radiance vs altitude for balloon flight 25 Jan. 1968. (See Table XXX)

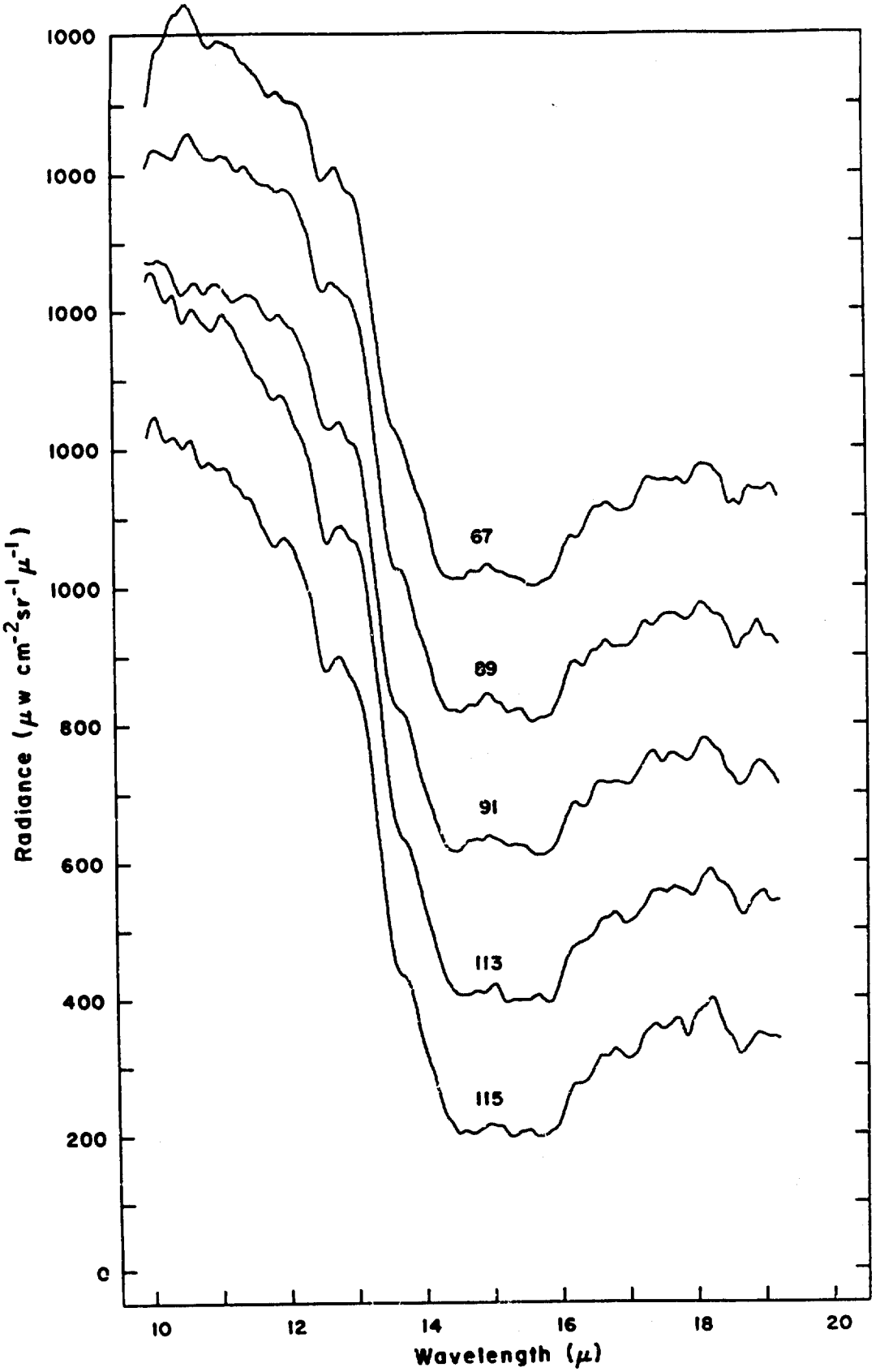

Figure 107 Spectral radiance vs altitude for balloon flight 25 June 1968. (See Table IVI)

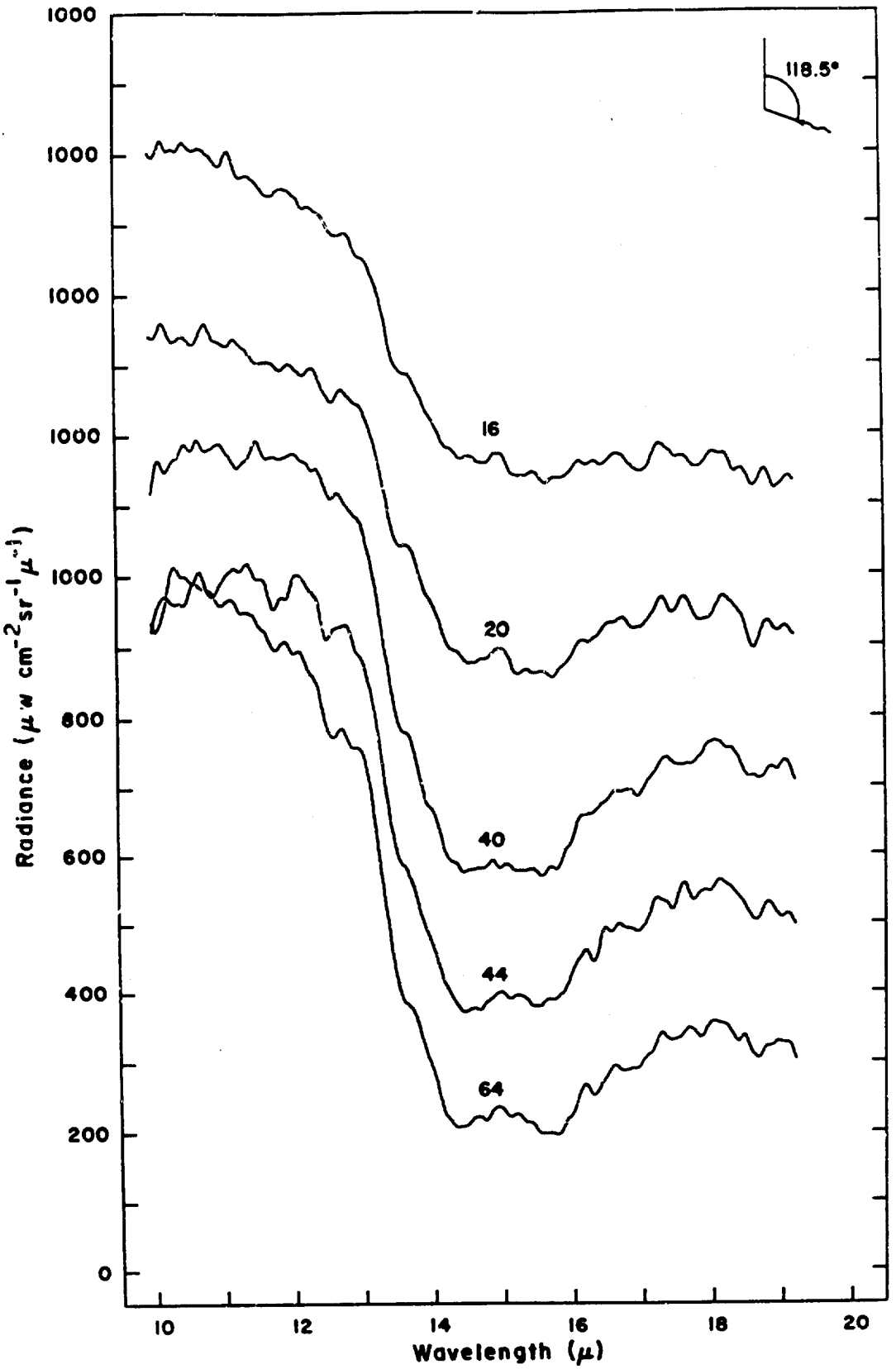

Figure 108 Spectral radiance vs altitude for balloon flight 25 June 1968. (See Table III)

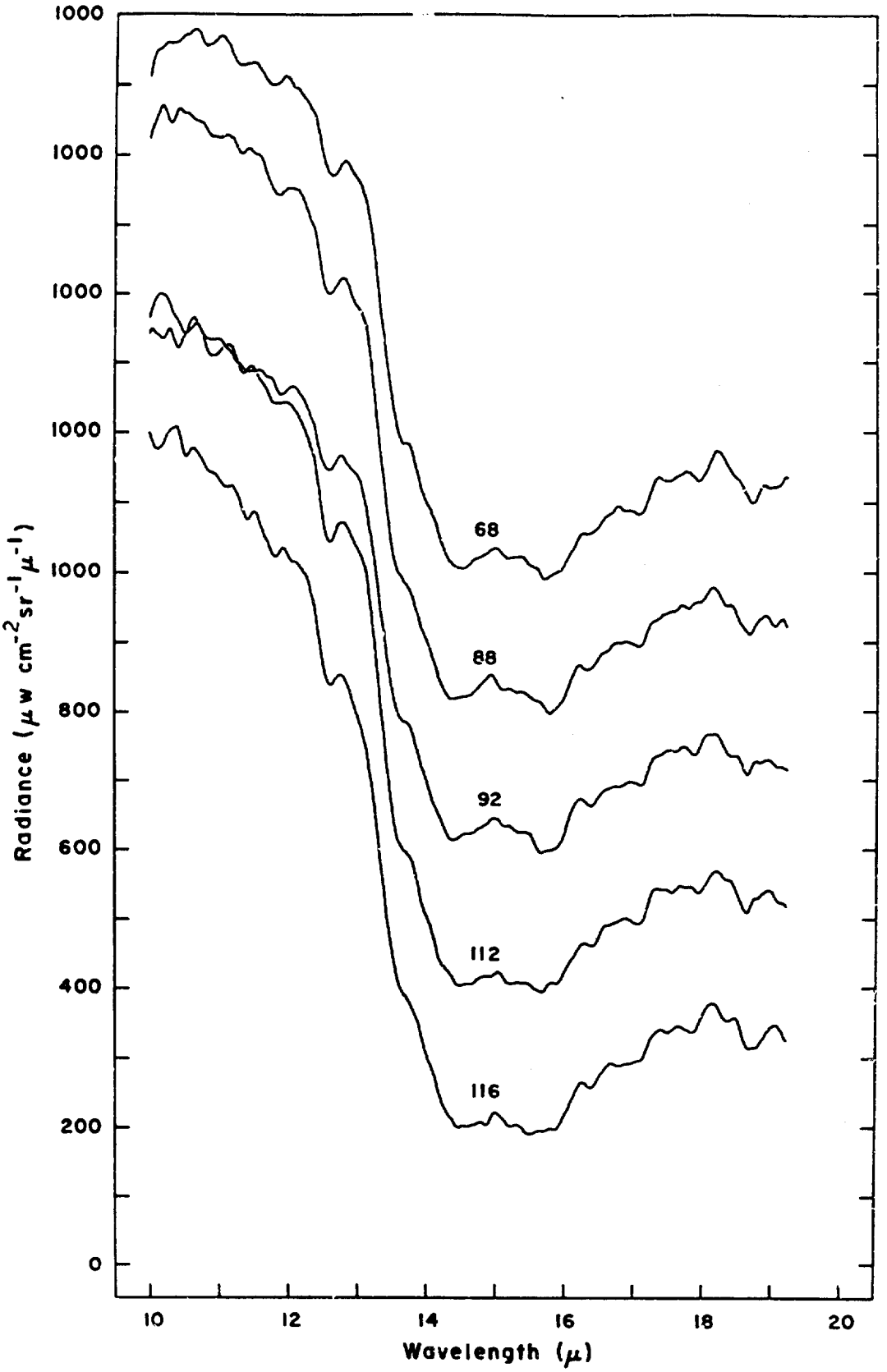

Figure 109 Spectral radiance vs altitude for balloon flight 25 June 1956. (See Table XVI)

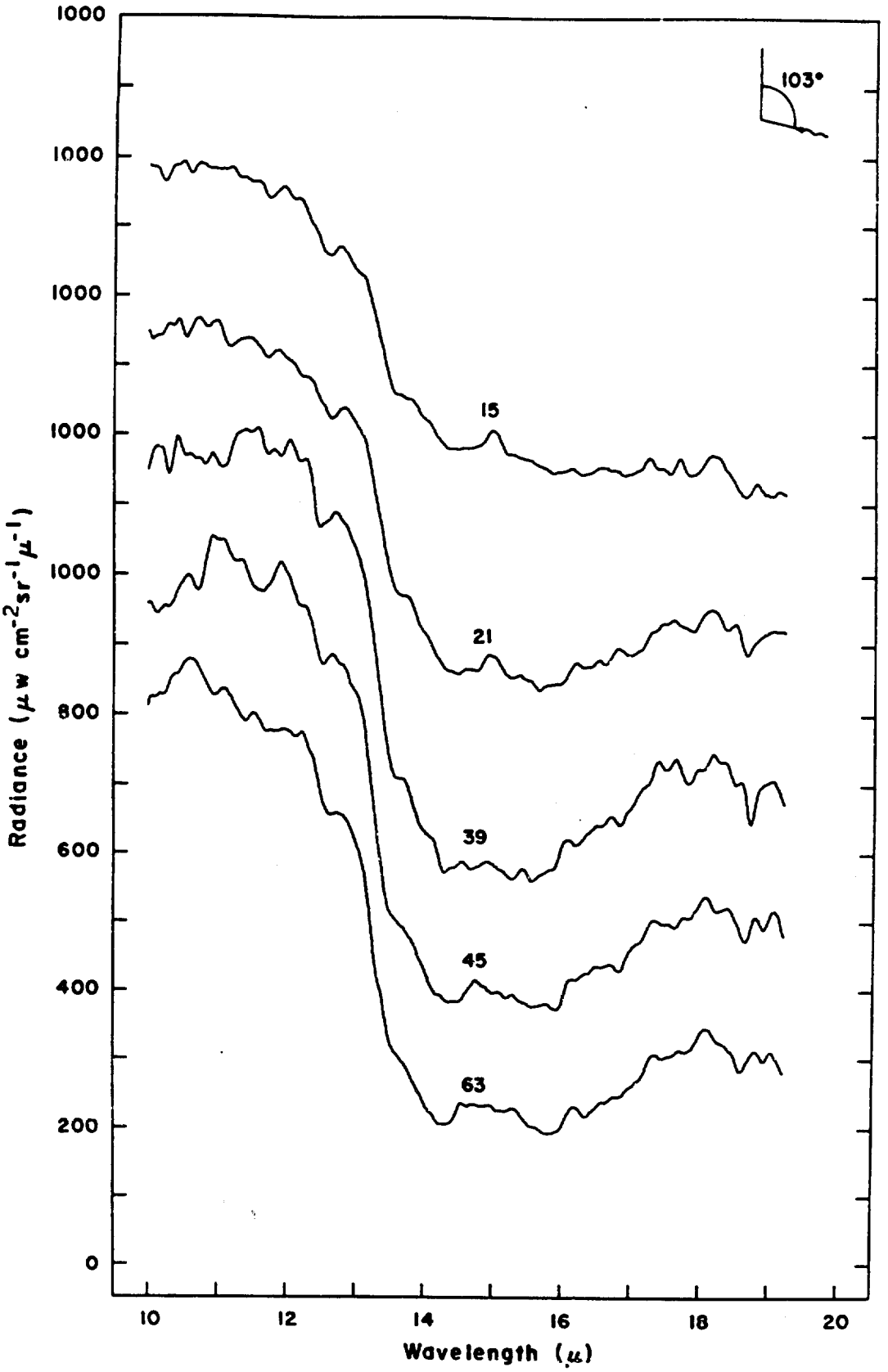

Figure 110 Spectral radiance vs altitude for balloon flight 25 June 1968. (See Table III)

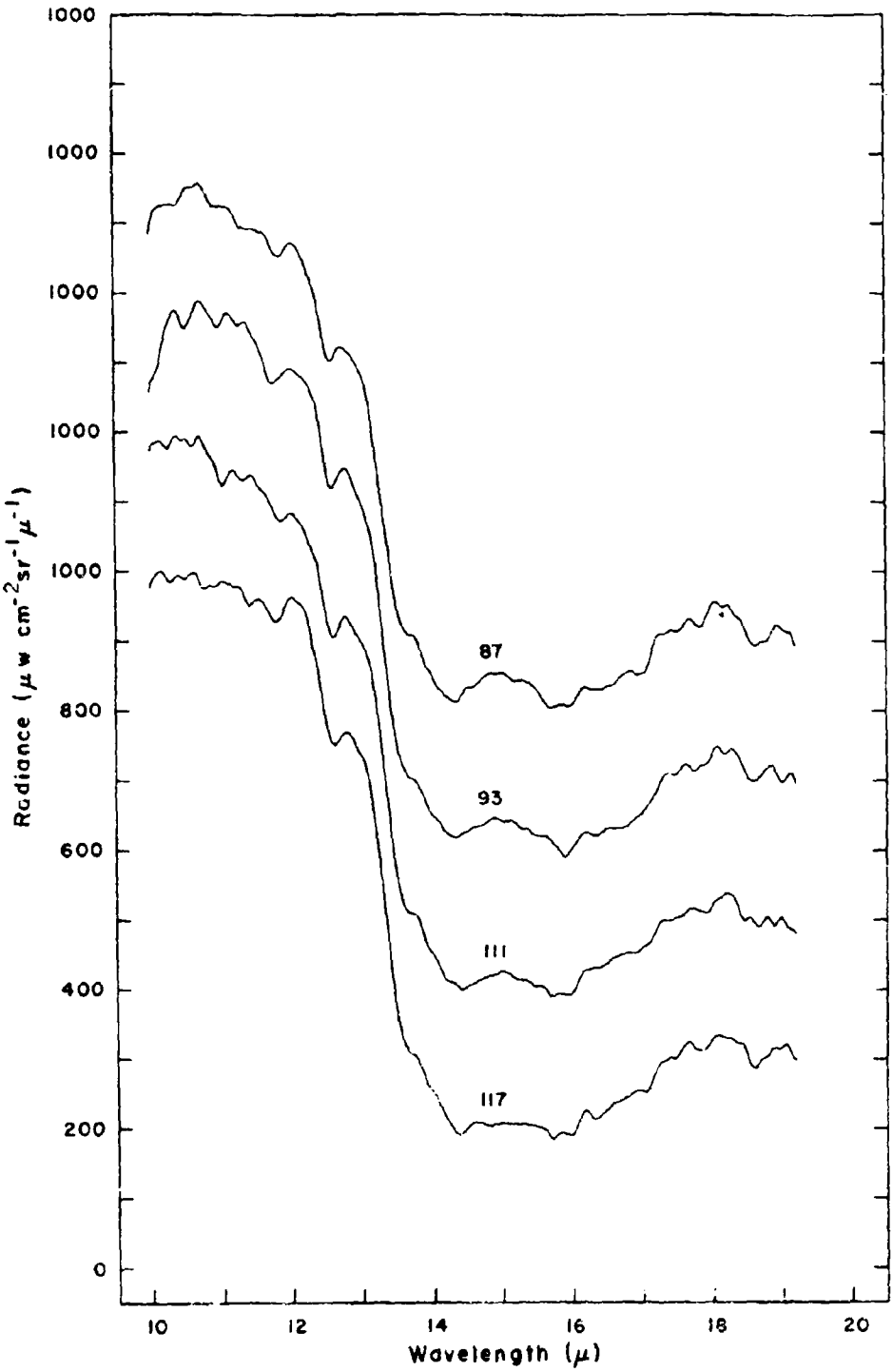

Figure 111 Spectral radiance vs altitude for Tellico flight 25 June 1968. (See Table III)

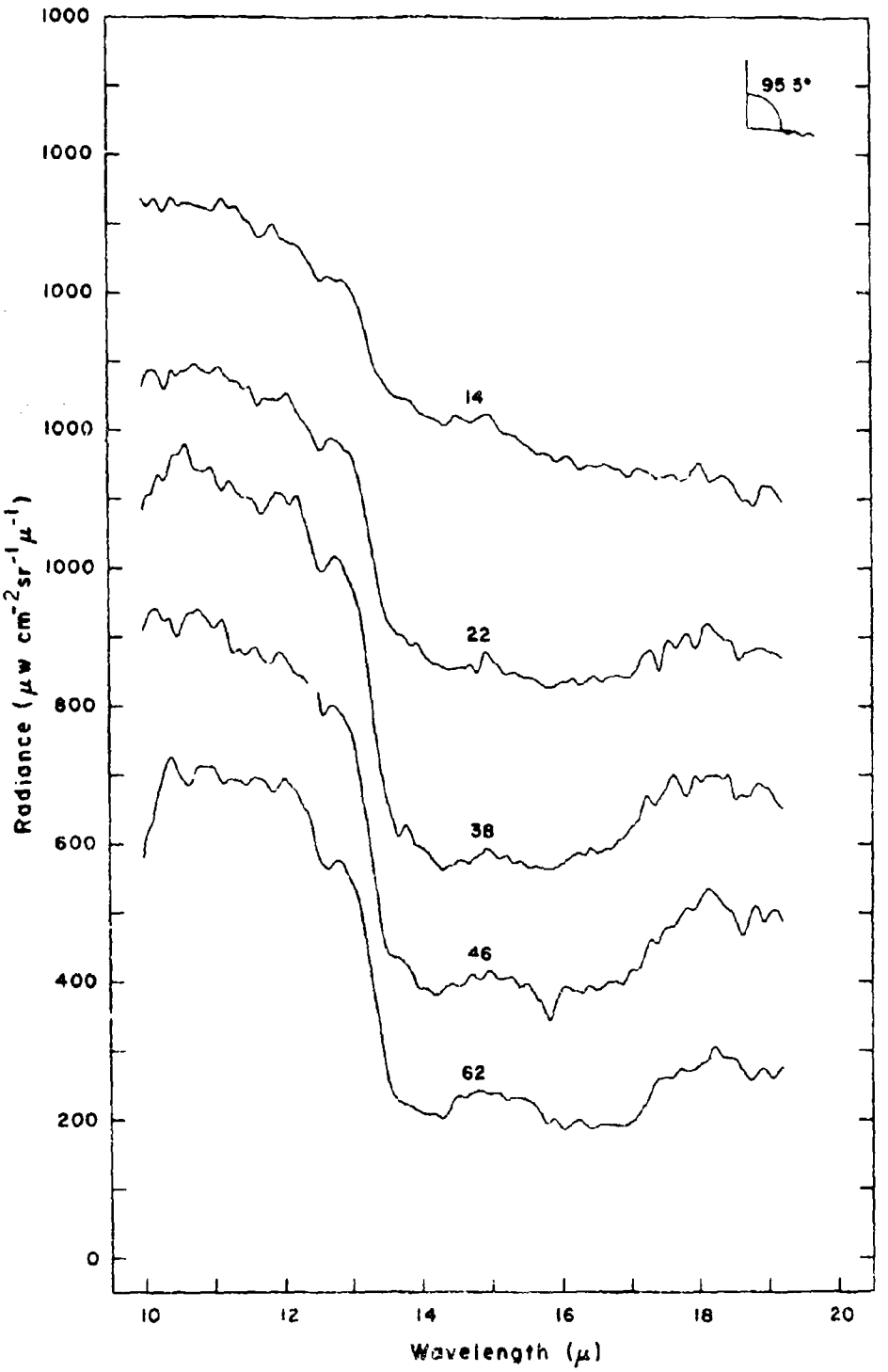

Figure 112 Spectral radiance vs altitude for balloon flight 25 June 1968. (See Table III)

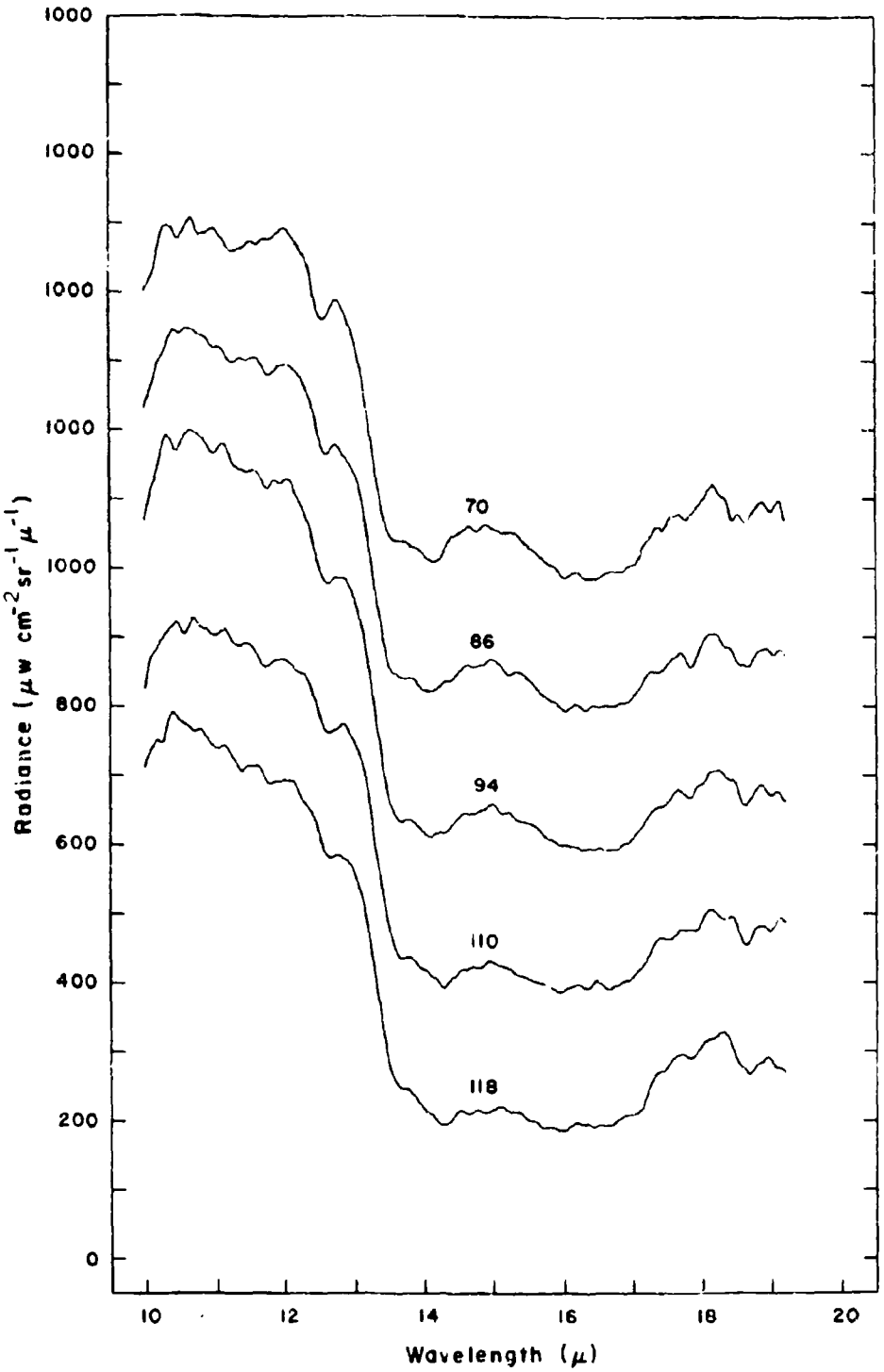

Figure 113 Spectral radiance vs altitude for balloon flight 25 June 1968. (See Table III)

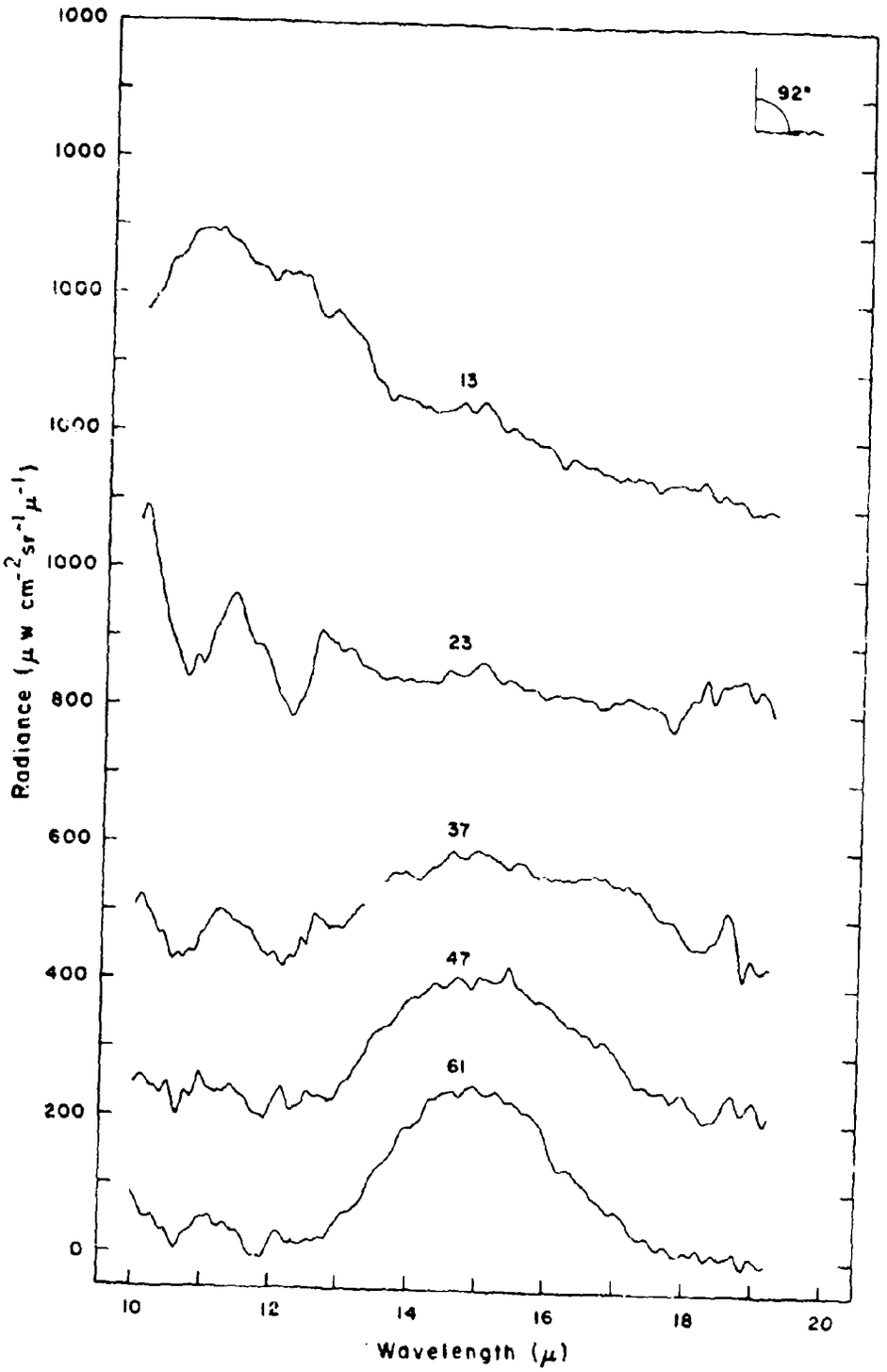

Figure 114 Spectral radiance vs altitude for balloon flight 25 June 1968. (See Table III)

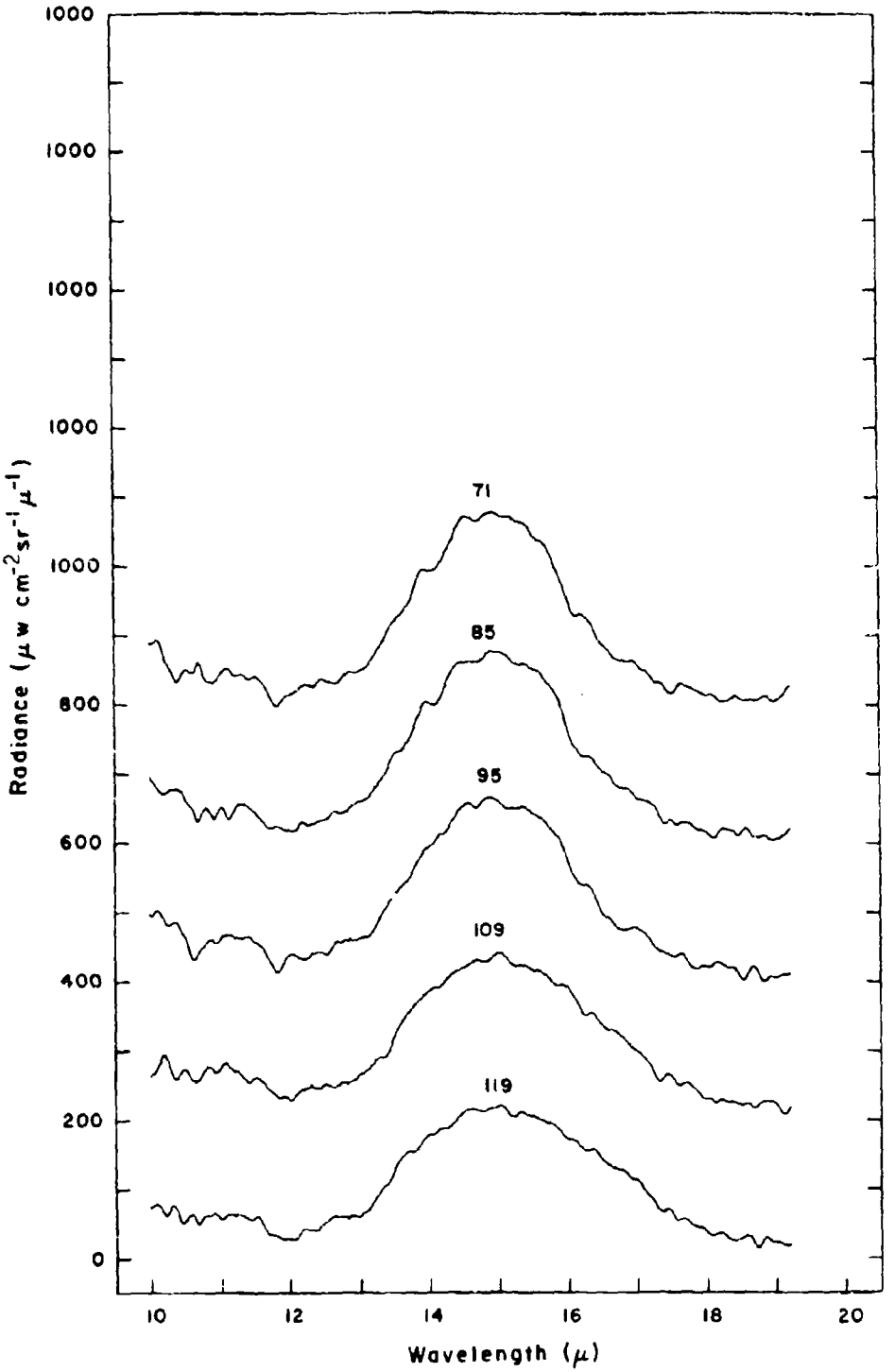

Figure 115 Spectral radiance vs altitude for balloon flight 25 June 1968. (See Table III)

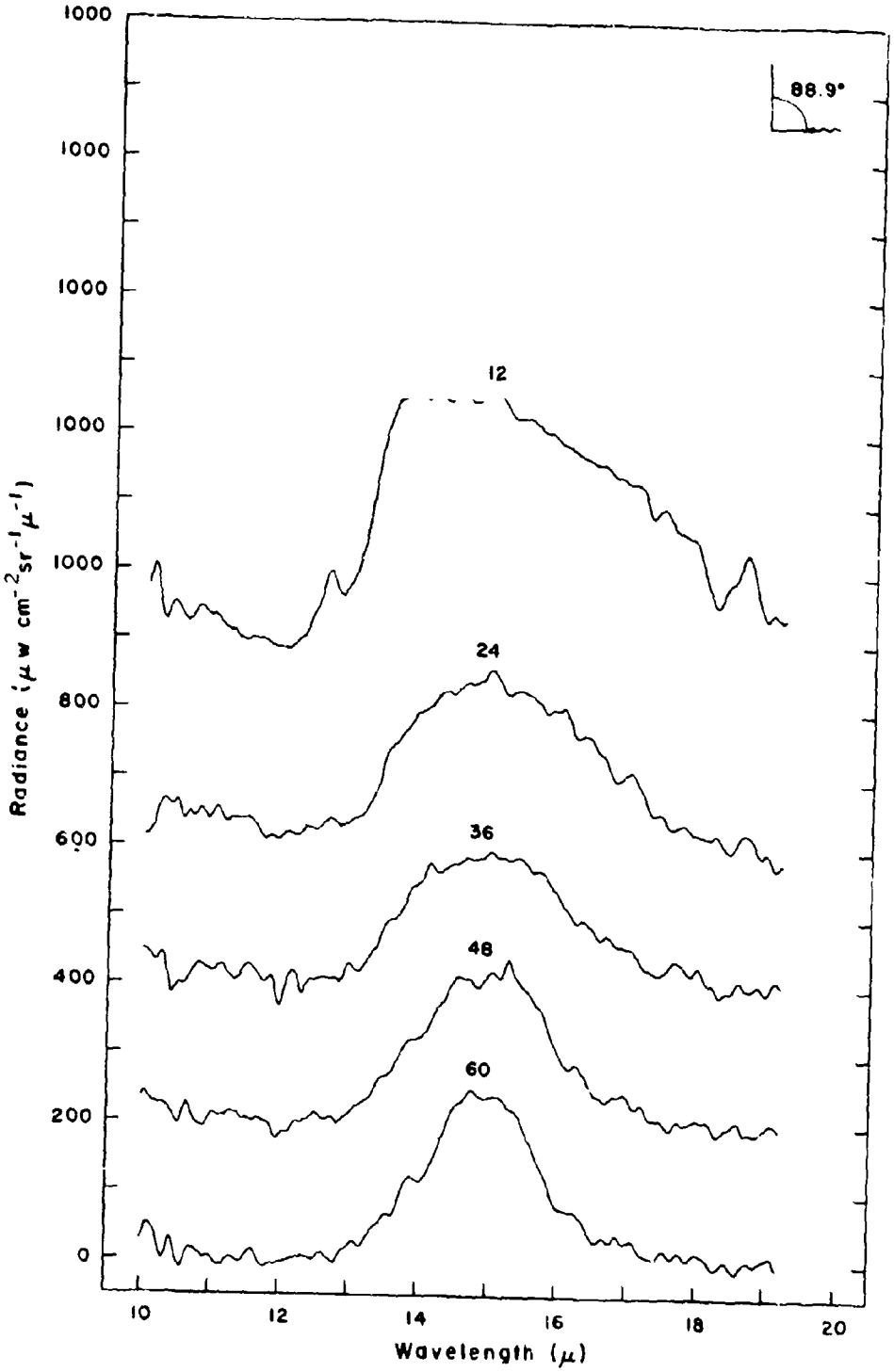

Figure 116 Spectral radiance vs altitude for balloon flight 25 June 1968. (See Table III)

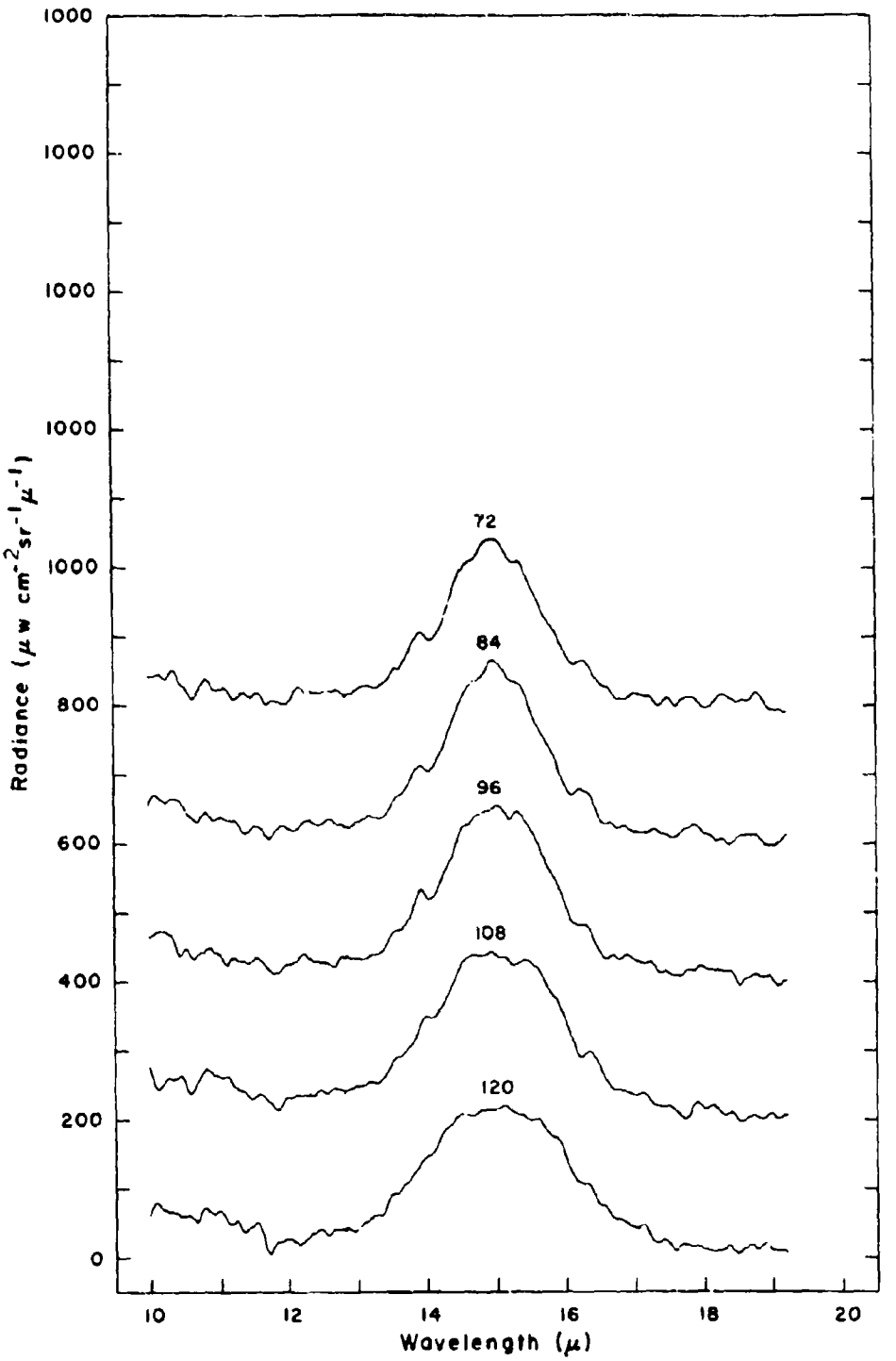

Figure 117 Spectral radiance vs altitude for balloon flight 25 June 1968. (See Table 12-1)

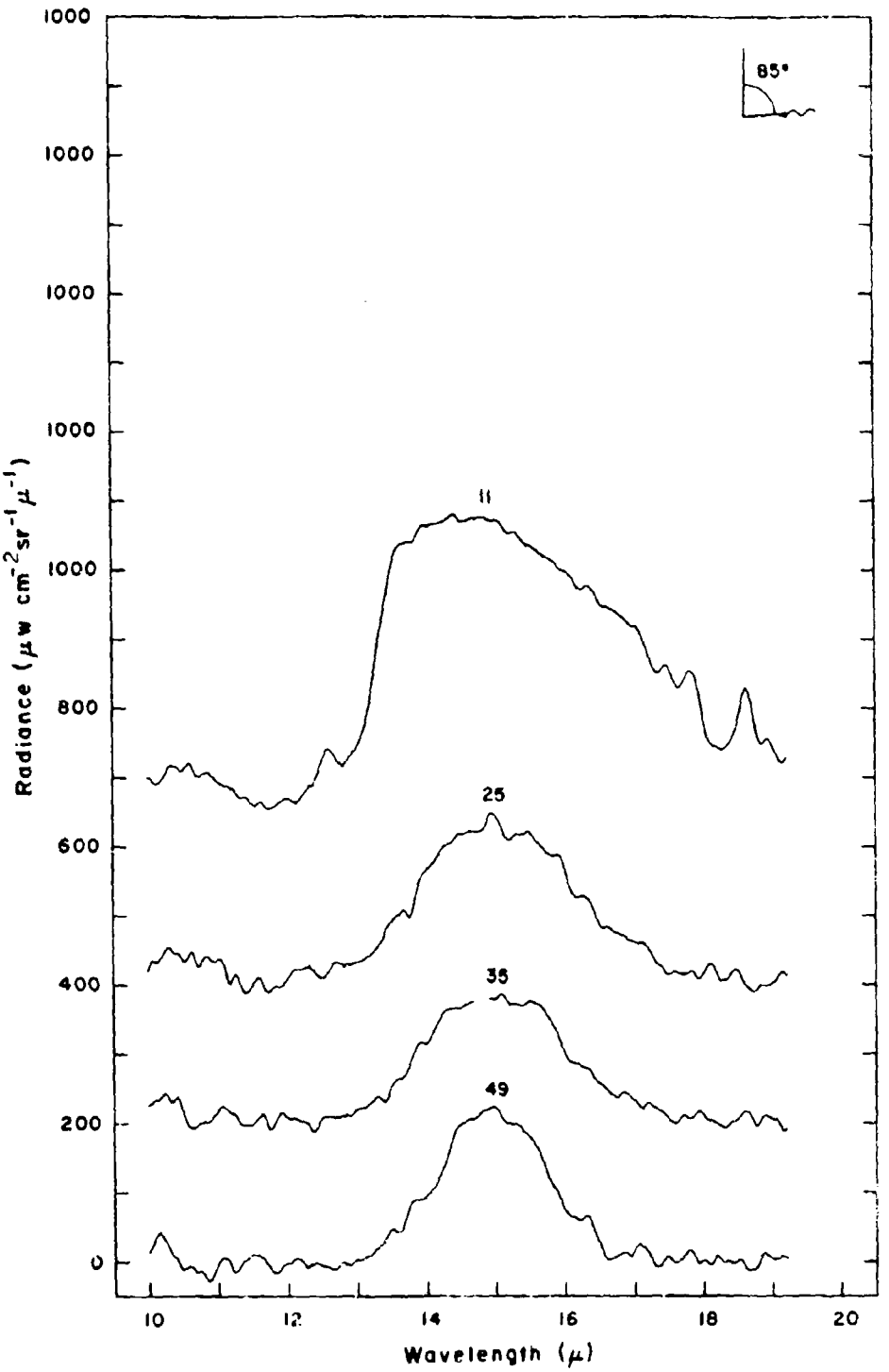

Figure 118 Spectral radiance vs altitude for balloon flight 25 June 1968. (See Table III)

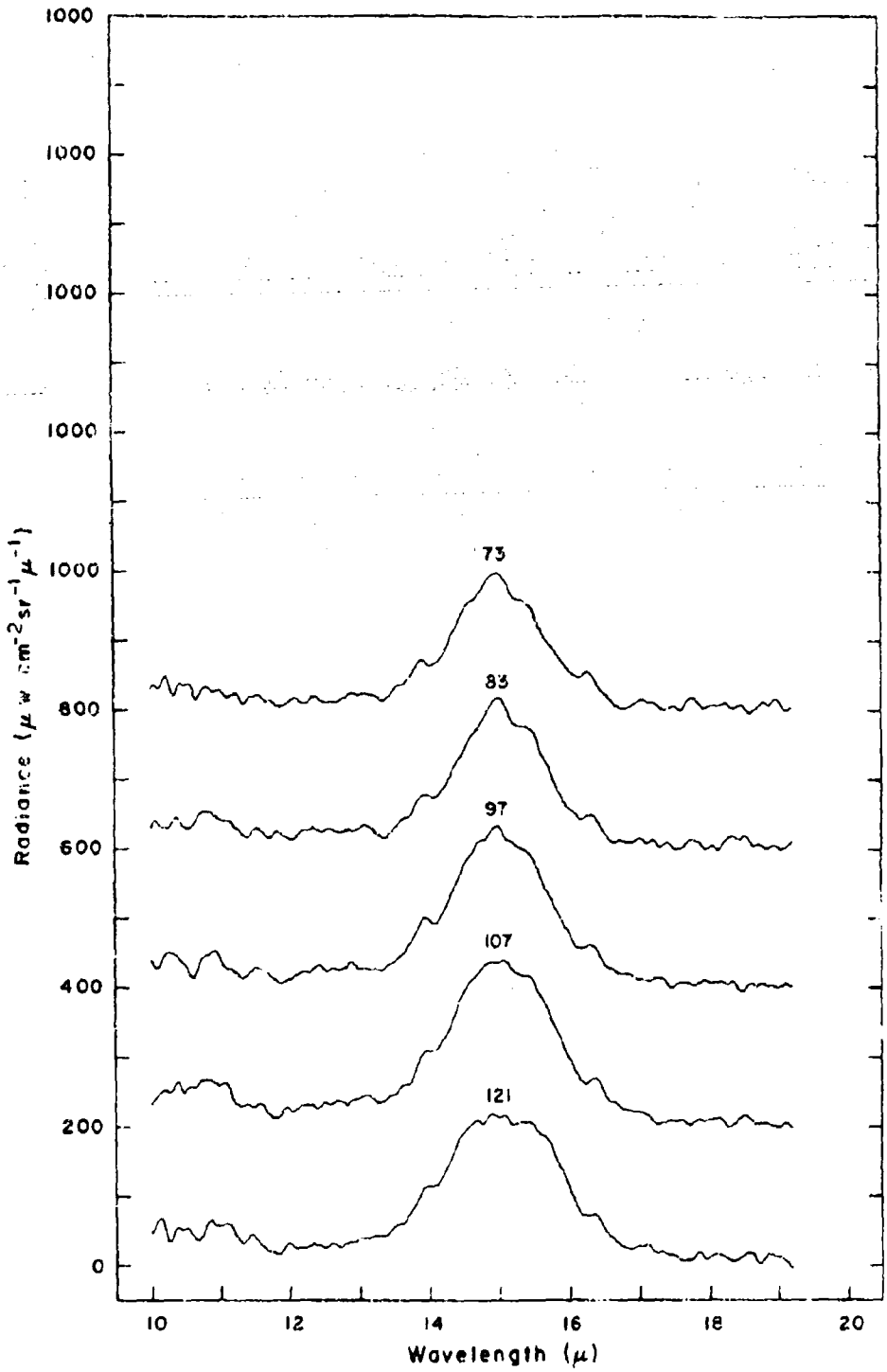

Figure 119 Spectral radiance vs altitude for balloon flight, 25 June 1968. (See Table III)

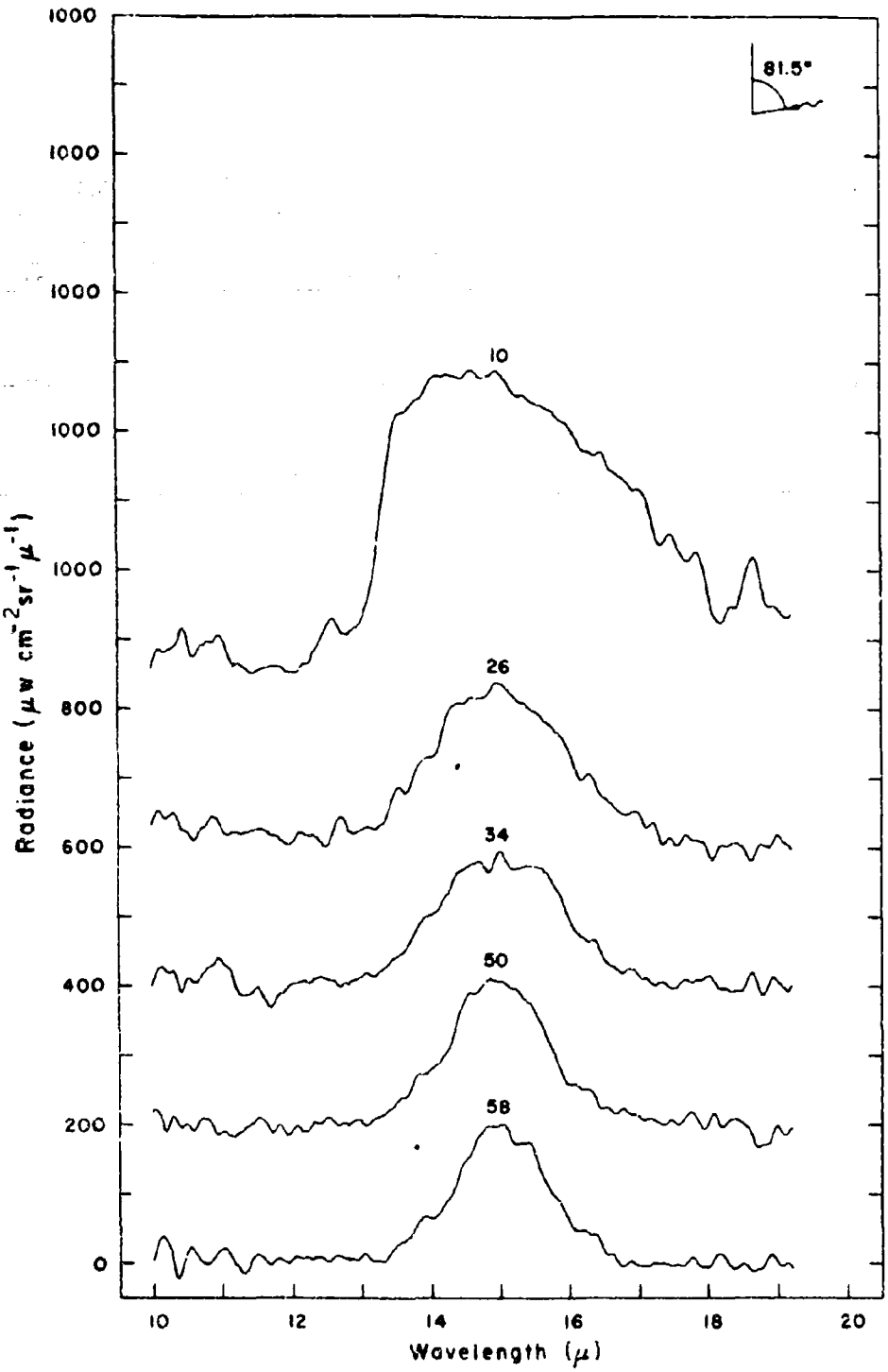

Figure 120 Spectral radiance vs altitude for balloon flight 25 June 1968. (See Table III)

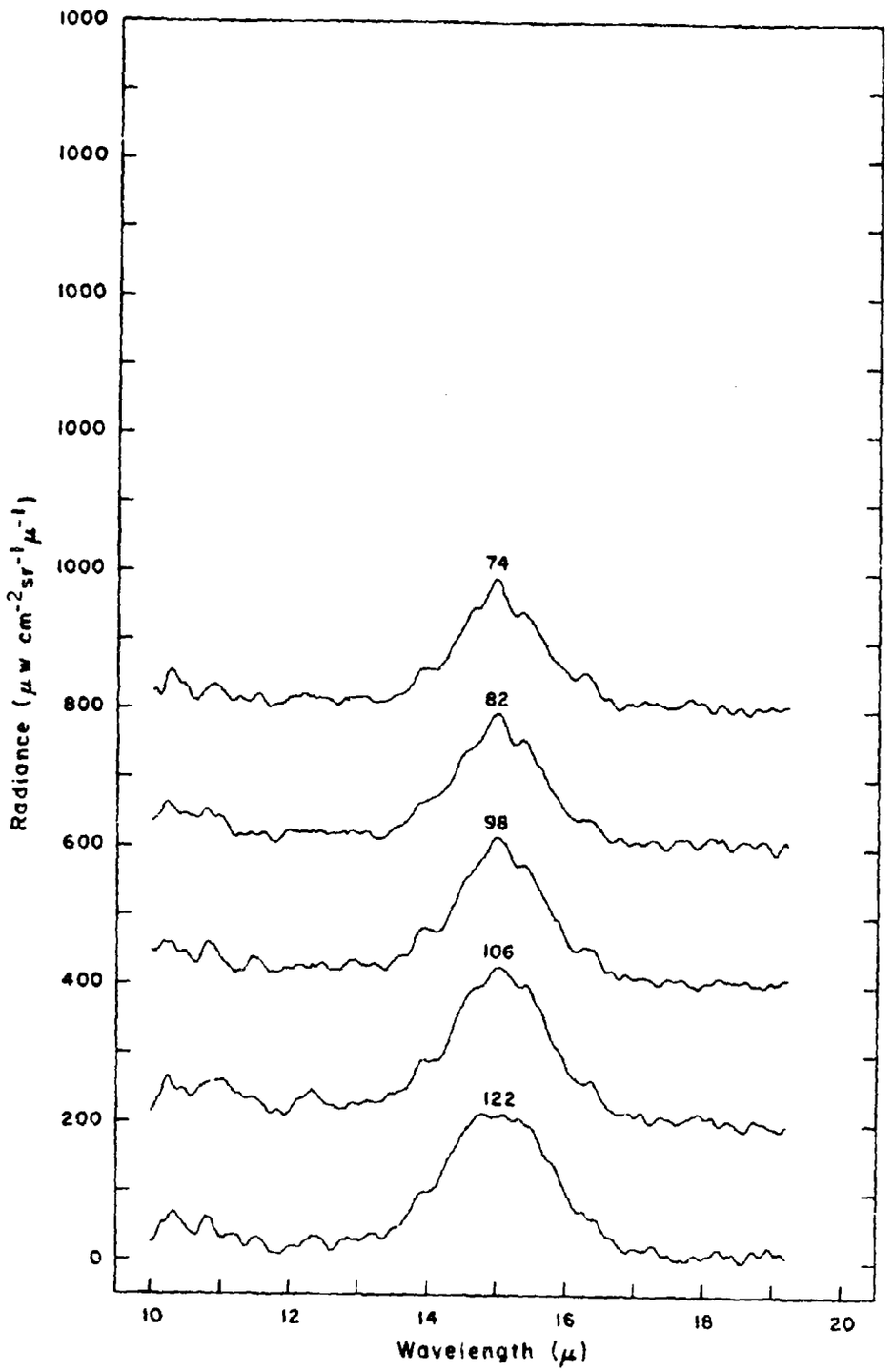

Figure121 Spectral radiance vs altitude for balloon flight 25 June 1968. (See Table III)

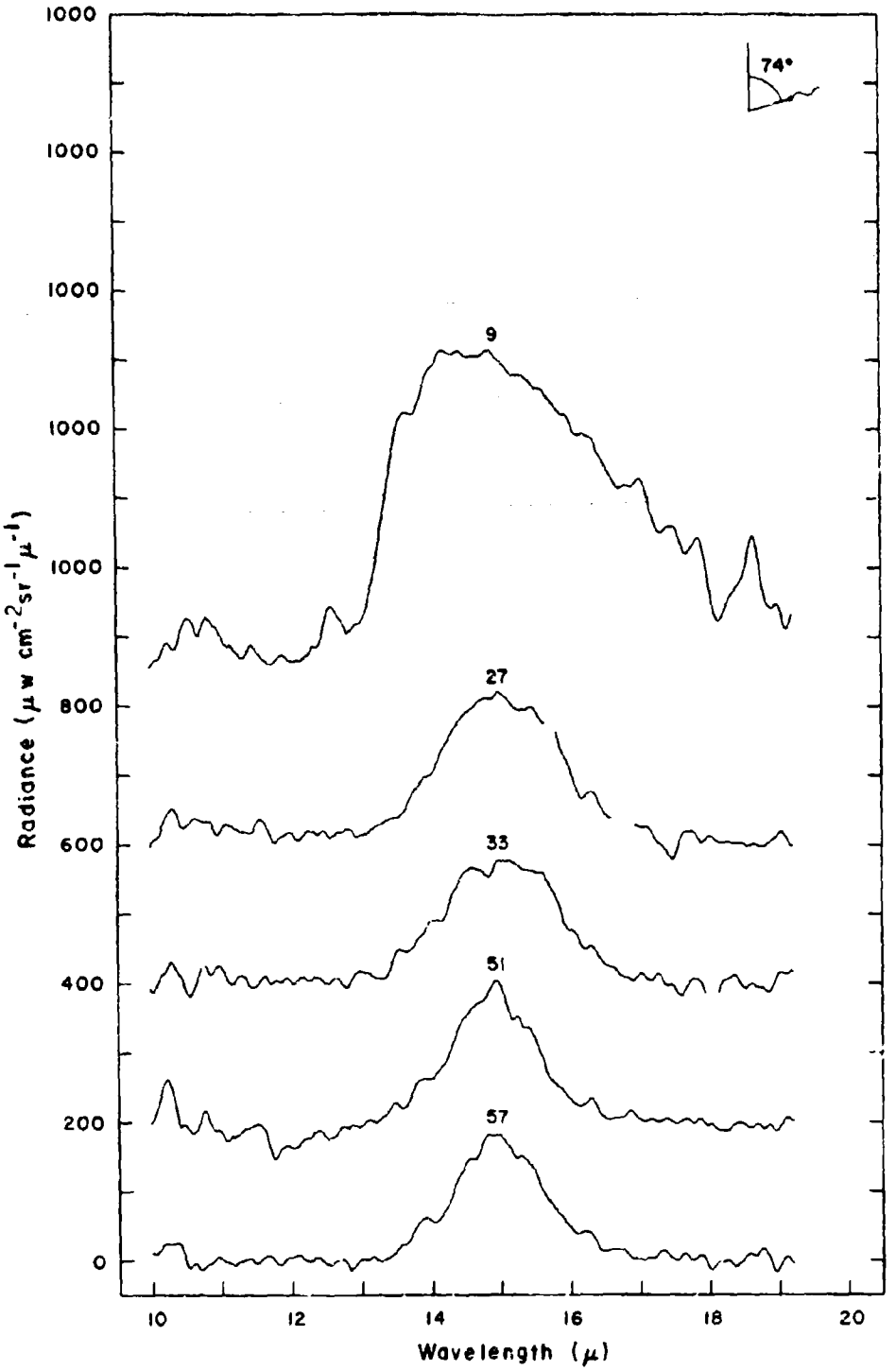

Figure 122 Spectral radiance vs altitude for balloon flight 25 June 1968. (See Table III)

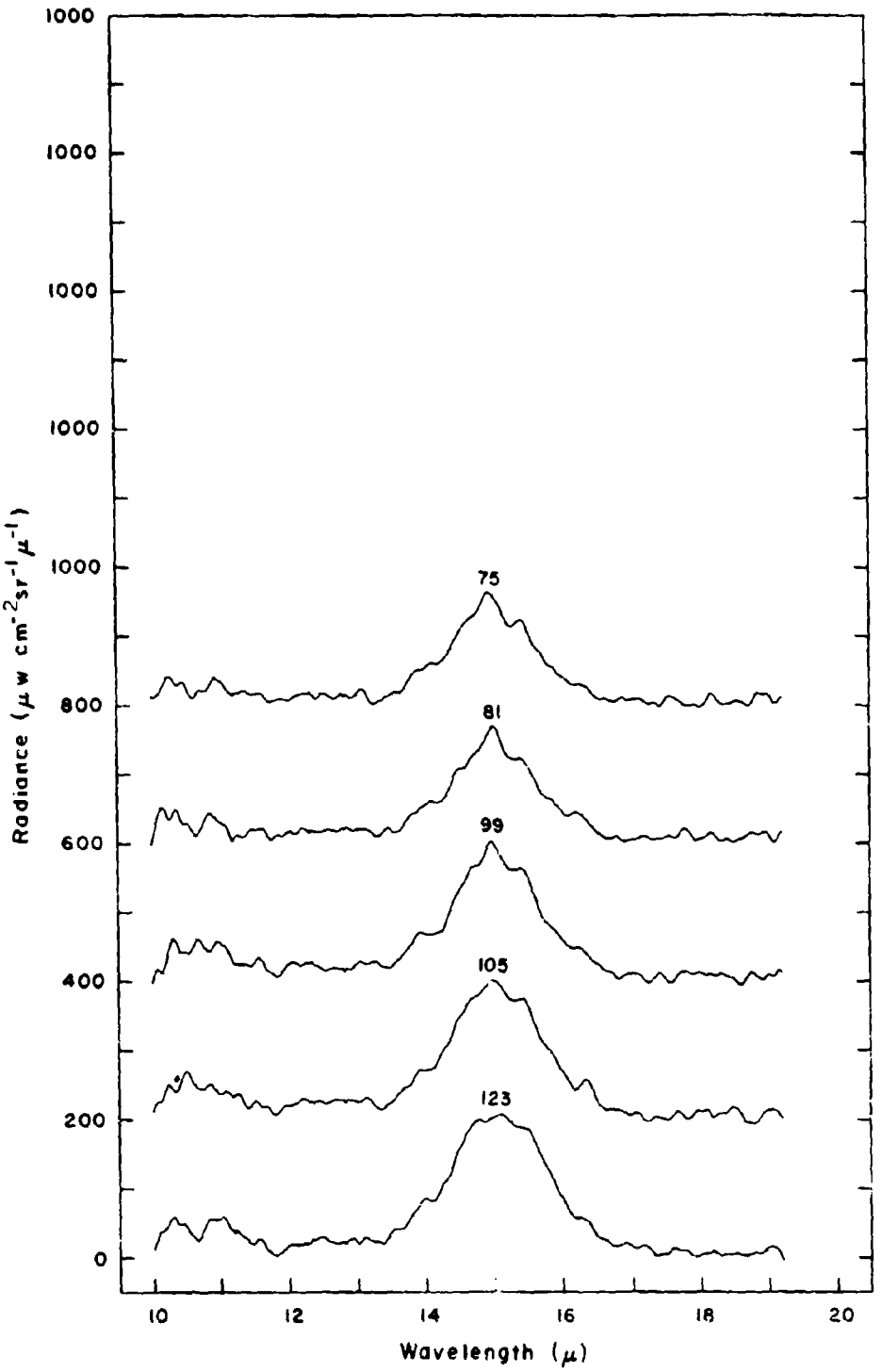

Figure 123 Spectral radiance vs altitude for balloon flight 25 June 1968. (See Tab. III)

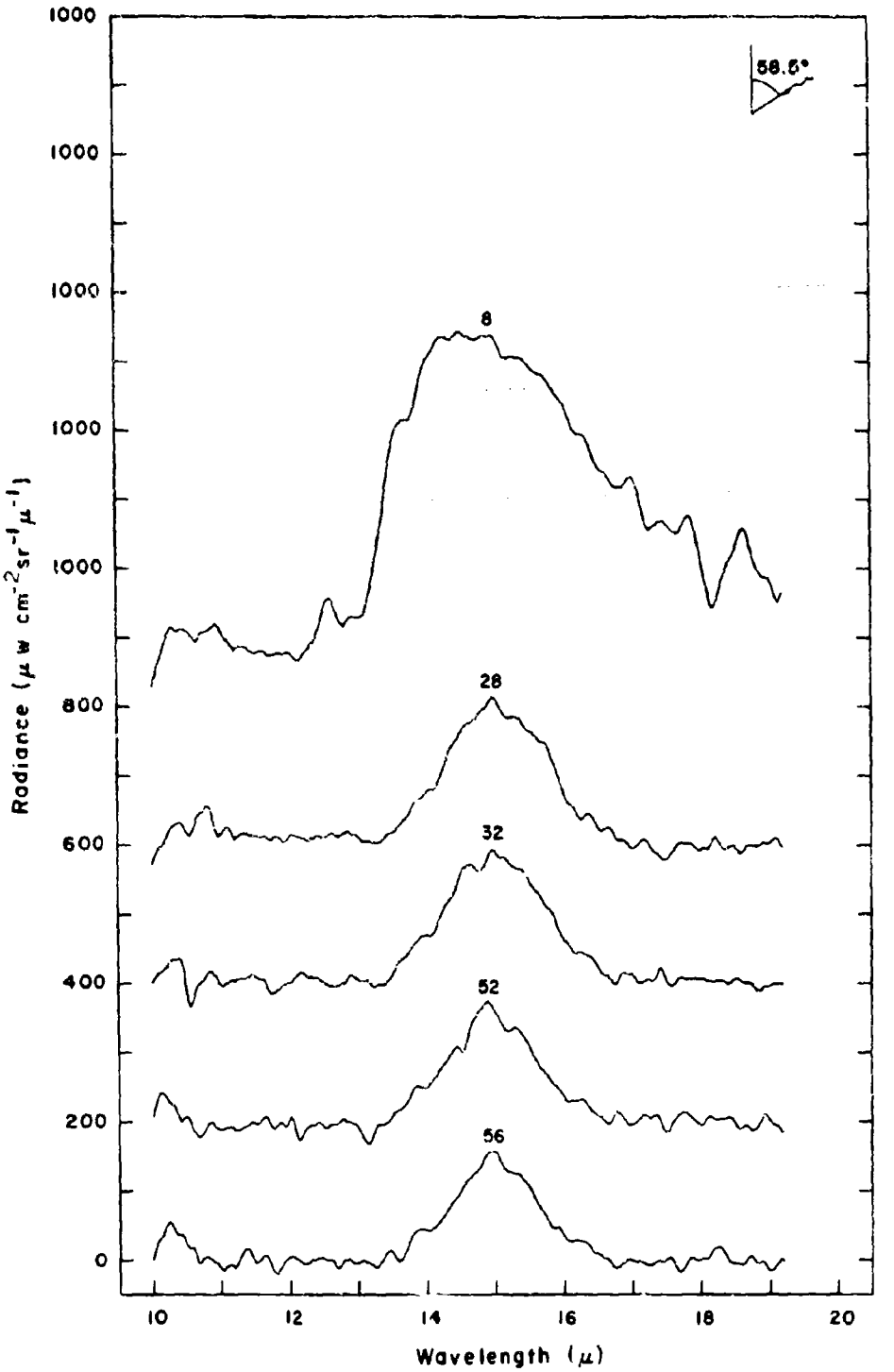

Figure 124 Spectral radiance vs. altitude for balloon flight 25 June 1968. (See Table III)

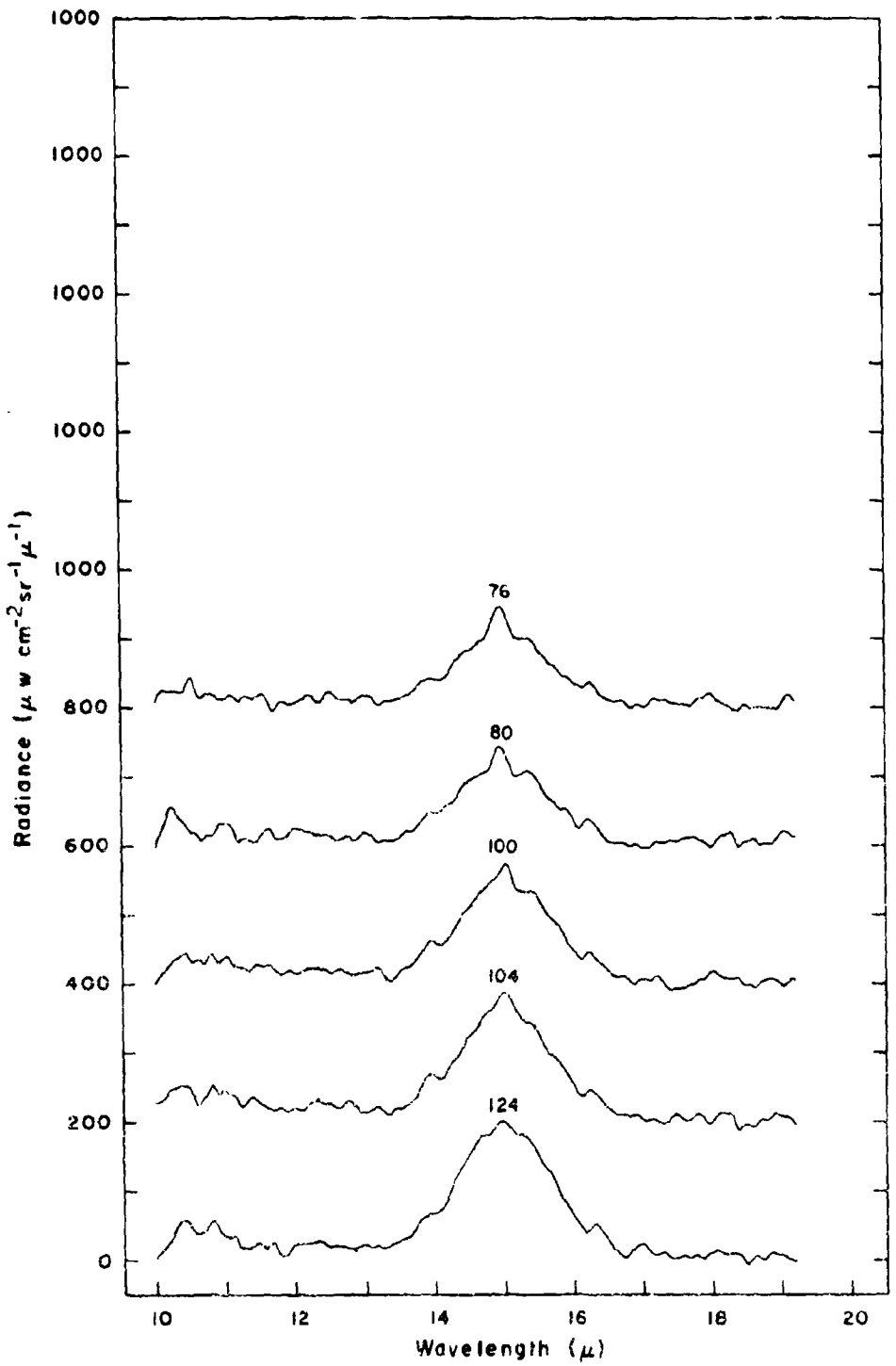

Figure 325 Spectral radiance vs altitude for 1 31 to 11 [illegible] 25 June 1965. (See Table 33)

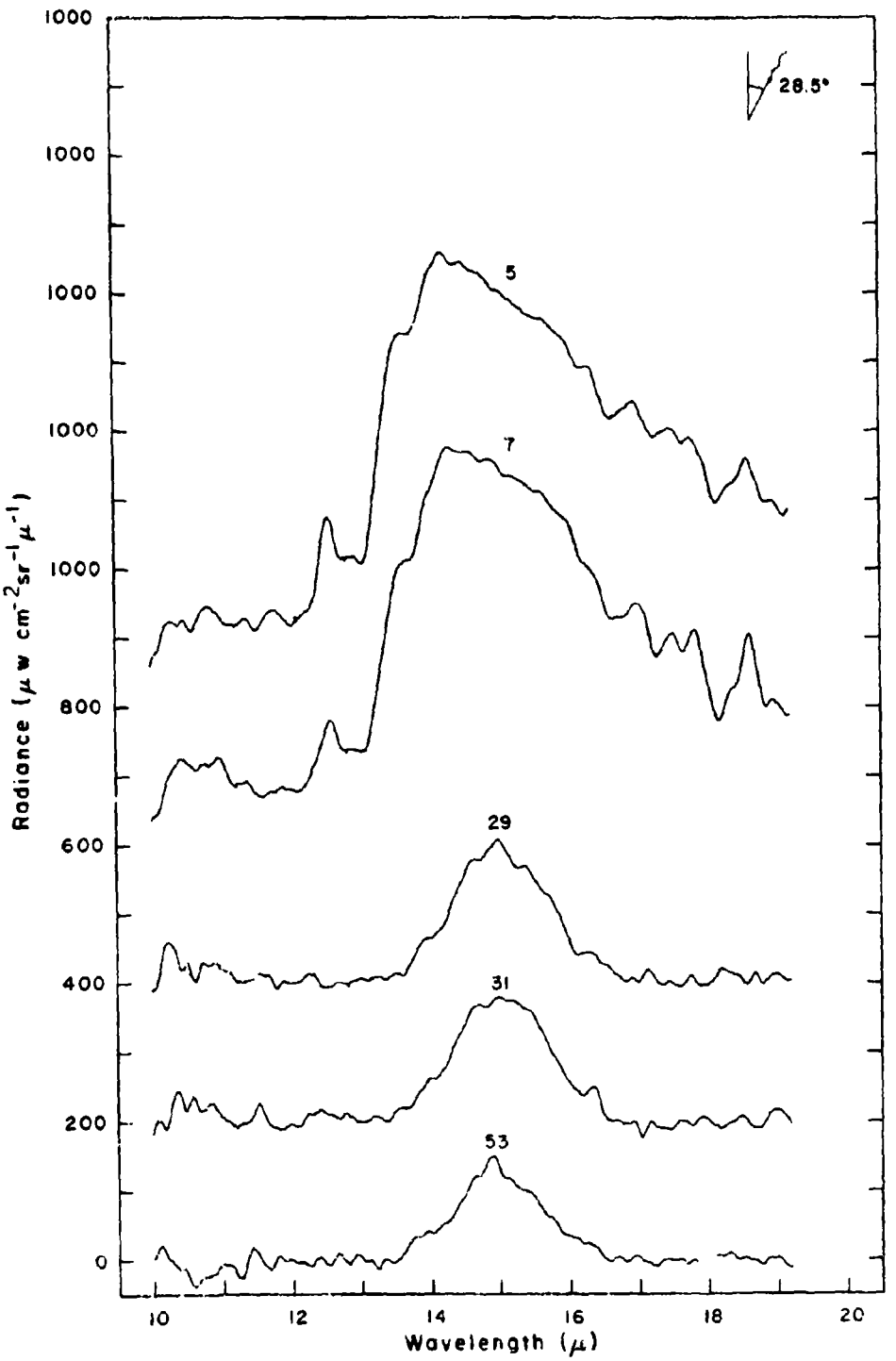

Figure 126 Spectral radiance vs. altitude for balloon flight 25 June 1968. (See Table 3)

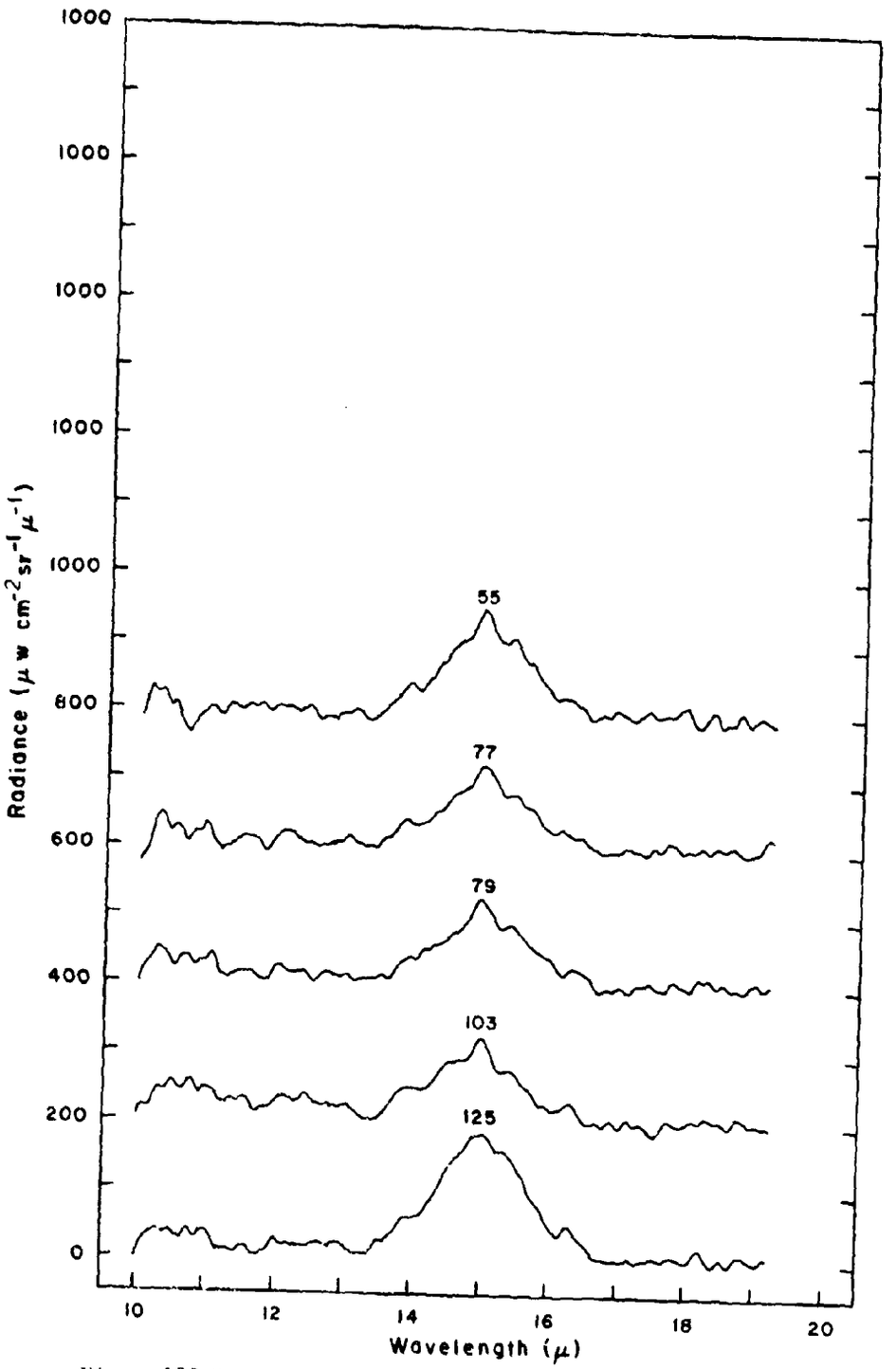

Figure 127 Spectral radiance vs altitude for balloon flight 25 June 1966. (See Table 14)

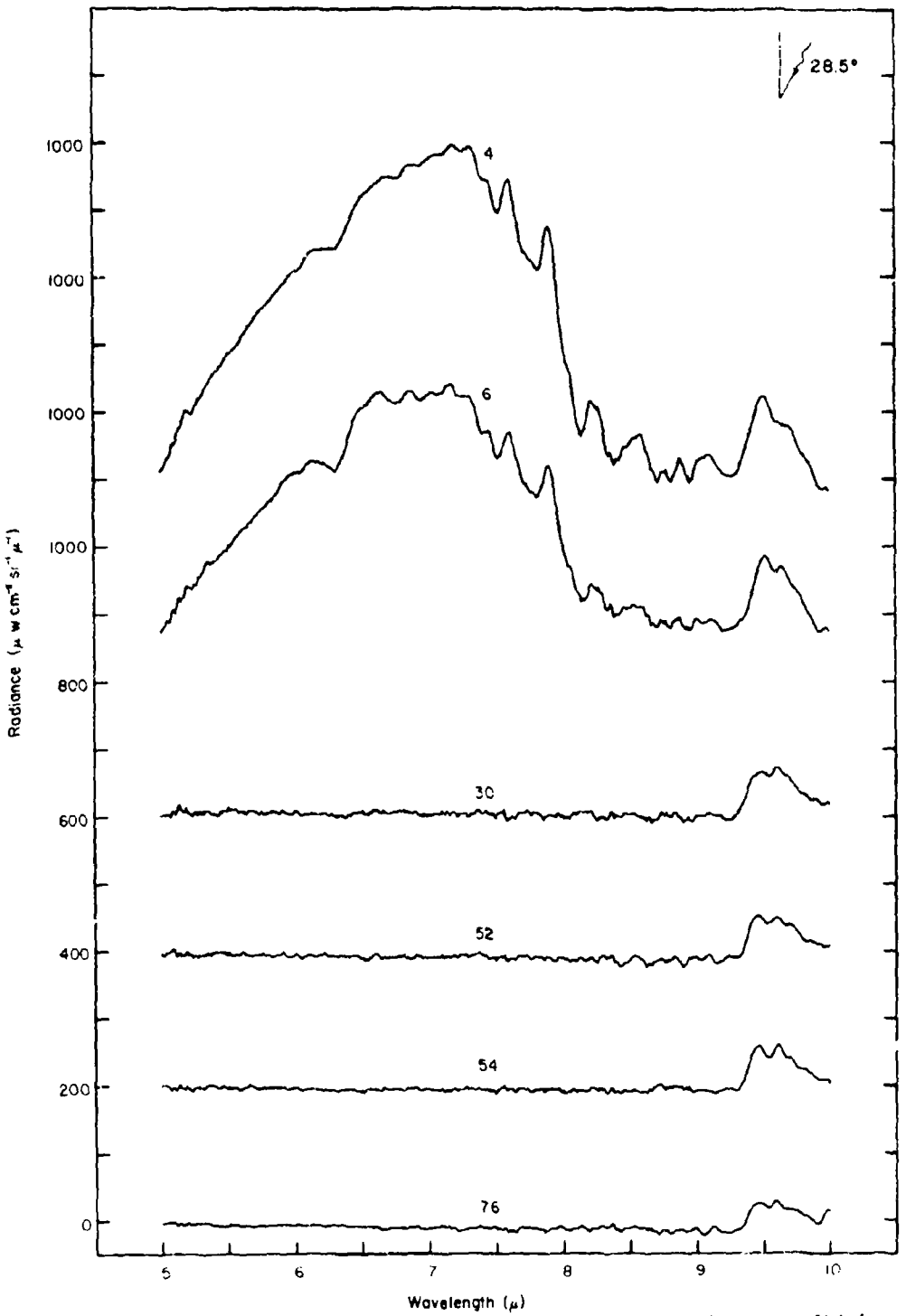

Figure 128. Spectral radiance vs altitude for balloon flight 1 July 1968. (See Table IV).

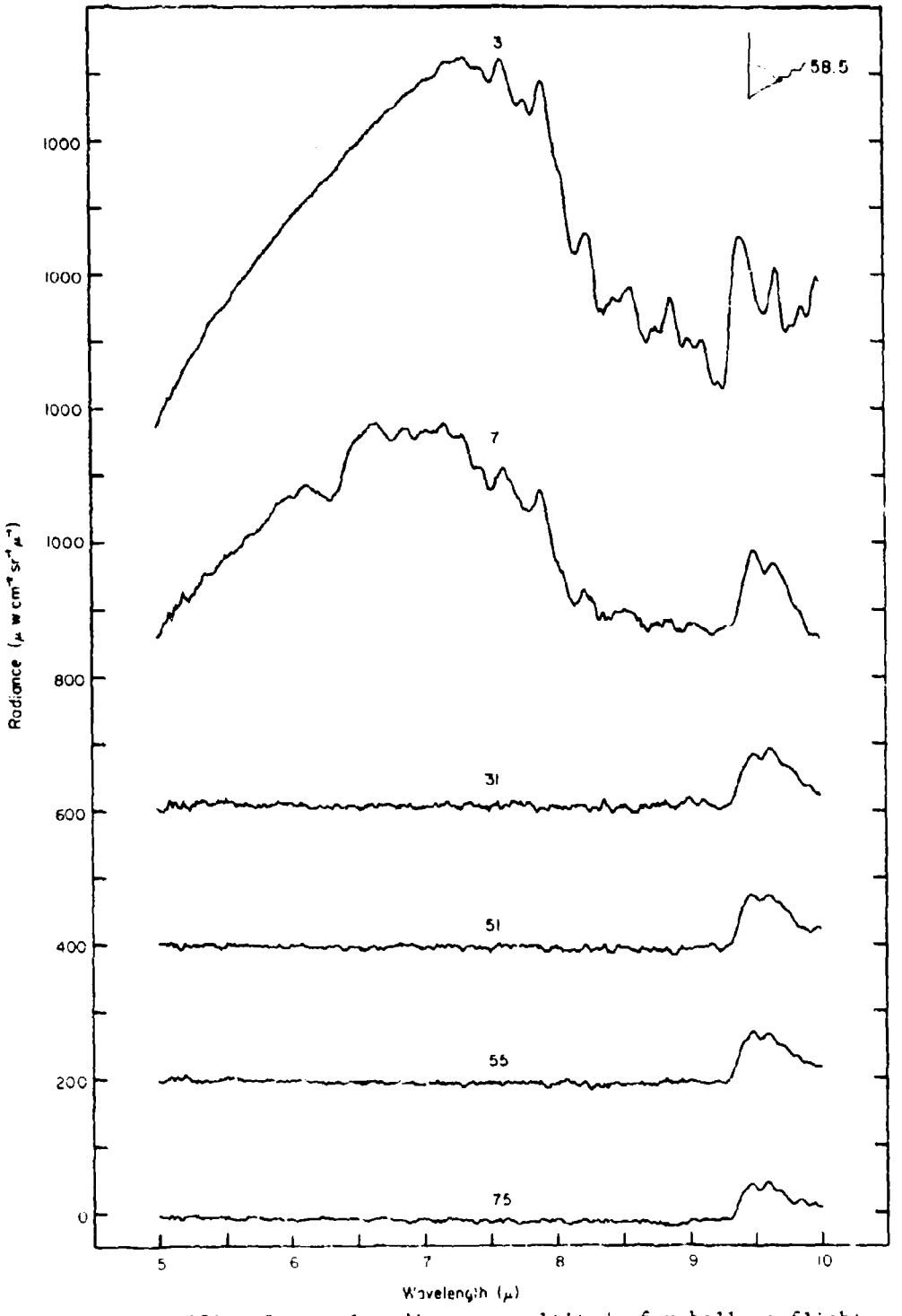

Figure 129. Spectral radiance vs altitude for balloon flight 1 July 1968. (See Table IV.)

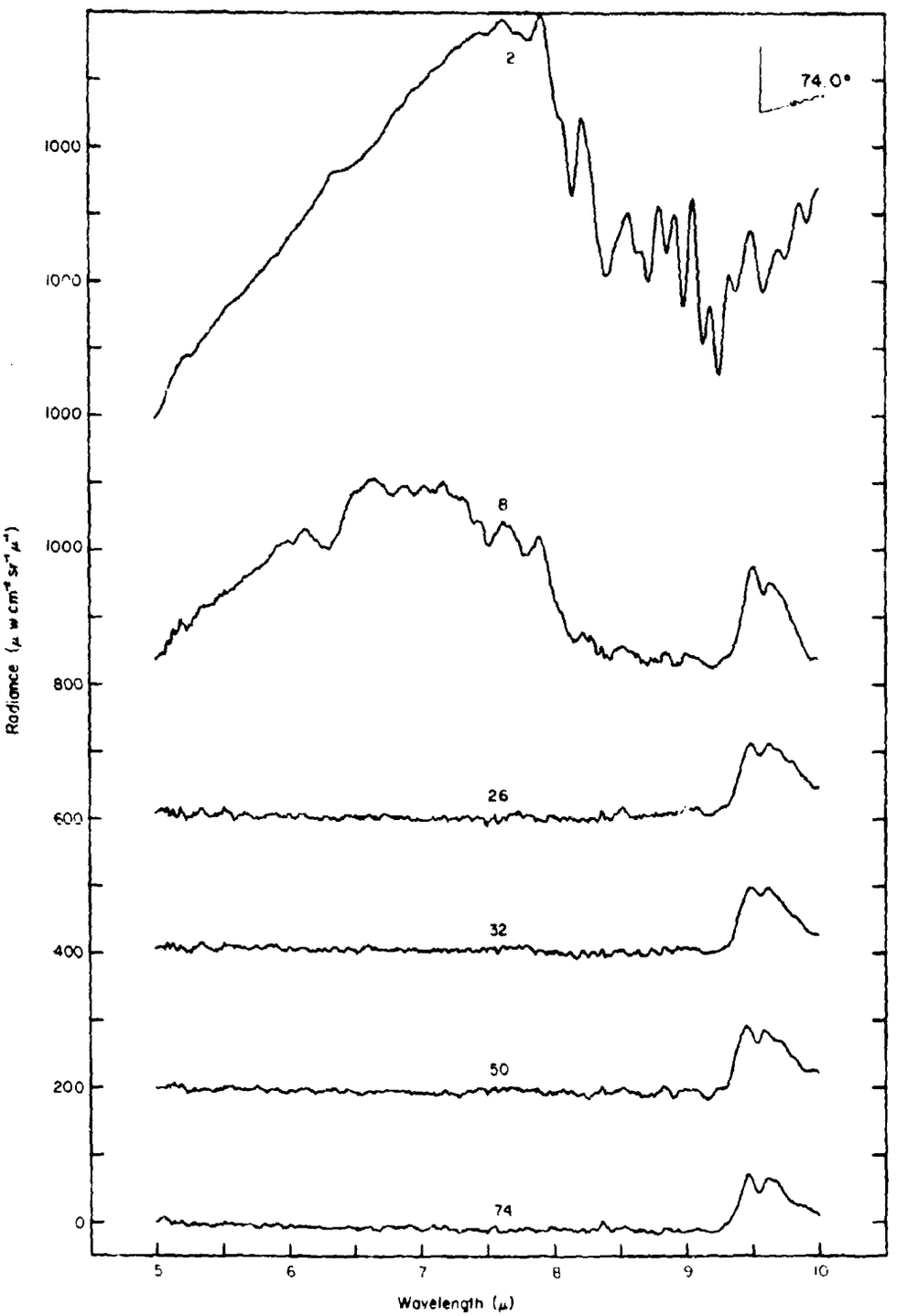

Figure 130. Spectral radiance vs altitude for balloon flight 1 July 1968. (See Table IV).

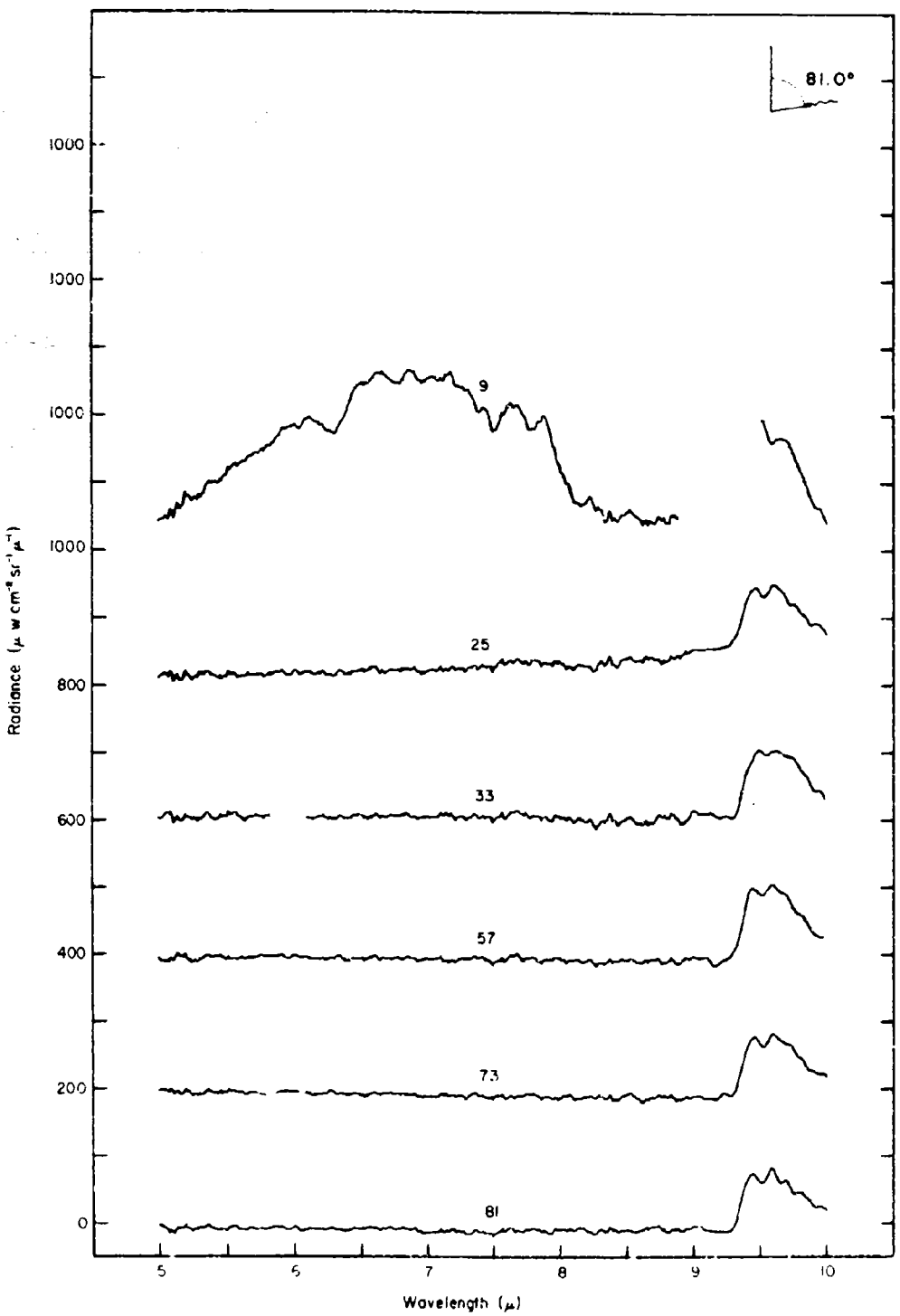

Figure 131. Spectral radiance vs altitude for balloon flight 1 July 1968. (See Table IV).

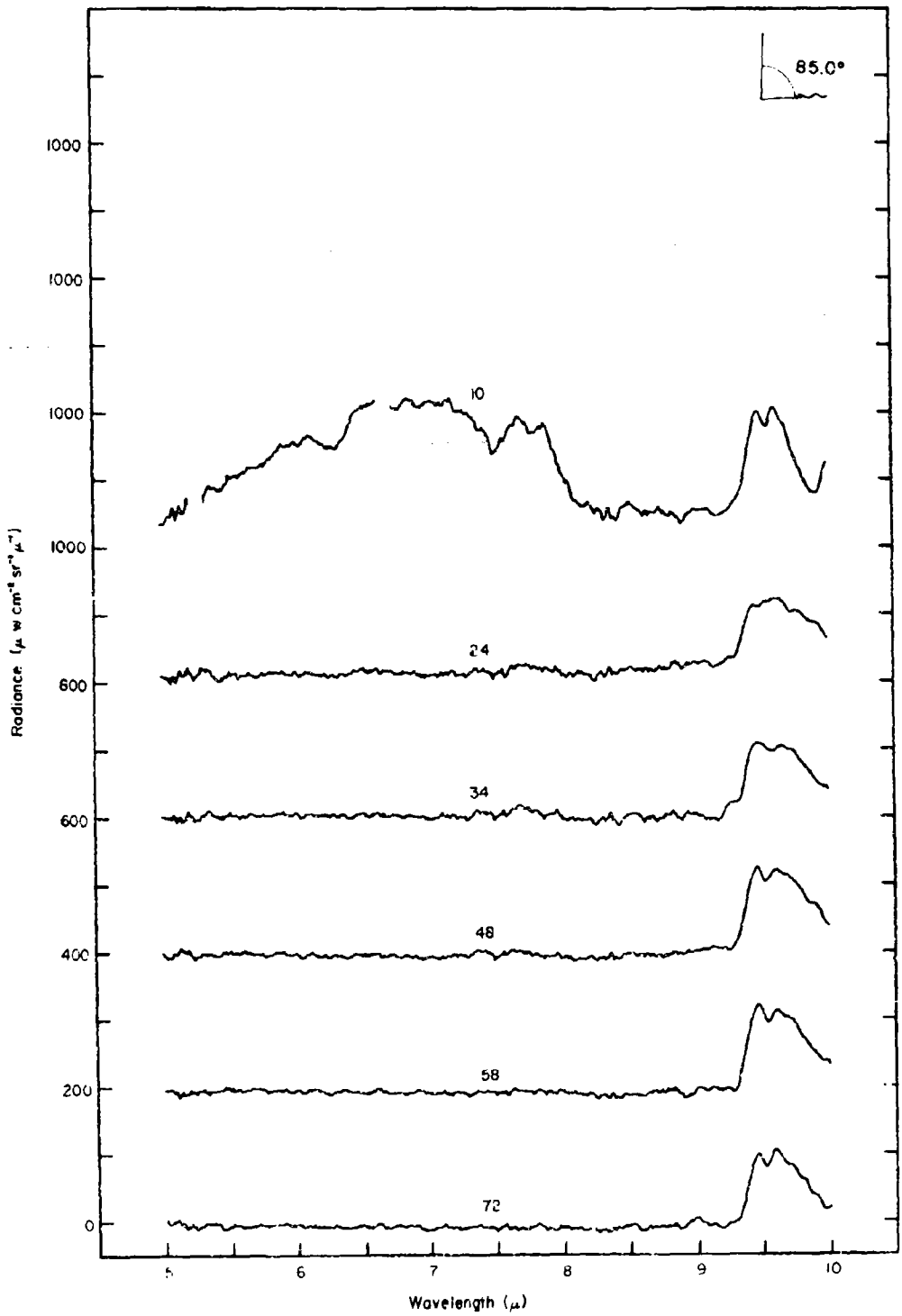

Figure 132. Spectral radiance vs altitude for balloon flight 1 July 1968. (See Table IV).

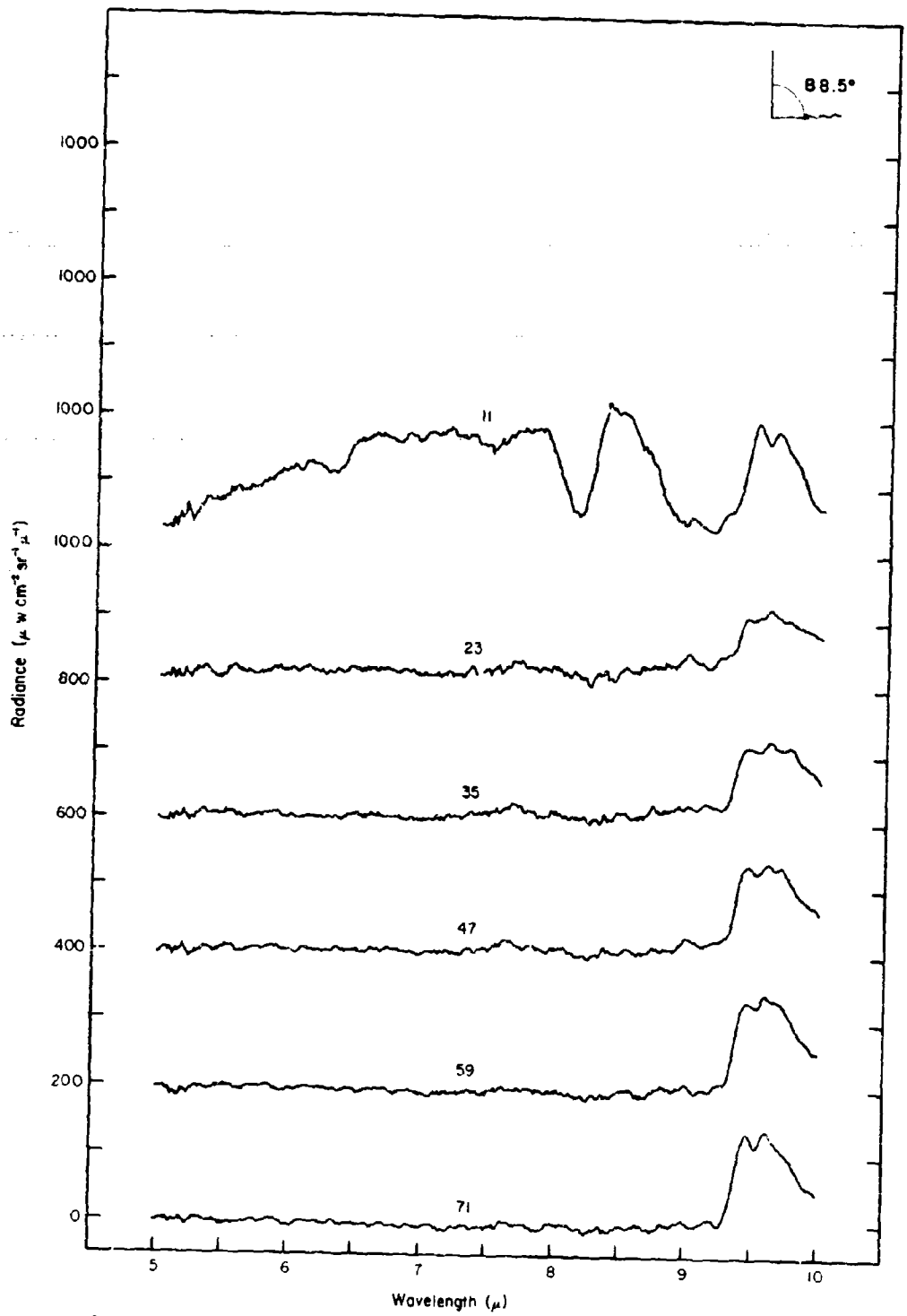

Figure 133. Spectral radiance vs altitude for balloon flight 1 July 1968. (See Table IV).

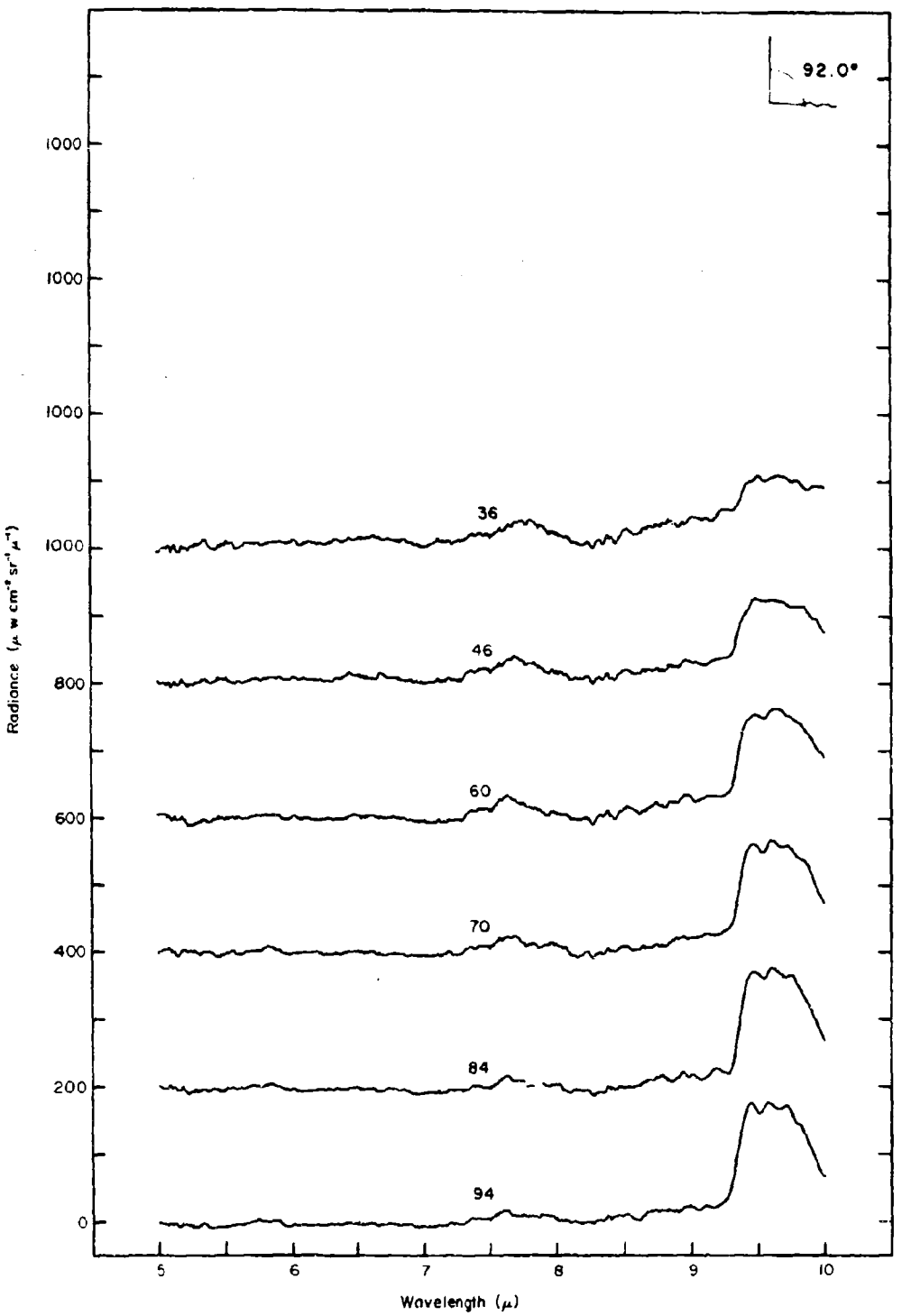

Figure 134. Spectral radiance vs altitude for balloon flight 1 July 1968. (See Table IV).

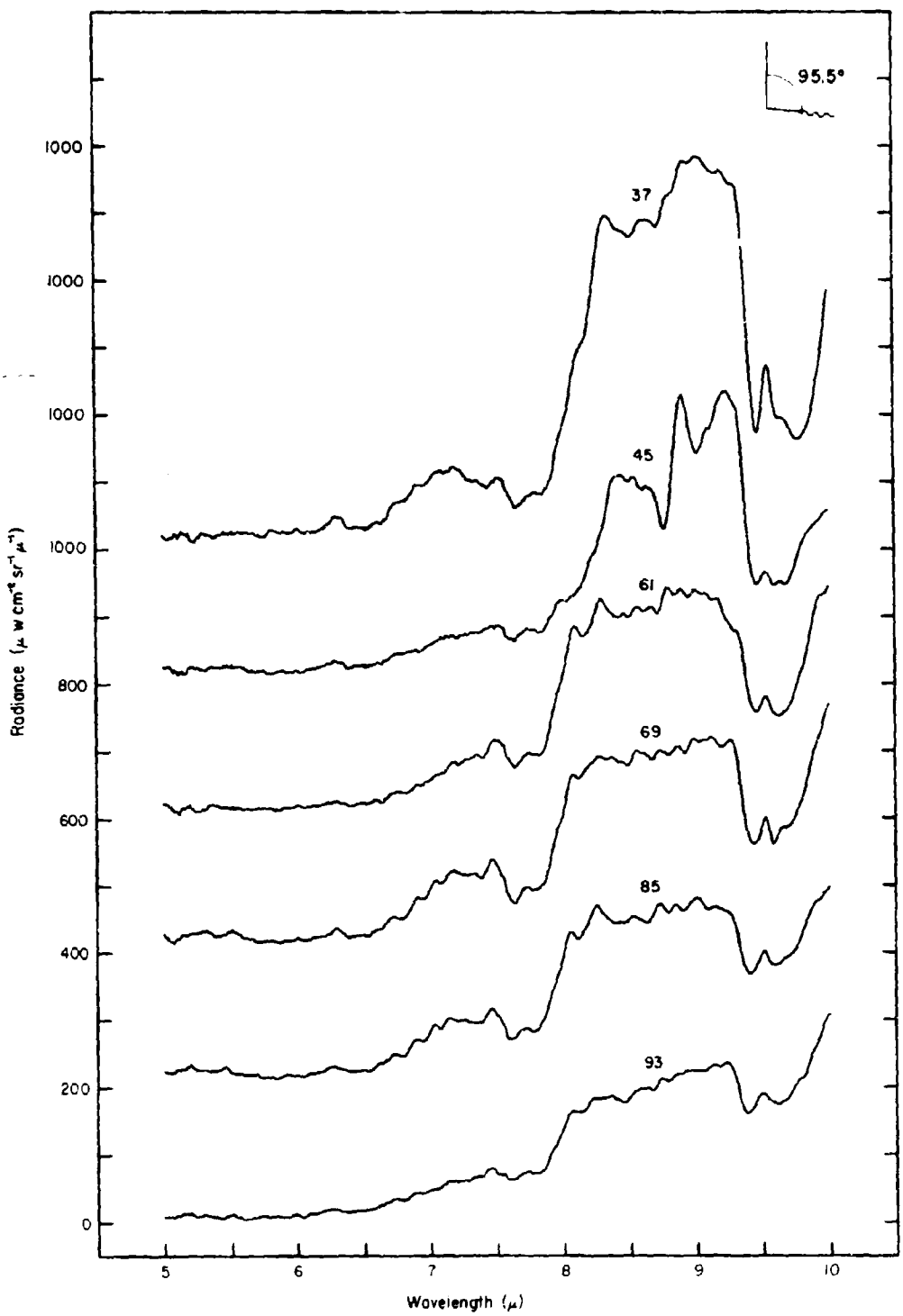

Figure 135. Spectral radiance vs altitude for balloon flight 1 July 1968. (See Table IV).

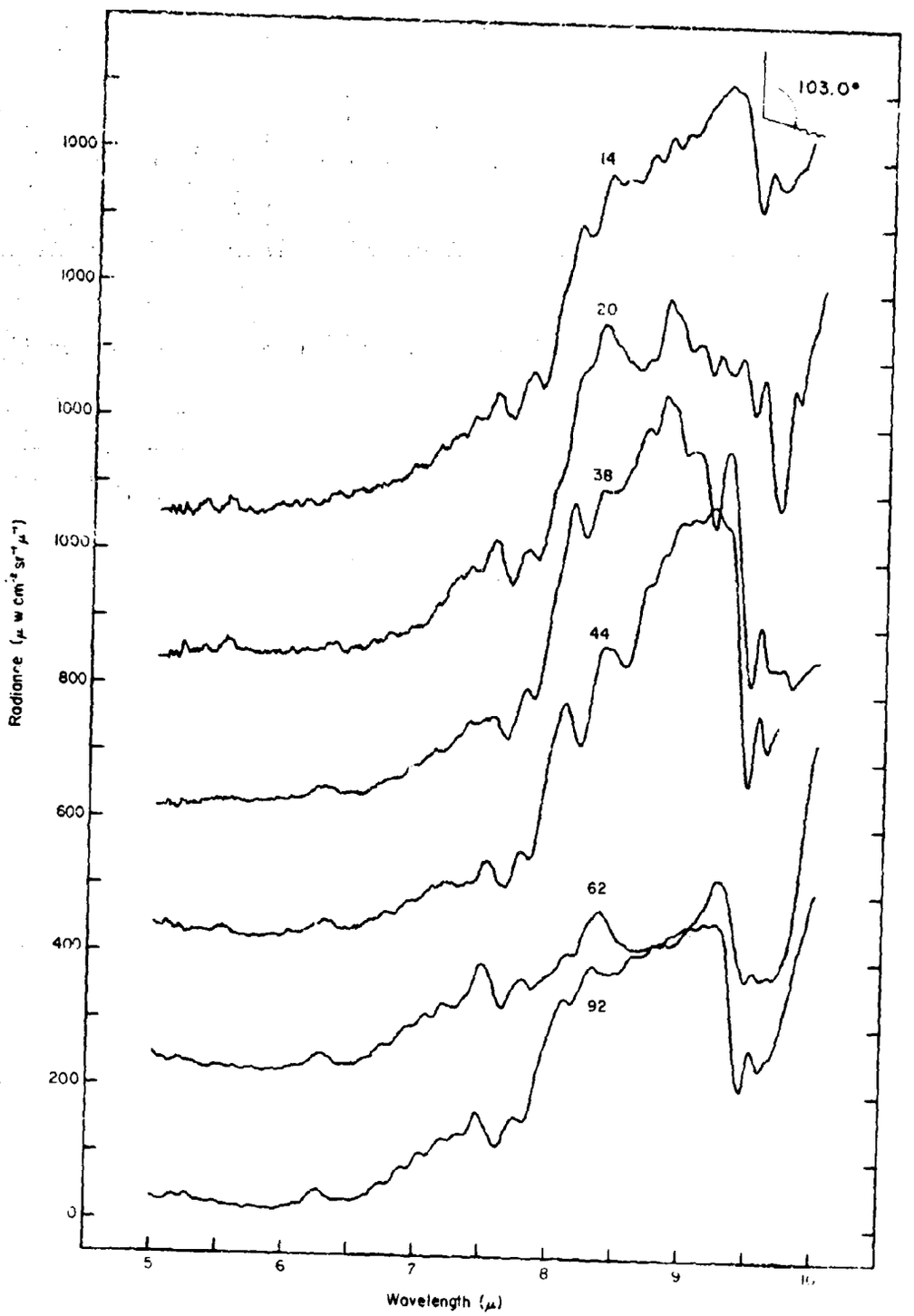

Figure 136. Spectral radiance vs altitude for balloon flight 1 July 1968. (See Table IV).

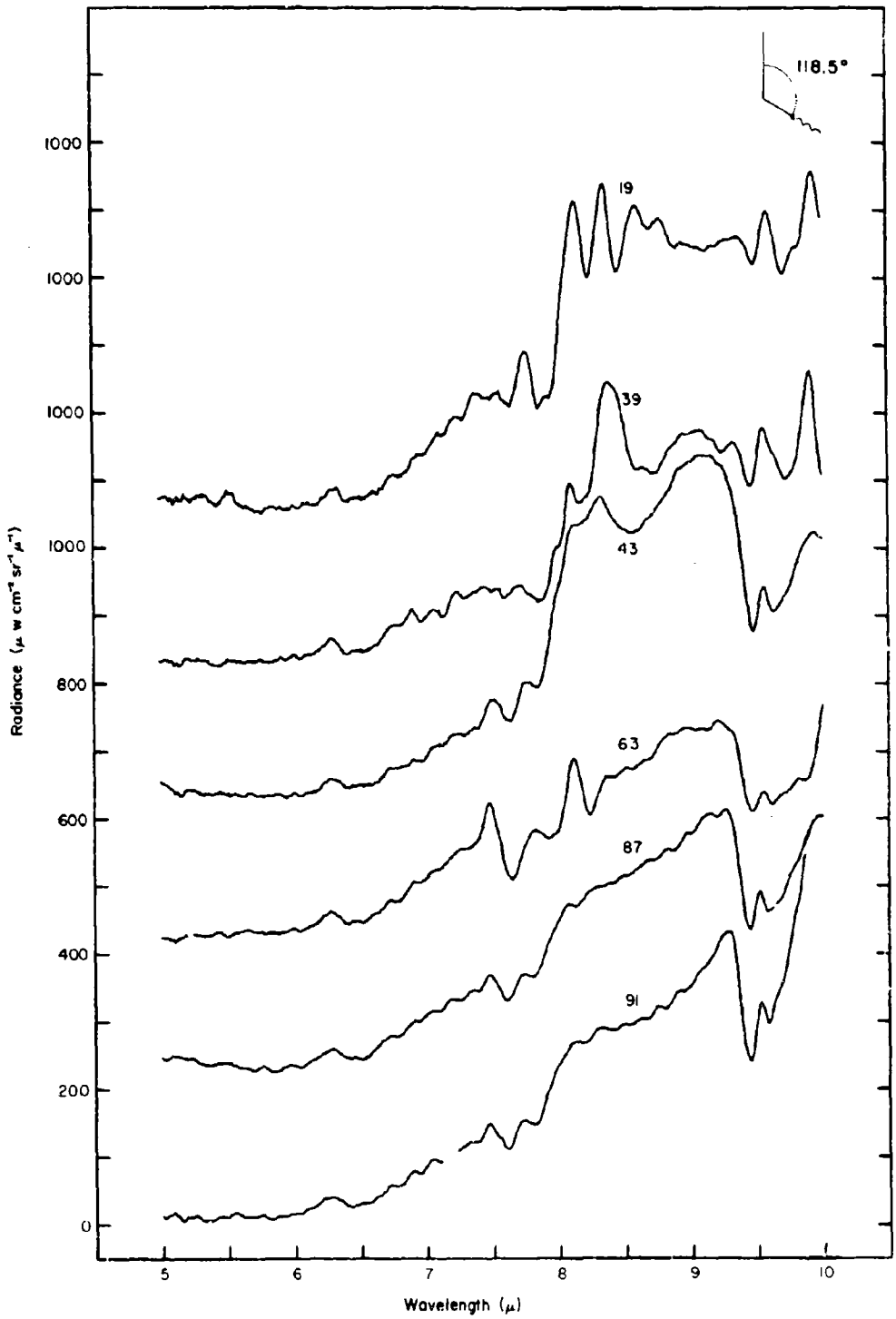

Figure 137. Spectral radiance vs altitude for balloon flight 1 July 1968. (See Table IV).

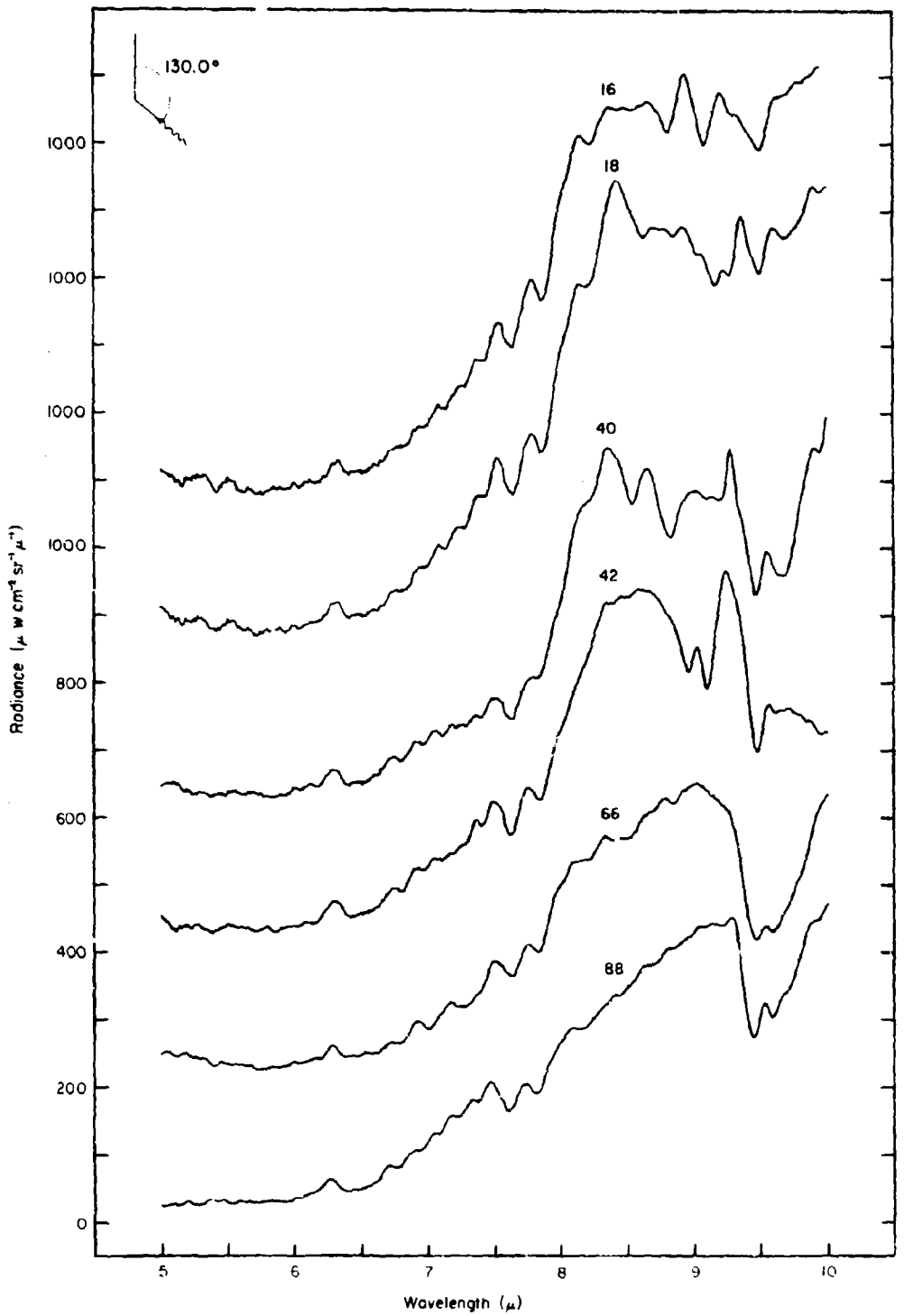

Figure 138. Spectral radiance vs altitude for balloon flight 1 July 1968. (See Table IV).

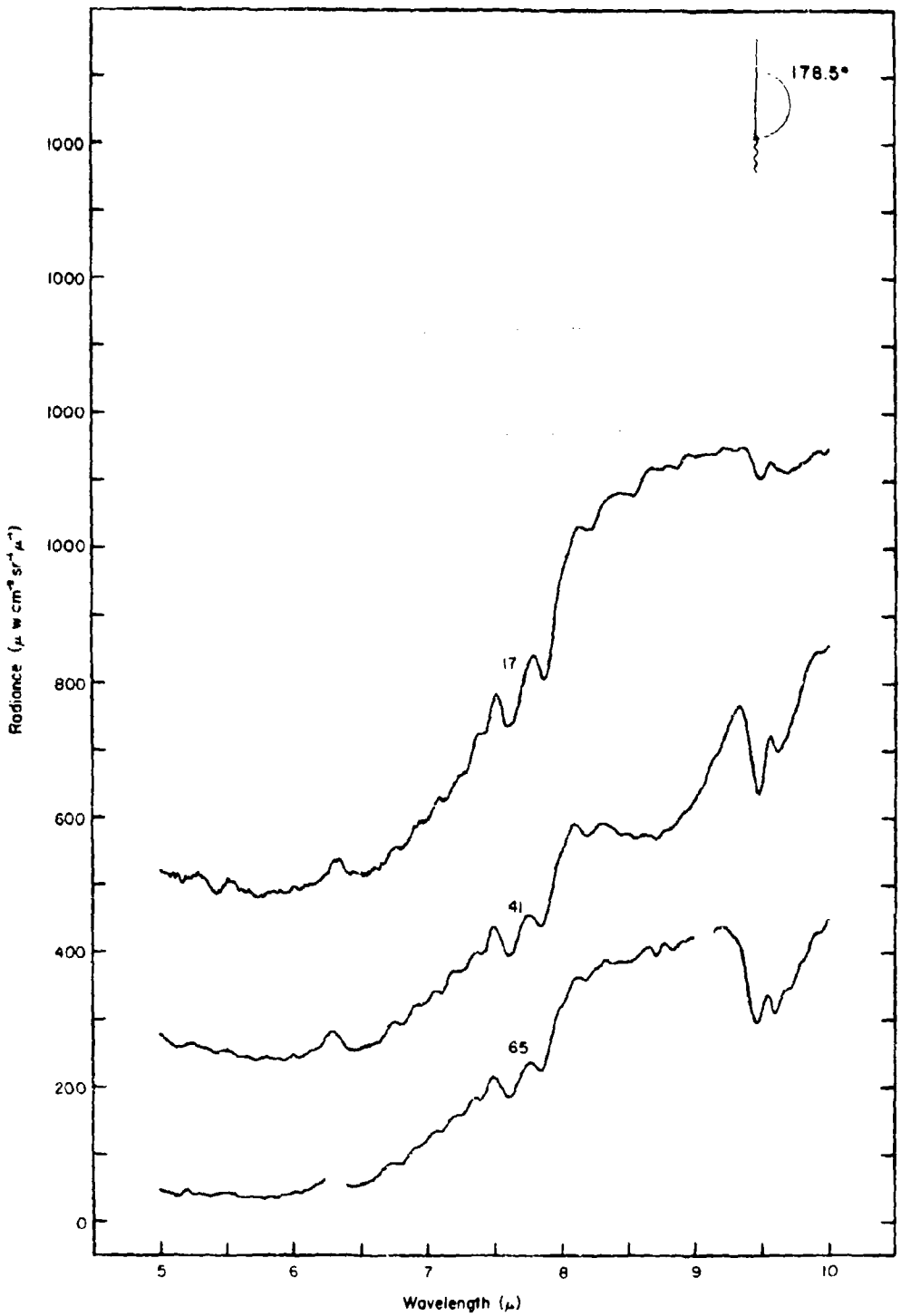

Figure 139. Spectral radiance vs altitude for balloon flight 1 July 1968. (See Table IV).

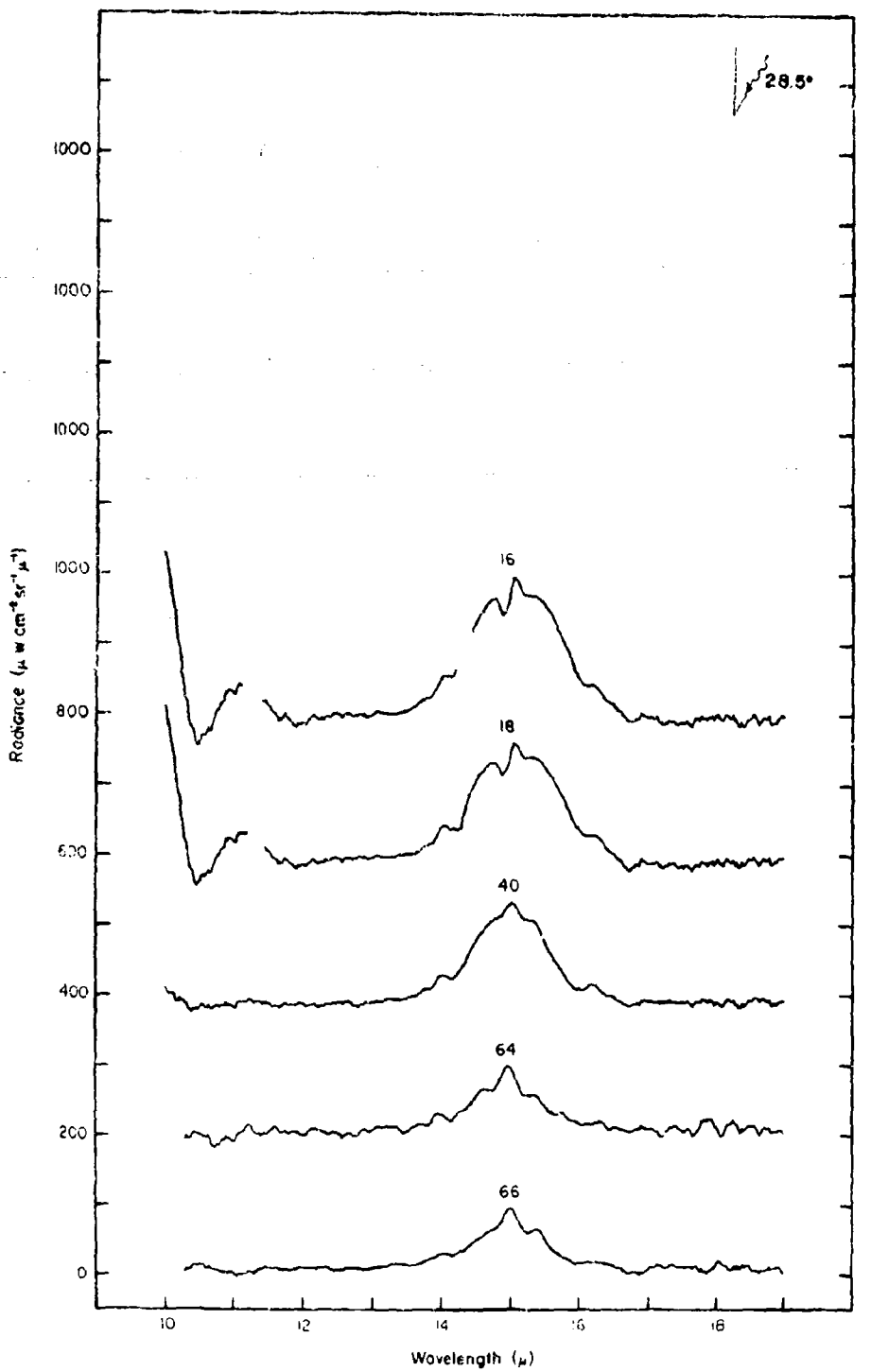

Figure 140. Spectral radiance vs altitude for balloon flight 1 July 1968. (See Table IV).

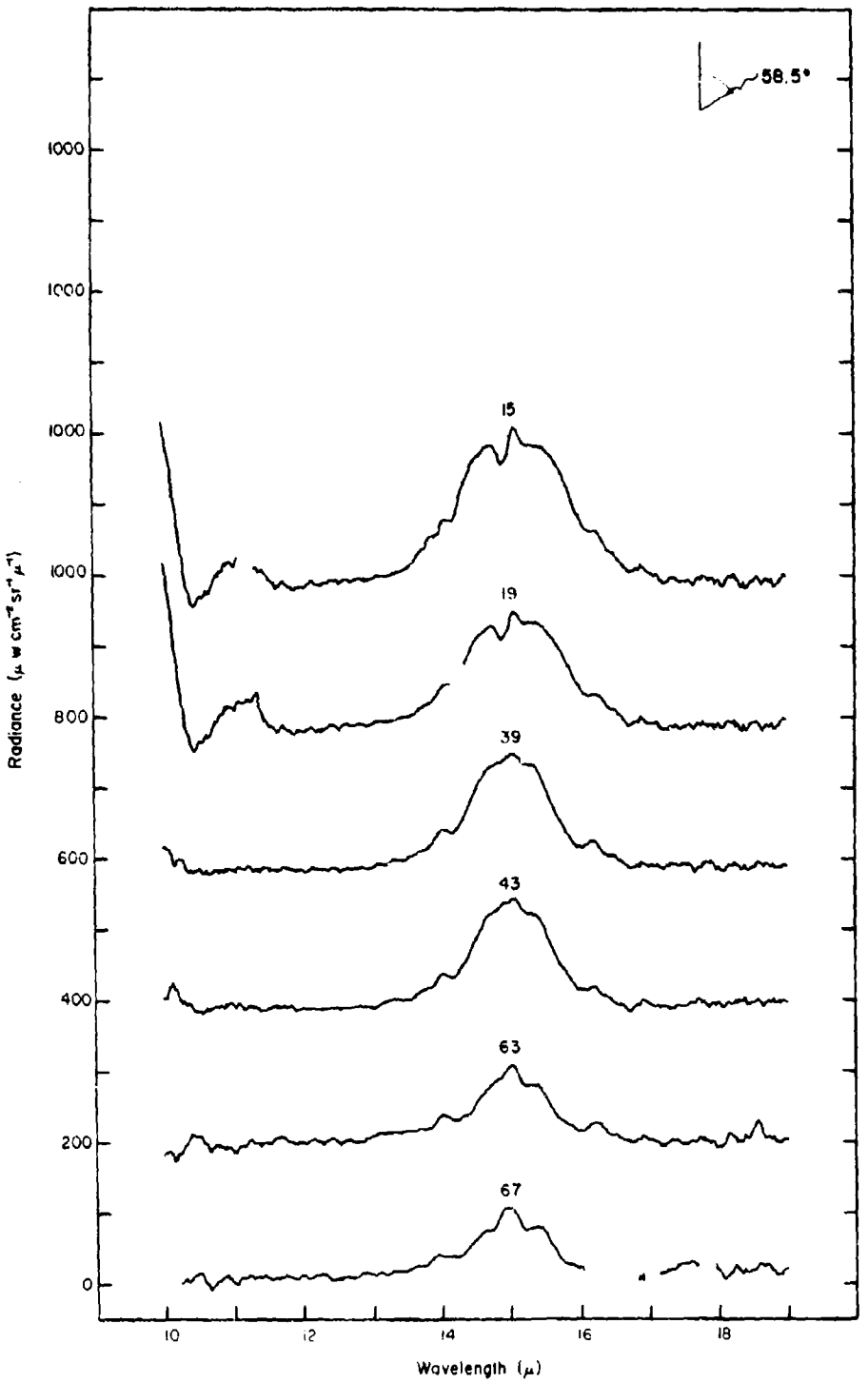

Figure 141. Spectral radiance vs altitude for balloon flight 1 July 1968. (See Table IV).

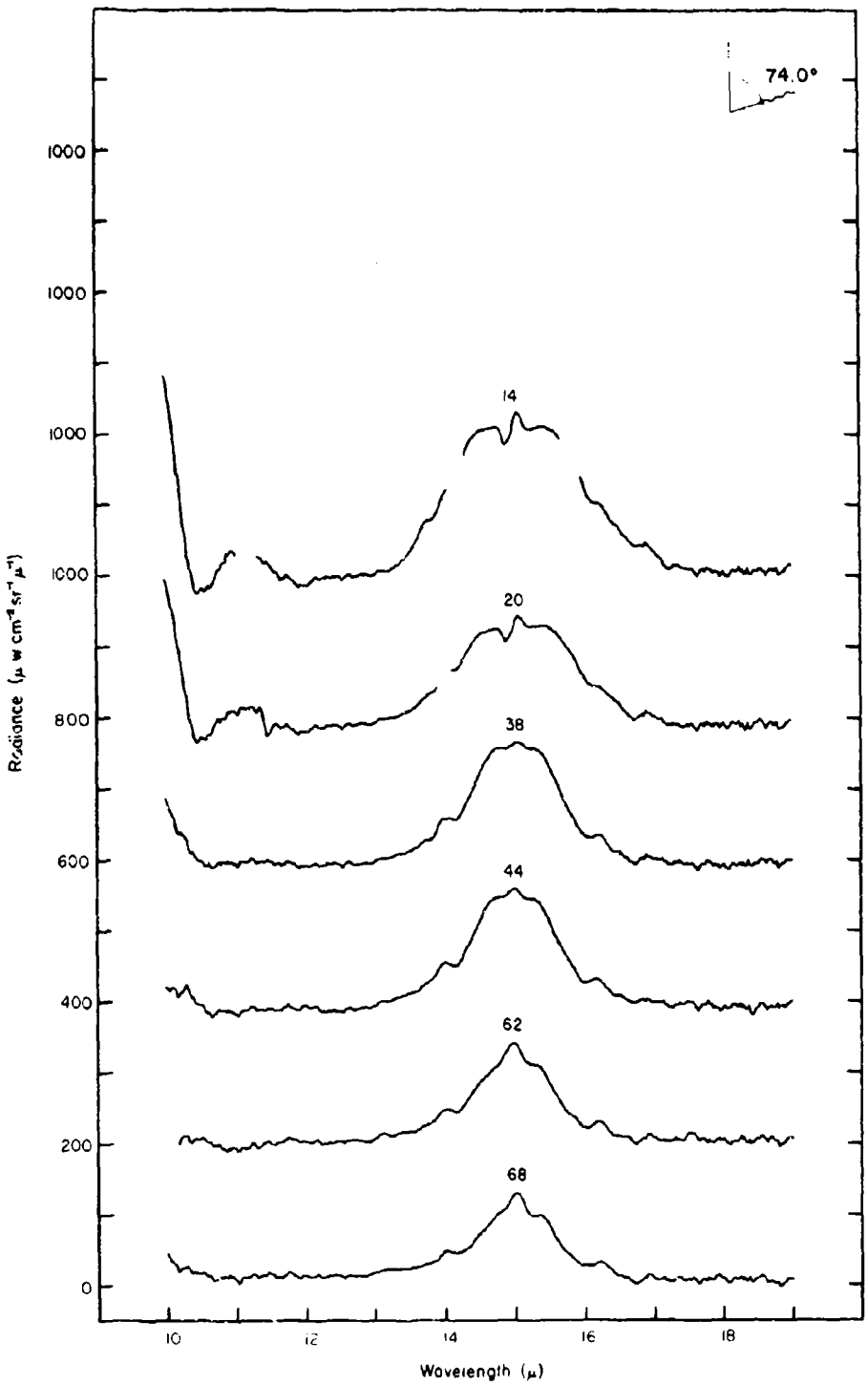

Figure 142. Spectral radiance vs altitude for balloon flight 1 July 1968. (See Table IV).

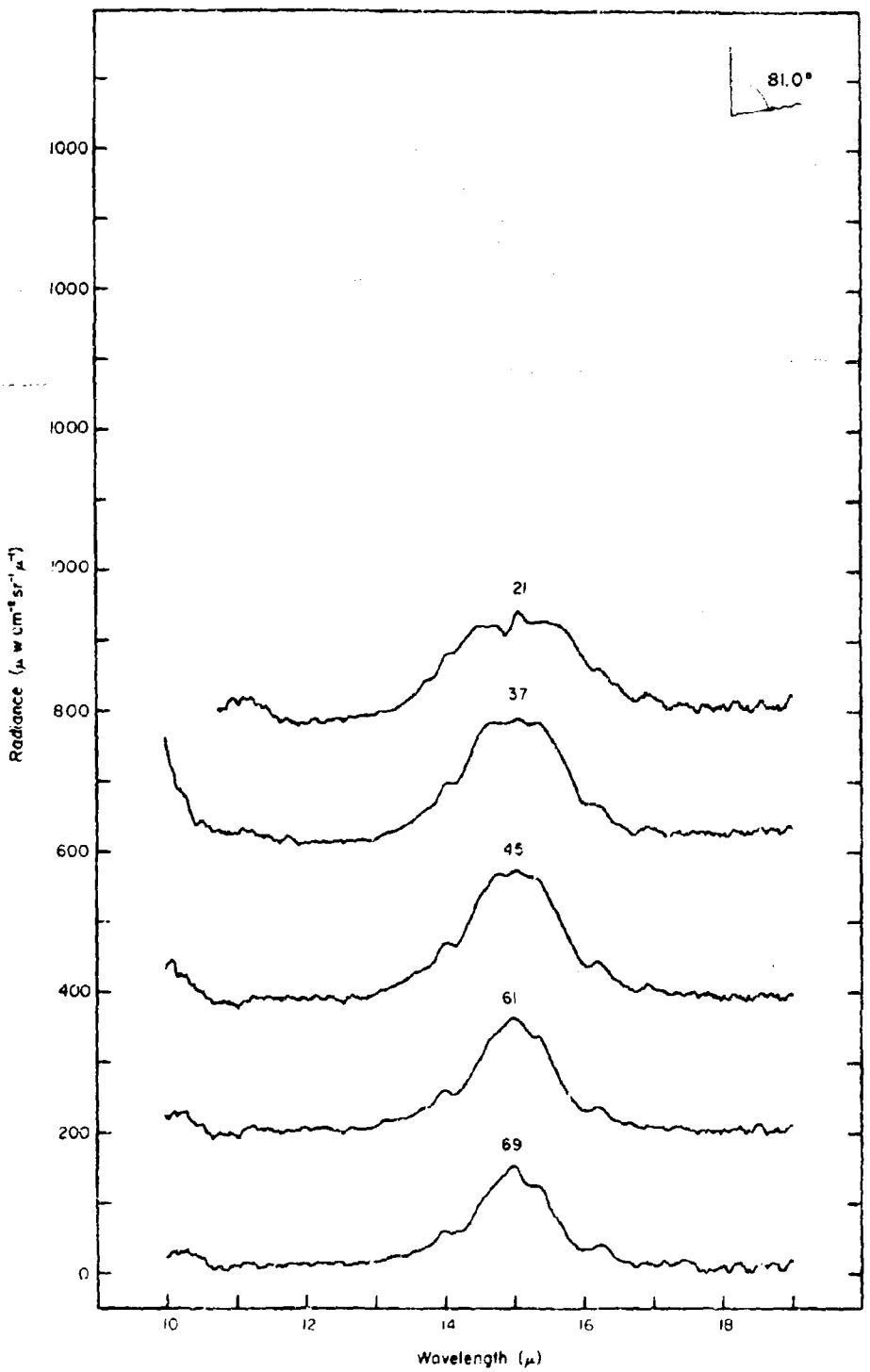

Figure 143. Spectral radiance vs altitude for balloon flight 1 July 1968. (See Table IV).

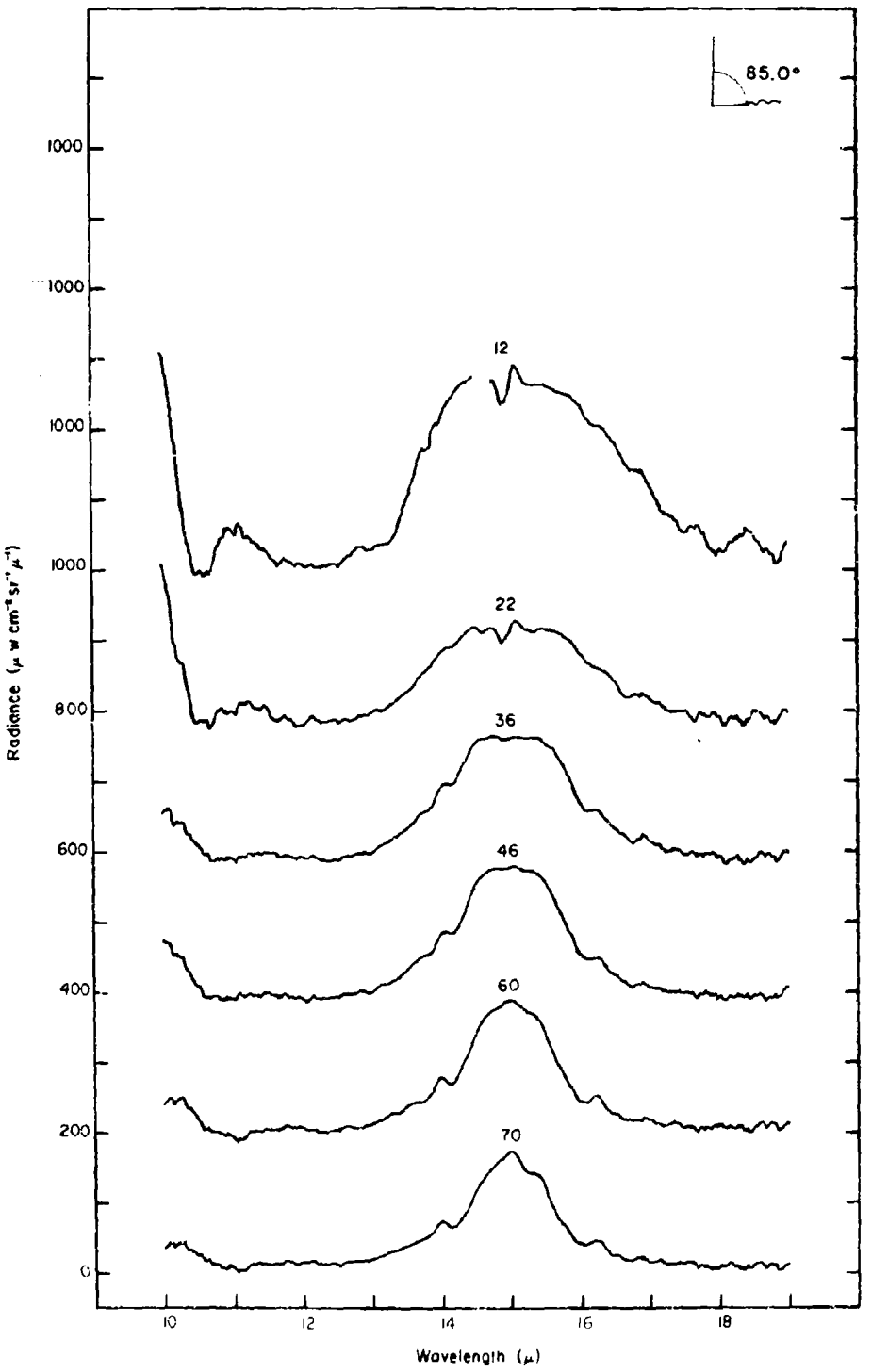

Figure 144. Spectral radiance vs altitude for balloon flight 1 July 1968. (See Table IV).

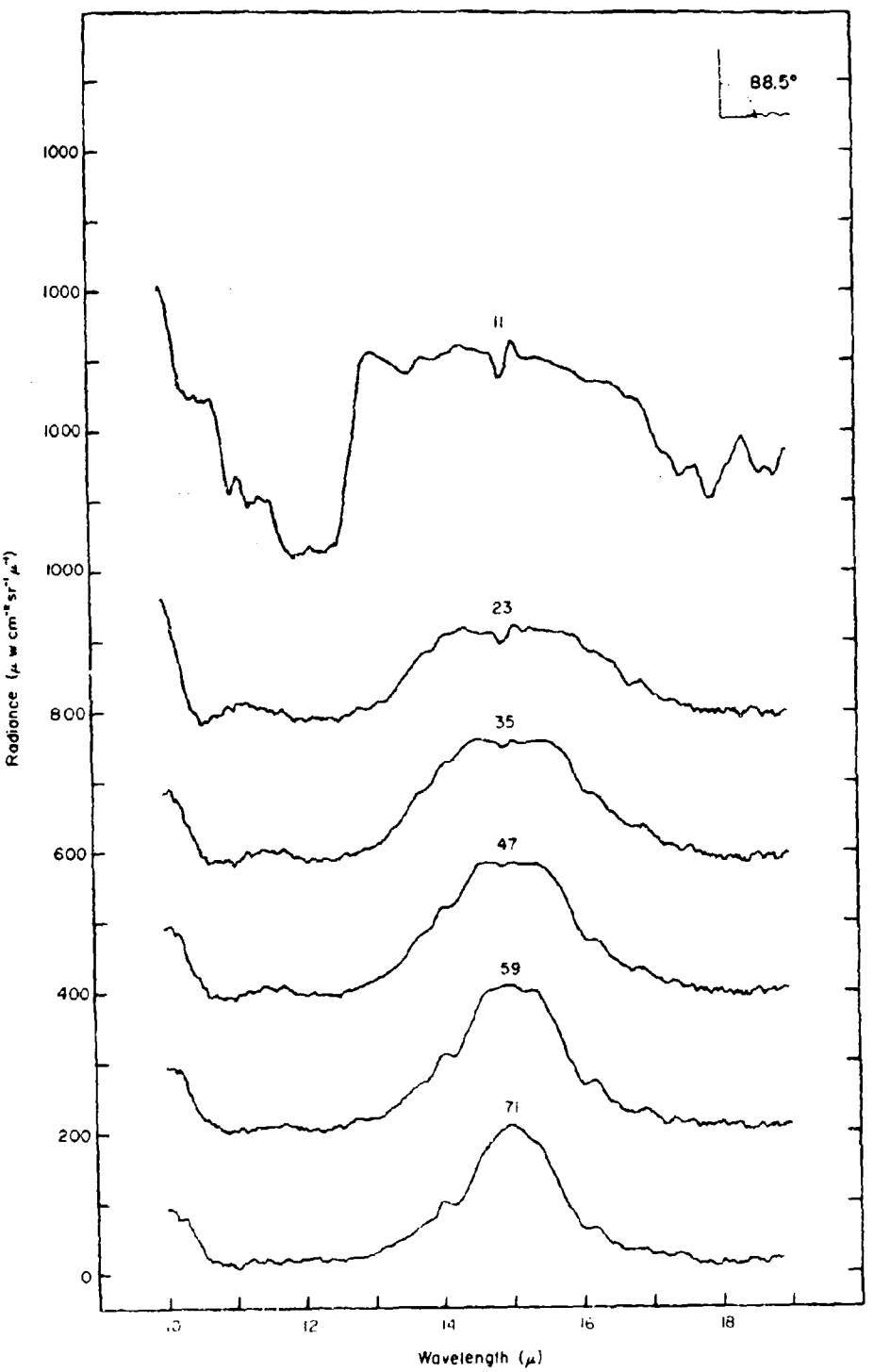

Figure 145. Spectral radiance vs altitude for balloon flight 1 July 1968. (See Table IV).

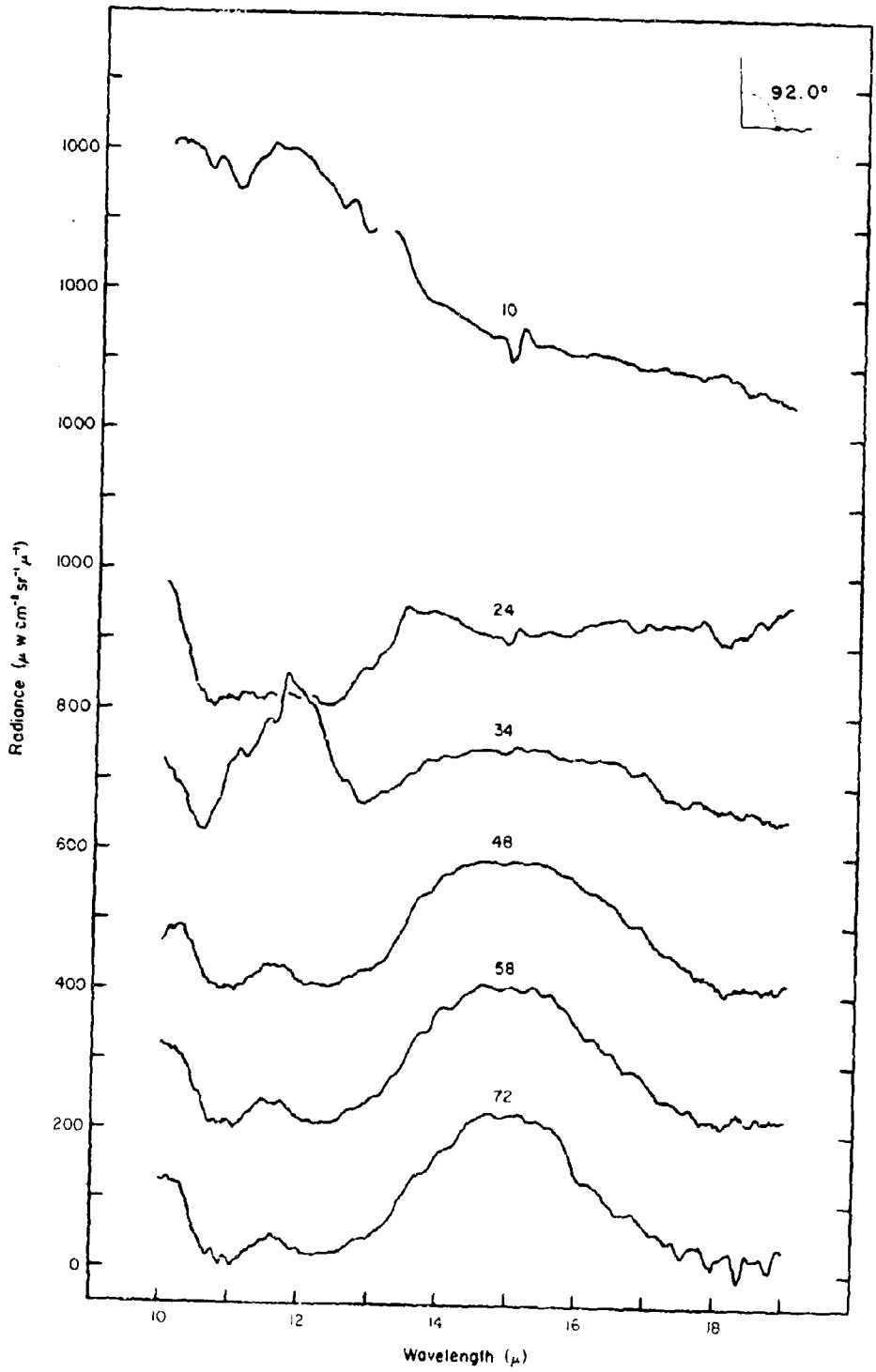

Figure 146. Spectral radiance vs altitude for balloon flight 1 July 1968. (See Table IV).

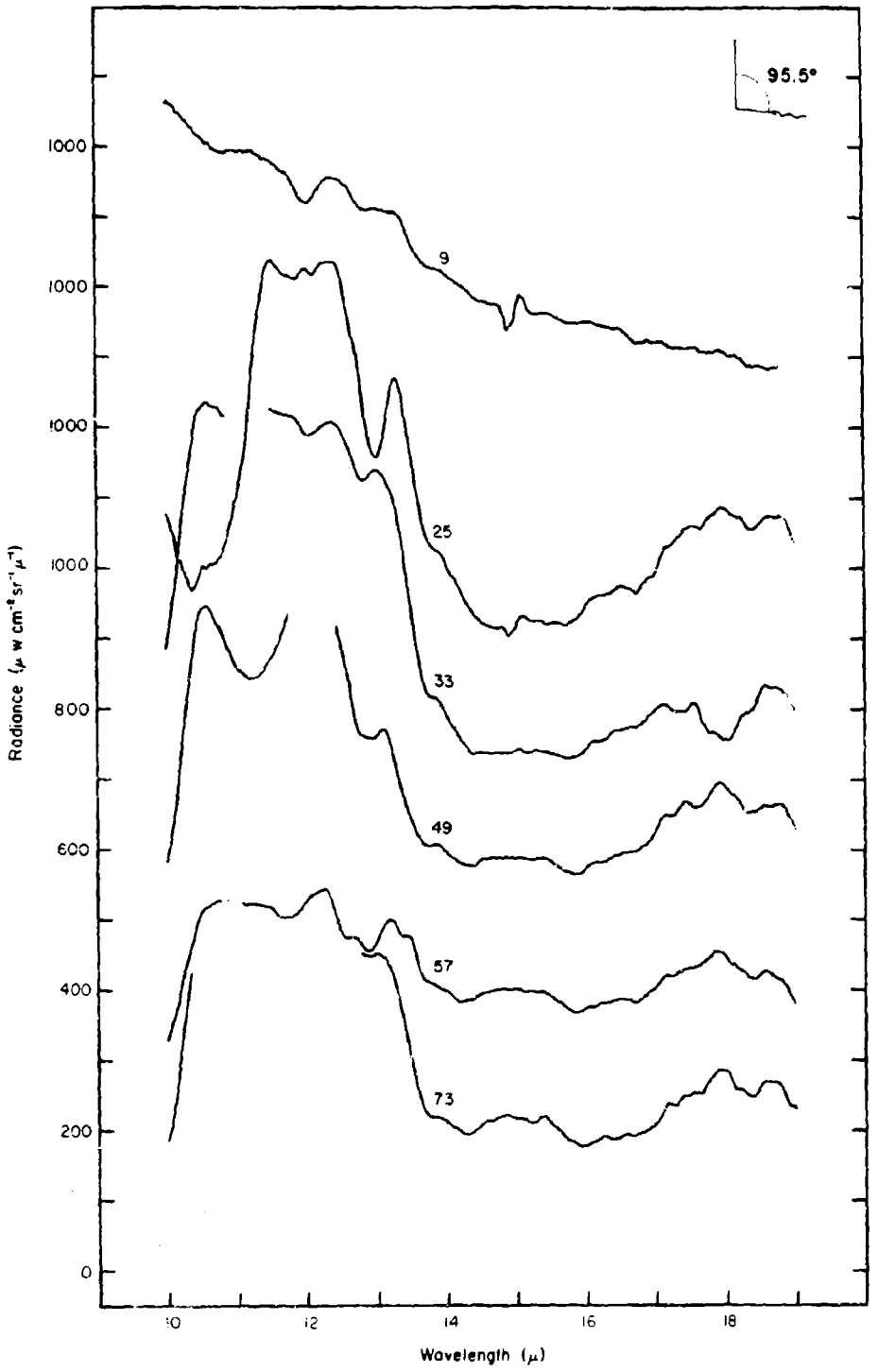

Figure 147. Spectral radiance vs altitude for balloon flight 1 July 1968. (See Table IV).

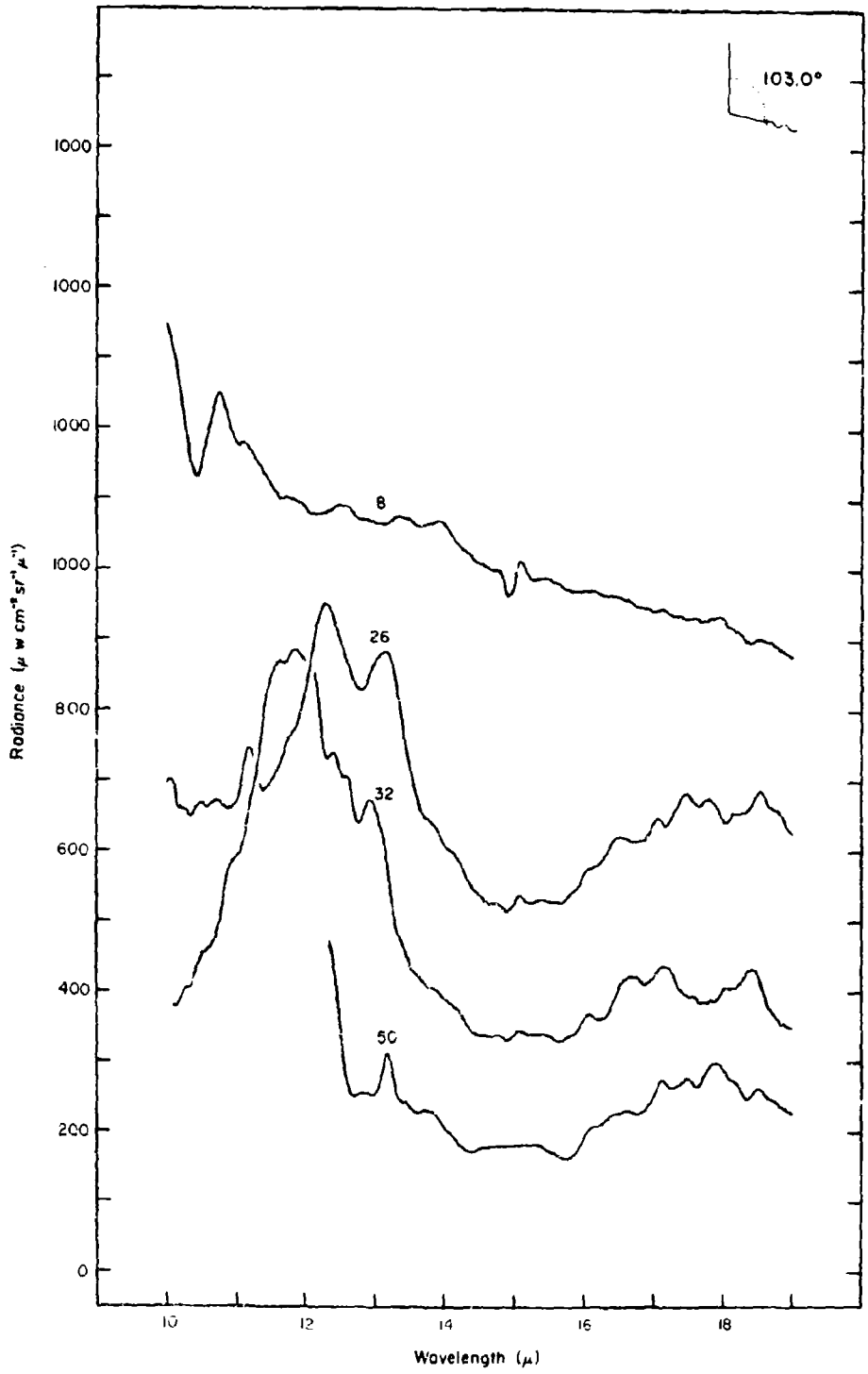

Figure 148. Spectral radiance vs altitude for balloon flight 1 July 1968. (See Table IV).

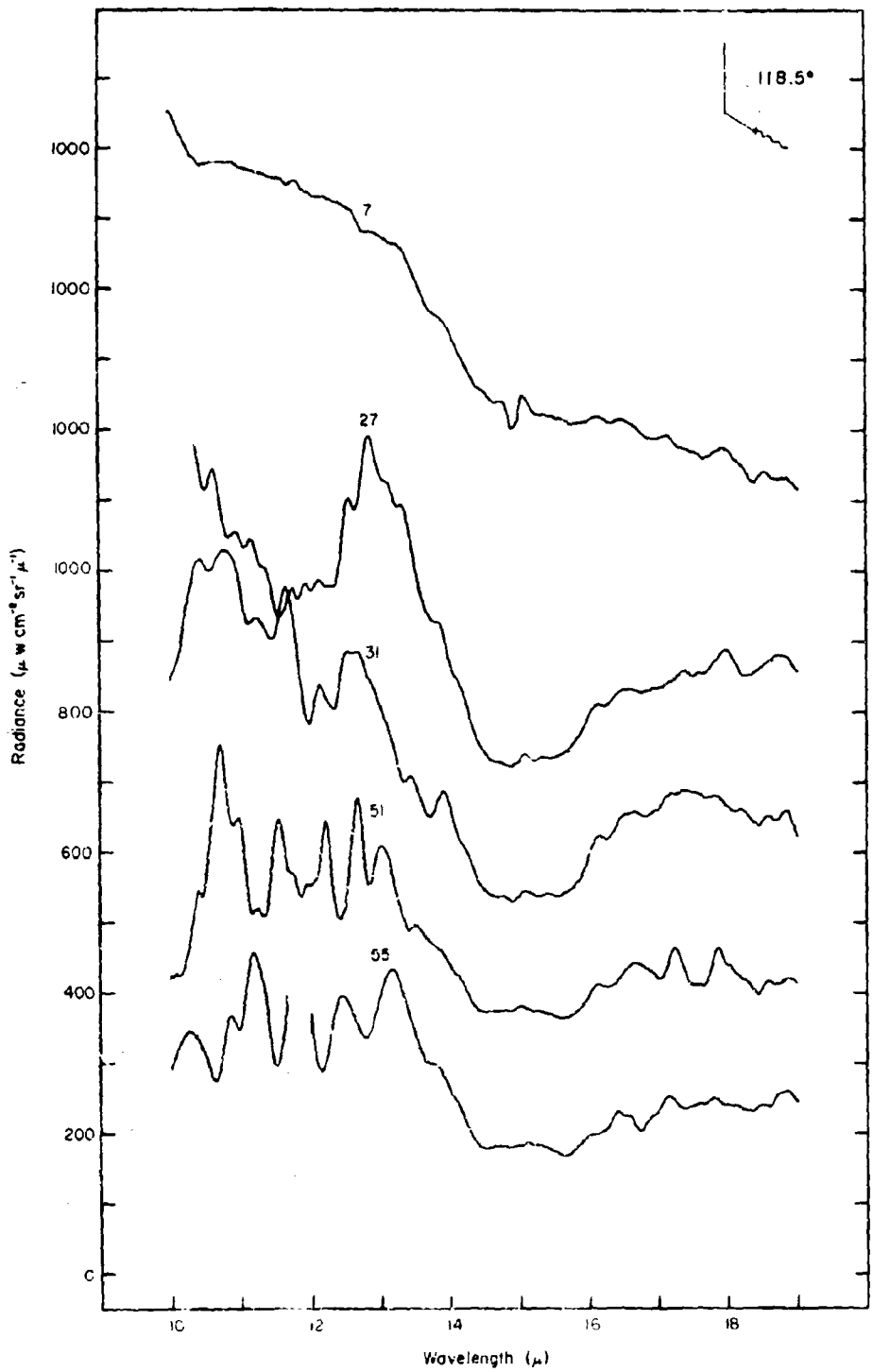

Figure 149. Spectral radiance vs altitude for balloon flight 1 July 1968. (See Table IV).

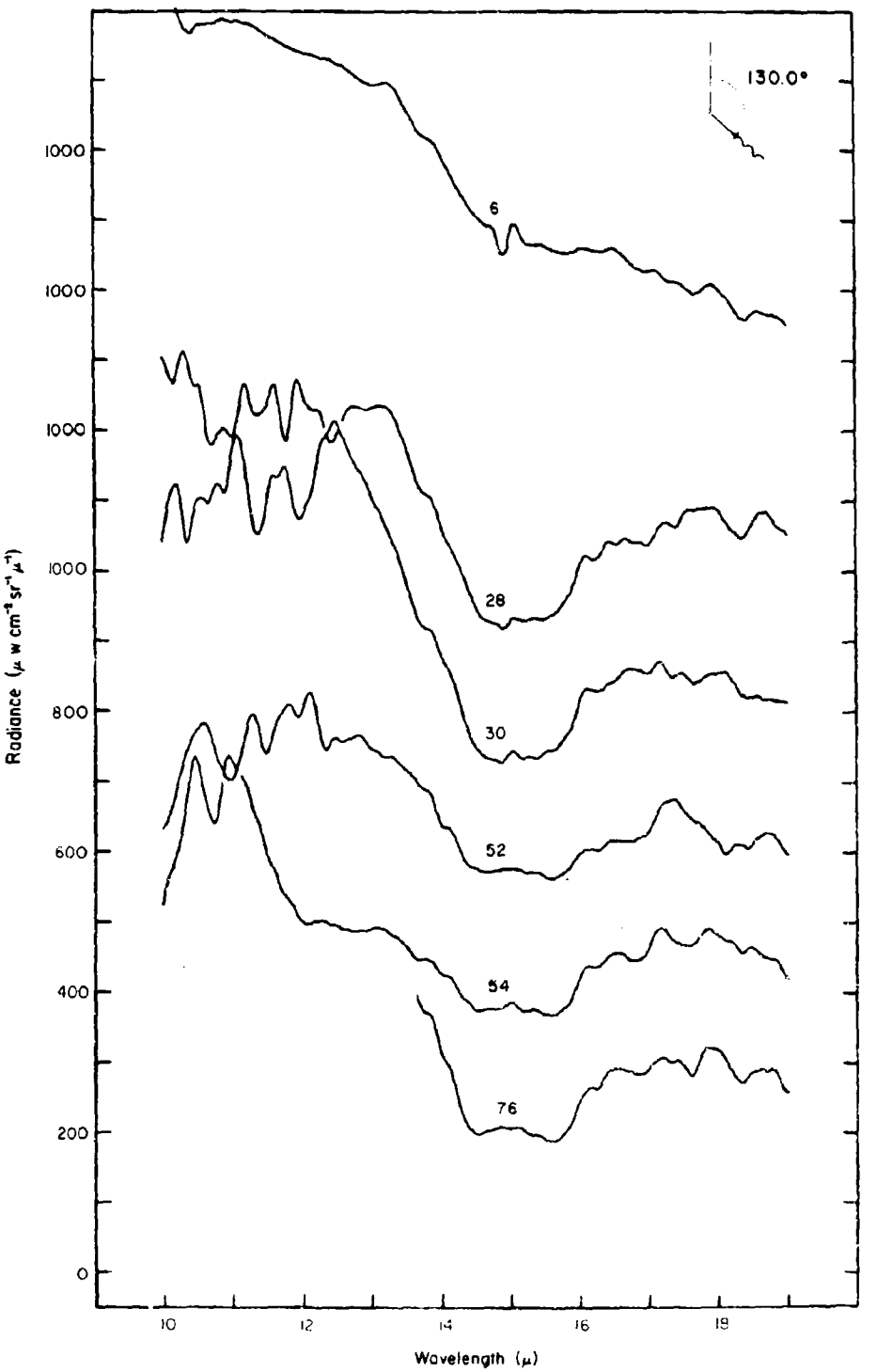

Figure 150. Spectral radiance vs altitude for balloon flight 1 July 1968. (See Table IV).

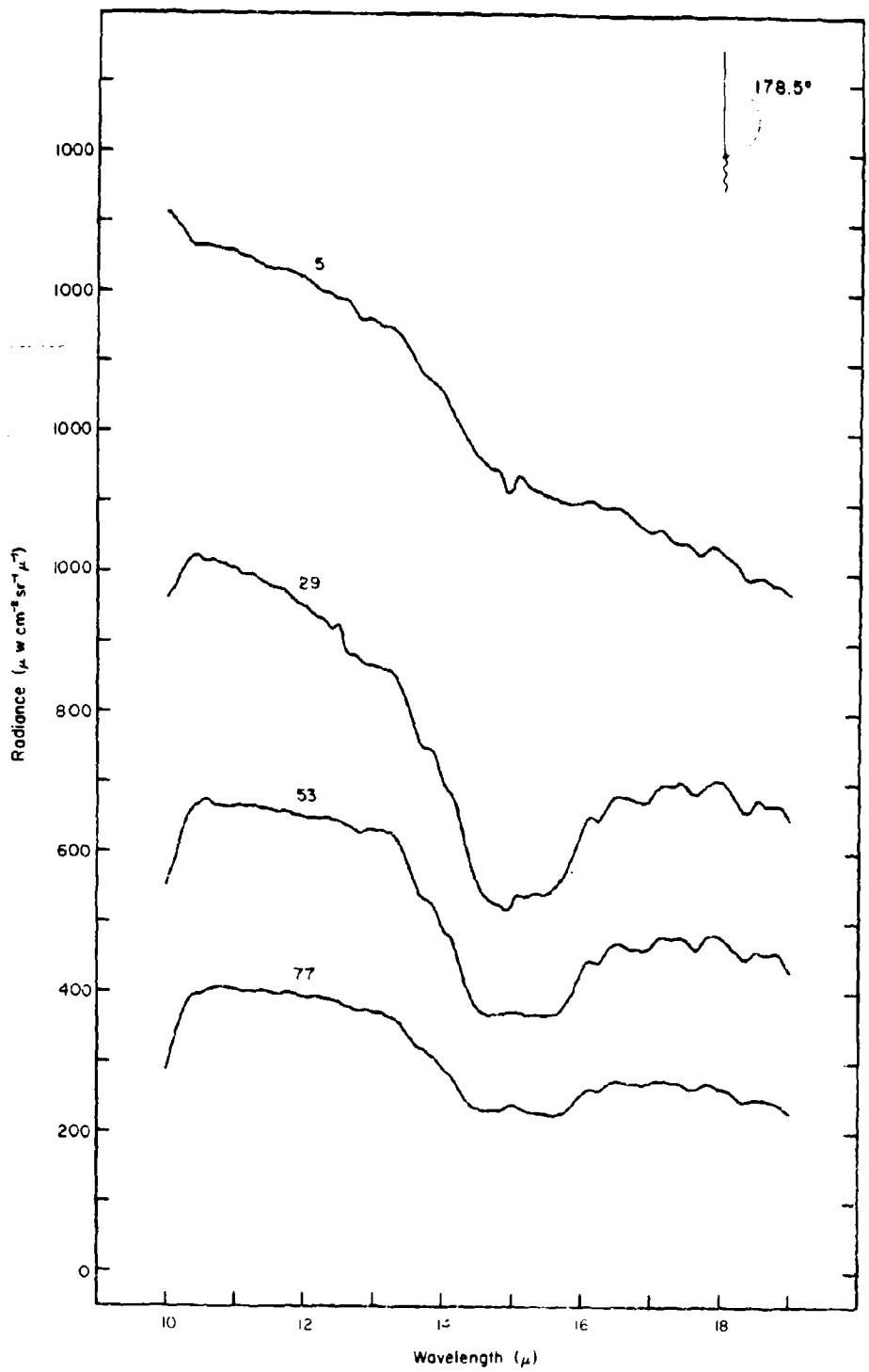

Figure 151. Spectral radiance vs altitude for balloon flight 1 July 1968. (See Table IV).

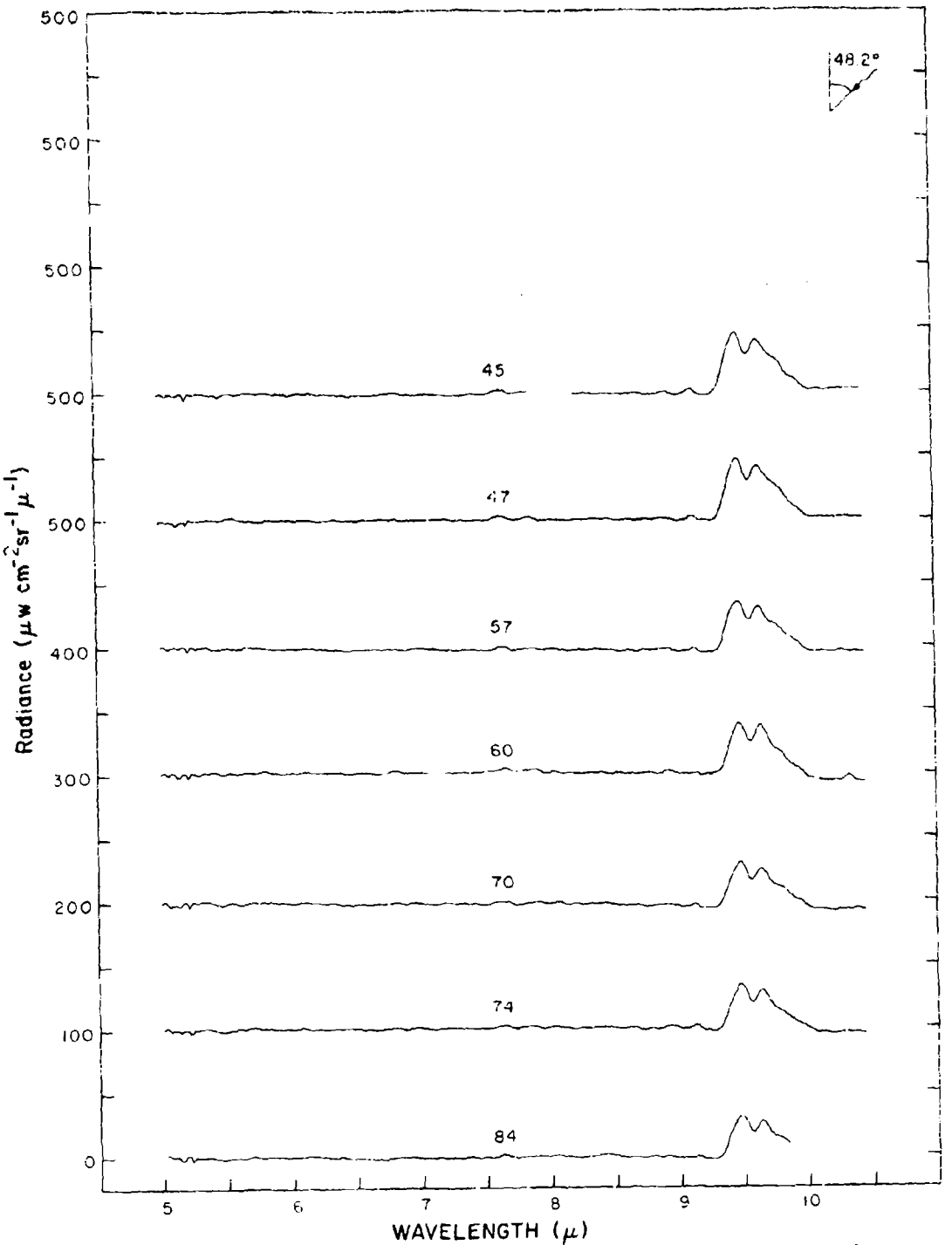
48.2°
45
47
57
60
70
74
84
Radiance (μw cm^{-2}sr$^{-1}\mu^{-1}$)
WAVELENGTH (μ)
500
500
500
500
500
400
300
200
100
0
5
6
7
8
9
10

Figure 152 [illegible]

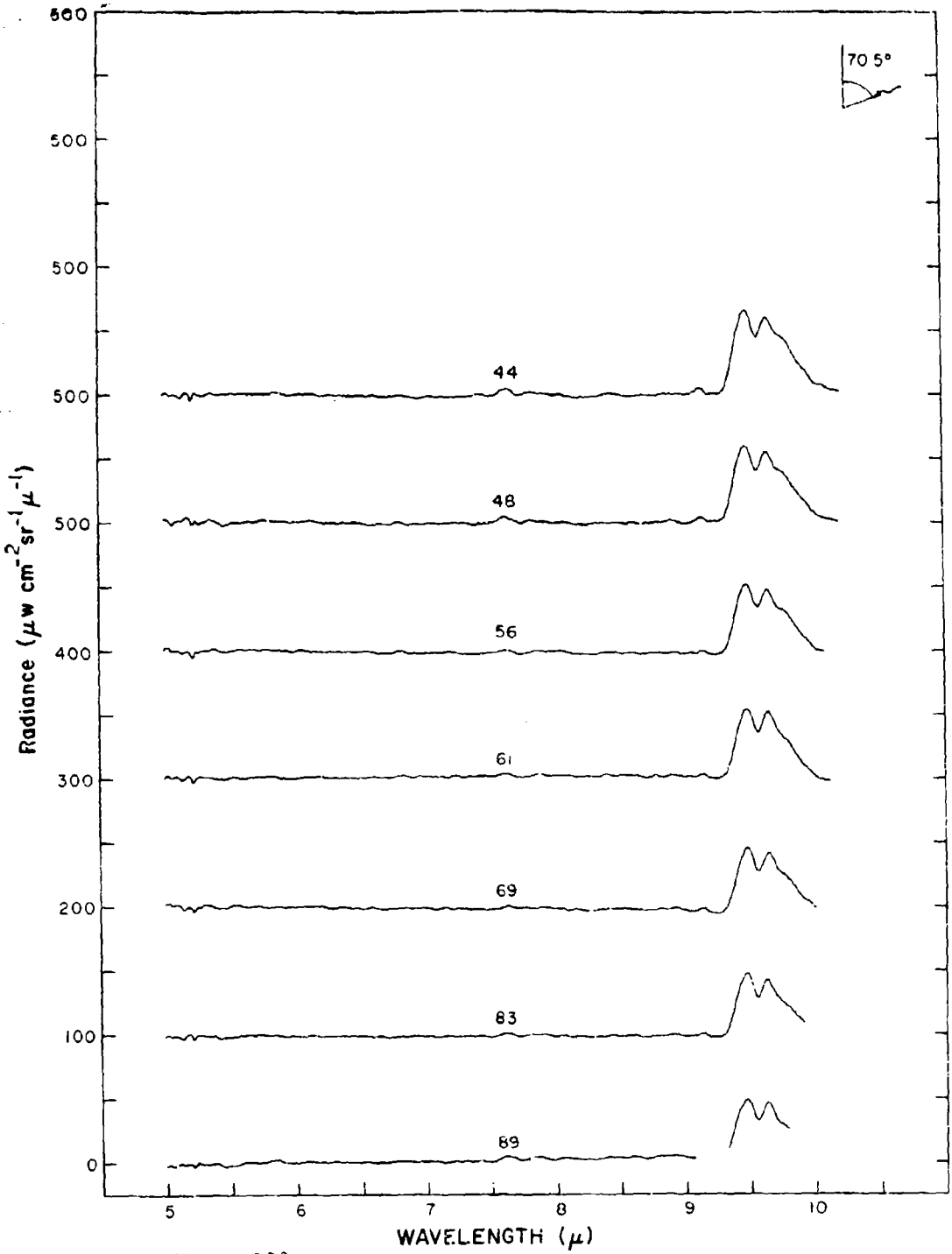

Figure 153 Spectral radiance vs altitude for balloon flight 25 February 1969. (See Table V)

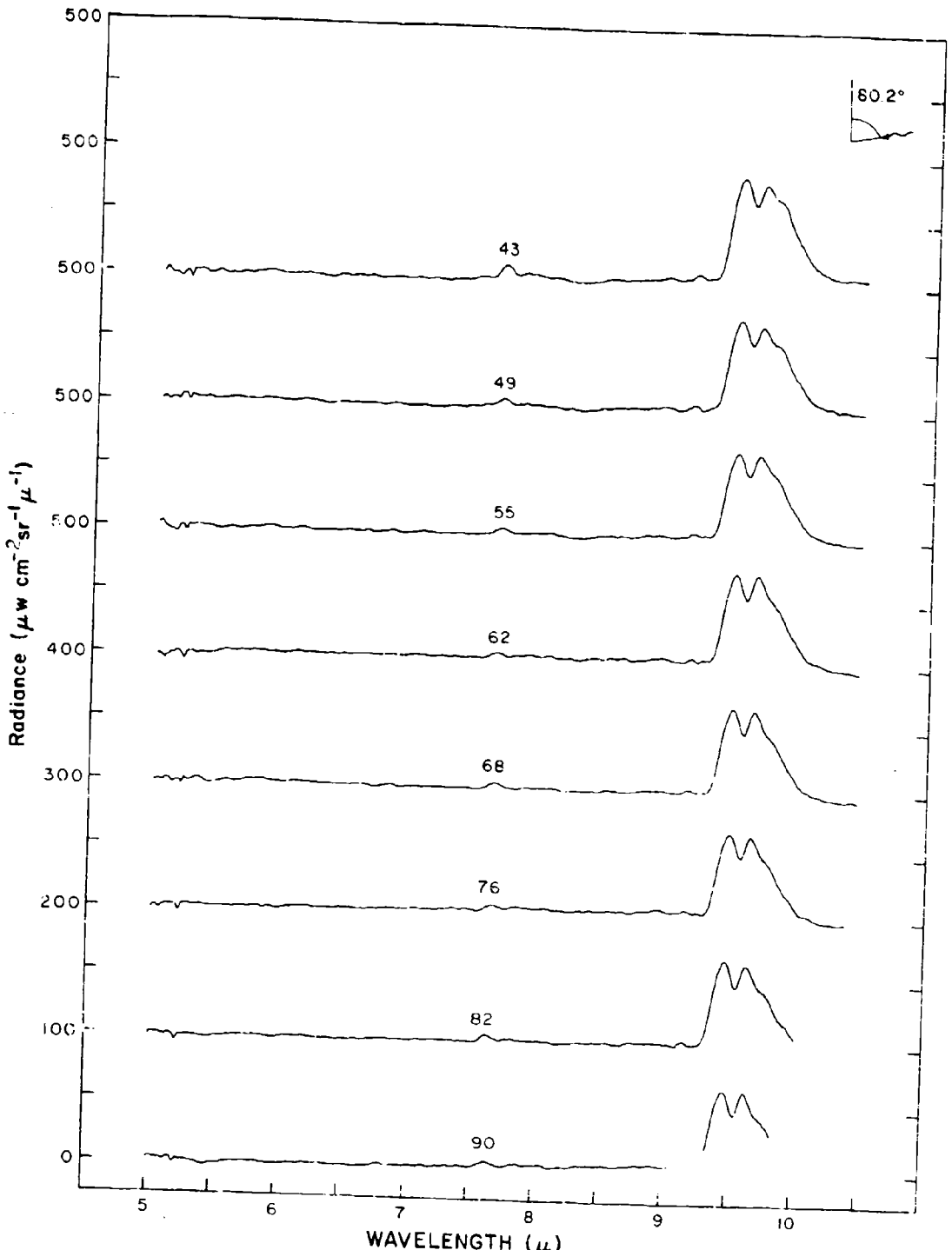

Fig. 154 Spectral radiance vs altitude for Nimbus flight 26 February 1969. (See Table V)

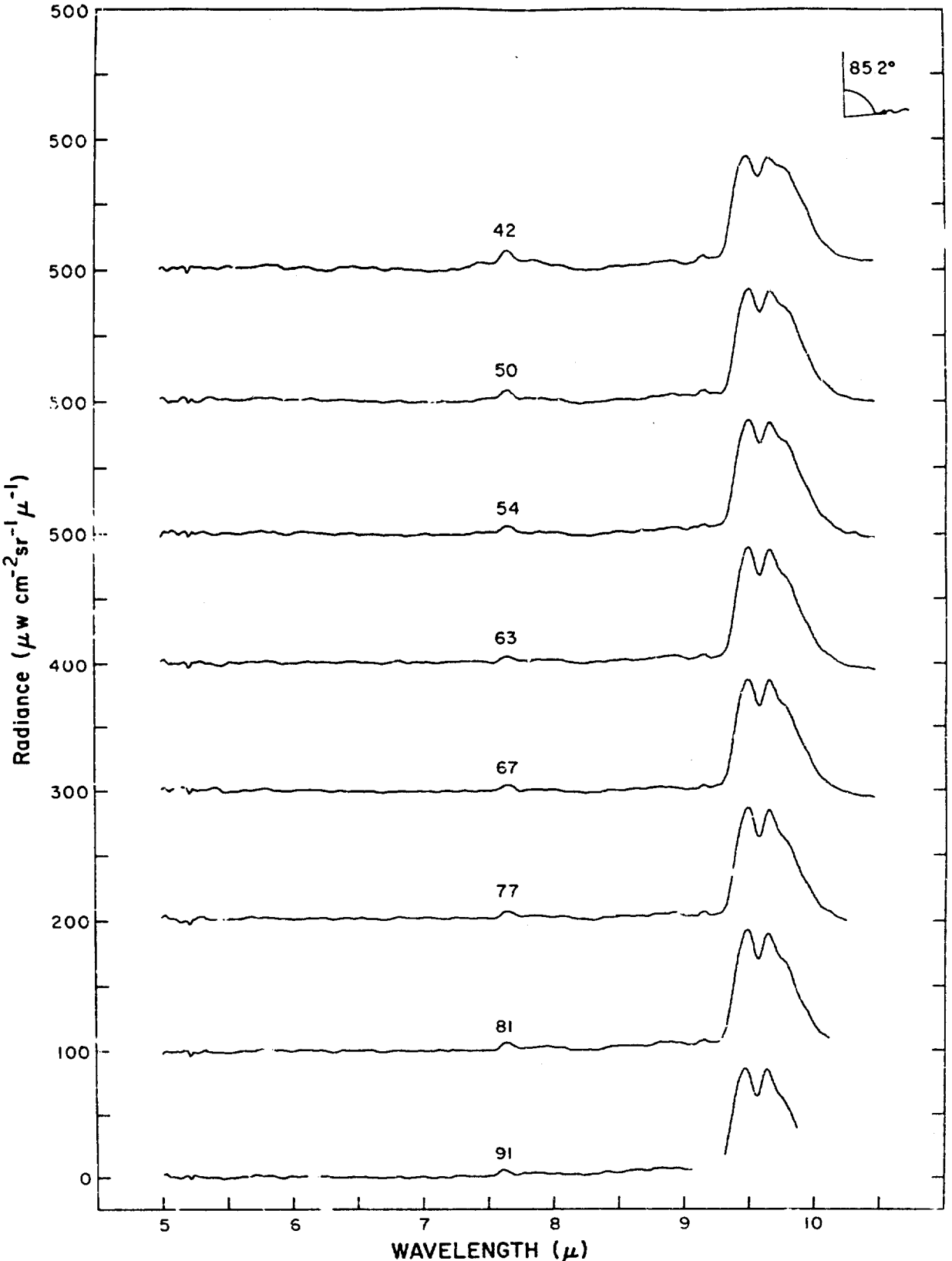

Figure 155 Spectral radiance vs altitude for balloon flight 25 January 1969. (See Table V)

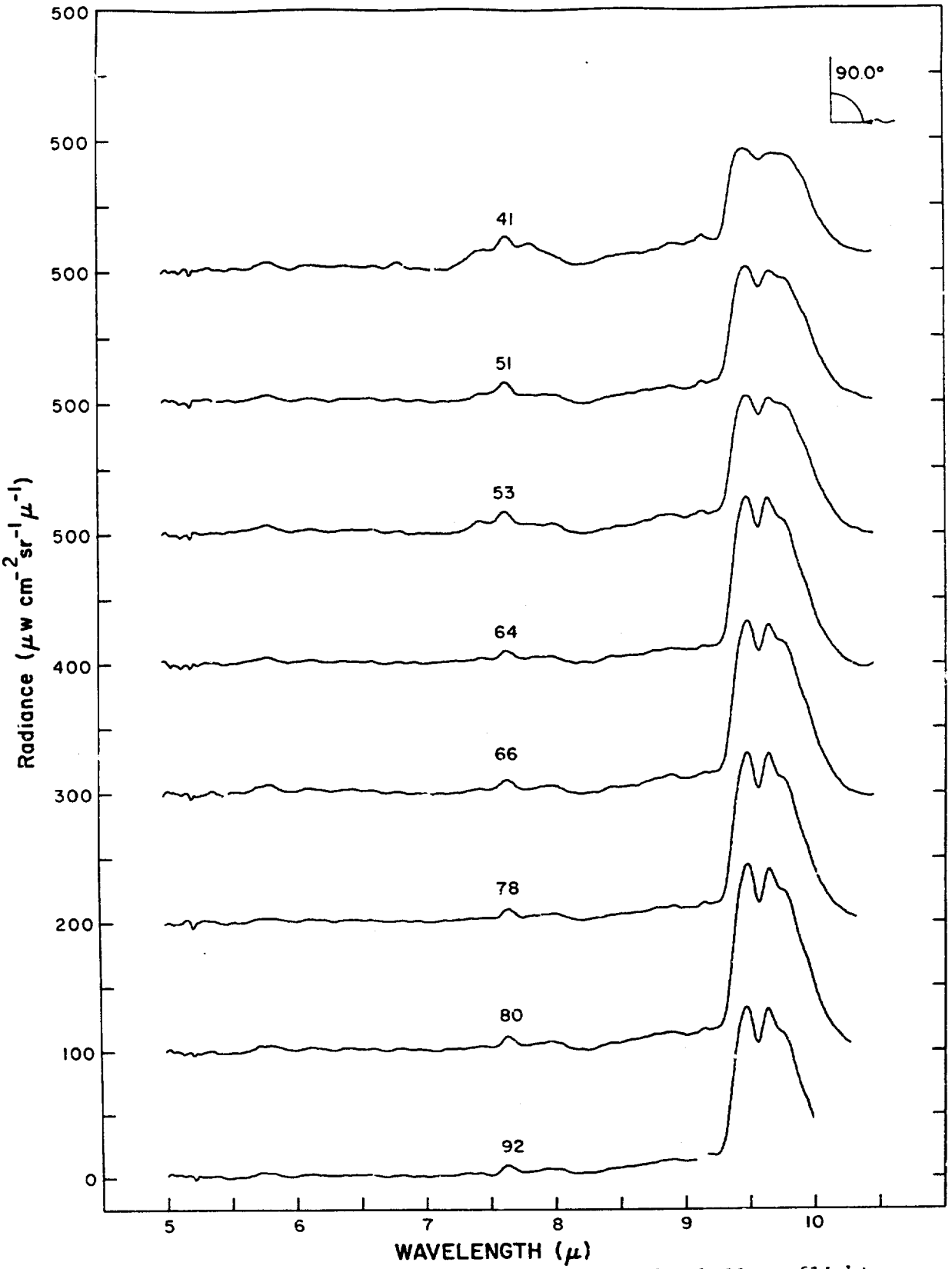

Figure 56 Spectral radiance vs altitude for balloon flight 25 February 1969. (See Table V)

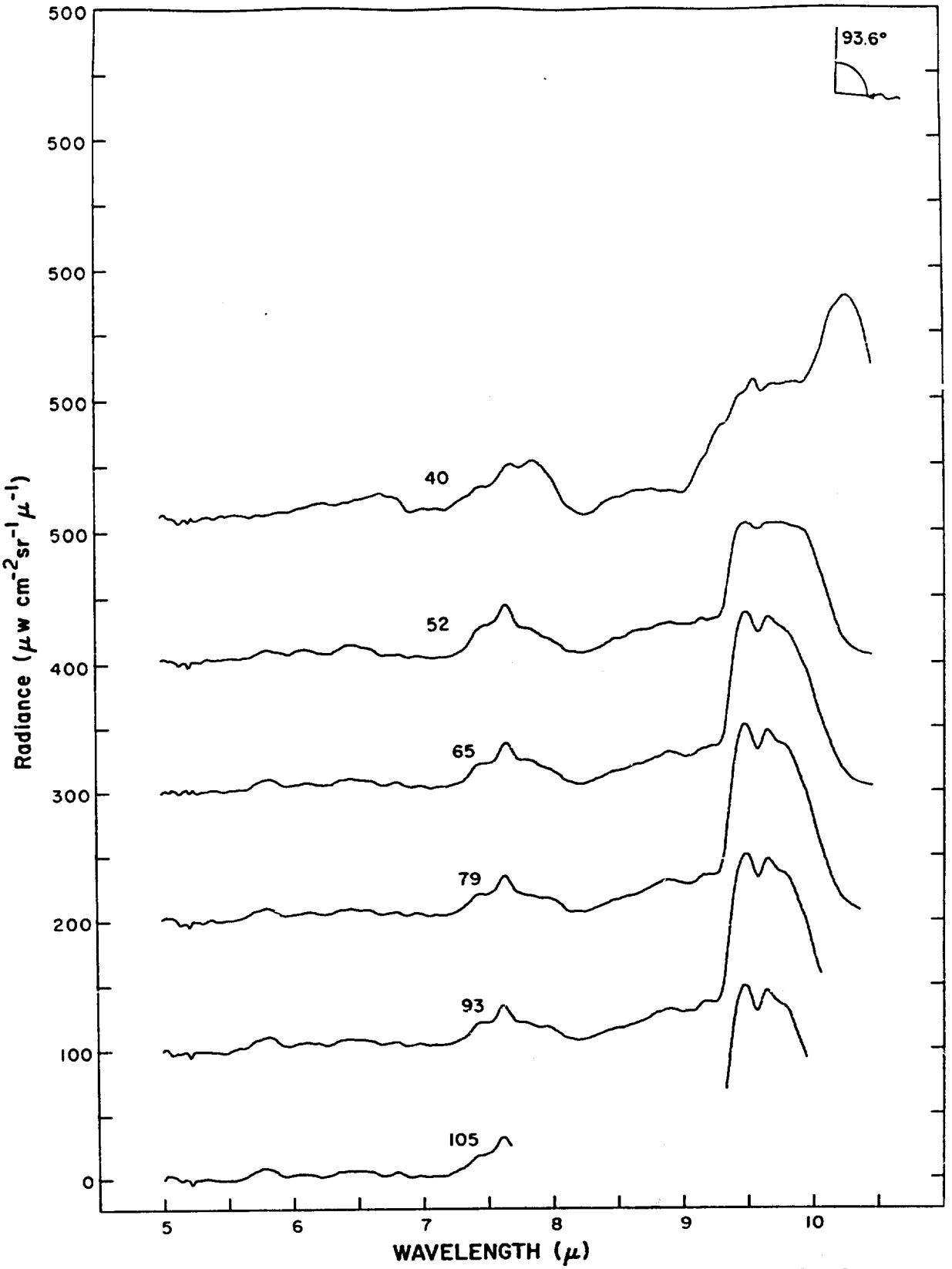

Figure 157 Spectral radiance vs altitude for balloon flight 25 February 1969. (See Table V)

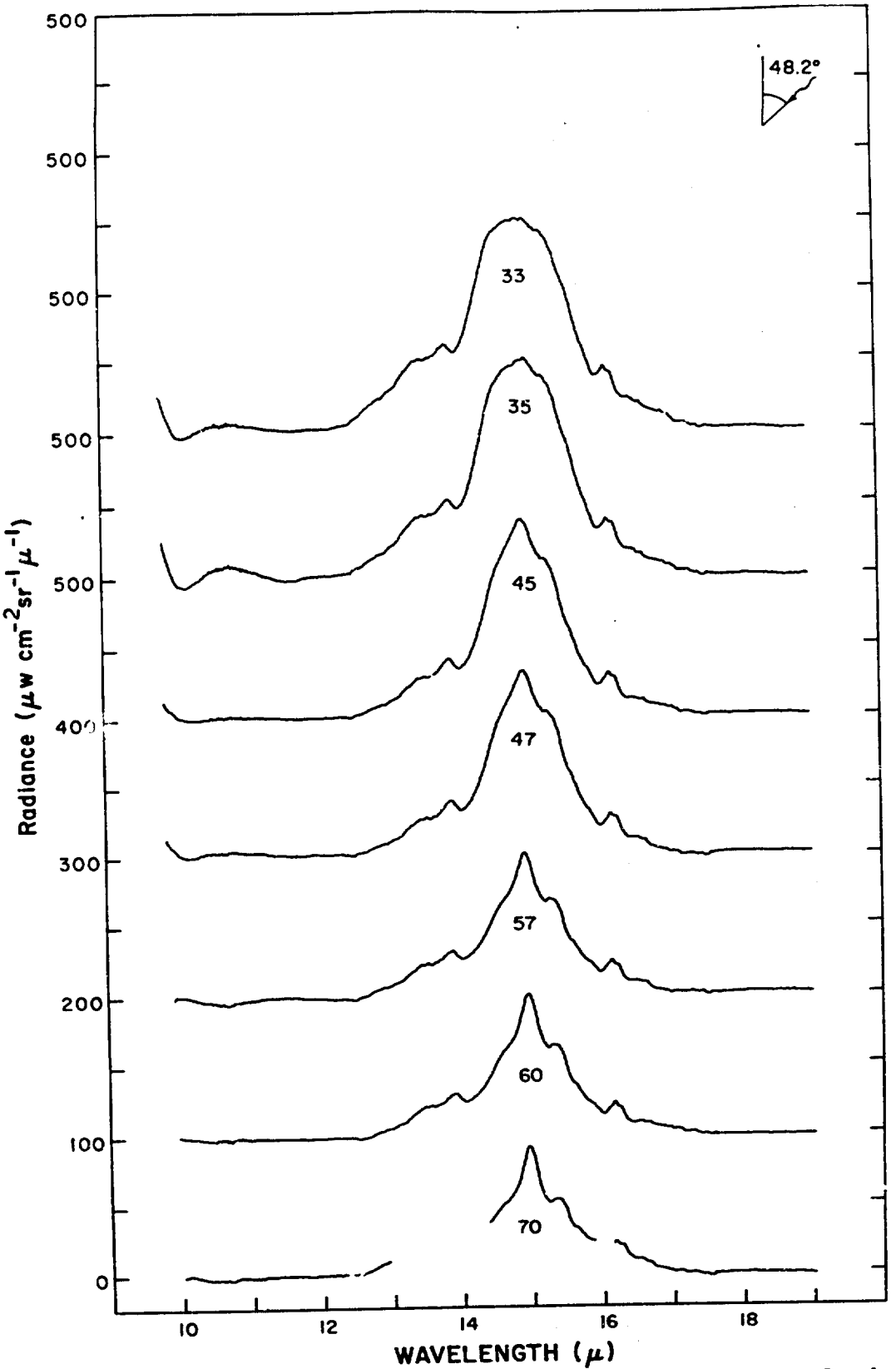

Figure 158 Spectral radiance vs altitude for balloon flight 25 February 1969. (See Table V)

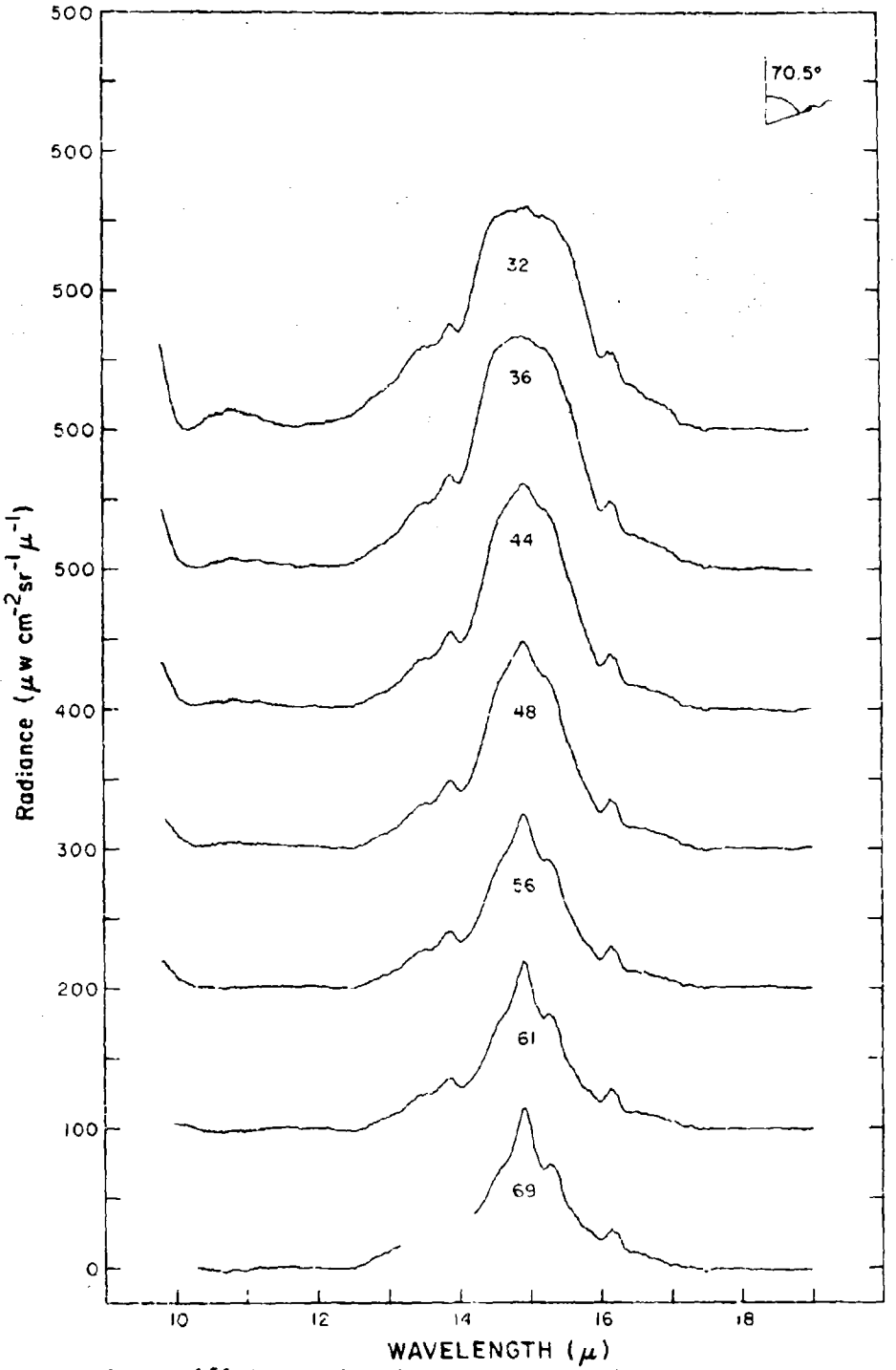

Figure 159 Spectral radiance vs altitude for balloon flight 25 February 1963. (See Table V)

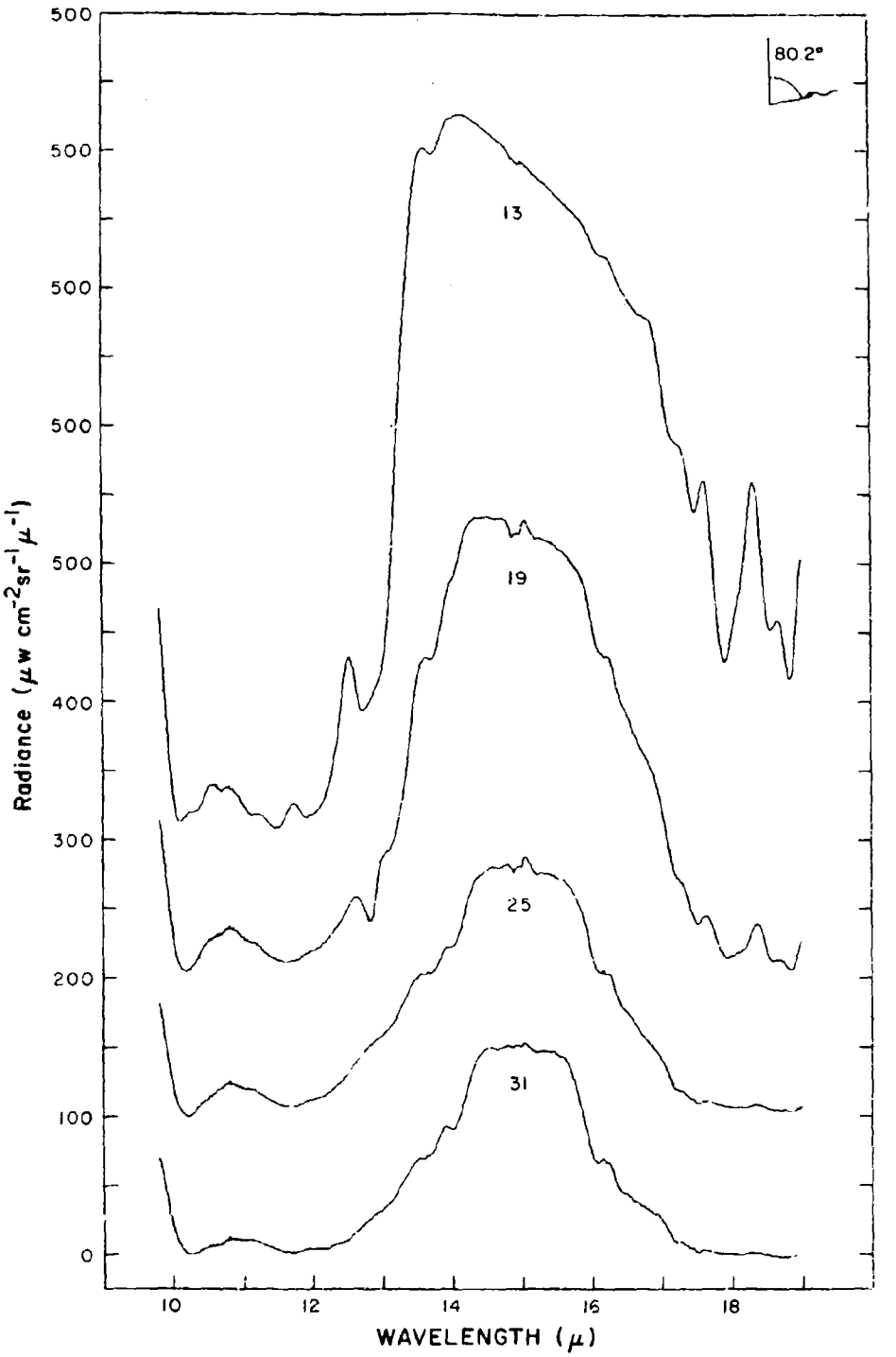

Figure 160 Spectral radiance vs altitude for balloon flight 25 February 1969. (See Table V)

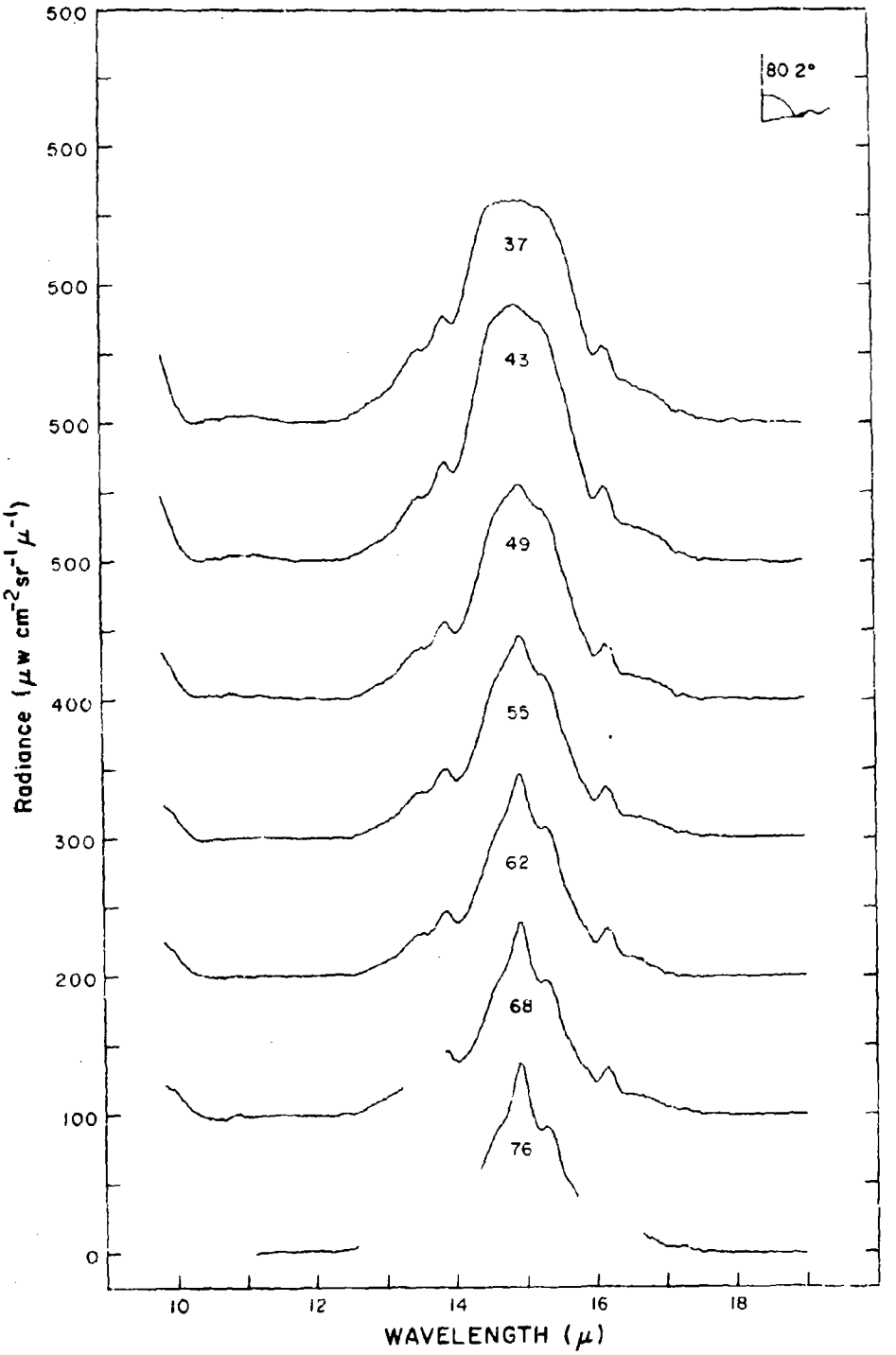

Fig. 161 Spectra [illegible] for [illegible] flight, 25 [illegible] 1966. (See Table V)

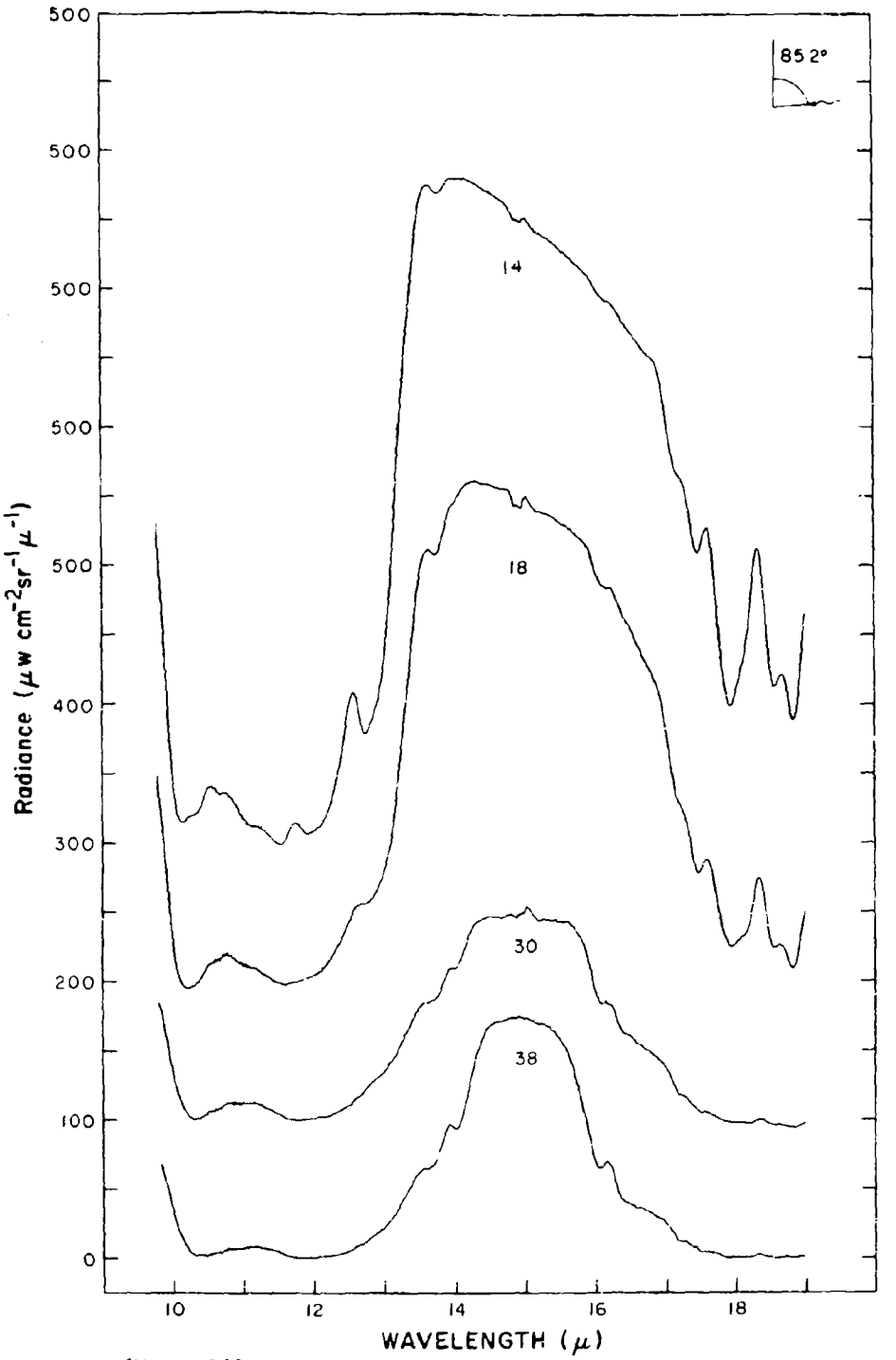

Figure 162 Spectral radiance vs altitude for balloon flight 25 February 1963. (See Table V)

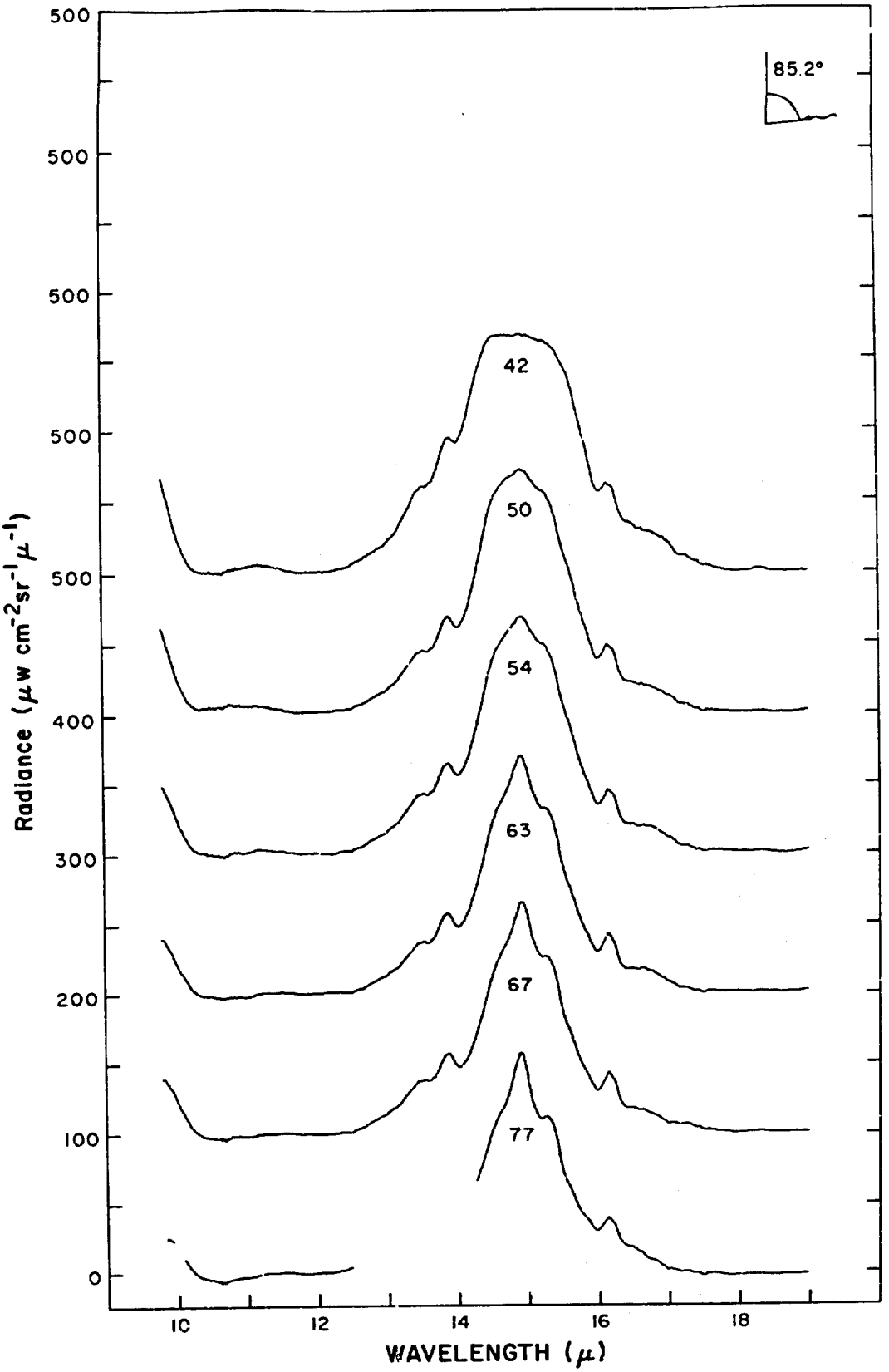

Figure 163 Spectral radiance vs altitude for balloon flight 25 February 1969. (See Table V)

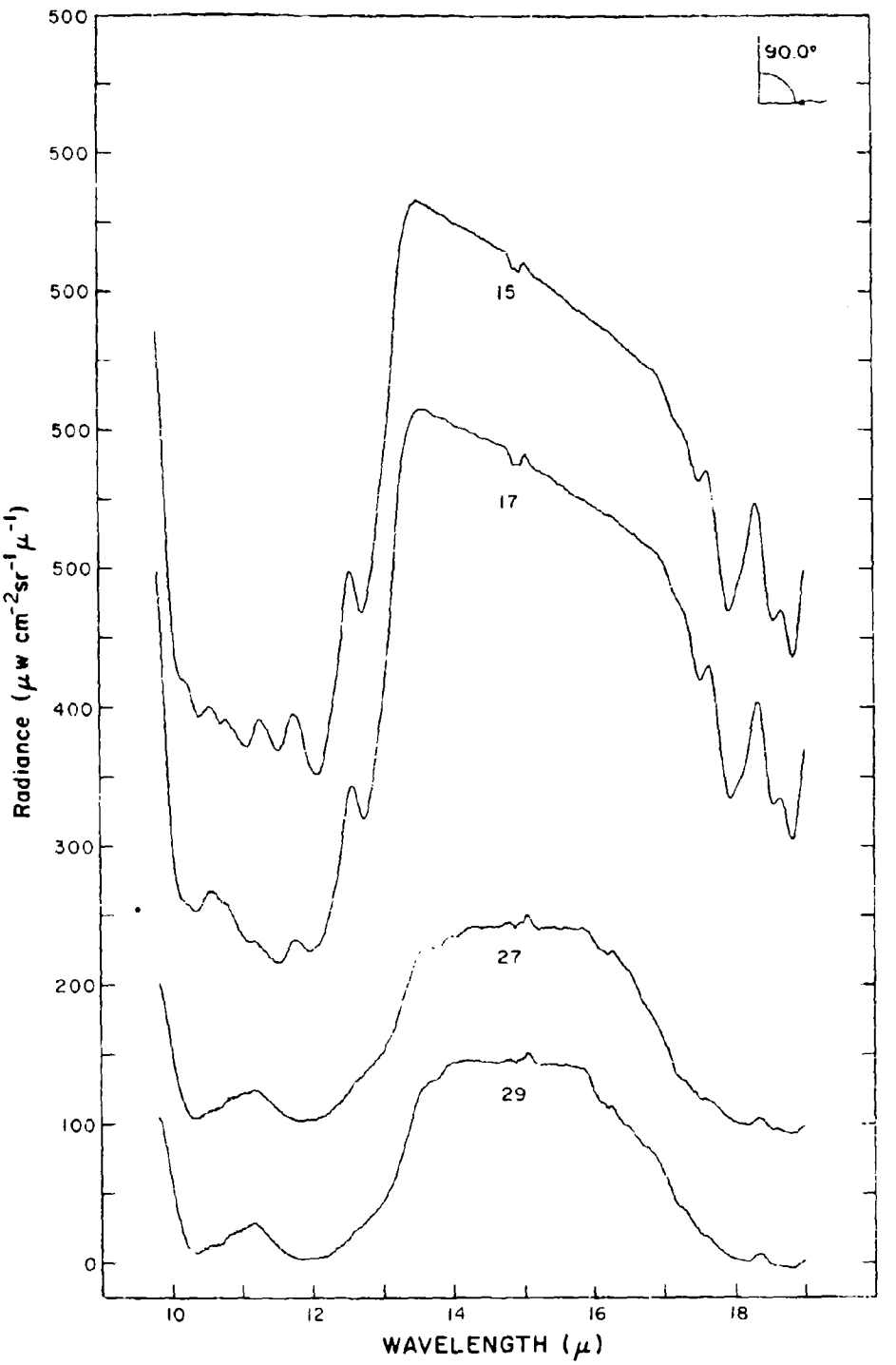

Figure 164 Spectral radiance vs altitude for Nimbus flight 25 February 1969. (See Table V)

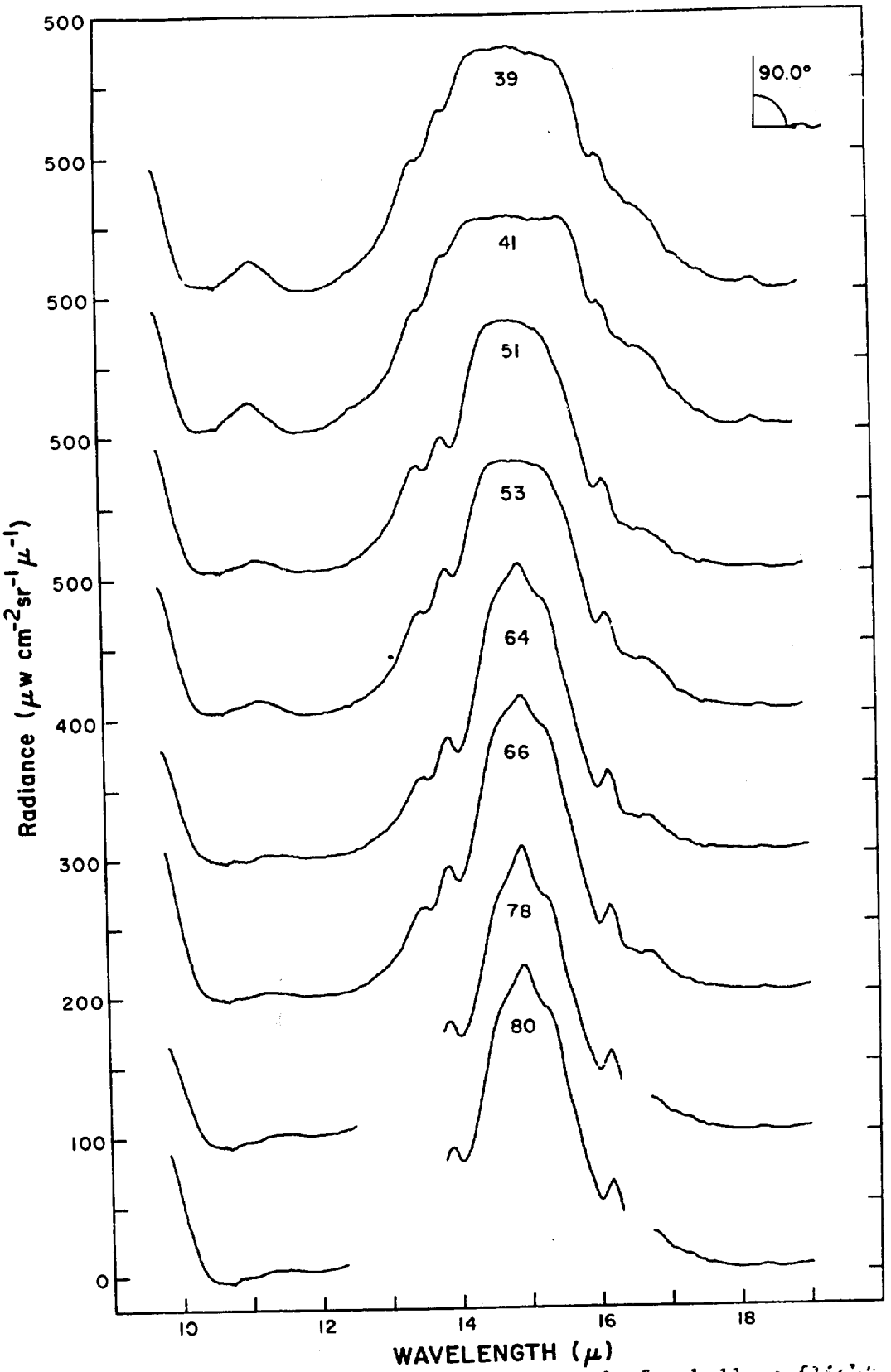

Fig. 165 Spectral radiance vs altitude for balloon flight 25 February 1966. (See Table V)

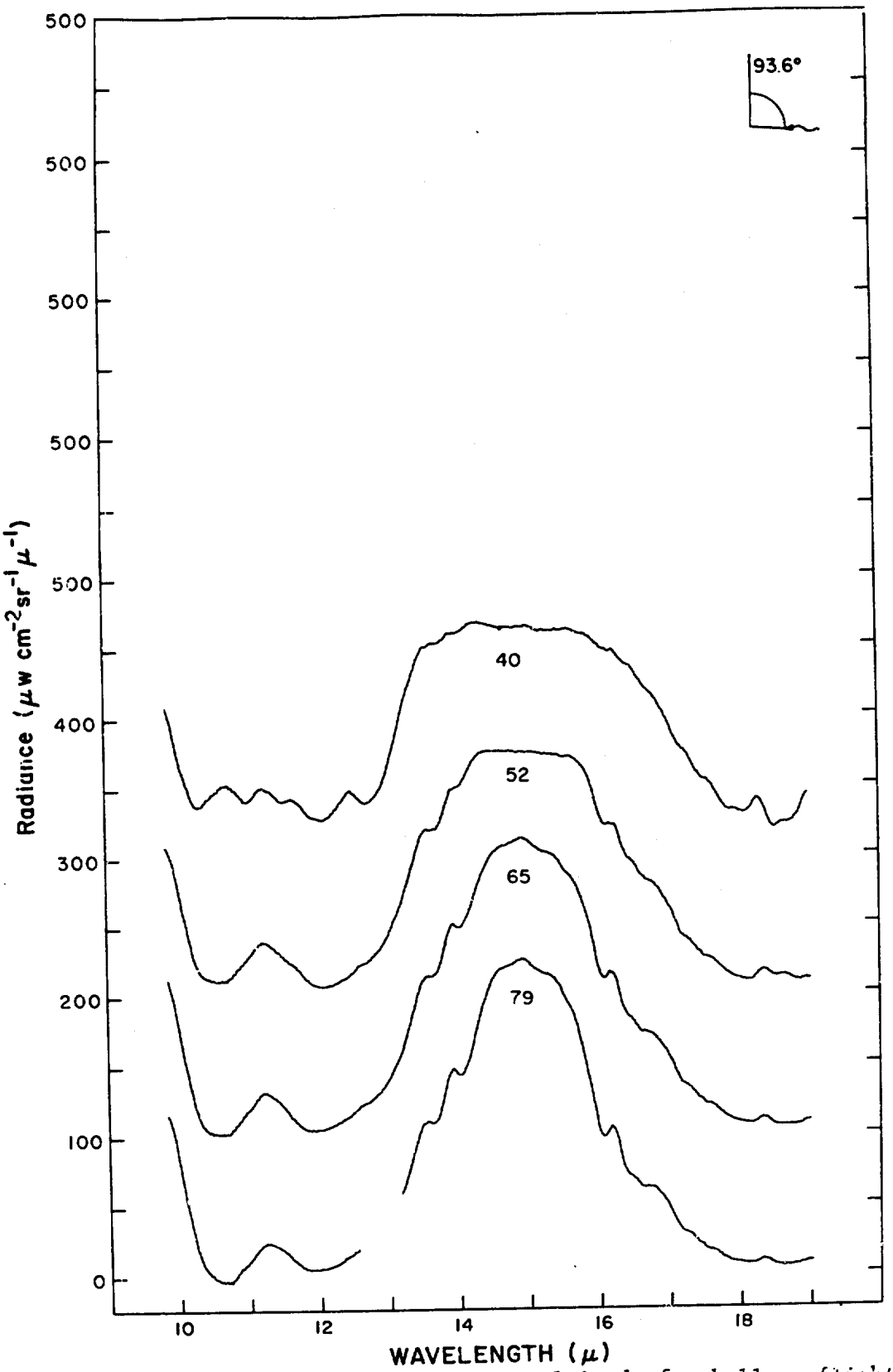

Figure 166 Spectral radiance vs altitude for balloon flight 25 February 1966. (See Table V)

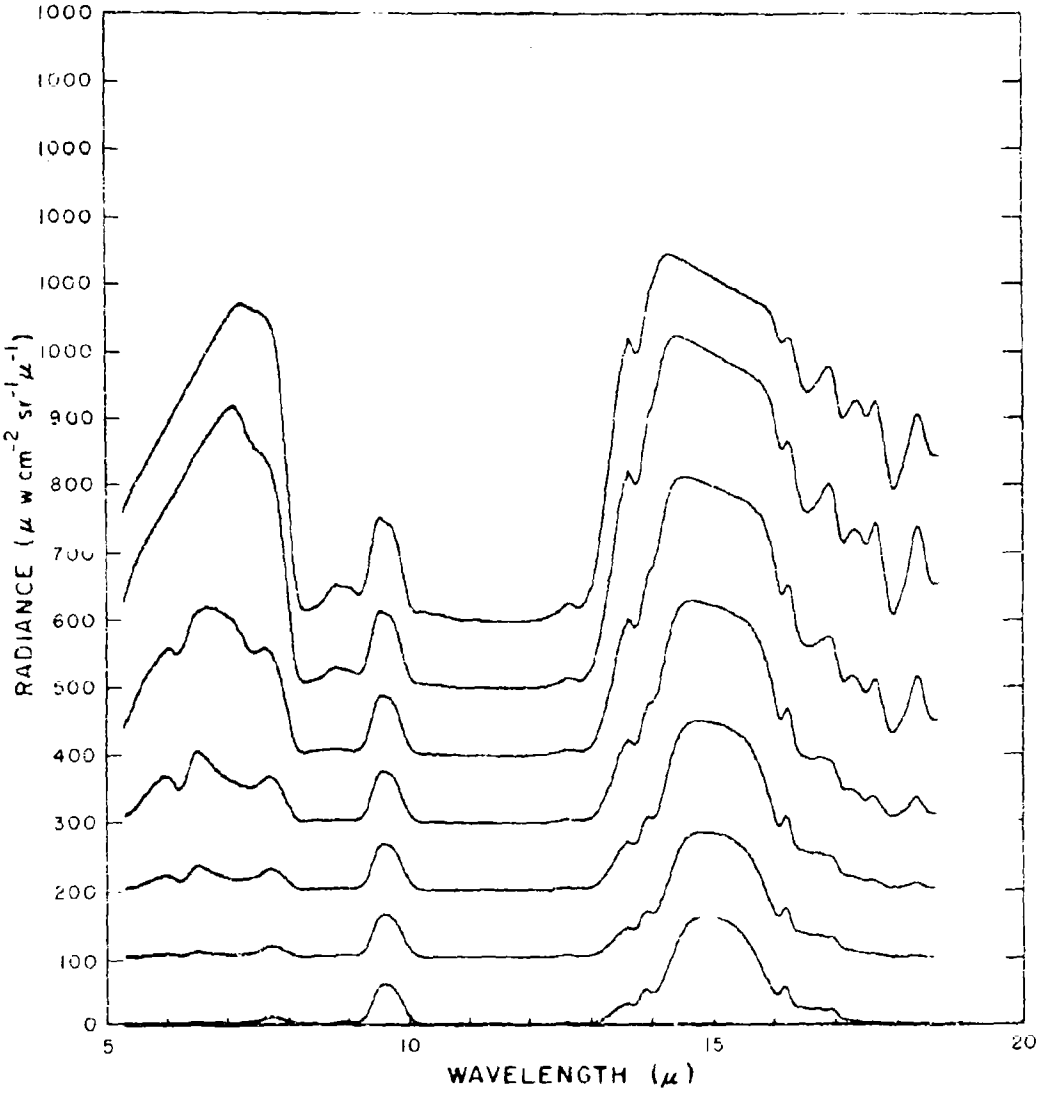

Figure 167. Calculated spectral radiance from 5 to 18μ vs altitude for 2 km intervals from 2 to 14 km (top to bottom) at a zenith observation angle of 0^{o} (sec = 1) for 1 June 1967. Successive records have a 100 μw cm^{-2} sr^{-1} μ^{-1} offset for clarity.

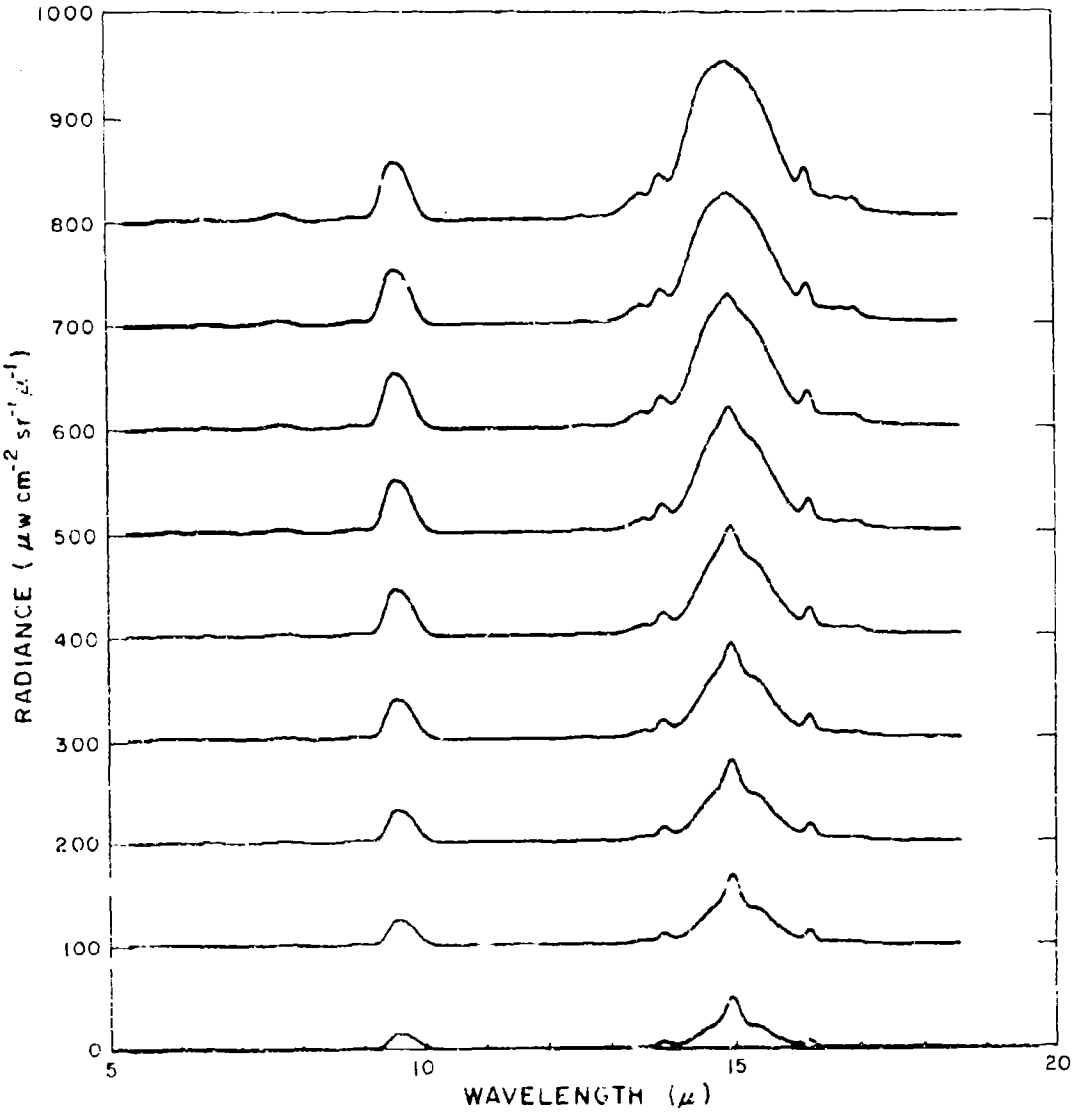

Figure 167. Cont. Calculated spectral radiance from 5 to 18μ vs altitude for 2 km intervals from 16 to 32 km (top to bottom) at a zenith observation angle of 0^{0} (sec = 1) for 1 June 1967. Successive records have a 100 $\mu w\ cm^{-2}\ sr^{-1}\ \mu^{-1}$ offset for clarity.

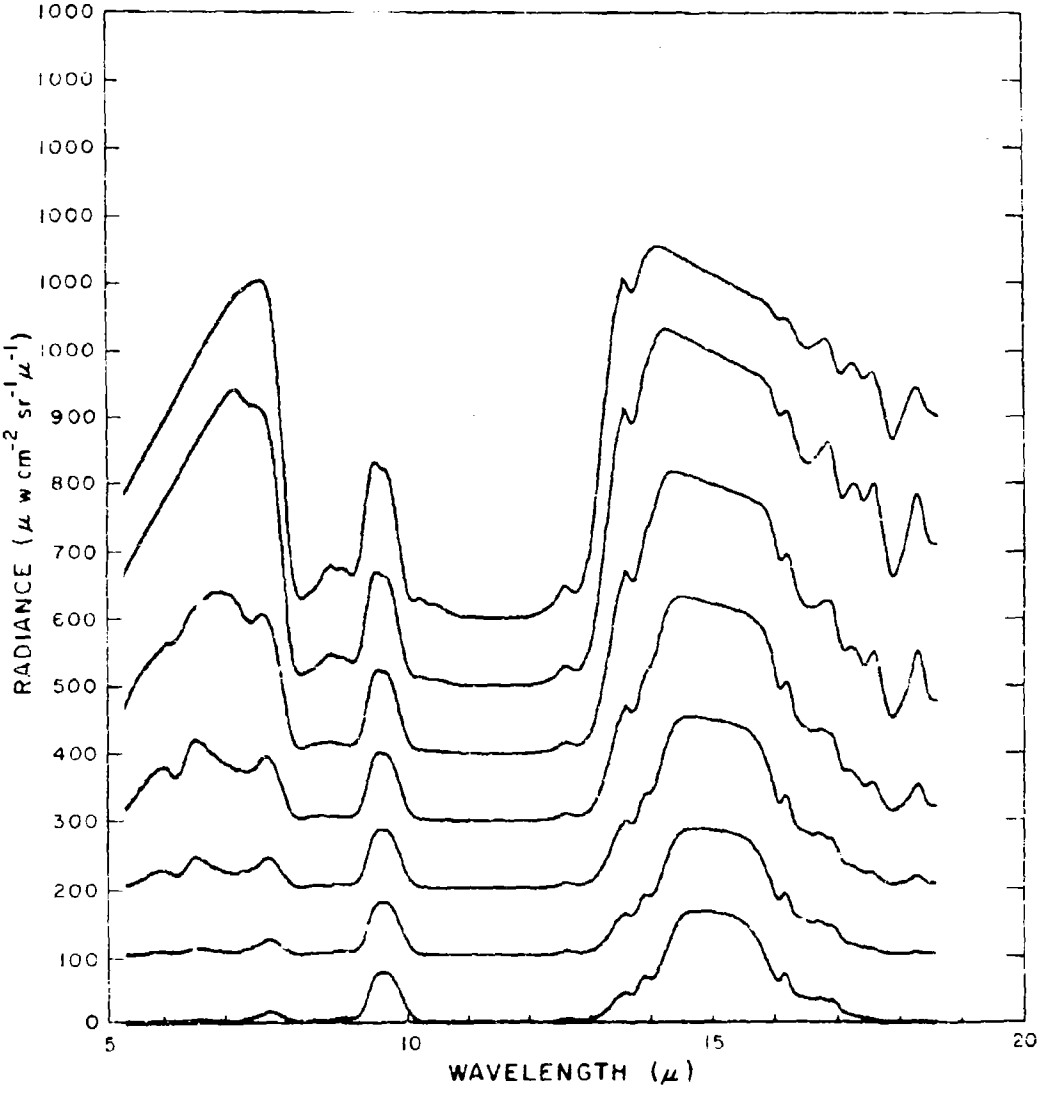

Figure 168. Calculated spectral radiance from 5 to 18μ vs altitude for 2 km intervals from 2 to 14 km (top to bottom) at a zenith observation angle of 60^{0} (sec = 2) for 1 June 1967. Successive records have a 100 $\mu w\ cm^{-2}\ sr^{-1}\ \mu^{-1}$ offset for clarity.

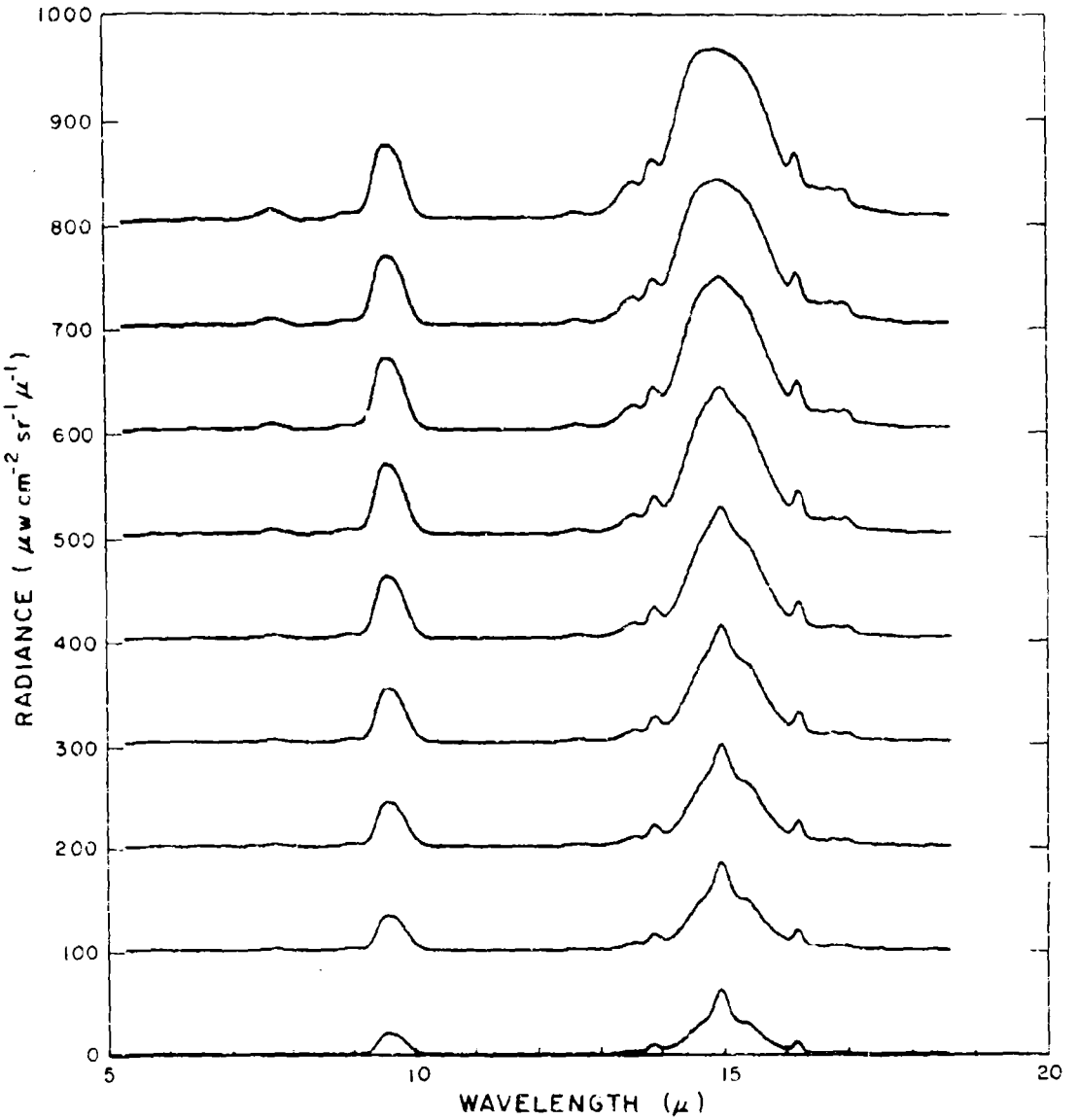

Figure 168. Cont. Calculated spectral radiance from 5 to 18μ vs altitude for 2 km intervals from 16 to 32 km (top to bottom) at a zenith observation angle of 60° (sec = 2) for 1 June 1967. Successive records have a 100 μw cm^{-2} sr^{-1} μ^{-1} offset for clarity.

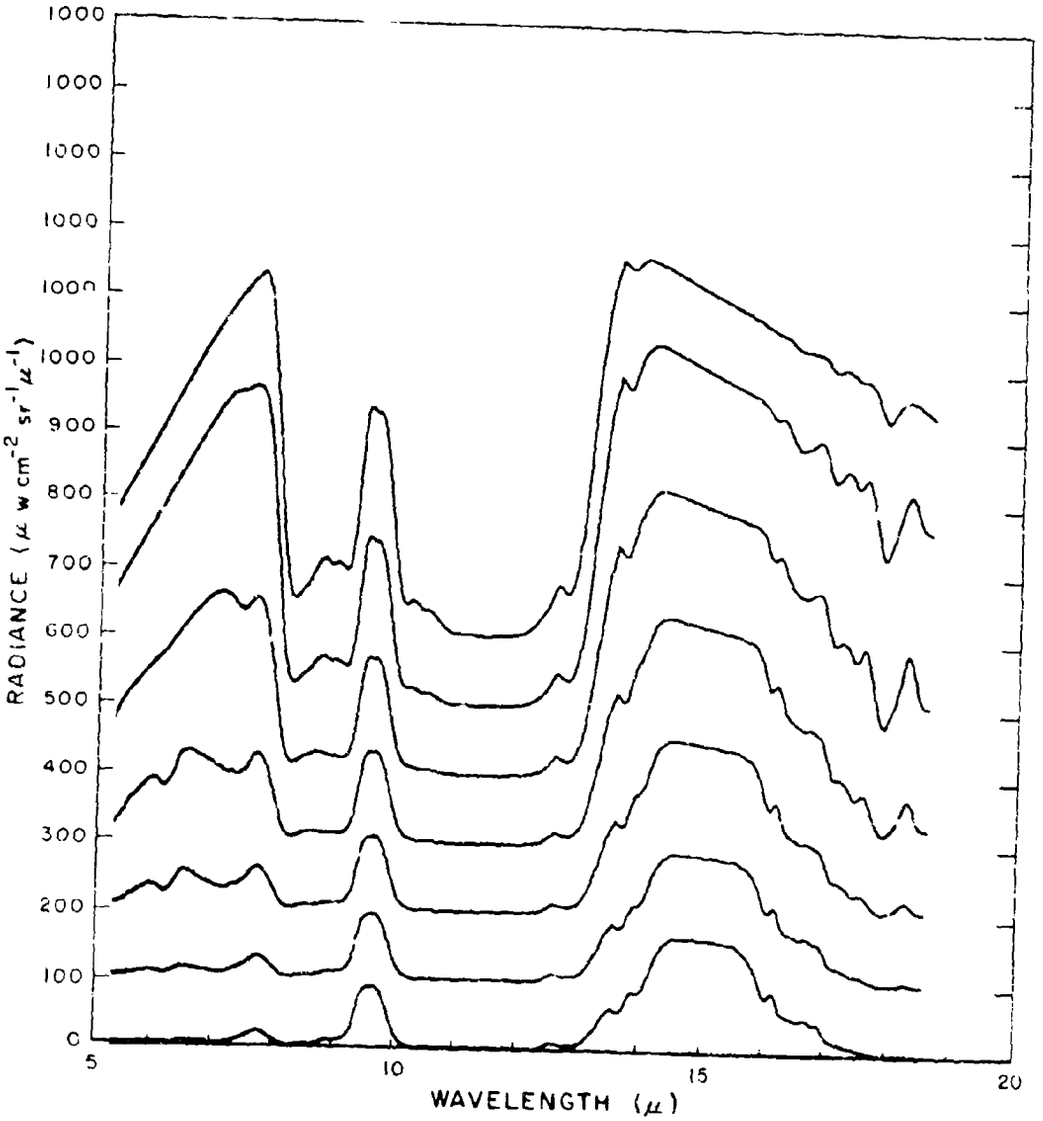

Figure 169. Calculated spectral radiance from 5 to 18μ vs altitude for 2 km intervals from 2 to 14 km (top to bottom) at a zenith observation angle of 75.5° (sec = 4) for 1 June 1967. Successive records have a 100 μw cm^{-2} sr^{-1} μ^{-1} offset for clarity.

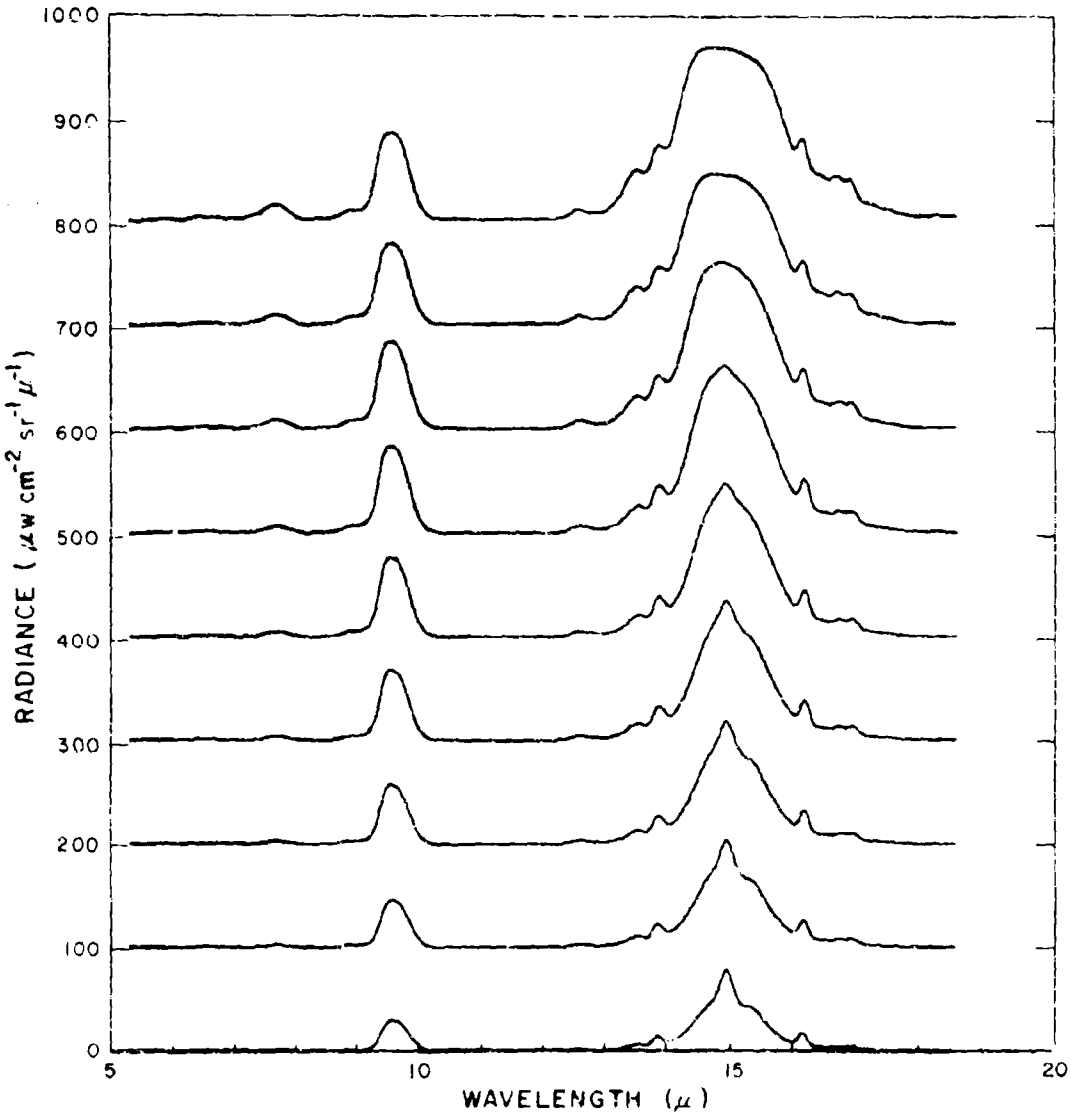

Figure 169. Cont. Calculated spectral radiance from 5 to 18$_\mu$ vs altitude for 2 km intervals from 16 to 32 km (top to bottom) at a zenith observation angle of 75.5° (sec = 4) for 1 June 1967. Successive records have a 100 μw cm ^{2} sr^{-1} μ^{-1} offset for clarity.

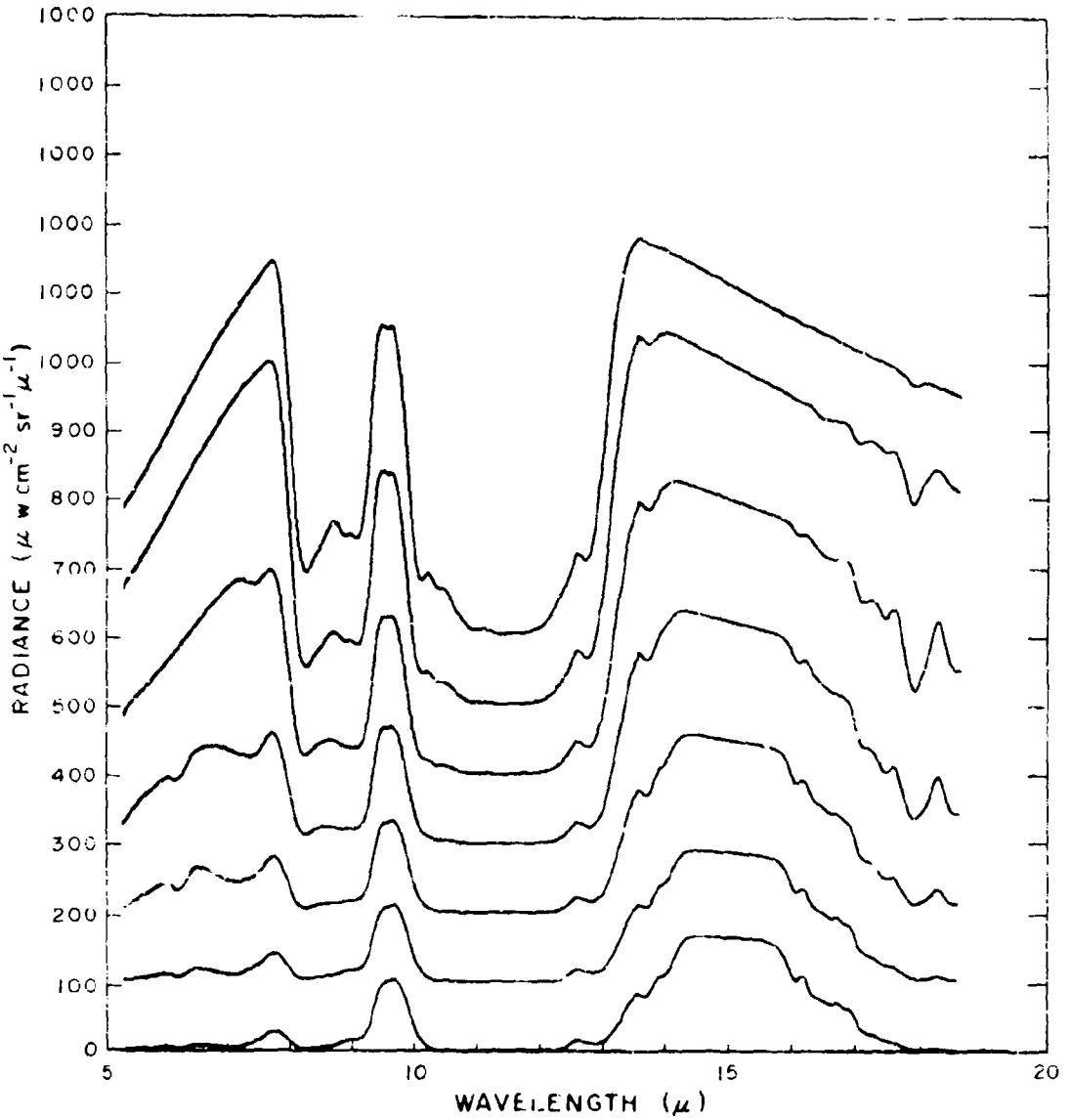

Figure 170. Calculated spectral radiance from 5 to 18μ vs altitude for 2 km intervals from 2 to 14 km (top to bottom) at a zenith observation angle of 82.8° (sec = 8) for 1 June 1967. Successive records have a 100 μw cm^{-2} sr^{-1} μ^{-1} offset for clarity.

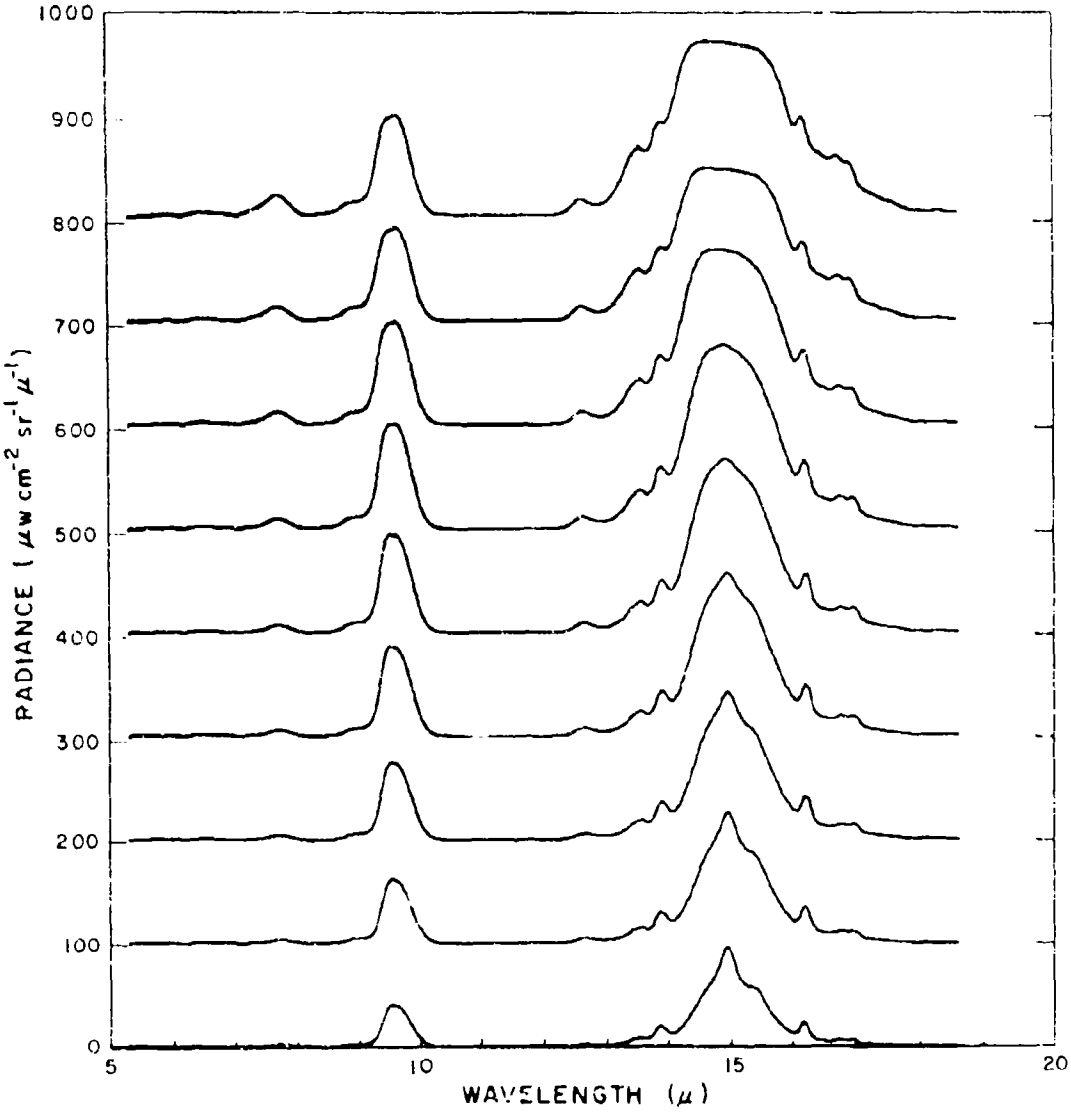

Figure 170. Cont. Calculated spectral radiance from 5 to 18μ vs altitude for 2 km intervals from 16 to 32 km (top to bottom) at a zenith observation angle of 82.8° (sec = 8) for 1 June 1967. Successive records have a 100μw cm^{-2} sr^{-1} μ^{-1} offset for clarity.

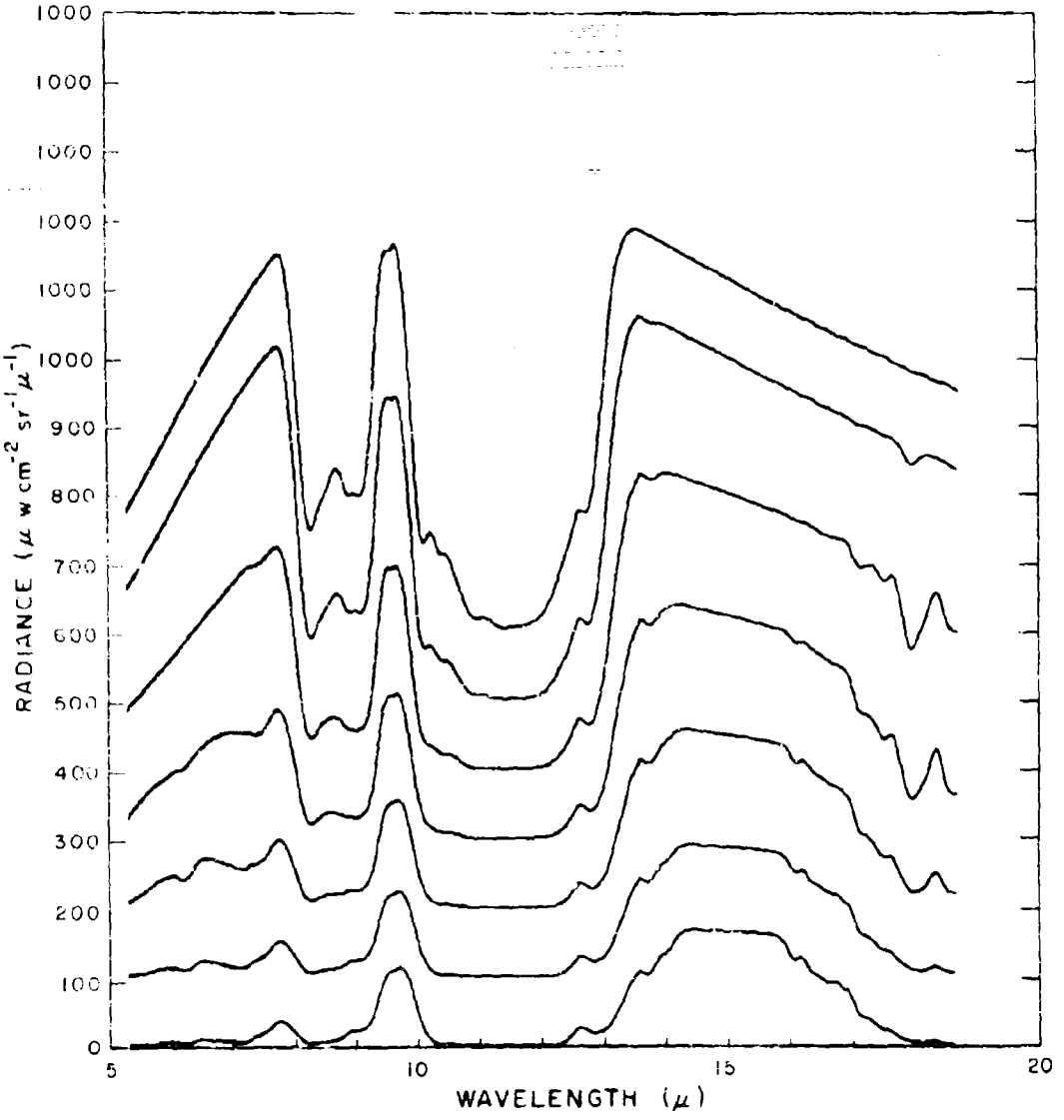

Figure 171. Calculated spectral radiance from 5 to 18μ vs altitude for 2 km intervals from 2 to 14 km (top to bottom) at a zenith observation angle of 86.4° (sec = 16) for 1 June 1967. Successive records have a 100 $\mu w\ cm^{-2}\ sr^{-1}\ \mu^{-1}$ offset for clarity.

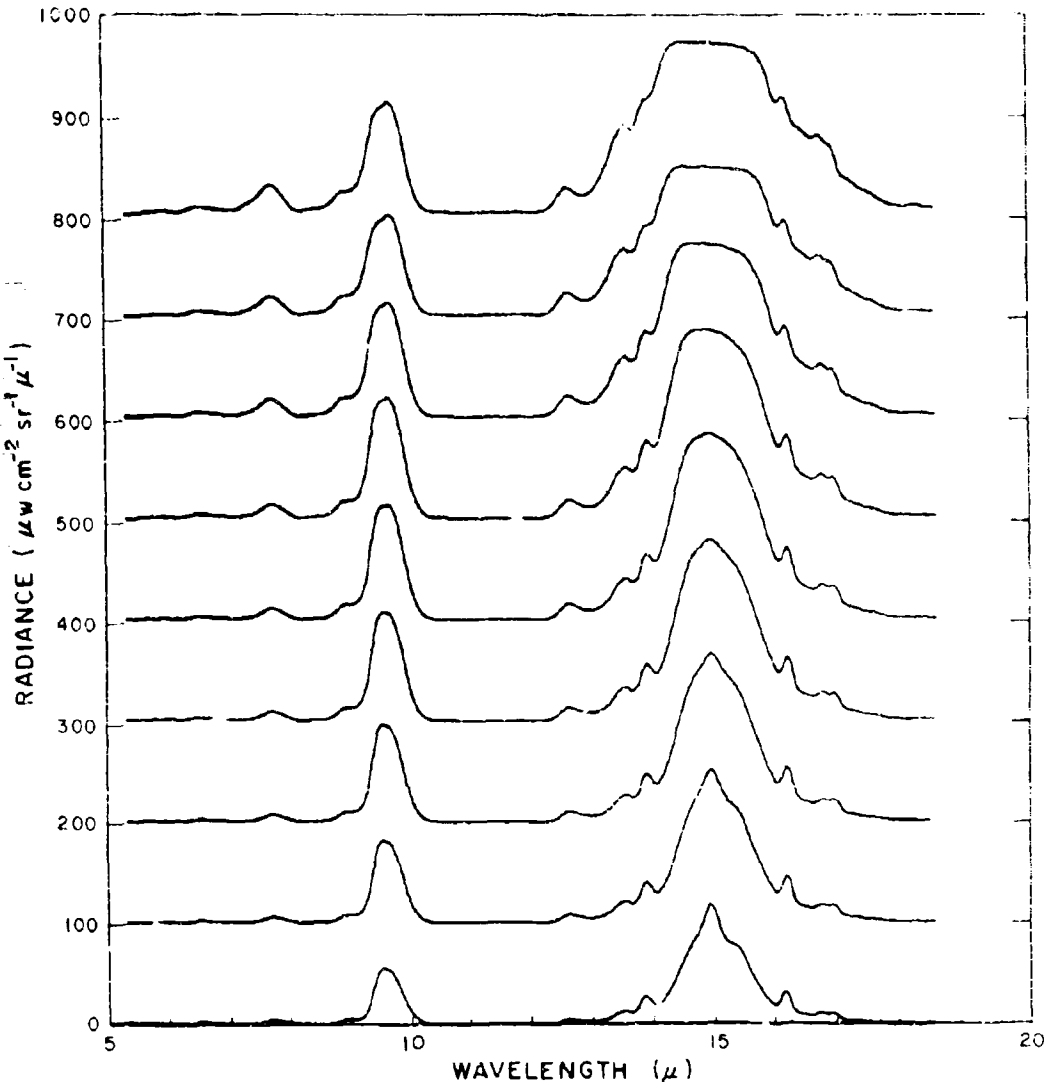

Figure 171. Cont. Calculated spectral radiance from 5 to 18μ vs altitude for 2 km intervals from 16 to 32 km (top to bottom) at a zenith observation angle of 86.5° (sec = 16) for 1 June 1967. Successive records have a 100 μw cm^{-2} sr^{-1} μ^{-1} offset for clarity.

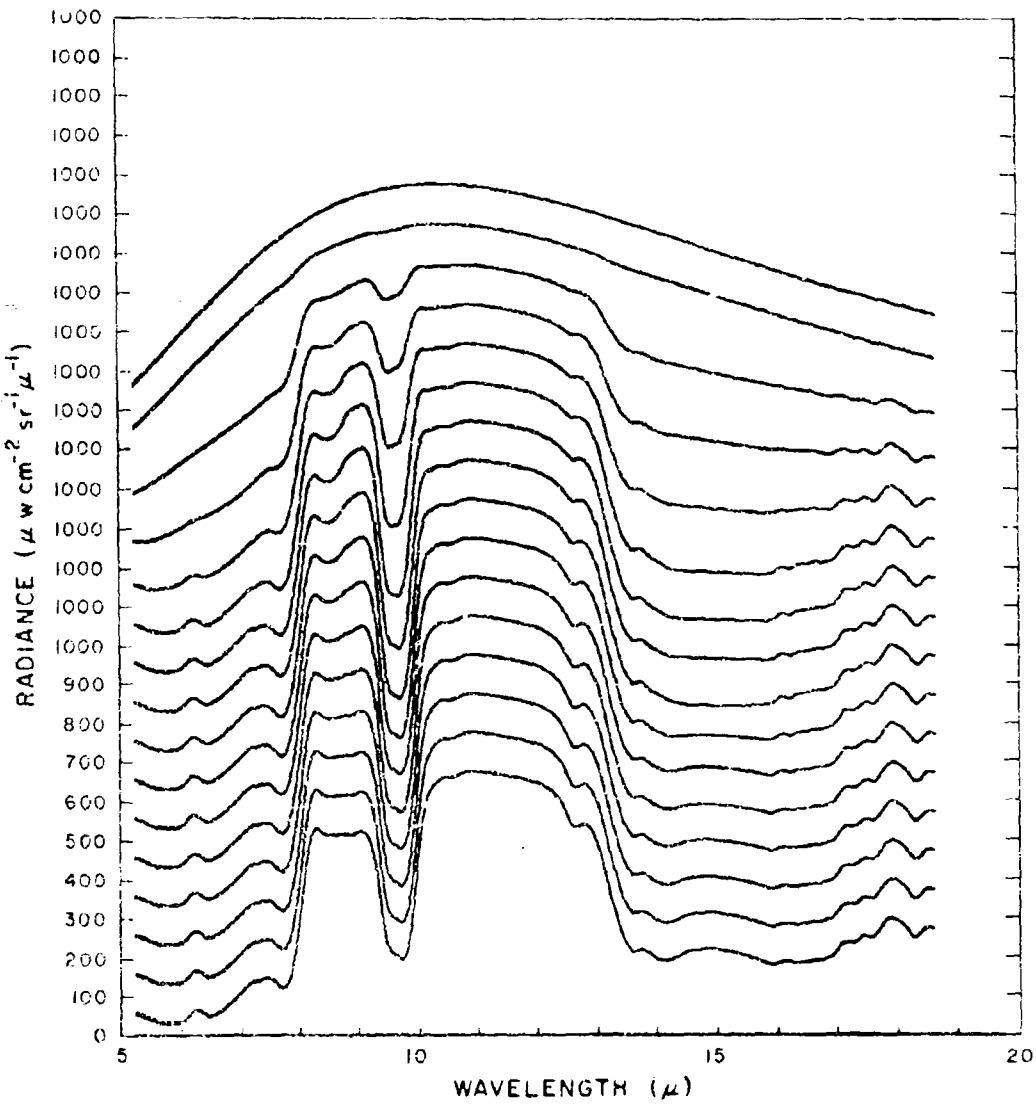

Figure 172. Calculated spectral radiance from 5 to 18u vs altitude for 2 km intervals from 2 - 32 km (top to bottom) at a zenith observation angle of 93.6° (sec = 16) for 1 June 1967. Successive records have a 100 $\mu w\ cm^{-2}\ sr^{-1}\ \mu^{-1}$ offset for clarity.

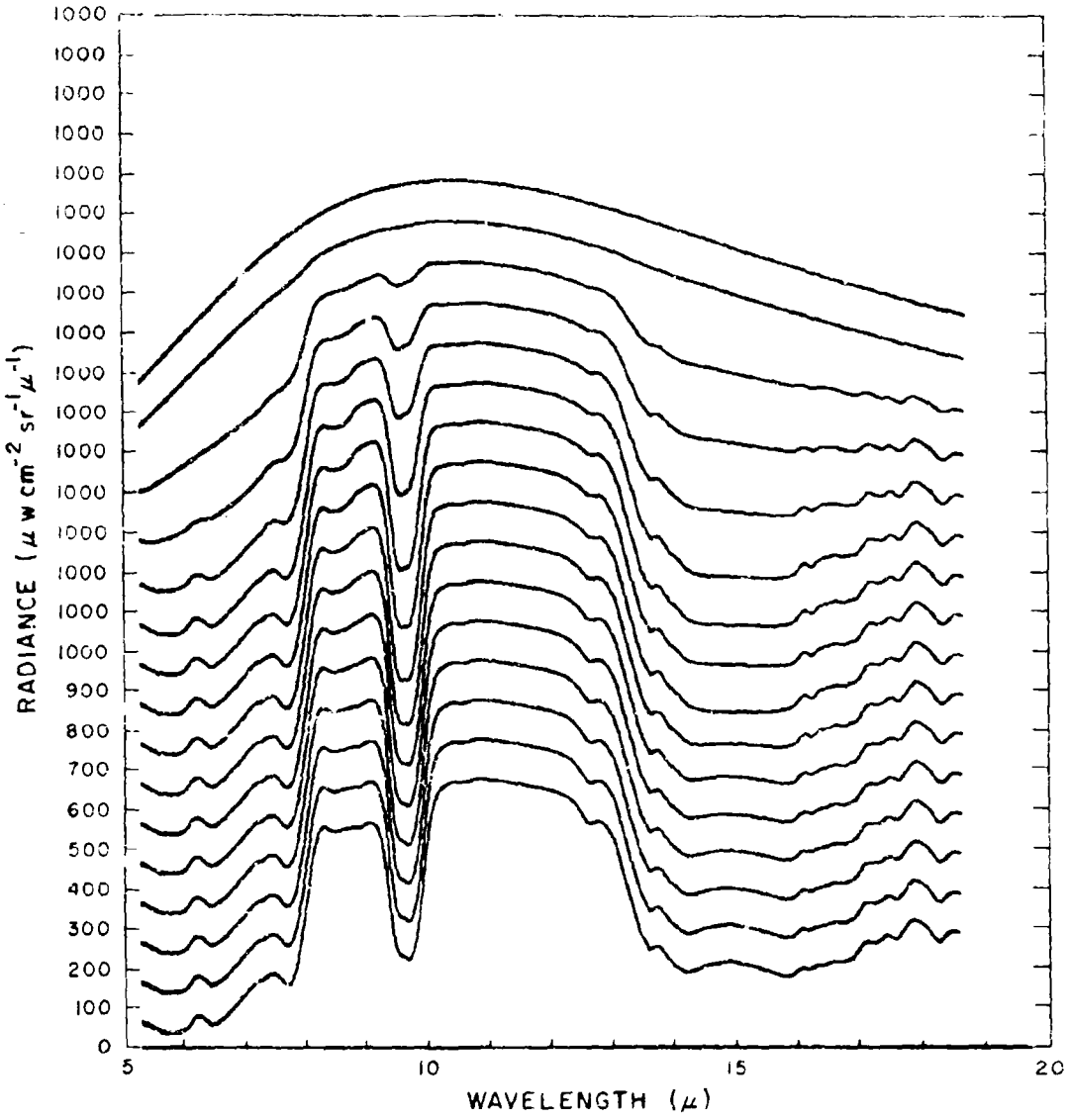

Figure 173. Calculated spectral radiance from 5 to 18μ vs altitude for 2 km intervals from 2 - 32 km (top to bottom) at a zenith observation angle of 97.2° (sec = 8) for 1 June 1967. Successive records have a 100 μw cm^{-2} sr^{-1} μ^{-1} offset for clarity.

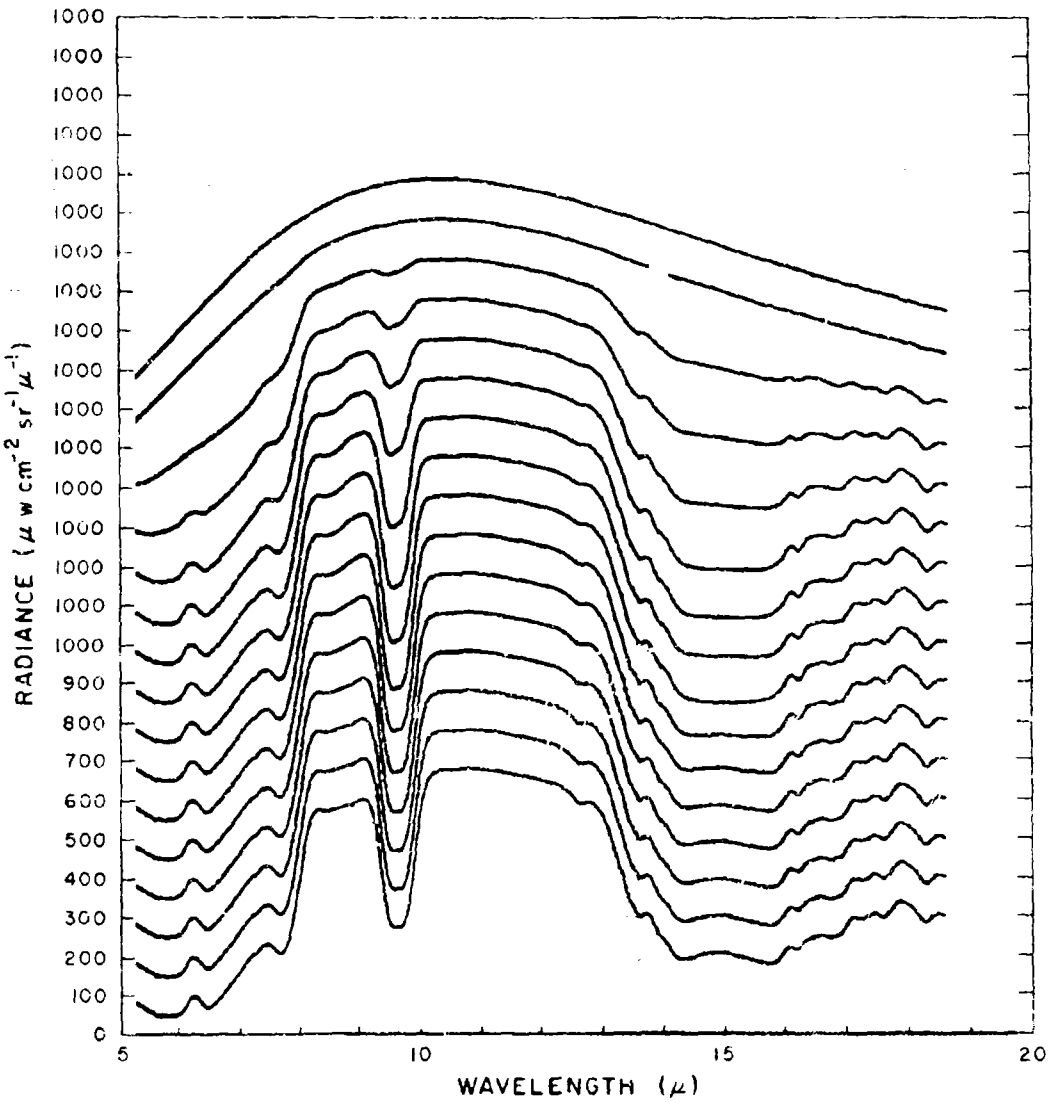

Figure 174. Calculated spectral radiance from 5 to 18μ vs altitude for 2 km intervals from 2 - 32 km (top to bottom) at a zenith observation angle of 104.5° (sec.=4) for 1 June 1967. Successive records have a 100 μw cm^{-2} sr^{-1} μ^{-1} offset for clarity.

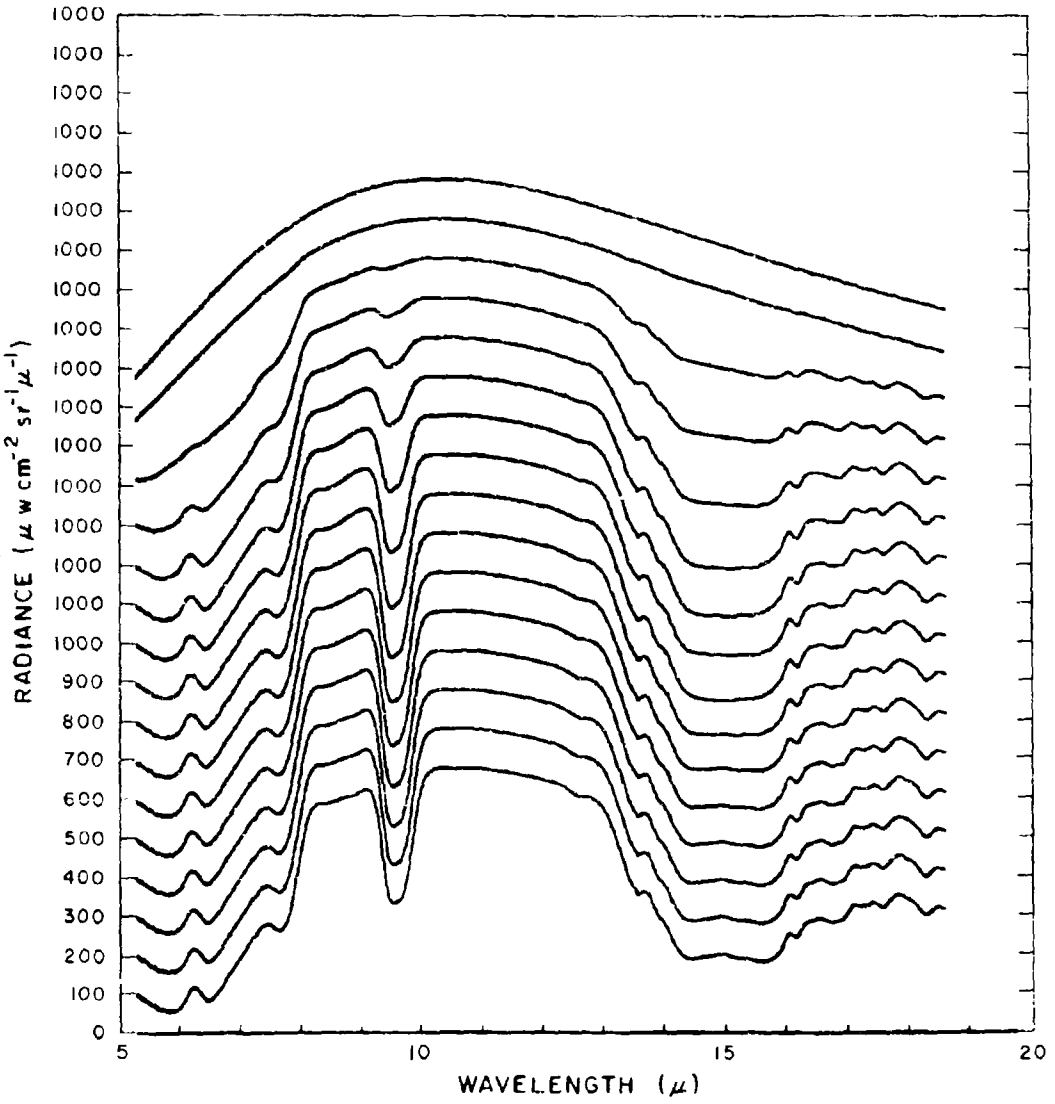

Figure 175. Calculated spectral radiance from 5 to 18μ vs altitude for 2 km intervals from 2 - 32 km (top to bottom) at a zenith observation angle of 120^{o} (sec.=2) for 1 June 1967. Successive records have a 100 μw cm^{-2} sr^{-1} μ^{-1} offset for clarity.

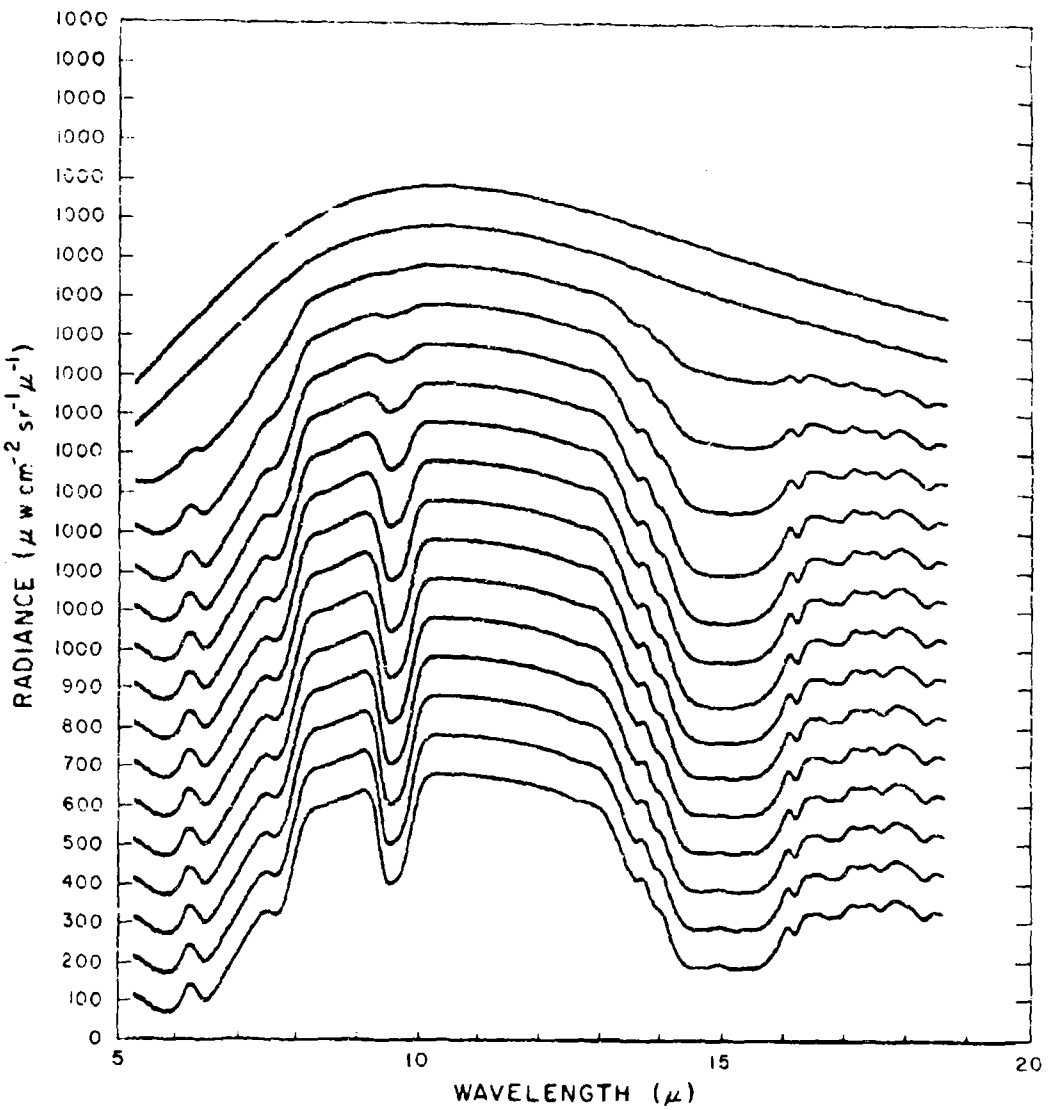

Figure 176. Calculated spectral radiance from 5 to 18μ vs altitude for 2 km intervals from 2 - 32 km (top to bottom) at a zenith observation angle of 180° (sec. = 1) for 1 June 1967. Successive records have a 100 μw cm^{-2} sr^{-1} μ^{-1} offset for clarity.

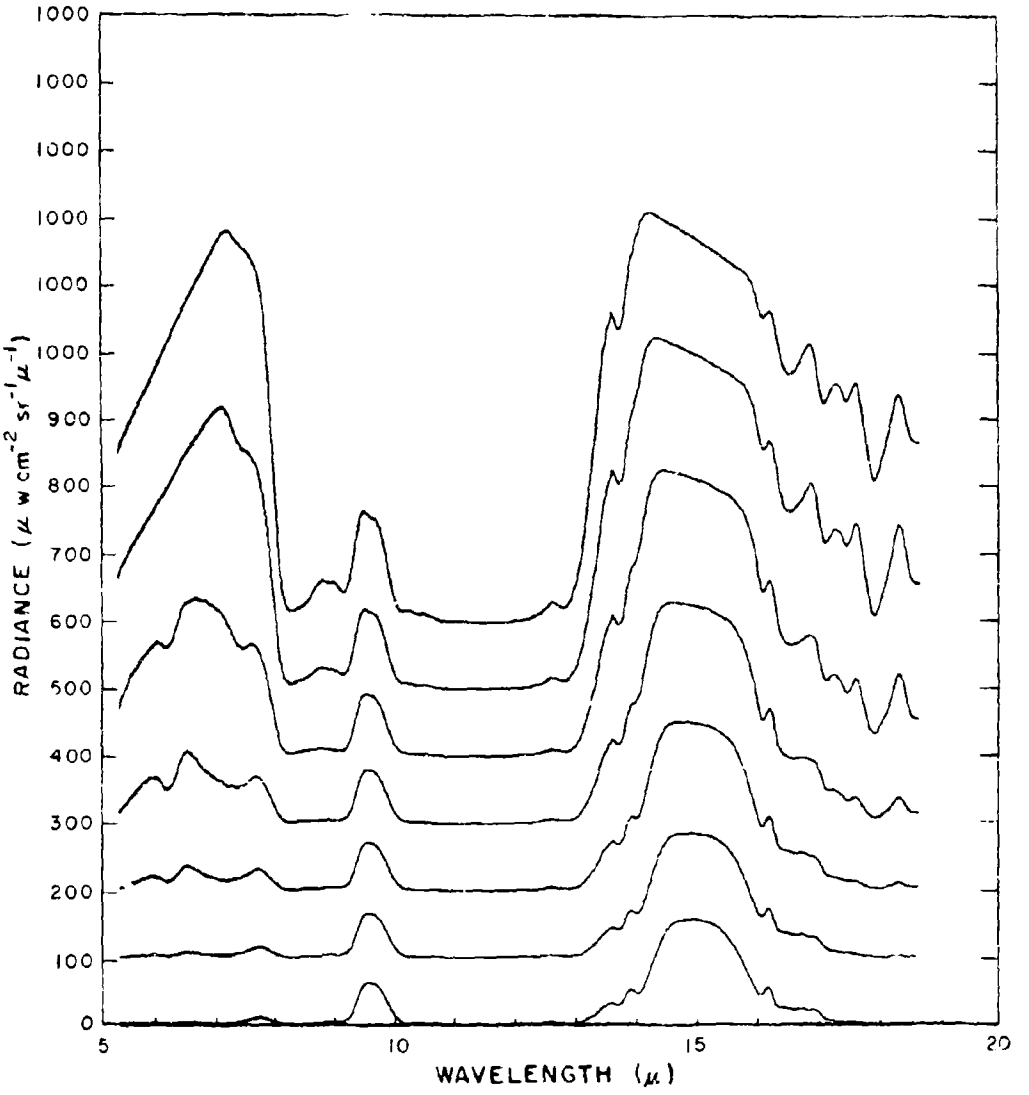

Figure 177. Calculated spectral radiance from 5 to 18μ vs altitude for 2 km intervals from 2 to 14 km (top to bottom) at a zenith observation angle of 0^{0} (sec = 1) for 30 November 1967. Successive records have a 100 $\mu w\ cm^{-2}\ sr^{-1}\ \mu^{-1}$ offset for clarity.

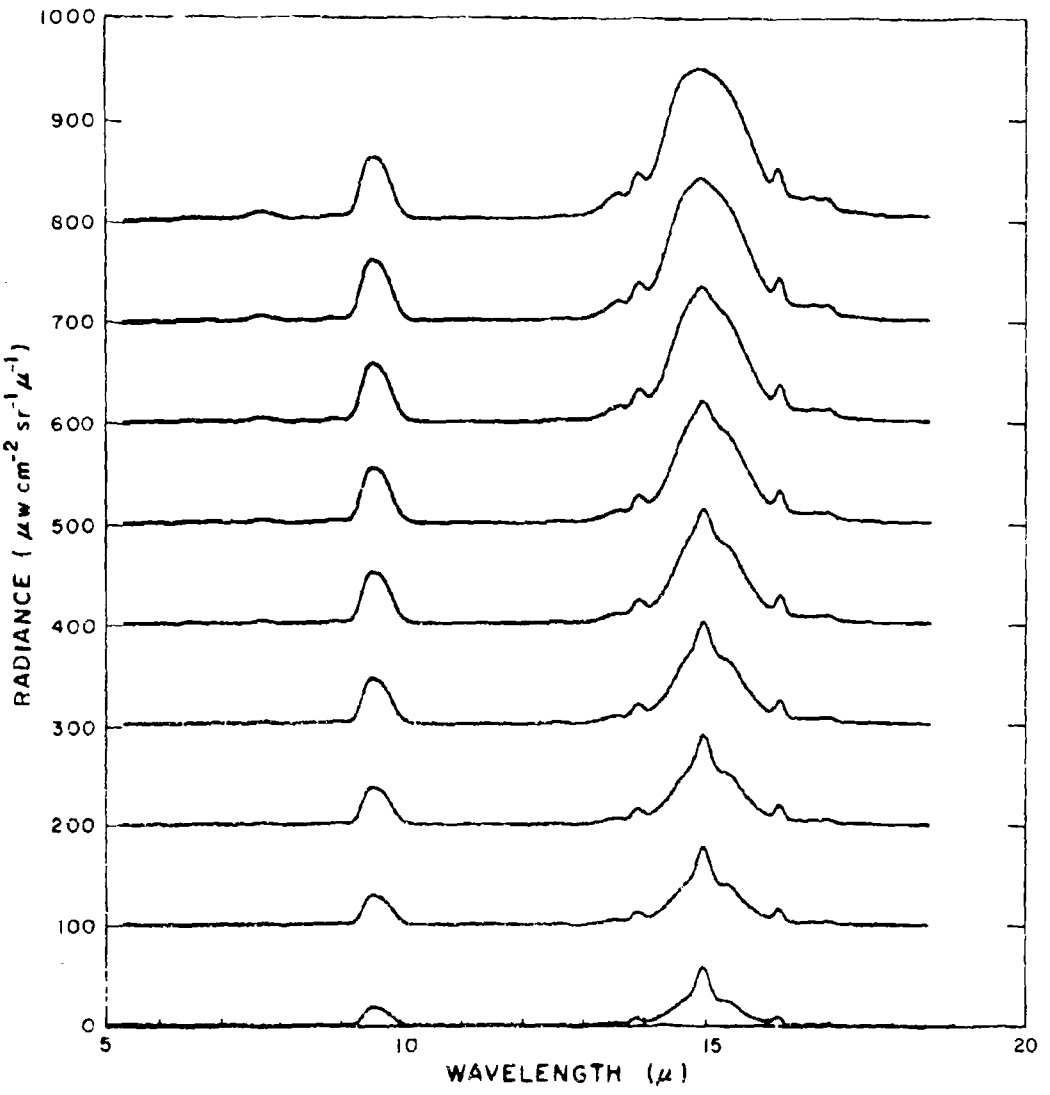

Figure 177. Cont. Calculated spectral radiance from 5 to 18μ vs altitude for 2 km intervals from 16 to 32 km (top to bottom) at a zenith observation angle of 0^{o} (sec = 1) for 30 November 1967. Successive records have a 100 μw cm^{-2} sr^{-1} μ^{-1} offset for clarity.

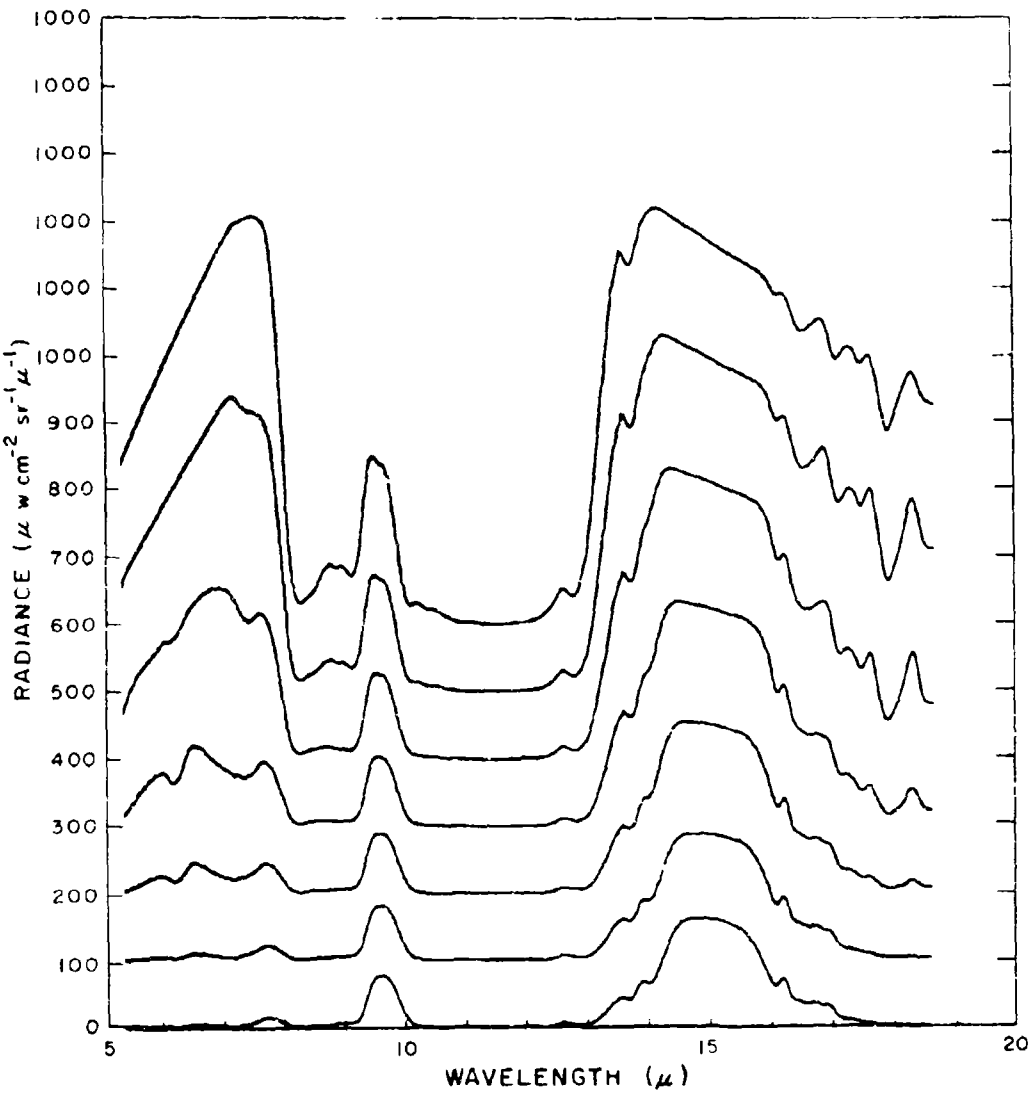

Figure 178. Calculated spectral radiance from 5 to 18μ vs altitude for 2 km intervals from 2 t0 14 km (top to bottom) at a zenith obversation angle of 60^{o} (sec = 2) for 30 November 1967. Successive records have a 100 μw cm^{-2} sr^{-1} μ^{-1} offset for clarity.

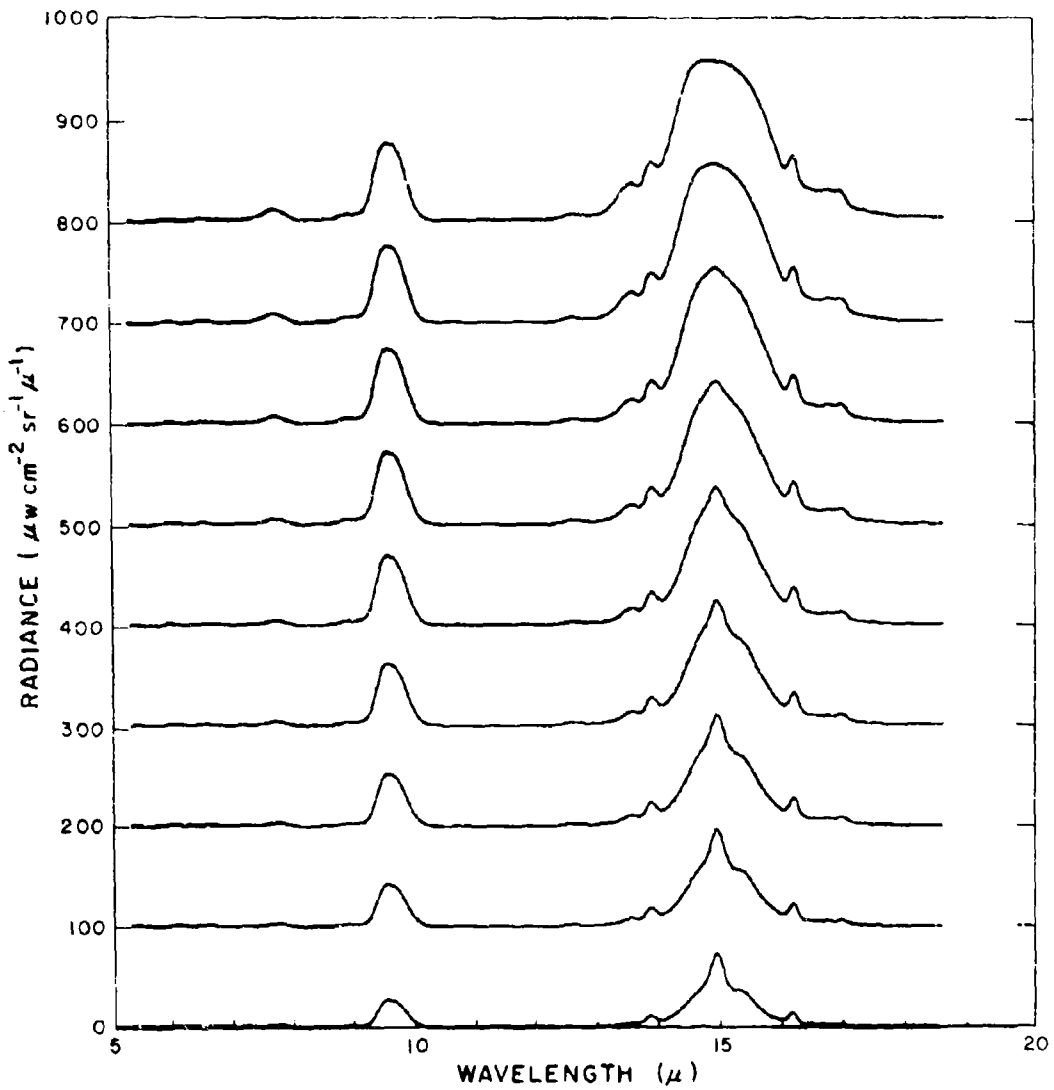

Figure 178. Cont. Calculated spectral radiance from 5 to 18μ vs altitude for 2 km intervals from 16 to 32 km (top to bottom) at a zenith observation angle of 60° (sec = 2) for 30 November 1967. Successive records have a 100 μw cm^{-2} sr^{-1} μ^{-1} offset for clarity.

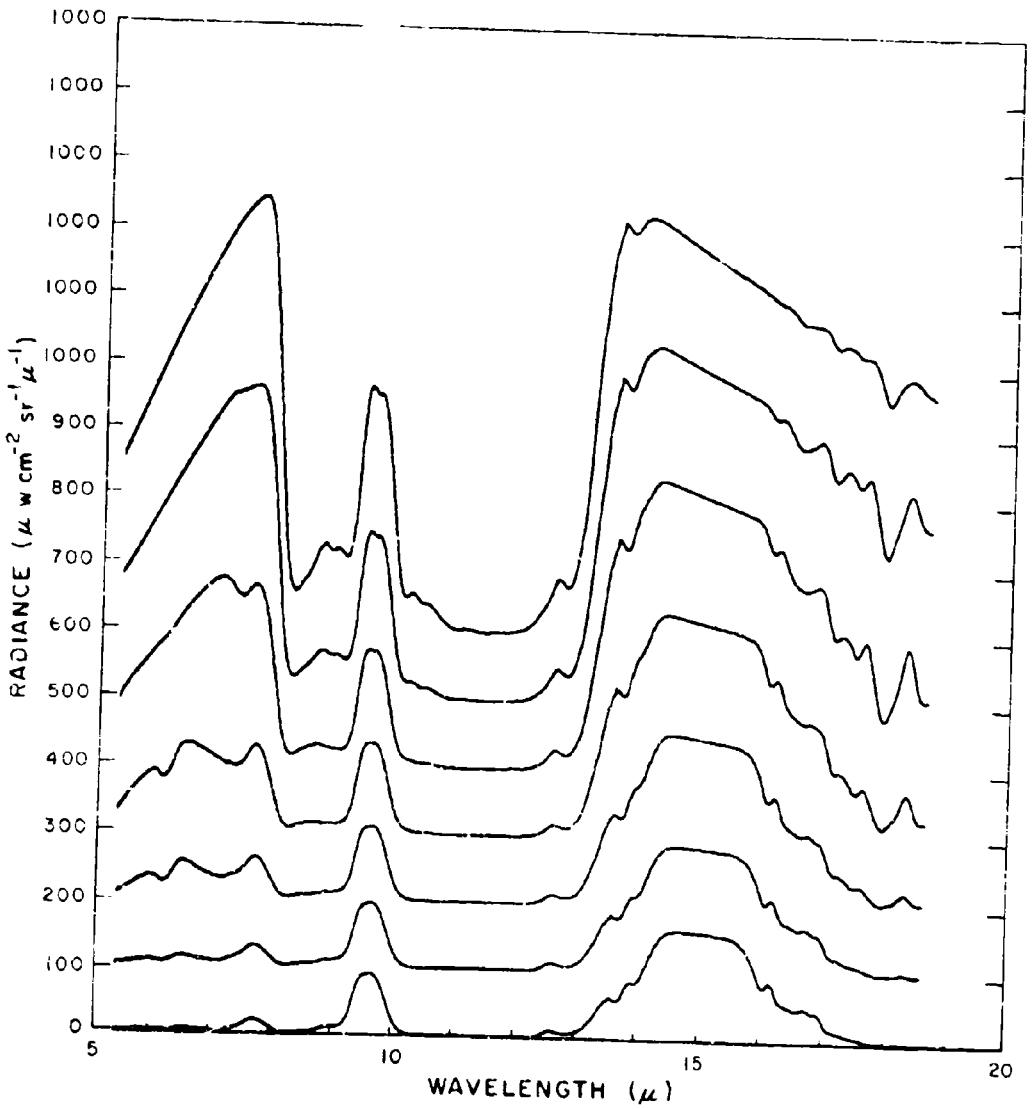

Figure 179. Calculated spectral radiance from 5 to 18μ vs altitude for 2 km intervals from 2 to 14 km (top to bottom) at a zenith observation angle of 75.5° (sec = 4) for 30 November 1967. Successive records have a 100 μw cm^{-2} sr^{-1} μ^{-1} offset for clarity.

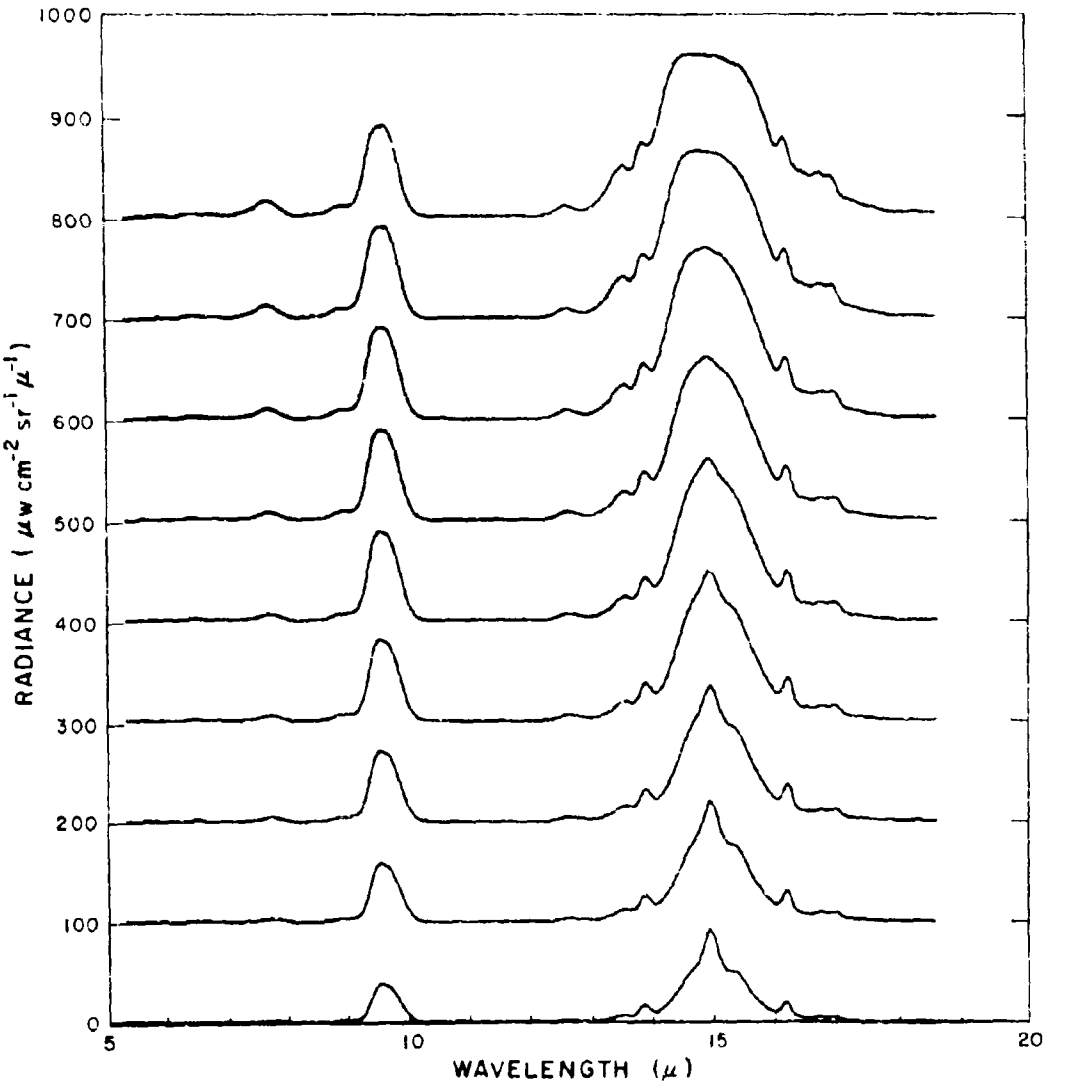

Figure 179. Cont. Calculated spectral radiance from 5 to 18μ vs altitude for 2 km intervals from 16 to 32 km (top to bottom) at a zenith observation angle of 75.5° (sec = 4) for 30 November 1967. Successive records have a 100 μw cm^{-2} sr^{-1} μ^{-1} offset for clarity.

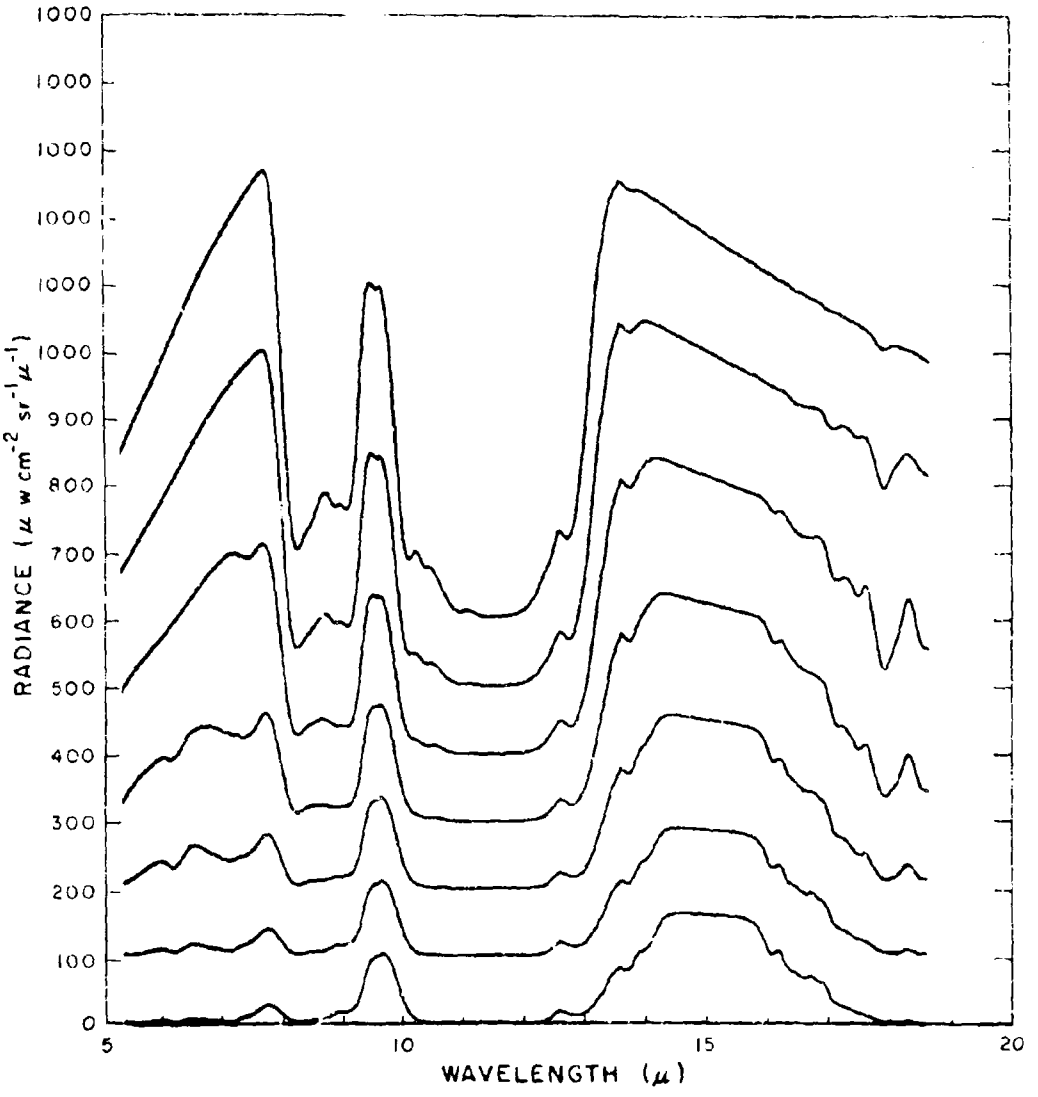

Figure 180. Calculated spectral radiance from 5 to 18μ vs altitude for 2 km intervals from 2 to 14 km (top to bottom) at a zenith observation angle of 82.8° (sec = 8) for 30 November 1967. Successive records have a 100 μw cm^{-2} sr^{-1} μ^{-1} offset for clarity.

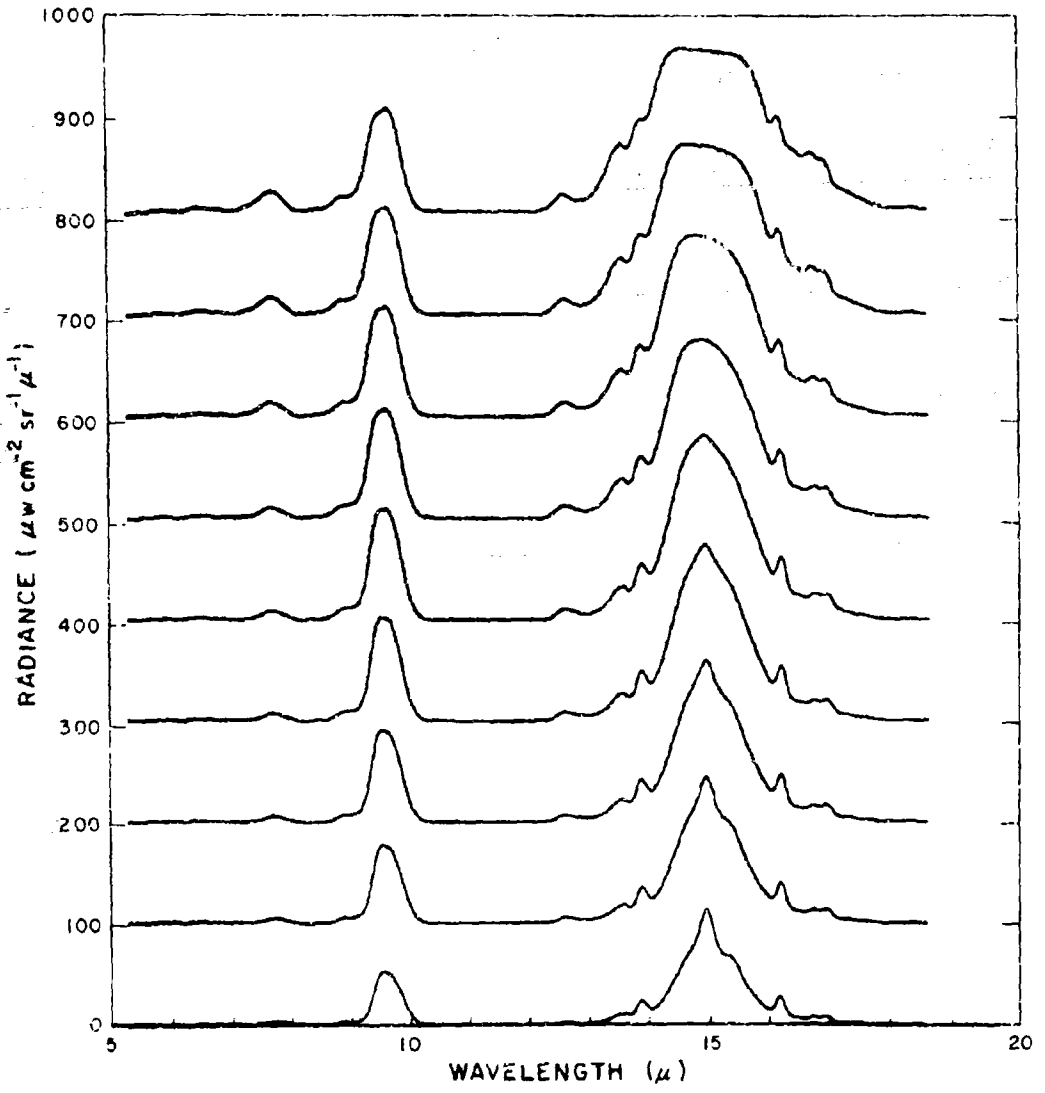

Figure 80. Cont. Calculated spectral radiance from 5 to 18μ vs altitude for 2 km intervals from 16 to 32 km (top to bottom) at a zenith observation angle of 82.6° (sec = 8) for 30 November 1967. Successive records have a 100 μw cm^{-2} sr^{-1} μ^{-1} offset for clarity.

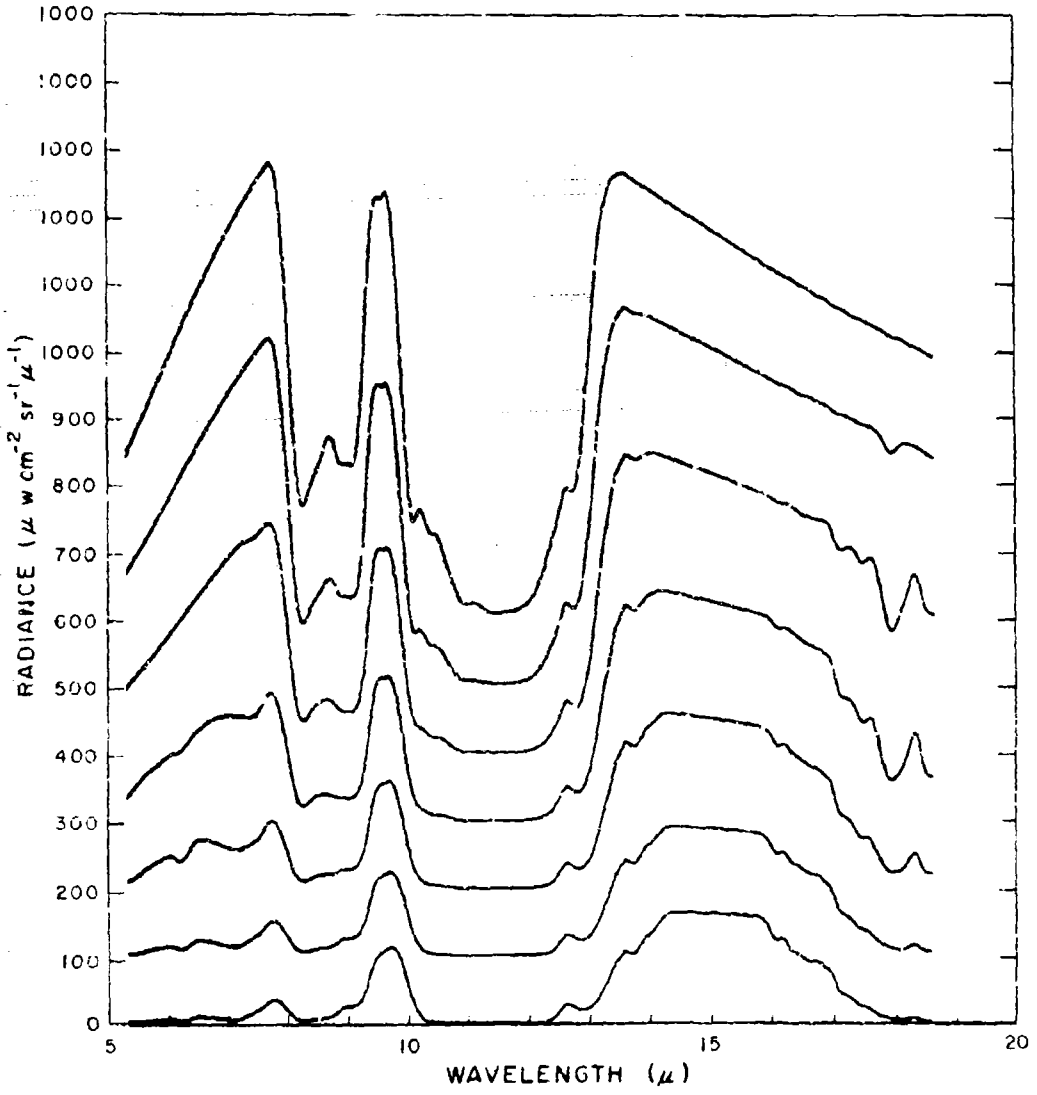

Figure 181. Calculated spectral radiance from 5 to 18μ vs altitude for 2 km intervals from 2 to 14 km (top to bottom) at a zenith observation angle of 86.4° (sec = 16) for 30 November 1967. Successive records have a 100 μw cm^{-2} sr^{-1} μ^{-1} offset for clarity.

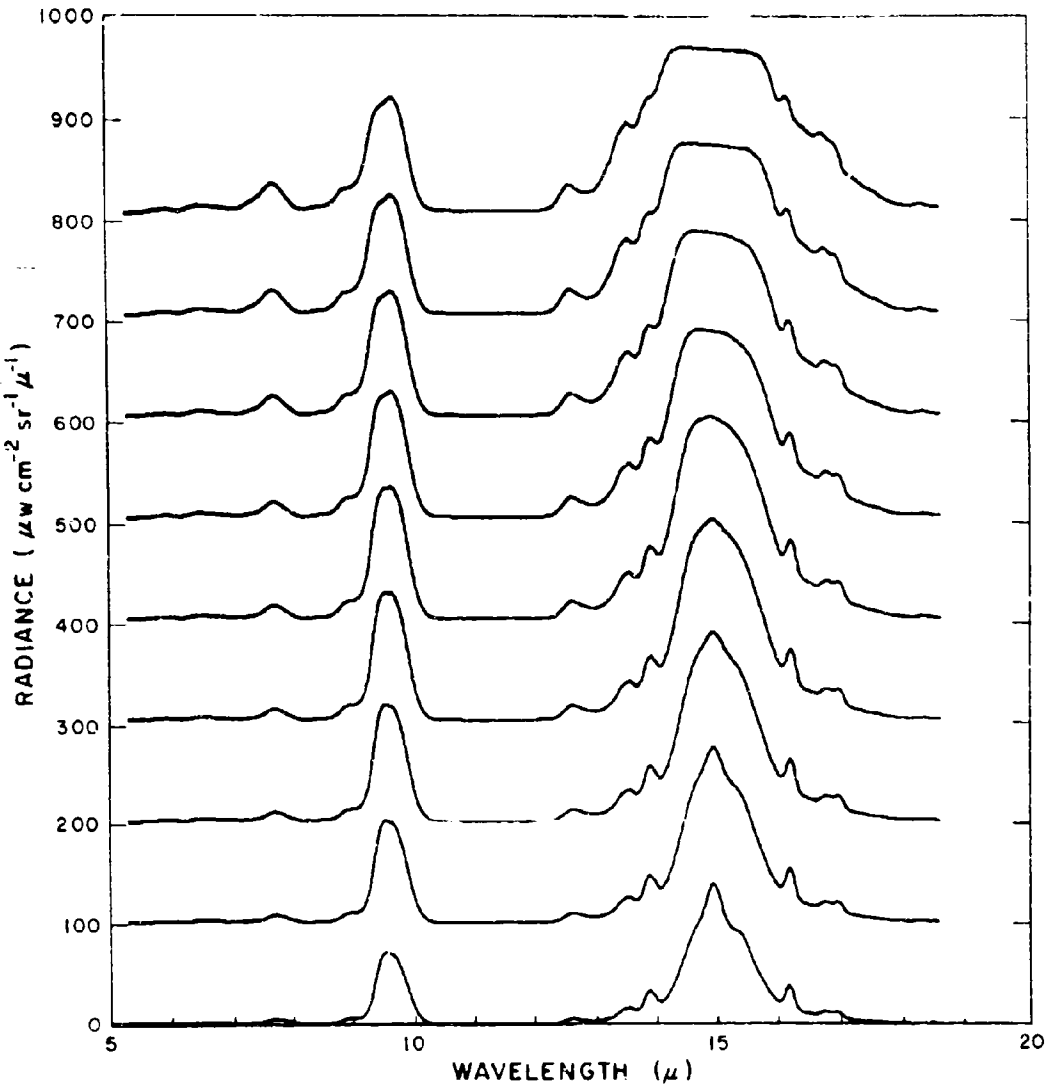

Figure 181. Cont. Calculated spectral radiance from 5 to 18μ vs altitude for 2 km intervals from 16 to 32 km (top to bottom) at a zenith observation angle of 86.4° (sec = 16) for 30 November 1967. Successive records have a 100 $\mu w\ cm^{-2}\ sr^{1}\ \mu^{-1}$ offset for clarity.

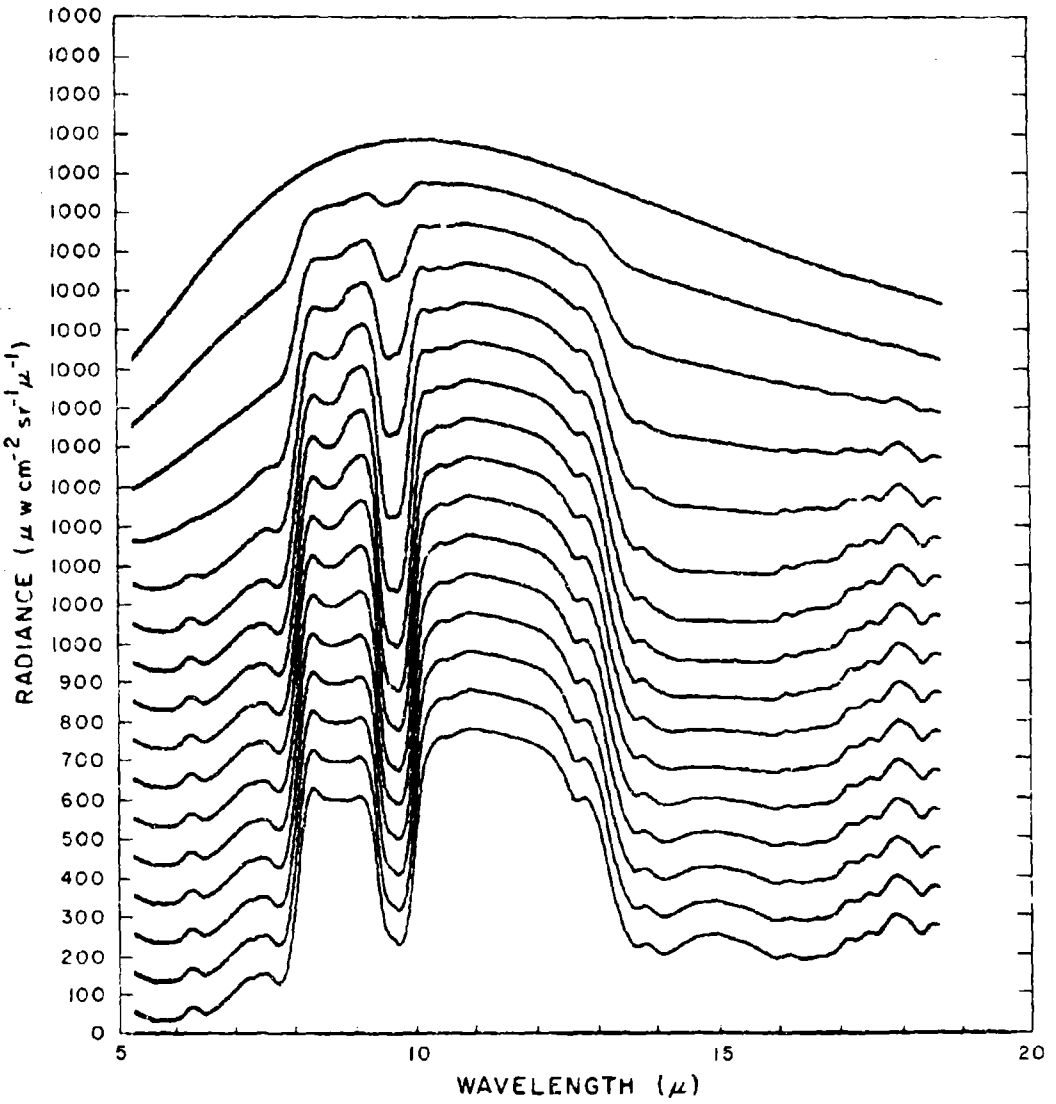

Figure 182. Calculated spectral radiance from 5 to 18μ vs altitude for 2 km intervals from 2 - 32 km (top to bottom) at a zenith observation angle of 93.6° (sec = 16) for 30 November 1967. Successive records have a 100 μw cm^{-2} sr^{-1} μ^{-1} offset for clarity.

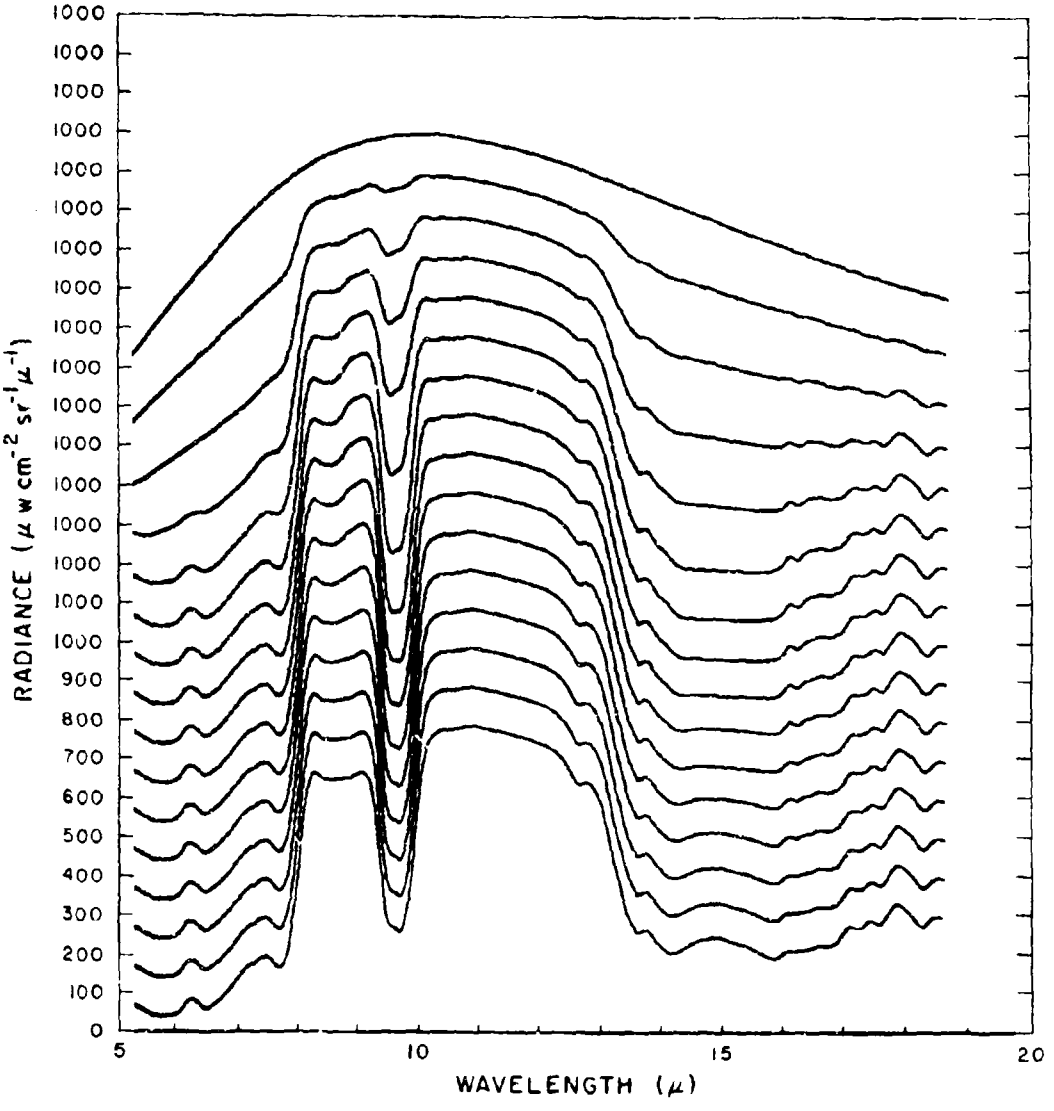

Figure 183. Calculated spectral radiance from 5 to 18μ vs altitude for 2 km intervals from 2 - 32 km (top to bottom) at a zenith observation angle of 97.2^{o} (sec = 8) for 30 November 1967. Successive records have a 100 μw cm^{-2} sr^{-1} μ^{-1} offset for clarity.

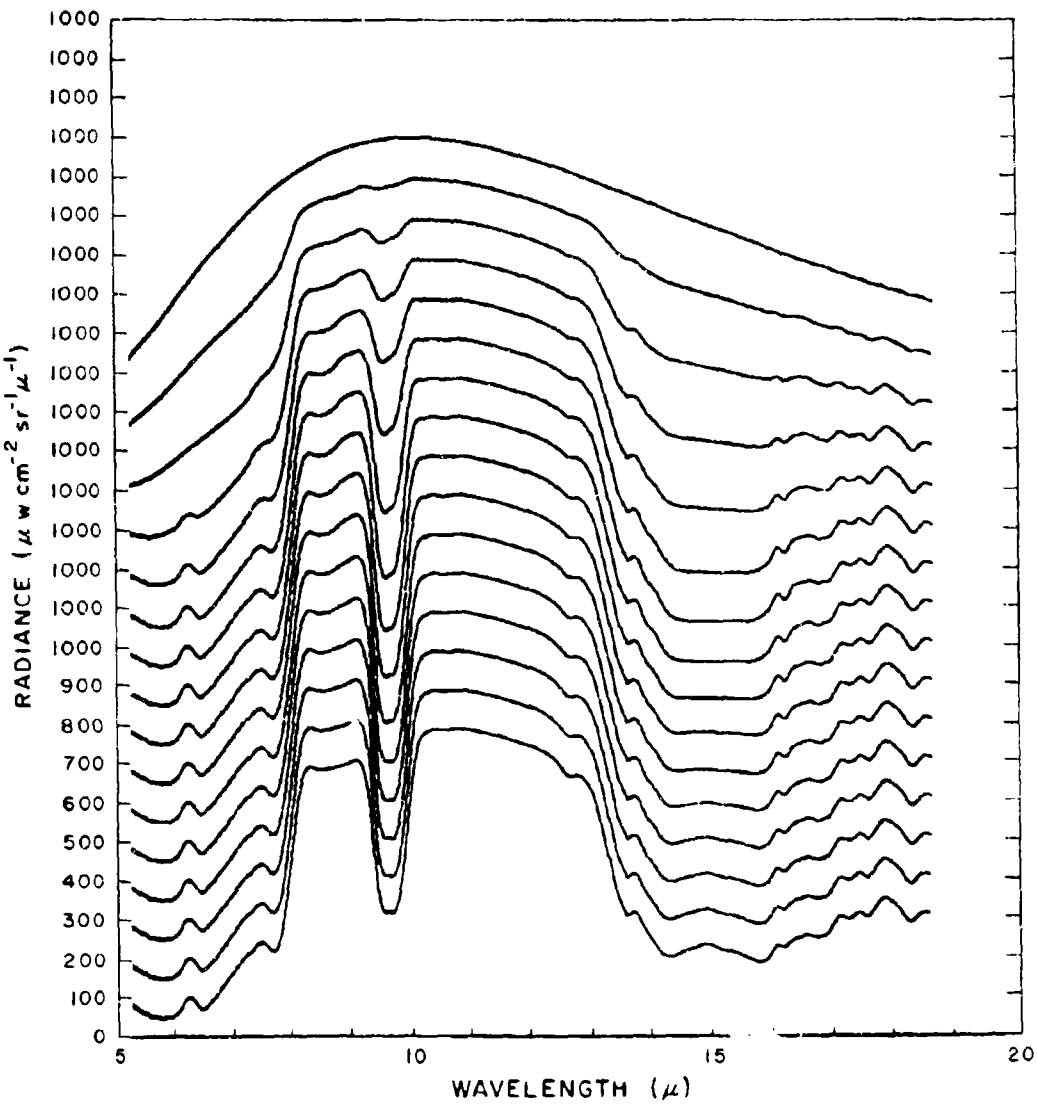

Figure 184. Calculated spectral radiance from 5 to 18.5μ vs altitude for 2 km intervals from 2 - 32 km (top to bottom) at a zenith observation angle of 104.5° (sec = 4) for 30 November 1967. Successive records have a 100 μw cm^{-2} sr^{-1} μ^{-1} offset for clarity.

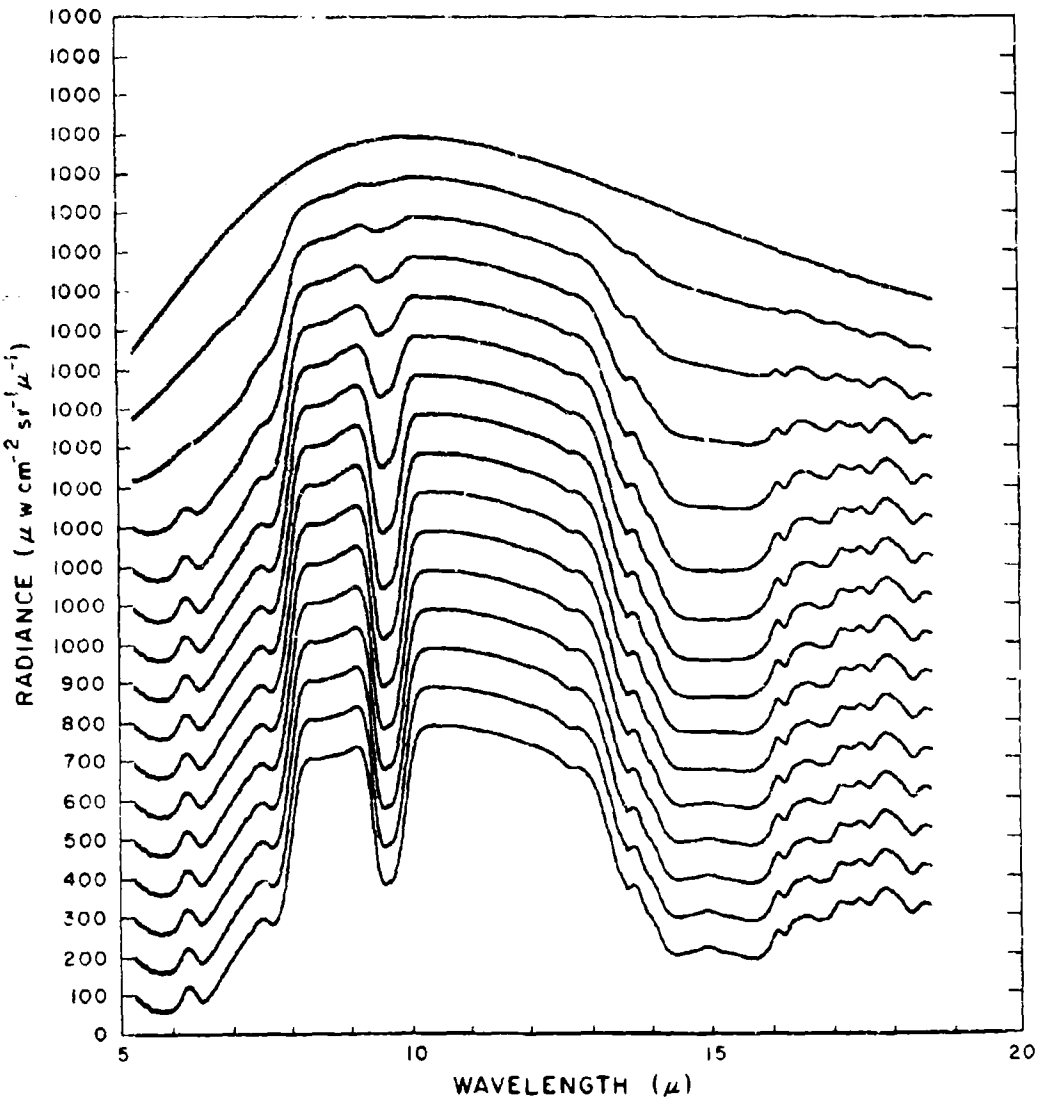

Figure 185. Calculated spectral radiance from 5 to 18.5μ vs altitude for 2 km intervals from 2 - 32 km (top to bottom) at a zenith observation angle of 120° (sec = 2) for 30 November 1967. Successive records have a 100 μw cm^{-2} sr^{-1} μ^{-1} offset for clarity.

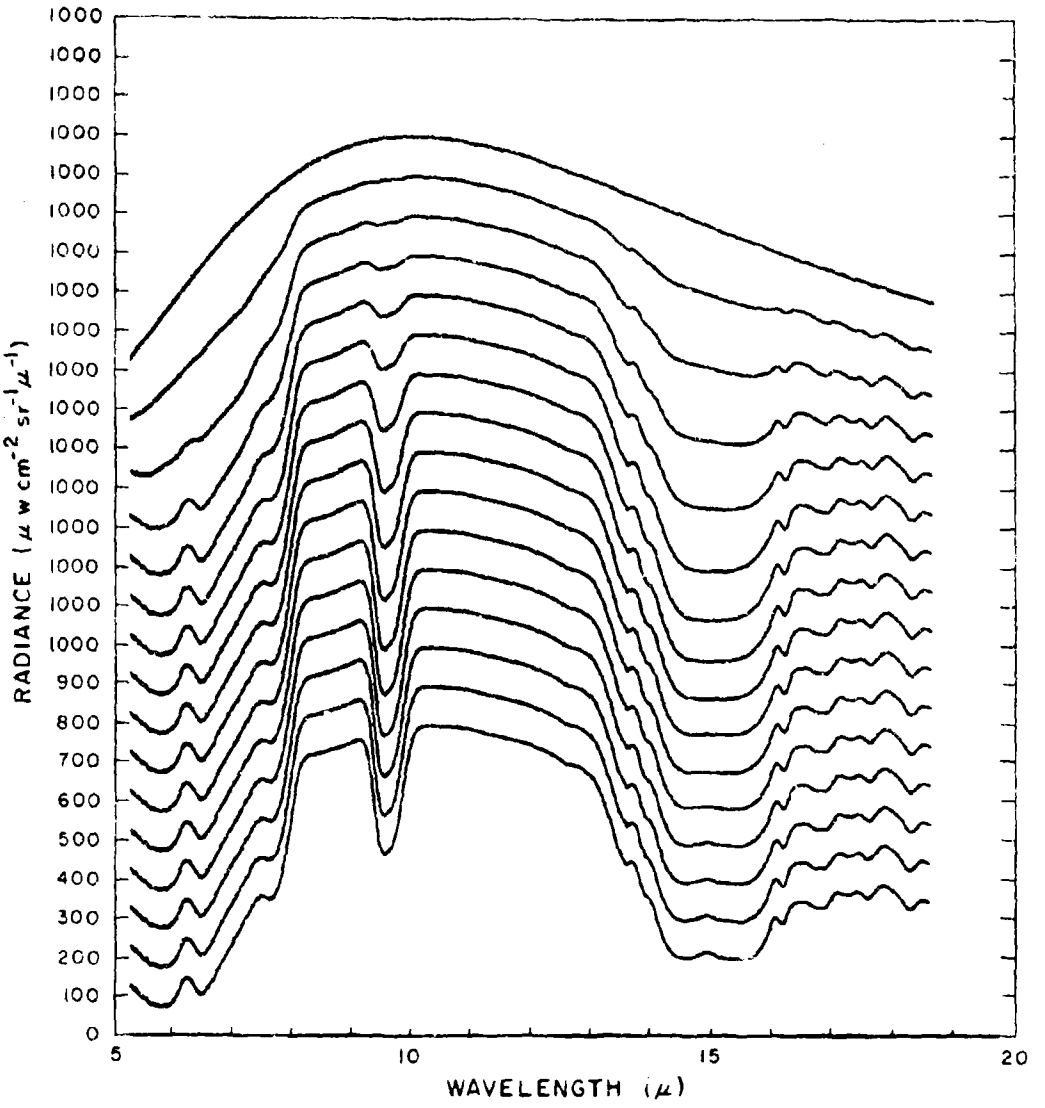

Figure 186. Calculated spectral radiance from 5 to 18.5μ vs altitude for 2 km intervals from 2 - 32 km (top to bottom) at a zenith observation angle of 180° (sec = 1) for 30 November 1967. Successive records have a 100 μw cm^{-2} sr^{-1} μ^{-1} offset for clarity.

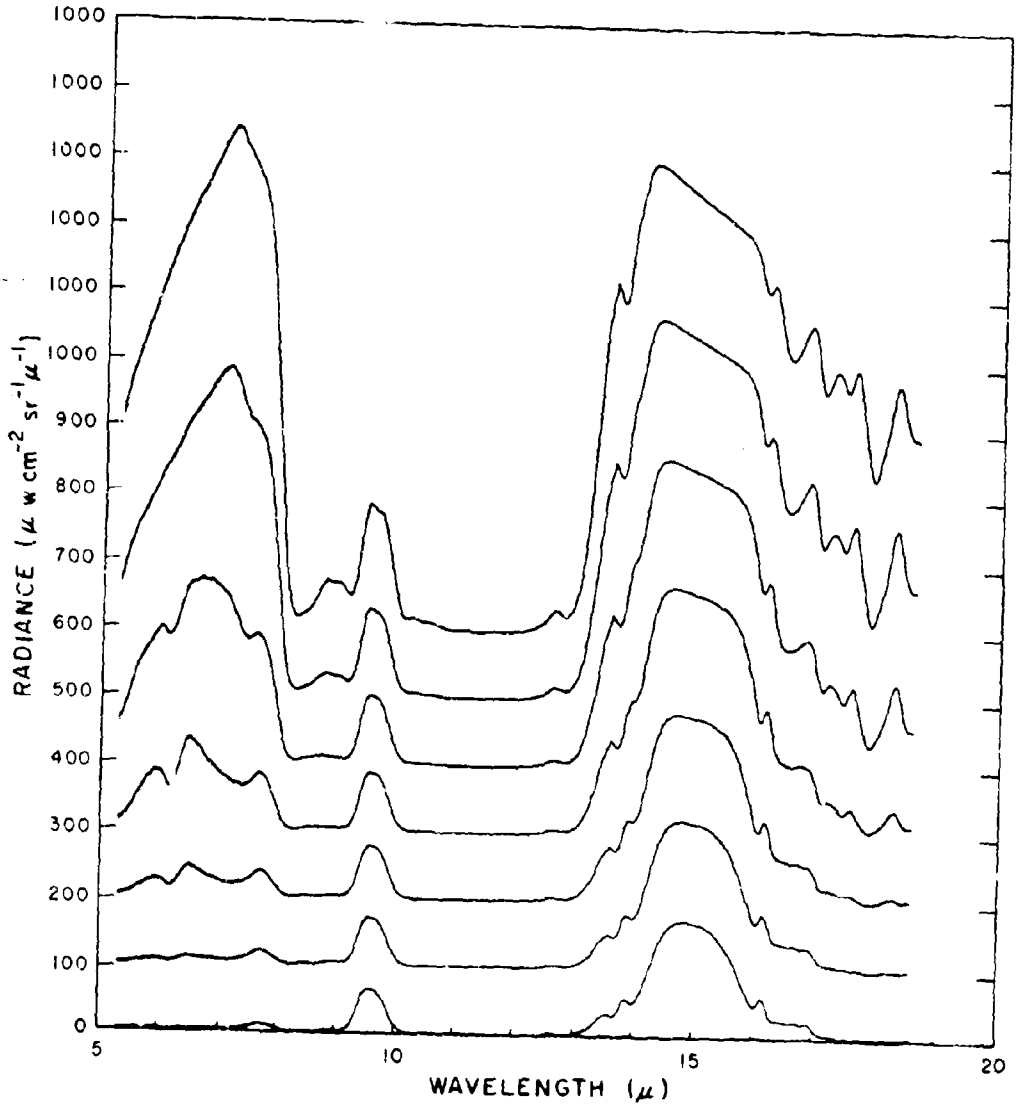

Figure 187. Calculated spectral radiance from 5 to 18.5μ vs altitude for 2 km intervals from 2 to 14 km (top to bottom) at a zenith observation angle of 0^{o} (sec = 1) for 1 July 1968. Successive records have a 100 μw cm^{-2} sr^{-1} μ^{-1} offset for clarity.

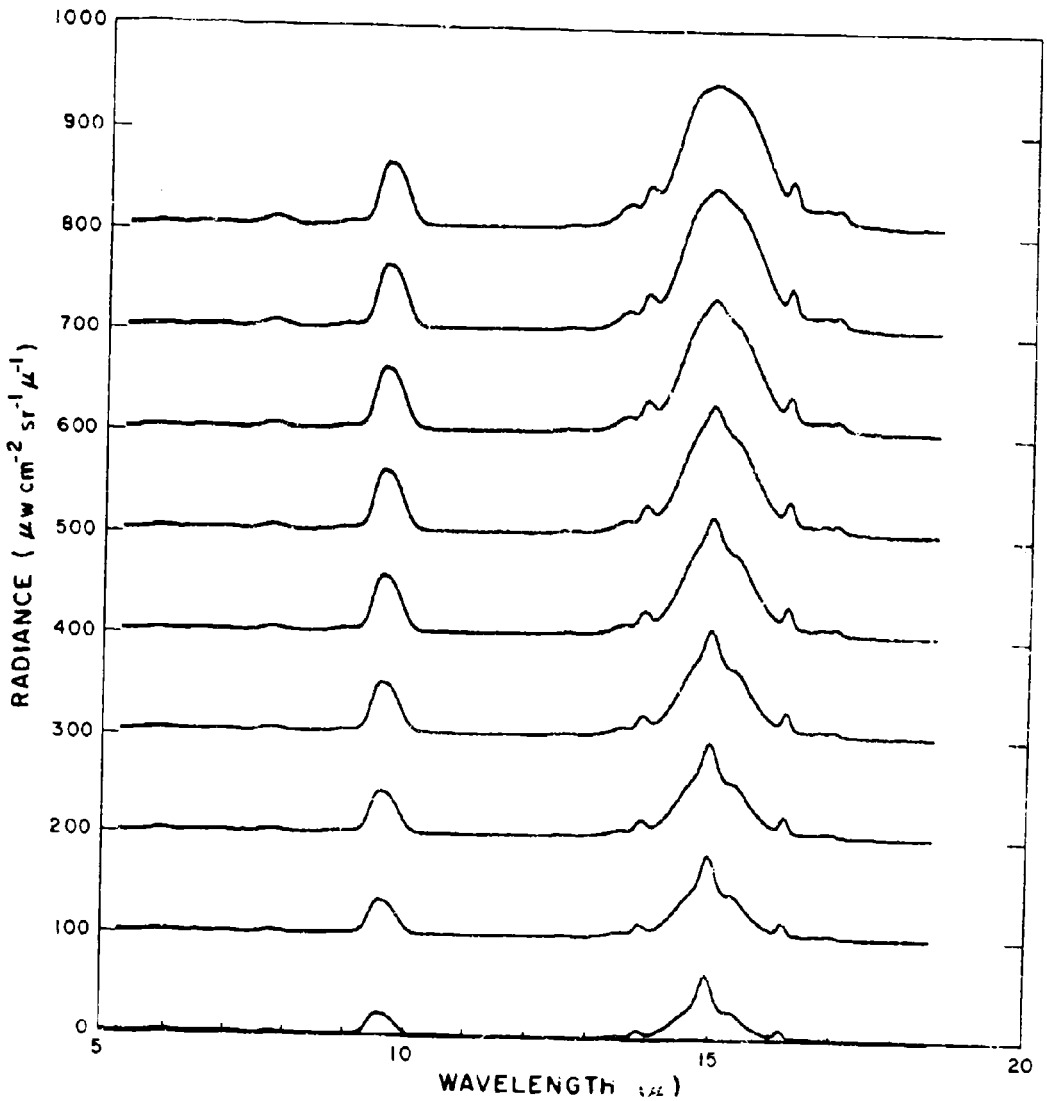

Figure 187. Cont. Calculated spectral radiance from 5 to 18.5μ vs altitude for 2 km intervals from 16 to 32 km (top to bottom) at a zenith observation angle of 0° (sec = 1) for 1 July 1968. Successive records have a 100 μw cm^{-2} sr^{-1} μ^{-1} offset for clarity.

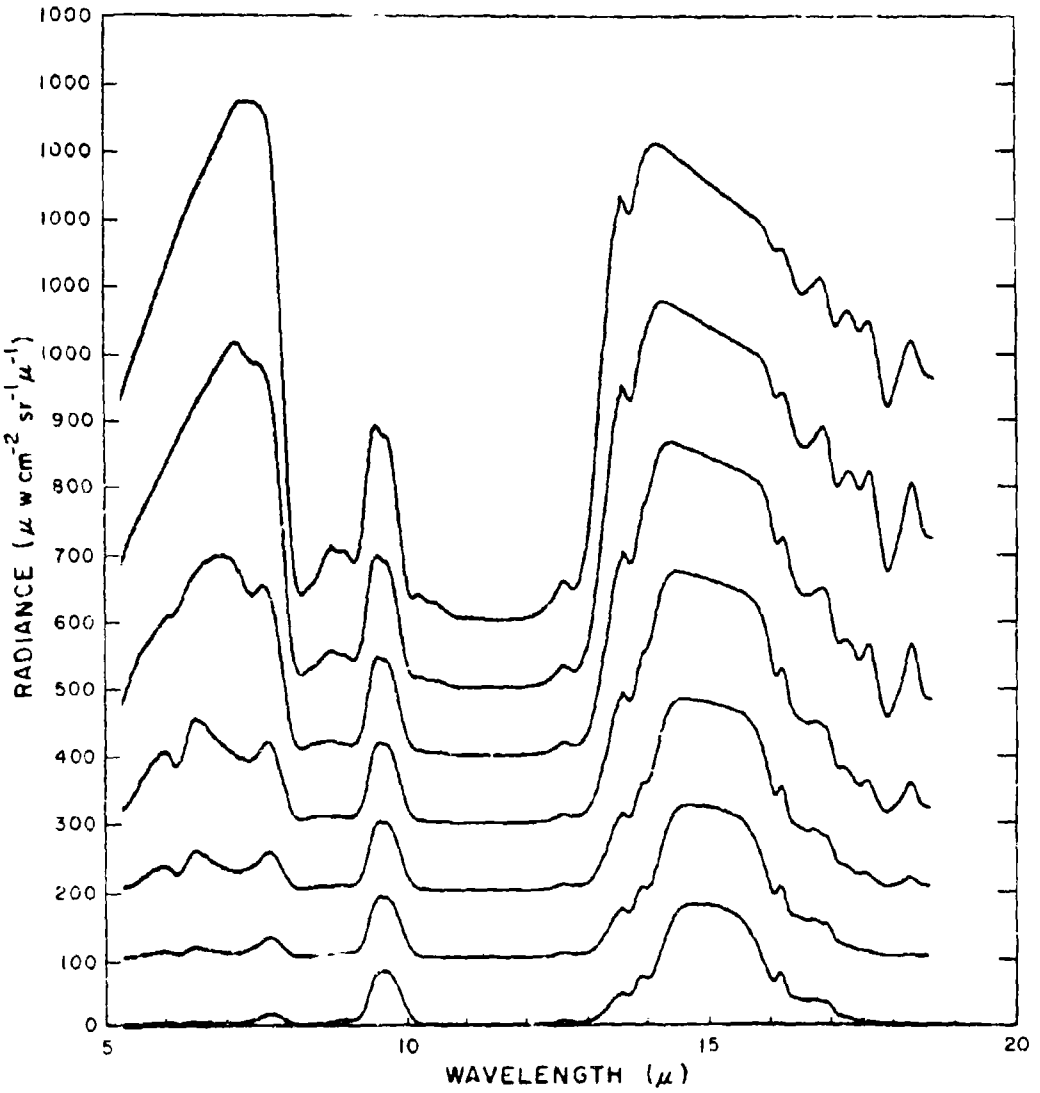

Figure 188. Calculated spectral radiance from 5 to 18.5 vs altitude for 2 km intervals from 2 to 14 km (top to bottom) at a zenith observation angle of 60° (sec = 2) for 1 July 1968. Successive records have a 100 μw cm^{-2} sr^{-1} μ^{-1} offset for clarity.

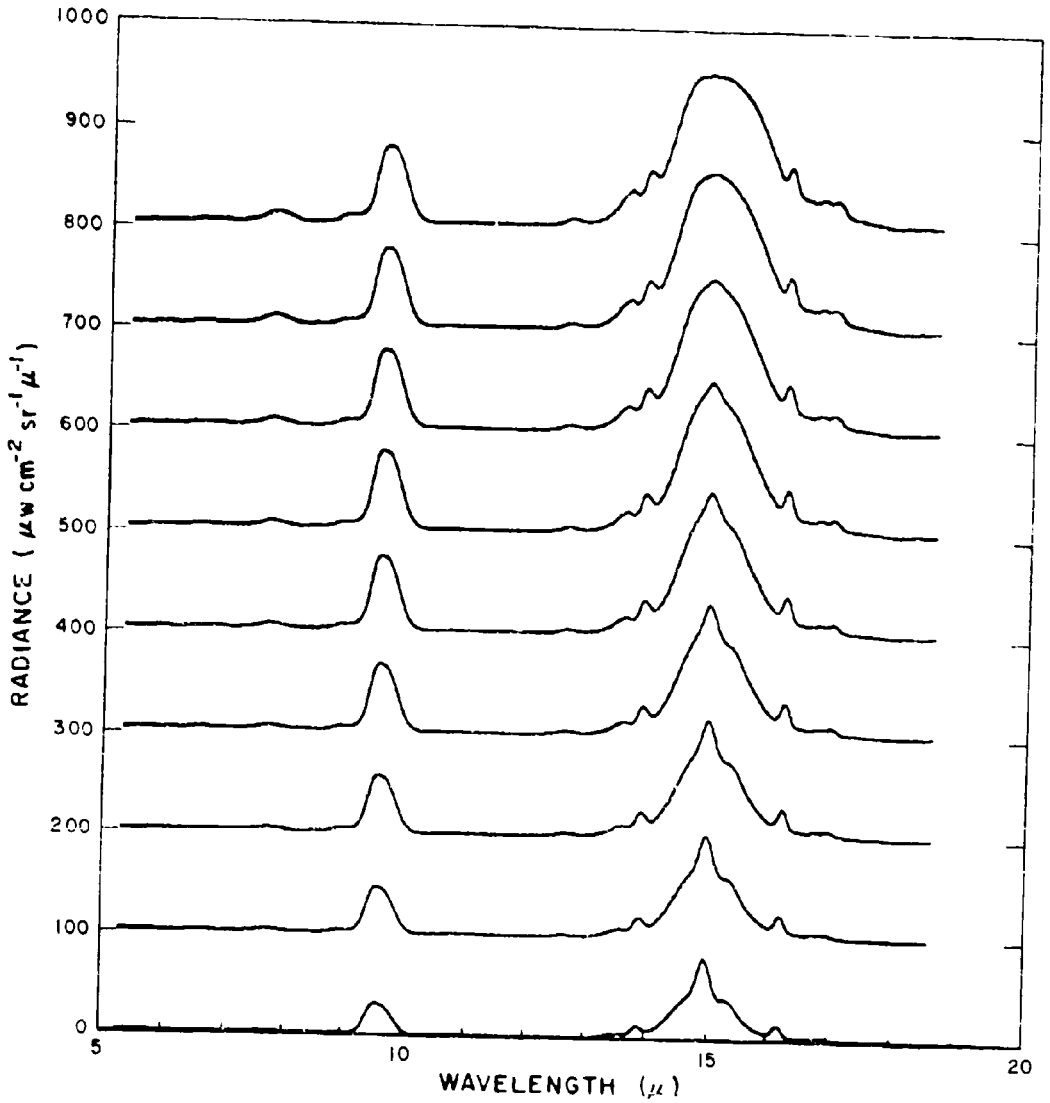

Figure 188. Cont. Calculated spectral radiance from 5 to 18.5μ vs altitude for 2 km intervals from 16 to 32 km (top to bottom) at a zenith observation angle of 60° (sec = 2) for 1 July 1968. Successive records have a 100 $\mu w\ cm^{-2}\ sr^{-1}\ \mu^{-1}$ offset for clarity.

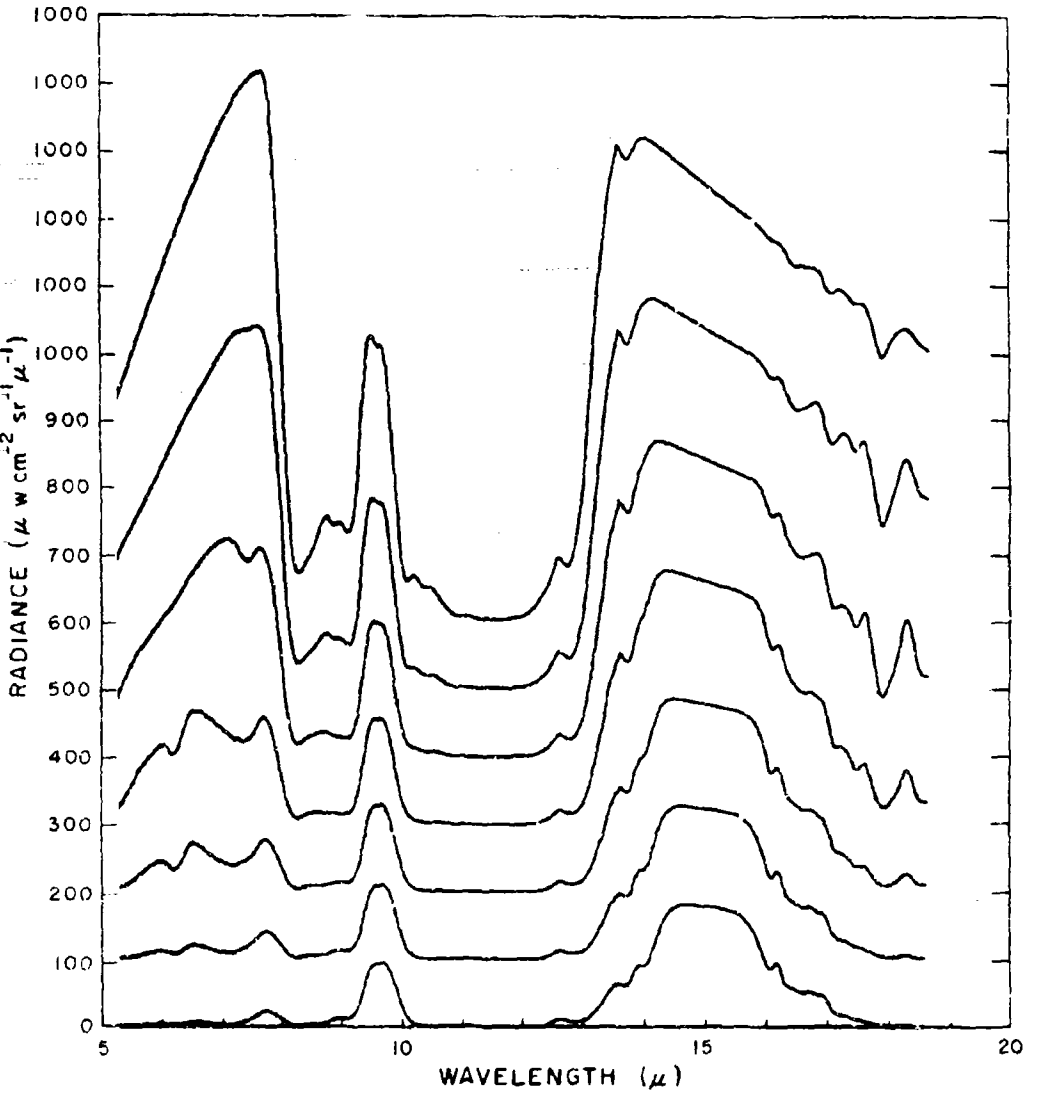

Figure 189. Calculated spectral radiance from 5 to 18.5μ vs altitude for 2 km intervals from 2 to 14 km (top to bottom) at a zenith observation angle of 75.5 (sec = 4) for 1 July 1968. Successive records have a 100 μw cm^{-2} sr^{-1} μ^{-1} offset for clarity.

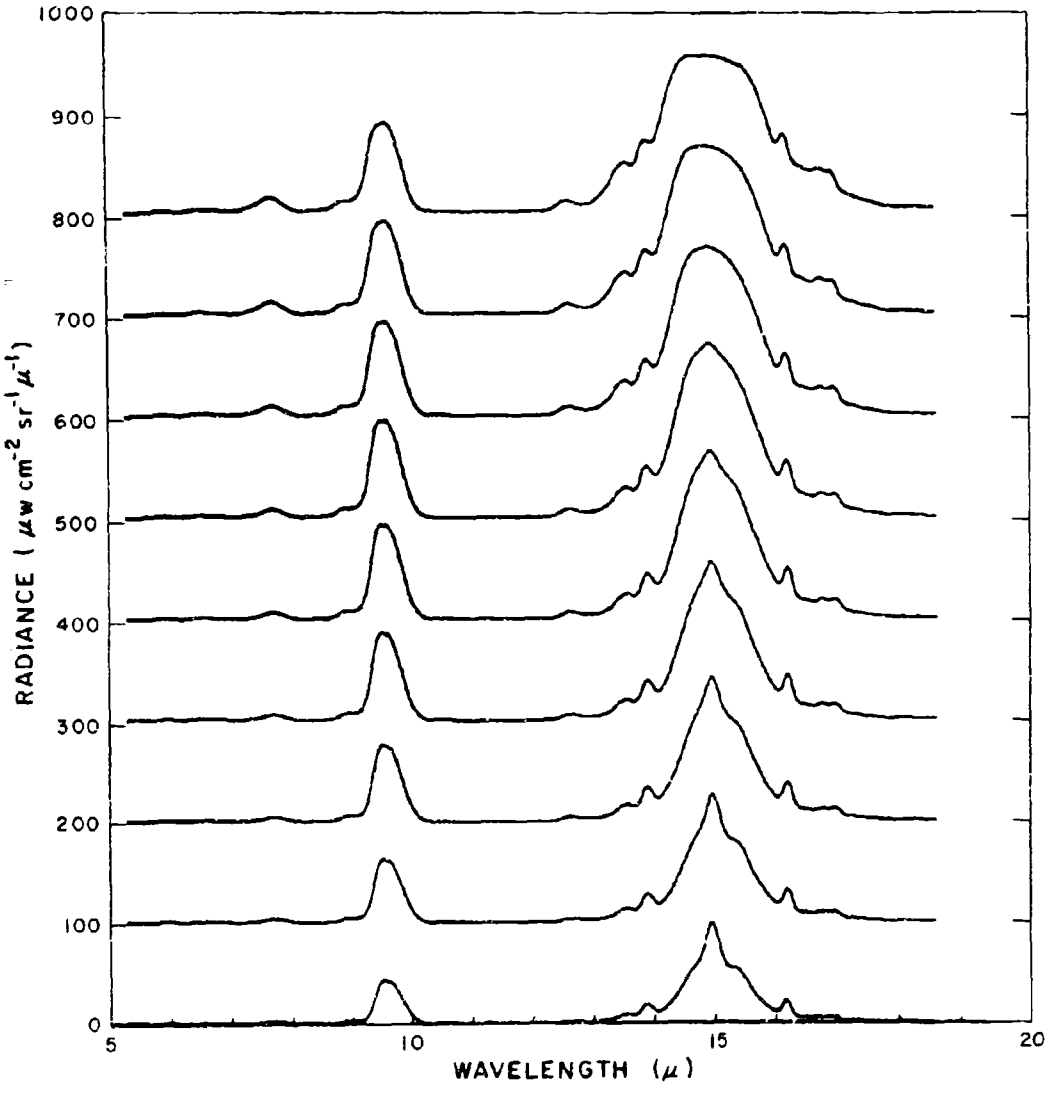

Figure 189. Cont. Calculated spectral radiance from 5 to 18.5μ vs altitude for 2 km intervals from 16 to 32 km (top to bottom) at a zenith observation angle of 75.5° (sec = 4) for 1 July 1968. Successive records have a 100 μw cm^{-2} sr^{-1} μ^{-1} offset for clarity.

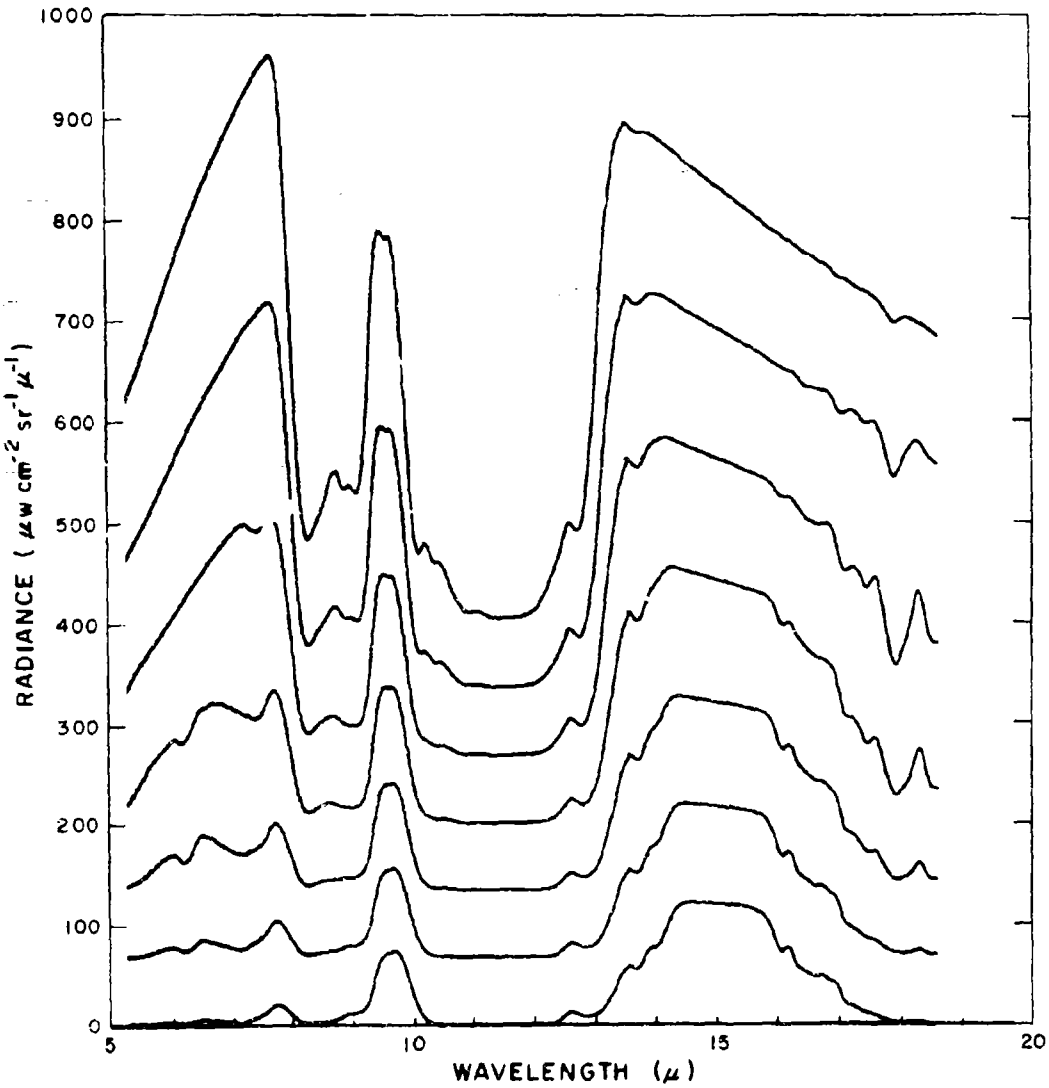

Figure 190. Calculated spectral radiance from 5 to 18.5μ vs altitude for 2 km intervals from 2 to 14 km (top to bottom) at a zenith observation angle of 82.8° (sec = 8) for 1 July 1968. Successive records have a 100 μw cm^{-2} sr^{-1} μ^{-1} offset for clarity.

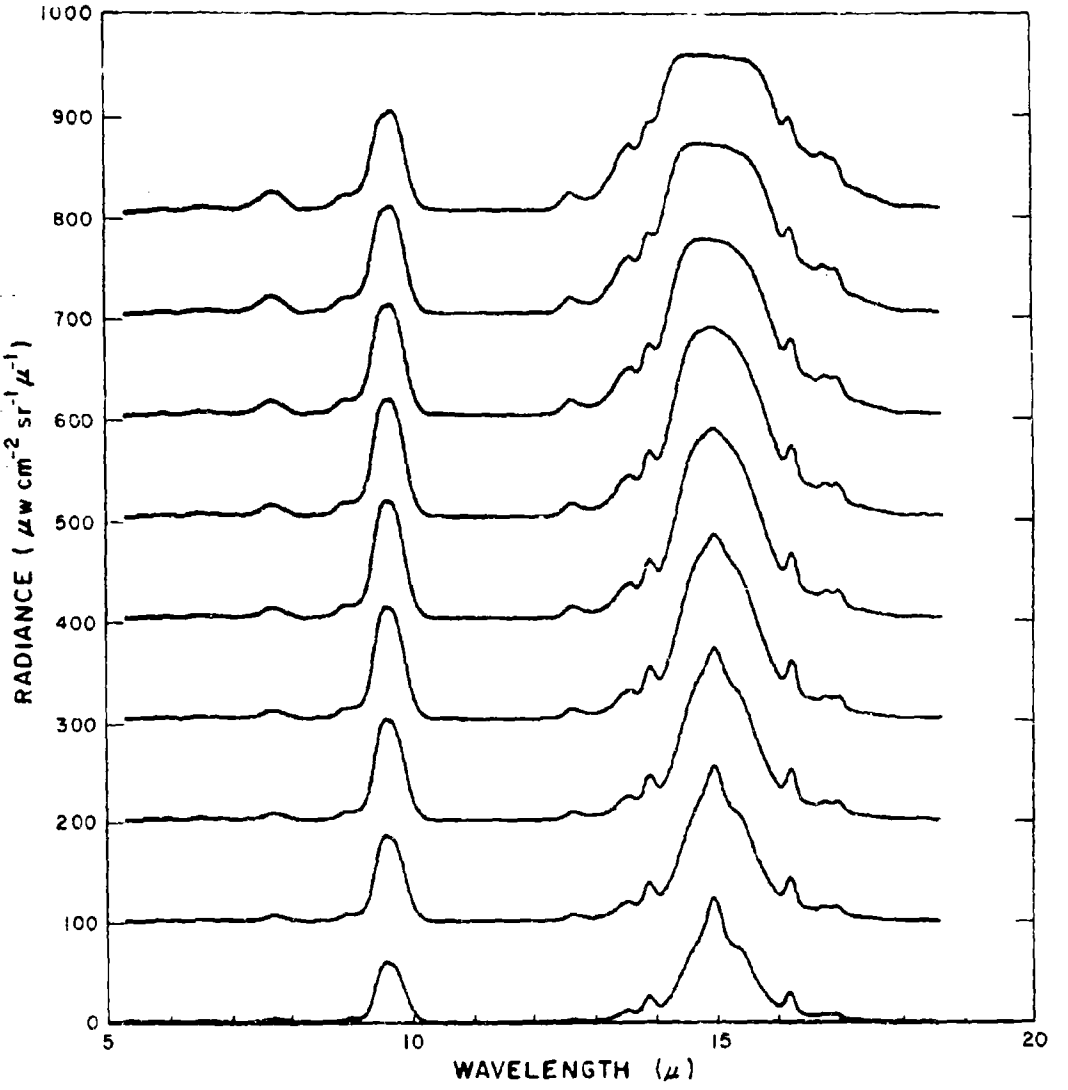

Figure 190. Cont. Calculated spectral radiance from 5 to 18.5μ vs altitude for 2 km intervals from 16 to 32 km (top to bottom) at a zenith observation angle of 82.8° (sec = 8) for 1 July 1968. Successive records have a 100 $\mu w\ cm^{-2}\ sr^{-1}\ \mu^{-1}$ offset for clarity.

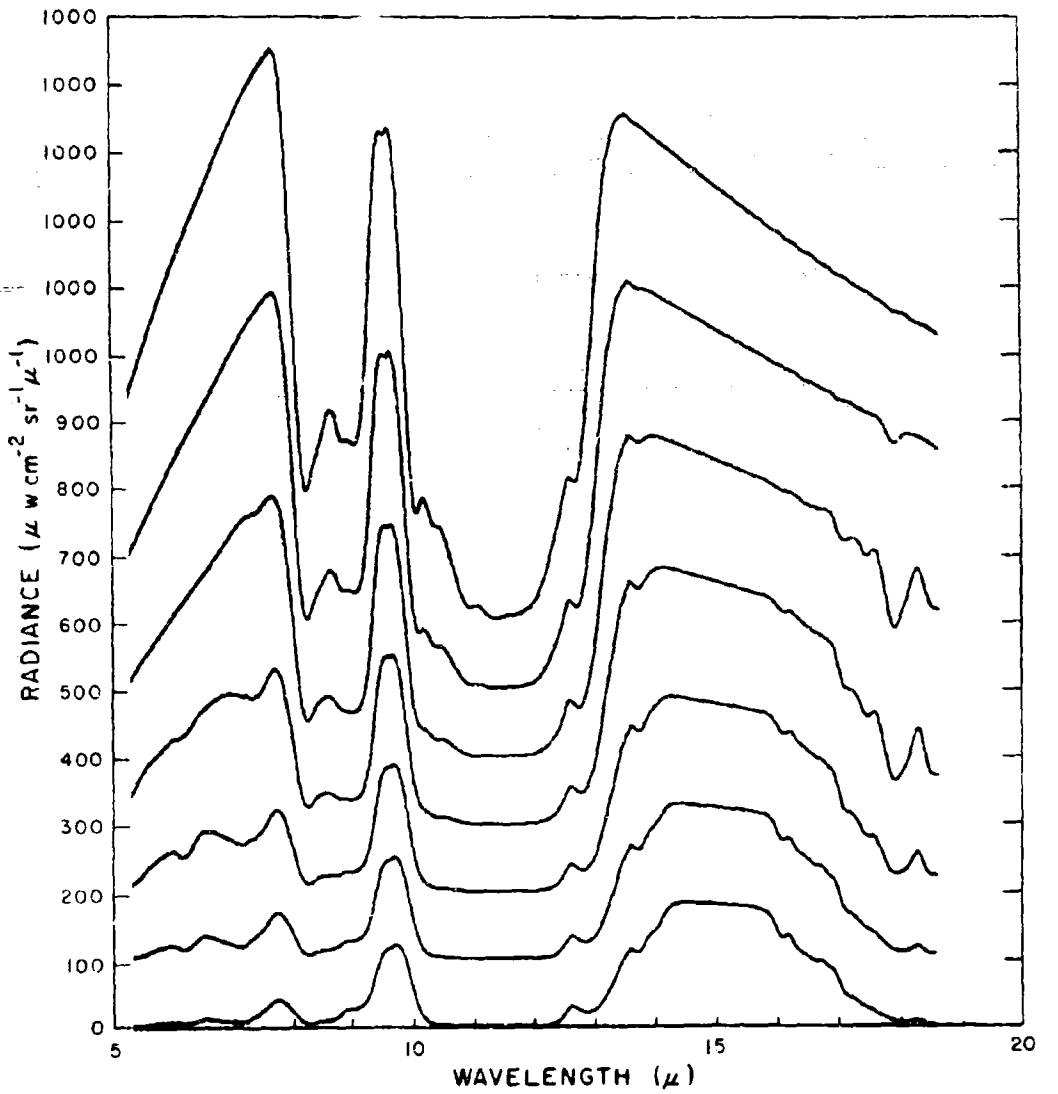

Figure 191. Calculated spectral radiance from 5 to 18.5μ vs altitude for 2 km intervals from 2 to 14 km (top to bottom) at a zenith observation angle of 86.4° (sec = 16) for 1 July 1968. Successive records have a 100 μw cm^{-2} sr^{-1} μ^{-1} offset for clarity.

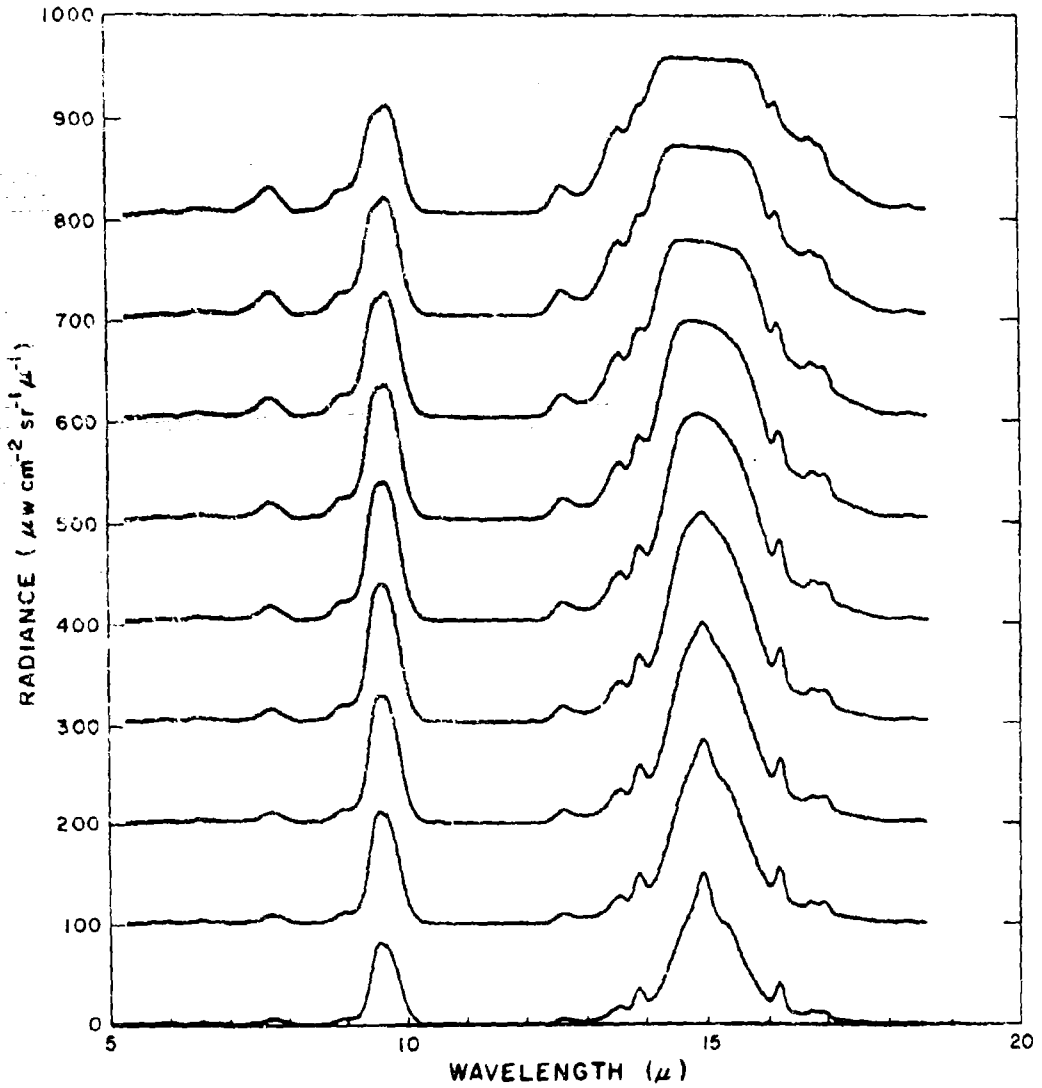

Figure 191. Cont. Calculated spectral radiance from 5 to 18.5μ vs altitude for 2 km intervals from 16 to 32 km (top to bottom) at a zenith observation angle of 86.4° (sec = 16) for 1 July 1968. Successive records have a 100 μw cm^{-2} sr^{-1} μ^{-1} offset for clarity.

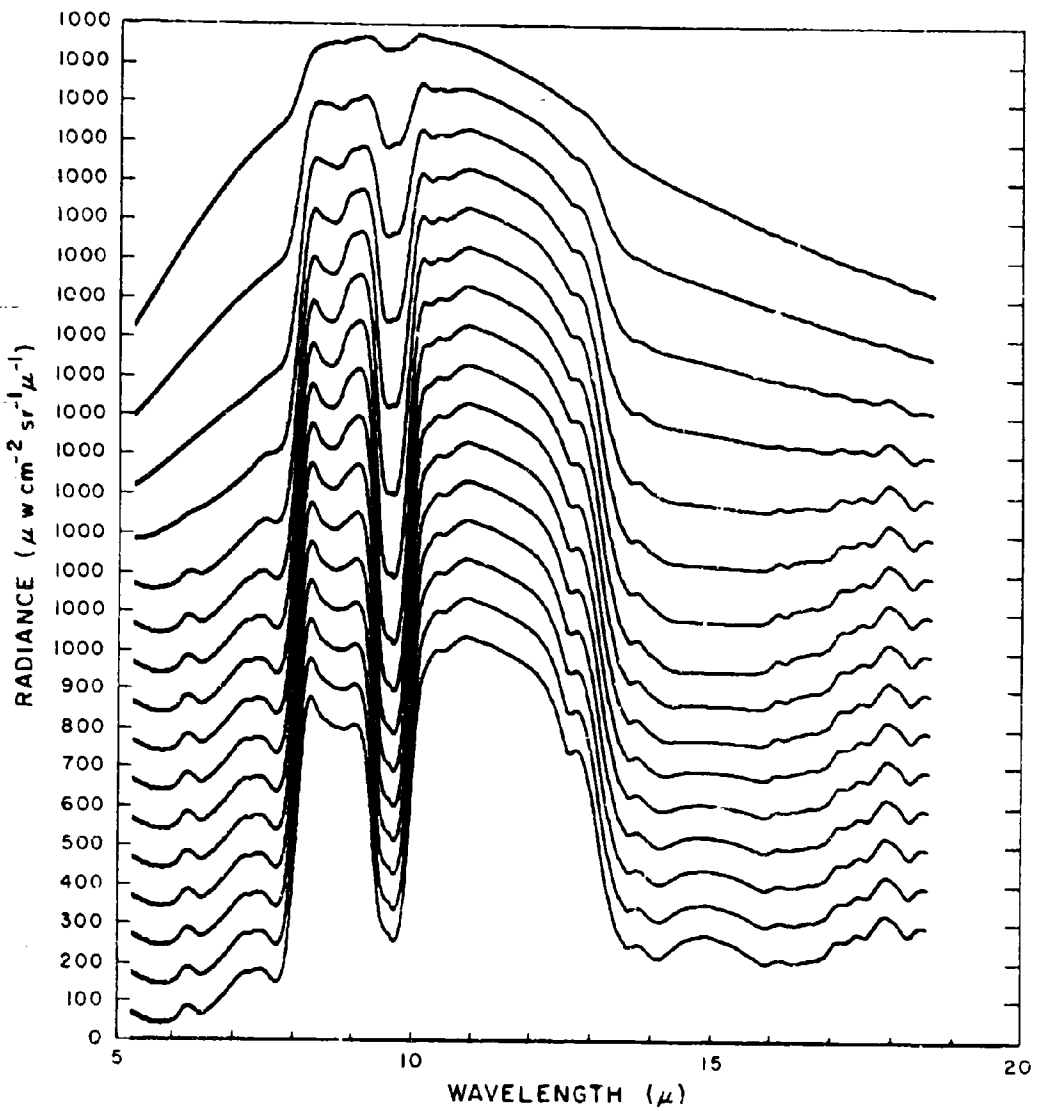

Figure 192. Calculated spectral radiance from 5 to 18.5μ vs altitude for 2 km intervals from 2 - 32km (top to bottom) at a zenith observation angle of 93.6^{o}(sec = 16) for 1 July 1968. Successive records have a 100 μw cm^{-2} sr^{-1} μ^{-1} offset for clarity.

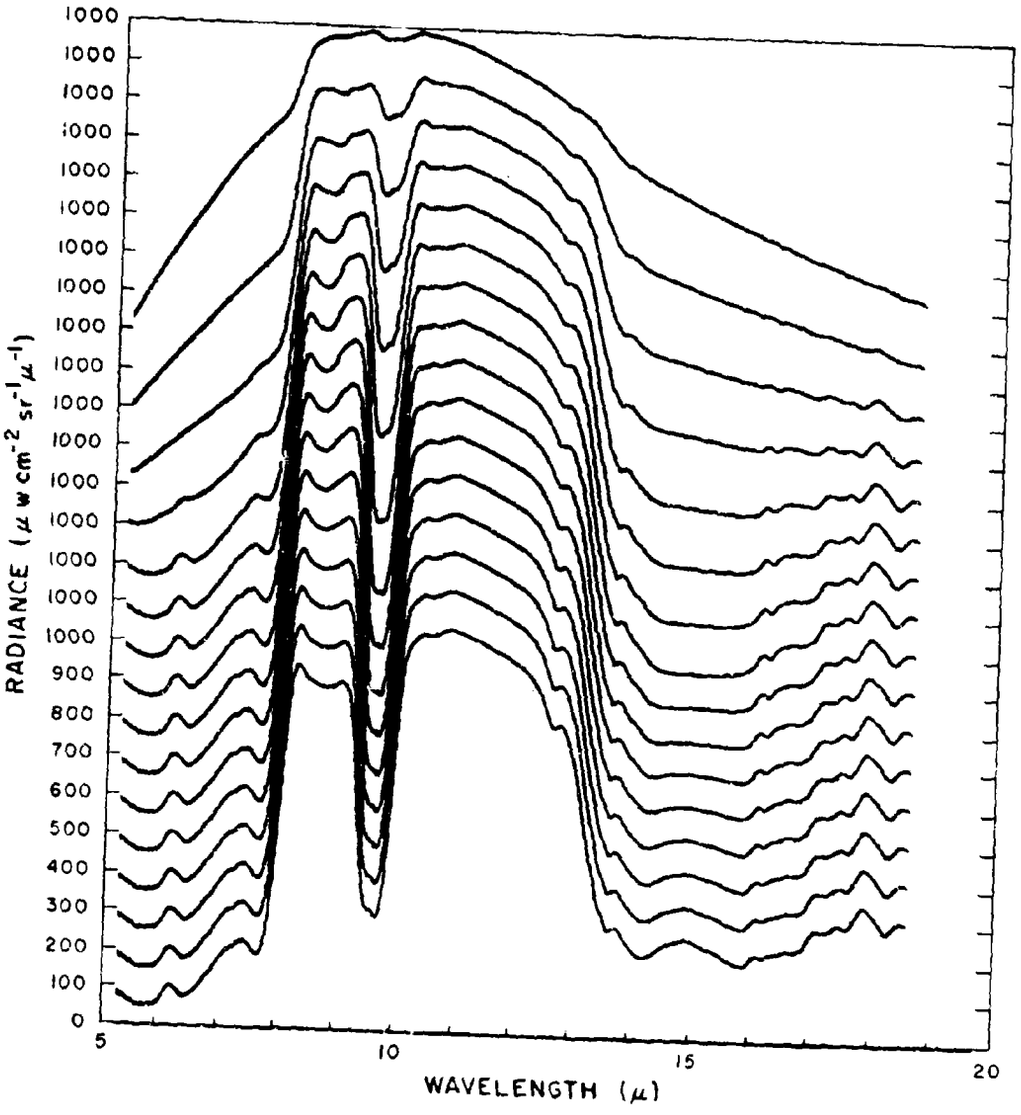

Figure 193. Calculated spectral radiance from 5 to 18.5μ vs altitude for 2 km intervals from 2 - 32 km (top to bottom) at a zenith observation angle of 97.2°(sec = 8) for 1 July 1968. Successive records have a 100 μw cm^{-2} sr^{-1} μ^{-1} offset for clarity.

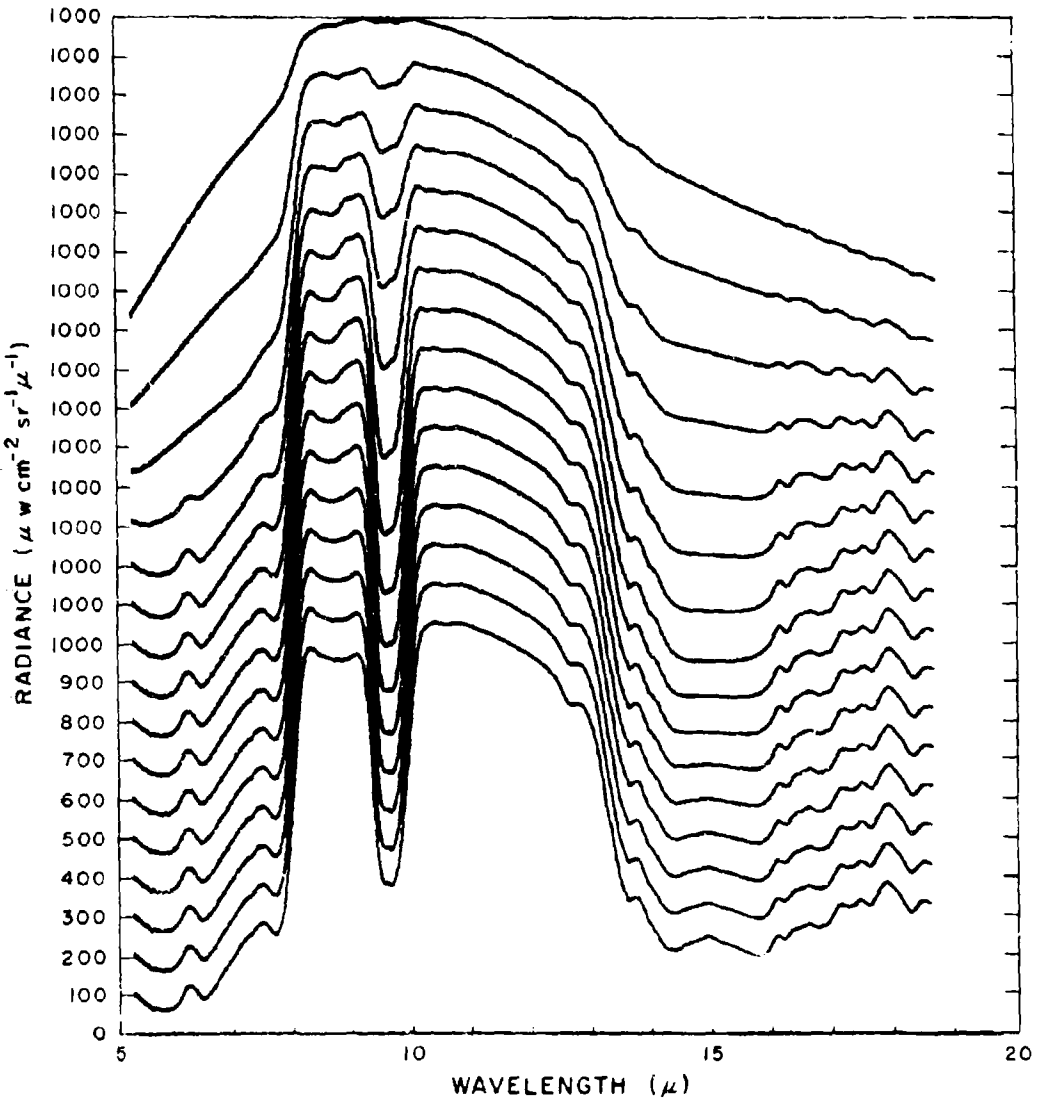

Figure 194. Calculated spectral radiance from 5 to 18.5μ vs altitude for 2 km intervals from 2 - 32 km (top to bottom) at a zenith observation angle of 104.5° (sec = 4) for 1 July 1968. Successive records have a 100 μw cm^{-2} sr^{-1} μ^{-1} offset for clarity.

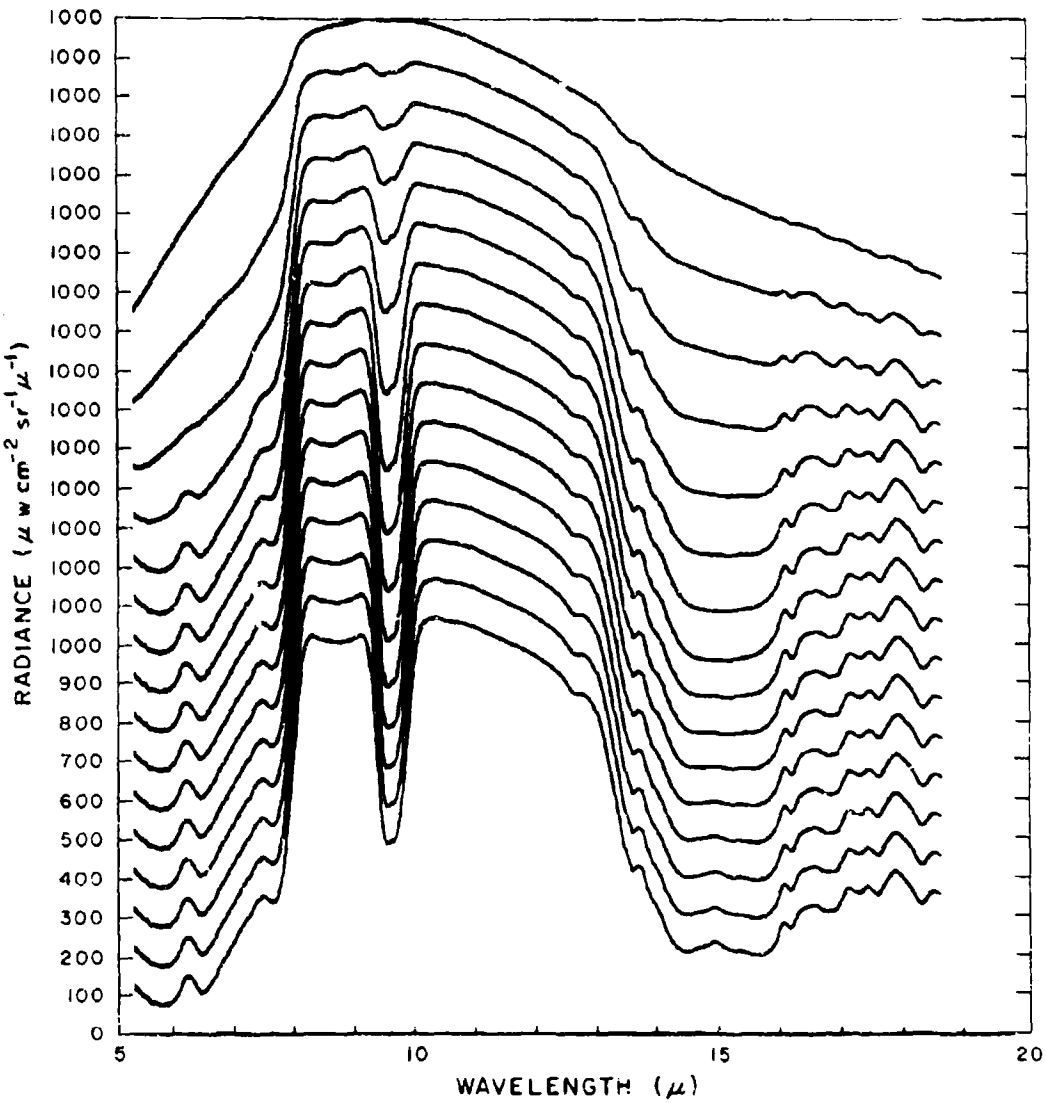

Figure 195. Calculated spectral radiance from 5 to 18.5μ vs altitude for 2 km intervals from 2 - 32 km (top to bottom) at a zenith observation angle of 120° (sec = 2) for 1 July 1968. Successive records have a 100 μw cm^{-2} sr^{-1} μ^{-1} offset for clarity.

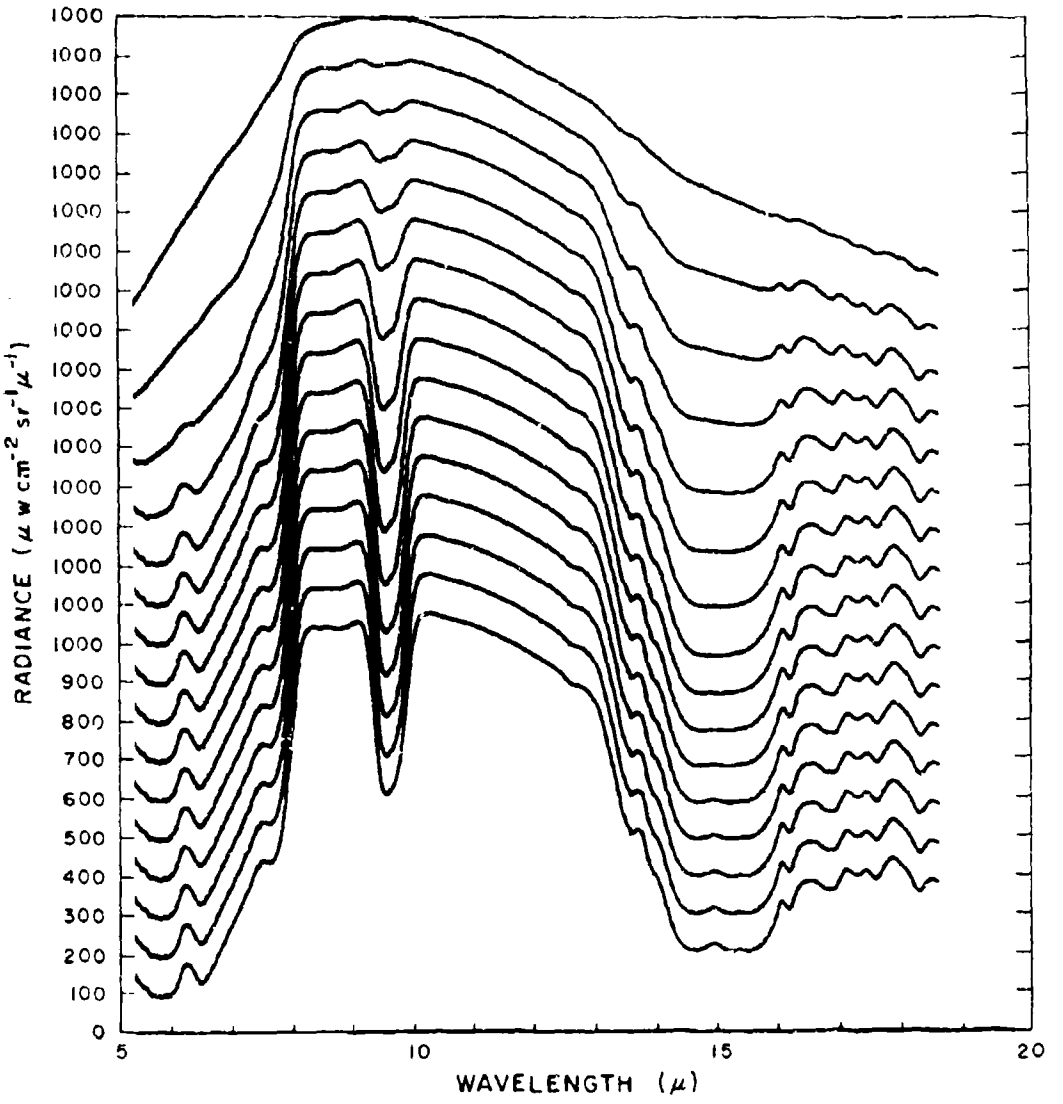

Figure 196. Calculated spectral radiance from 5 to 18.5μ vs altitude for 2 km intervals from 2 - 32 km (top to bottom) at a zenith observation angle of 180^{o} (sec = 1) for 1 July 1968. Successive records have a 100 μw cm^{-2} sr^{-1} μ^{-1} offset for clarity.

Table I

1 June 1967

Record	Time (MDT)	Alt (km)	Press (mb)	Air Temp (°C)	Source Angle (deg)	
13	0649	2.0	791	14.1		180
14	0651	2.6	738	9.8		131.8
15	0654	3.0	697	6.3	60	120
16	0657	3.5	660	2.9	75.5	104.5
17	0659	3.9	627	-0.2	82.8	97.2
18	0702	4.4	583	-4.5	86.4	93.6
19	0705	4.8	558	-6.8	90	90
20	0707	5.6	496	-12.5	93.6	86.4
21	0710	5.8	487	-13.2	97.2	82.8
22	0713	6.1	465	-15.2	104.5	75.5
23	0715	6.5	441	-18.2	120	60
24	0718	7.0	410	-22.8	131.8	30
25	0721	7.7	373	-28.1	180	BB
26	0723	8.2	344	-32.4	131.8	30
27	0726	8.7	322	-35.9	120	60
28	0729	9.1	304	-38.9	104.5	75.5
29	0731	9.5	285	-42.3	97.2	82.8
30	0734	10.1	262	-46.7	93.6	86.4
31	0737	11.0	228	-53.3	90	90
32	0739	11.1	223	-54.2	86.4	93.6
33	0742	11.6	206	-57.3	82.8	97.2
34	0745	12.0	193	-60.3	75.5	104.5
35	0748	12.5	180	-62.2	60	120
36	0750	13.0	167	-64.9	30	131.8
37	0753	13.3	158	-63.9	BB	180
38	0756	13.7	148	-63.5	30	131.8
39	0758	14.2	138	-64.1	60	120
40	0801	14.3	129	-64.8	75.5	104.5
41	0804	15.0	122	-65.3	82.8	97.2
42	0806	15.4	114	-65.3	86.4	93.6
43	0809	15.8	107	-65.1	90	90
44	0812	16.3	98.5	-64.7	93.6	86.4
45	0814	16.7	93.0	-64.5	97.2	82.8
46	0817	17.1	88.0	-63.9	104.5	75.5
47	0820	17.5	82.0	-62.9	120	60
48	0822	17.8	78.0	-62.0	131.8	30
49	0825	18.0	76.0	-61.9	180	BB
50	0828	18.4	71.0	-61.0	131.8	30
51	0830	18.9	66.0	-59.8	120	60
52	0833	19.4	61.5	-58.9	104.5	75.5
53	0836	19.8	57.5	-58.0	97.2	82.8
54	0838	20.3	53.0	-58.5	93.6	86.4
55	0841	20.8	49.0	-58.9	90	90
56	0844	21.2	46.0	-58.7	86.4	93.6
57	0846	21.5	44.0	-57.7	82.8	97.2

Table I. Cont'd.

Record	Time (MDT)	Alt (km)	Press (mb)	Air Temp (°C)	Source Angle (deg)	
58	0849	21.9	41.0	-56.1	75.5	104.5
59	0852	22.3	39.0	-55.1	60	120
60	0854	22.6	37.0	-54.2	30	131.8
61	0857	23.2	34.0	-52.4	BB	180
62	0900	23.5	32.5	-51.9	30	131.8
63	0902	23.9	30.0	-51.0	60	120
64	0905	24.4	28.0	-50.3	75.5	104.5
65	0908	24.6	27.0	-49.9	82.8	97.2
66	0910	25.1	25.0	-49.1	86.4	93.6
67	0913	25.6	23.2	-48.2	90	90
68	0916	25.8	22.7	-48.0	93.6	86.4
69	0918	26.3	21.0	-47.2	97.2	82.8
70	0921	26.9	19.2	-46.1	104.5	75.5
71	0924	27.3	17.8	-45.3	120	60
72	0927	28.1	15.8		131.8	30
73	0929	28.3	15.4		180	BB
74	0932	28.6	14.7		131.8	30
75	0935	28.8	14.2		120	60
76	0937	29.0	13.6		104.5	75.5
77	0940	29.3	13.2		97.2	82.8
78	0943	29.6	12.5		93.6	86.4
79	0945	30.0	11.8		90	90
80	0948	30.2	11.4		86.4	93.6
81	0951	30.5	10.9		82.8	97.2
82	0953	30.8	10.4		75.5	104.5
83	0956	30.9	10.2		60	120
84	0959	31.4	9.5		30	131.8
85	1001	31.3	9.6		BB	180
86	1004	31.3	9.7		30	131.8
87	1007	31.2	9.8		60	120
88	1009	31.2	9.8		75.5	104.5
89	1012	31.2	9.8		82.8	97.2
90	1015	31.2	9.8		86.4	93.6
91	1017	31.2	9.8		90	90
92	1020	31.2	9.8		93.6	86.4
93	1023	31.1	9.9		97.2	82.8
94	1026	31.1	9.9		104.5	75.5
95	1028	31.1	9.9		120	60
96	1031	30.9	10.2		131.8	30
97	1034	30.8	10.4		180	BB
98	1036	30.7	10.6		131.8	30
99	1039	30.6	10.8		120	60
100	1042	30.5	10.9		104.5	75.5
101	1044	30.2	11.5		97.2	82.8
102	1047	30.0	11.7		93.6	86.4
103	1050	29.7	12.2		90	90
104	1052	29.4	12.6		86.4	93.6

Table I. Cont'd.

Record	Time (MDT)	Alt (km)	Press (mb)	Air Temp (°C)	Source Angle (deg)	
105	1055	29.3	13.2		82.8	97.2
106	1058	29.1	13.5		75.5	104.5
107	1100	29.0	13.7		60	120
108	1103	28.9	13.9		30	131.8
109	1106	28.9	14.0		BB	180
110	1108	28.3	15.2		30	131.8
111	1111	28.0	15.9		60	120
112	1114	27.9	16.3	-44.3	75.5	104.5
113	1117	27.7	16.7	-44.5	82.8	97.2
114	1119	27.4	17.5	-45.0	86.4	93.6
115	1122	27.4	17.6	-45.1	90	90
116	1125	26.8	19.3	-46.1	93.6	86.4
117	1127	26.5	20.2	-46.6	97.2	82.8
118	1130	26.2	21.2	-47.2	104.5	75.5
119	1133	25.9	22.2	-47.7	120	60
120	1135	25.8	22.7	-48.0	131.8	30
121	1138	25.3	24.4	-48.8	180	BB
122	1141	25.1	25.0	-49.0	131.8	30
123	1143	25.0	25.5	-49.2	120	60
124	1146	24.4	28.0	-50.3	104.5	75.5
125	1149	24.2	29.0	-50.7	97.2	
126	1151	23.6	31.5	-51.6	93.6	
127	1154	23.5	32.5	-51.9	90	
128	1157	23.3	33.5	-52.2	86.4	
129	1200	22.9	35.5	-52.2	82.8	
130	1202	22.7	36.5	-53.9	75.5	
131	1205	22.6	37.5	-54.4	60	
132	1208	21.9	41.0	-56.3	30	

Table II.

30 November 1967

Record	Time (MST)	Alt (km)	Press (mb)	Air Temp (°C)	Source Angle (deg)	
5	0720	1.3	865	2	131.8	30
6	0723	1.3	865	2		60
7	0726	1.3	865	2	180	75.5
8	0728	1.3	865	2	131.8	82.8
9	0731	1.3	865	2	120	86.4
10	0734	1.3	865	2		90
11	0736	1.3	865	2	93.6	93.6
12	0739	1.3	865	2	90	97.2
13	0742	1.8	812	6.8	86.4	104.5
14	0744	2.1	776	7.1	82.8	120
15	0747	2.7	719	5.0	75.5	131.8
16	0750	3.5	665	2.4		180
17	0752	4.1	610	-2.4	60	131.8
18	0755	4.8	553	-8.1		120
19	0758	5.5	506	-12.7	30	104.5
20	0800	6.2	456	-18.3		97.2
21	0803	7.0	410	-23.9	BB	93.6
22	0806	7.7	373	-29.4		90
23	0808	8.5	329	-35.5	30	86.4
24	0811	9.1	301	-39.4		82.8
25	0814	9.8	275	-44.2	60	75.5
26	0816	10.8	235	-52.9		60
27	0819	11.6	208	-57.1	75.5	30
28	0822	12.5	180	-61.2	82.8	BB
29	0825	13.1	162	-62.5	86.4	30
30	0827	13.7	150	-62.2	90	60
31	0830	14.4	134	-61.5	93.6	75.5
32	0833	14.9	123	-62.6	97.2	82.8
33	0835	15.7	109	-63.7	104.5	86.4
34	0838	16.4	97.5	-65.6	120	90
35	0841	17.3	84.5	-69.9	131.8	93.6
36	0843	17.9	77.5	-68.1		97.2
37	0846	18.6	69.0	-67.6		104.5
39	0851	19.5	60.5	-61.8	180	120
41	0857	20.9	48.5	-57.8		131.8
43	0902	22.3	39.0	-56.9	131.8	
44	0905	23.0	35.0	-56.4	120	180
46	0910	24.4	28.0	-54.5	104.5	131.8
47	0913	25.1	25.0	-53.8	97.2	
51	0915	25.8	22.7	-53.1	93.6	120
52	0918	26.5	20.2	-52.0	90	
53	0921	27.4	17.6	-50.5	86.4	104.5
54	0923	28.0	16.1	-49.3	82.8	97.2
55	0926	28.7	14.1	-48.4	75.5	93.6

Table II. Cont'd.

Record	Time (MST)	Alt (km)	Press (mb)	Air Temp (°C)	Source Angle (deg)	
56	0929	29.3	13.1	-48.3		90
57	0931	29.6	12.6	-48.3	60	86.4
58	0934	29.6	12.6	-48.3		82.8
59	0937	29.6	12.6	-48.3		75.5
61	0942	29.6	12.6	-48.3		60
66	0950	29.6	12.6	-48.3	30	30
68	0955	29.6	12.6	-48.3	60	
69	0958	29.6	12.6	-48.3	75.5	BB
70	1001	29.6	12.6	-48.3	82.8	30
71	1003	29.6	12.6	-48.3	86.4	
72	1006	29.6	12.6	-48.3	90	60
73	1009	29.6	12.6	-48.3	93.6	
74	1011	29.6	12.6	-48.3	97.2	75.5
96	1017	29.6	12.6	-48.3	120	86.4
97	1019	29.6	12.6	-48.3	131.8	90
98	1022	29.6	12.6	-48.3		93.6
99	1025	29.6	12.6	-48.3		97.2
100	1027	29.4	12.9	-48.3	130	104.5
102	1033	29.4	12.9	-48.3		120
104	1038	29.4	12.9	-48.3	131.8	131.8
105	1041	29.3	13.1	-48.3	120	
106	1043	29.2	13.4	-48.3	104.5	180
107	1046	29.1	13.6	-48.4	97.2	131.8
108	1049	29.0	13.7	-48.4	93.6	
109	1051	29.0	13.8	-48.4	90	120
110	1054	28.9	14.0	-48.4	86.4	
111	1057	28.6	14.6	-48.5	82.8	104.5
112	1059	28.3	15.2	-48.5	75.5	97.2
113	1102	28.2	15.6	-48.8	60	93.6
114	1105	28.0	16.1	-49.3		90
115	1107	27.8	16.5	-49.7	30	86.4
116	1110	27.6	17.1	-50.2		82.4
117	1113	27.2	18.1	-50.9	BB	75.5
118	1116	26.9	19.1	-51.4		60
119	1118	26.6	20.0	-51.9	30	30
120	1121	26.4	20.7	-52.4		BB

Table III.

25 June 1968

Record	Time (MDT)	Alt. (km)	Press. (mb)	Air Temp. (°C)	Source Angle (deg)	
6	0633	2.9	683	10.6	178.5	DB
7	0636	3.7	619	4.1	130	28.5
8	0639	4.4	572	-0.6	118.5	58.5
9	0642	4.9	516	-6.5	103	74
10	0644	5.5	496	-8.4	95.5	81
11	0647	5.9	465	-12.1	92	85
12	0650	6.4	428	-17.4	88.5	88.5
13	0652	6.9	410	-19.7	85	92
14	0655	7.3	376	-24.7	81	95.5
15	0657	7.9	351	-28.3	74	103
16	0700	8.5	322	-33.7	58.5	118.5
17	0703	9.1	288	-40.0	28.5	130
18	0706	9.6	269	-43.9	BB	178.5
19	0708	10.1	251	-46.5	28.5	130
20	0711	10.7	234	-49.1	58.5	118.5
21	0713	11.0	223	-50.6	74	103
22	0716	11.2	212	-52.6	81	95.5
23	0719	11.7	193	-55.5	85	92
24	0721	12.2	180	-56.9	88.5	88.5
25	0724	12.8	163	-60.0	92	85
26	0727	13.4	149	-59.7	95.5	81
27	0729	13.9	142	-61.1	103	74
28	0732	14.2	135	-62.4	118.5	58.5
29	0735	14.6	123	-65.2	130	28.5
30	0737	15.2	112	-67.4	178.5	BB
31	0740	15.7	107	-67.0	130	28.5
32	0743	16.2	97	-66.3	118.5	58.5
33	0745	16.6	92.5	-65.9	103	74
34	0748	16.9	90	-63.8	95.5	81
35	0751	17.1	86	-62.2	92	85
36	0753	17.4	80	-63.4	88.5	88.5
37	0756	18.0	73	-63.2	85	92
38	0759	18.4	68	-61.9	81	95.5
39	0801	18.9	63	-60.8	74	103
40	0804	19.5	60	-60.0	58.5	118.5
41	0807	19.7	57.5	-59.2	28.5	130
42	0809	19.8	54.8	-58.4	BB	178.5
43	0812	20.3	51	-34.0	28.5	130
44	0815	20.7	48.5	-56.4	58.5	118.5
45	0817	21.0	45.5	-55.6	74	103
46	0820	21.6	42	-54.4	81	95.5
47	0823	21.9	39.5	-53.7	85	92

Table III. Cont'd.

Record	Time (MDT)	Alt. (km)	Press. (mb)	Air Temp. (°C)	Source Angle (deg)	
48	0825	22.3	37.5	-52.9	88.5	88.5
49	0828	22.6	35.5	-52.1	92	85
50	0831	23.0	33.5	-50.5	95.5	81
51	0833	23.5	31.5	-49.5	103	74
52	0836	23.8	29.5	-49.1	118.5	58.5
53	0839	24.2	27.5	-46.8	130	28.5
54	0841	24.7	25.5	-44.3	178.5	BB
55	0844	25.1	23.9	-44.4	130	28.5
56	0846	25.6	22.8	-44.9	118.5	58.5
57	0849	25.9	21.7	-44.9	103	74
58	0852	26.4	20.2	-44.1	95.5	81
59	0854	26.7	19.3	-43.4	92	85
60	0857	27.0	18.4	-42.4	88.5	88.5
61	0900	27.3	17.5	-41.4	85	92
62	0902	27.6	16.7	-40.2	81	95.5
63	0905	27.9	15.6	-39.0	74	103
64	0908	28.3	14.9	-38.2	58.5	118.5
65	0910	28.7	14.5	-37.3	28.5	130
66	0913	29.0	13.8	-36.4	BB	178.5
67	0916	29.1	13.5	-35.5	28.5	130
68	0918	29.4	12.9	-35.3	58.5	118.5
69	0921	29.6	12.6	-35.1	74	103
70	0924	29.9	12.0	-35.2	81	95.5
71	0926	30.0	11.7	-35.2	85	92
72	0929	29.9	12.0	-35.2	88.5	88.5
73	0932	29.9	12.0	-35.2	92	85
74	0934	29.9	12.0	-35.2	95.5	81
75	0937	29.9	12.0	-35.2	103	74
76	0940	29.9	12.0	-35.2	118.5	58.5
77	0942	29.9	12.0	-35.1	130	28.5
78	0945	29.7	12.3	-35.1	178.5	BB
79	0948	29.7	12.3	-35.1	130	28.5
80	0950	29.6	12.6	-35.1	118.5	58.5
81	0953	29.6	12.6	-35.3	103	74
82	0956	29.4	12.9	-35.5	95.5	81
83	0958	29.3	13.2	-36.0	92	85
84	1001	29.0	13.8	-36.4	88.5	88.5
85	1004	29.0	13.8	-36.4	85	92
86	1006	28.8	14.2	-37.0	81	95.5
87	1009	28.7	14.5	-37.3	74	103
88	1012	28.5	14.9	-37.9	58.5	118.5
89	1014	28.3	15.2	-38.3	28.5	130
90	1017	28.2	15.6	-39.0	BB	178.5
91	1020	28.0	16.3	-39.9	28.5	130
92	1022	27.7	16.7	-40.4	58.5	118.5
93	1025	27.4	17.5	-41.4	74	103
94	1028	27.3	18.4	-42.5	81	95.5

Table III. Cont'd.

Record	Time (MDT)	Alt. (km)	Press. (mb)	Air Temp. (°C)	Source Angle (deg)	
95	1030	27.0	19.3	-43.3	85	92
96	1033	26.8	19.7	-43.5	88.5	88.5
97	1036	26.7	20.7	-44.2	92	85
98	1038	26.4	21.2	-44.7	95.5	81
99	1041	25.9	22.8	-44.9	103	74
100	1044	25.6	23.9	-44.5	118.5	58.5
101	1046	25.5	24.4	-44.1	130	28.5
102	1049	25.3	25.5	-44.7	178.5	BB
103	1052	24.7	28.0	-47.7	130	28.5
104	1054	24.4	29.0	-48.9	118.5	58.5
105	1057	24.2	29.5	-49.1	103	74
106	1100	23.9	31.5	-49.6	95.5	81
107	1102	23.5	32.5	-49.7	92	85
108	1105	23.3	33.5	-50.6	88.5	88.5
109	1108	23.2	34.0	-50.9	85	92
110	1110	23.0	35.0	-51.8	81	95.5
111	1113	22.9	36.5	-52.5	74	103
112	1116	22.6	37.5	-53.0	58.5	118.5
113	1118	22.6	38.5	-53.2	28.5	130
114	1121	22.1	40.0	-53.8	BB	178.5
115	1124	21.9	41.0	-54.1	28.5	130
116	1126	21.9	42.0	-54.4	58.5	118.5
117	1129	21.6	43.0	-54.7	74	103
118	1132	21.5	44.0	-55.0	81	95.5
119	1134	21.3	45.5	-55.5	85	92
120	1137	21.0	48.5	-56.4	88.5	88.5
121	1140	20.7	51.0	-57.0	92	85
122	1142	20.4	53.5	-58.1	95.5	81
123	1145	20.1	56.0	-58.9	103	74
124	1148	19.8	57.5	-59.6	118.5	58.5
125	1150	19.7	59.0	-60.0	130	28.5
126	1158	19.5	60.0	-60.0	178.5	BB

Table IV.

1 July 1968

Record	Time (MDT)	Alt. (km)	Press. (mb)	Air Temp. (°C)	Source Angle (deg)	
1	0145	1.3	865	26.1	58.5	118.5
2	0148	1.3	865	26.1	74	103
3	0151	1.3	865	26.1	81	95.5
4	0153	1.3	865	26.1	85	92
5	0156	1.3	865	26.1	88.5	88.5
6	0159	1.3	865	26.1	92	85
7	0201	1.3	865	26.1	95.5	81
8	0204	1.3	865	26.1	103	74
9	0207	1.8	812	23.7	118.5	58.5
10	0209	2.3	767	20.1	130	28.5
11	0212	3.4	670	10.6	178.5	BB
12	0215	4.1	607	3.3	130	28.5
13	0217	5.3	516	-7.4	118.5	58.5
14	0220	5.8	485	-9.7	103	74
15	0223	6.9	428	-16.3	95.5	81
16	0225	7.5	384	-21.7	92	85
17	0228	8.4	337	-28.2	88.5	88.5
18	0231	8.8	315	-31.9	85	92
19	0233	9.4	288	-37.2	81	95.5
20	0236	10.4	251	-44.7	74	103
21	0239	11.1	223	-50.0	58.5	118.5
22	0241	11.6	207	-52.8	28.5	130
23	0244	12.2	188.5	-56.7	BB	178.5
24	0247	12.8	171	-61.0	28.5	130
25	0249	13.3	160	-63.0	58.5	118.5
26	0252	13.9	145	-65.7	74	103
27	0255	14.5	132	-67.5	81	95.5
28	0257	14.8	126	-67.9	85	92
29	0300	15.2	117	-68.2	88.5	88.5
30	0303	15.8	107	-67.9	92	85
31	0305	16.2	102	-66.5	95.5	81
32	0308	16.3	99	-66.1	103	74
33	0311	16.8	92.5	-65.3	118.5	58.5
34	0313	16.8	92.5	-65.3	130	28.5
35	0316	16.8	92.5	-65.3	178.5	BB
36	0319	17.1	88.0	-64.7	130	28.5
37	0321	17.7	80.0	-63.4	118.5	58.5
38	0324	18.0	76.5	-63.3	103	74
39	0327	18.4	71.0	-61.4	95.5	81
40	0329	18.6	69.5	-60.1	92	85
41	0332	18.7	68.0	-60.3	88.5	88.5
42	0335	19.4	61.5	-59.0	85	92
43	0337	19.5	60.0	-57.8	81	95.5
44	0340	19.8	57.5	-57.6	74	103

Table IV. Cont'd.

Record	Time (MDT)	Alt. (km)	Press. (mb)	Air Temp. (°C)	Source Angle (deg)	
45	0343	20.0	56.0	-56.9	58.5	118.5
46	0345	20.3	53.5	-55.9	28.5	130
47	0348	20.6	51.0	-55.0	BB	178.5
48	0351	21.0	47.5	-54.1	28.5	130
49	0353	21.2	46.5	-54.1	58.5	118.5
50	0356	21.5	44.0	-54.8	74	103
51	0359	21.6	43.0	-55.1	81	95.5
52	0401	21.8	42.0	-55.0	85	92
53	0404	22.3	39.5	-54.0	88.5	88.5
54	0407	22.6	37.5	-53.0	92	85
55	0409	22.9	35.5	-52.1	95.5	81
56	0412	23.3	33.5	-51.6	103	74
57	0415	23.9	30.0	-50.6	118.5	58.5
58	0417	24.1	29.5	-50.5	130	28.5
59	0420	24.5	27.5	-50.1	178.5	BB
60	0423	24.8	26.0	-49.8	130	28.5
61	0425	25.0	25.5	-49.5	118.5	58.5
62	0428	25.1	25.0	-49.2	103	74
63	0430	25.3	24.4	-48.9	95.5	81
64	0433	25.6	23.3	-48.2	92	85
65	0436	26.1	21.7	-47.2	88.5	88.5
66	0438	26.2	21.2	-46.9	85	92
67	0441	26.4	20.7	-46.6	81	95.5
68	0444	26.5	20.2	-46.2	74	103
69	0446	27.0	18.8	-45.4	58.5	118.5
70	0449	27.4	17.5	-45.2	28.5	130
71	0452	27.6	17.1	-45.2	BB	178.5
72	0454	27.7	16.7	-45.2	28.5	130
73	0457	28.0	15.9	-45.0	58.5	118.5
74	0500	28.2	15.6	-44.8	74	103
75	0502	28.3	15.2	-44.5	81	95.5
76	0505	28.7	14.5	-44.0	85	92
77	0508	28.8	14.2	-43.7	88.5	88.5
78	0510	28.8	14.2	-43.7	92	85
79	0513	29.0	13.8	-43.4	95.5	81
80	0516	29.6	12.6	-42.4	103	74
81	0518	29.7	12.3	-42.2	118.5	58.5
82	0521	30.2	11.5	-41.4	130	28.5
83	0524	30.3	11.3	-41.4	178.5	BB
84	0526	30.3	11.3	-41.4		28.5
85	0529	30.3	11.3	-41.4		58.5
86	0532	30.3	11.3	-41.4		74
87	0534	30.3	11.3	-41.4		81
88	0537	30.3	11.3	-41.4		85
89	0540	30.3	11.3	-41.4		88.5
90	0542	30.3	11.3	-41.4		92

Table IV. Cont'd.

Record	Time (MDT)	Alt. (km)	Press. (mb)	Air Temp. (°C)	Source Angle (deg)
91	0545	30.3	11.3	-41.4	95.5
92	0548	30.3	11.3	-41.4	103
93	0550	30.3	11.3	-41.4	118.5
94	0553	30.3	11.3	-41.4	130
95	0556	30.3	11.3	-41.4	178.5
96	0558	30.3	11.3	-41.4	130
97	0601	30.3	11.3	-41.4	118.5
98	0604	30.3	11.3	-41.4	103
99	0606	30.3	11.3	-41.4	95.5
100		30.3	11.3	-41.4	92

Table V.

25 February 1969

Record	Time (MST)	Alt. (km)	Press. (mb)	Air Temp. (°C)	Source Angle (deg)
11	0204	1.7	827	11.4	48.2
12	0206	2.1	782	8.2	70.5
13	0209	2.4	753	5.8	80.2
14	0212	4.0	619	-5.2	85.2
15	0214	4.3	595	-7.6	90.0
16	0217	5.2	527	-12.6	93.6
17	0220	5.8	485	-16.3	90.0
18	0222	6.2	456	-19.7	85.2
19	0225	7.0	410	-27.1	80.2
20	0228	7.6	376	-31.7	70.5
21	0230	8.1	352	-35.9	48.2
22	0233	8.8	315	-41.5	BB
23	0236	9.4	288	-46.2	48.2
24	0238	10.2	257	-52.9	70.5
25	0241	11.0	228	-58.0	80.2
26	0244	11.7	202	-61.6	85.2
27	0246	12.5	180	-63.9	90.0
28	0249	13.4	156	-65.1	93.6
29	0252	13.7	149	-65.0	90.0
30	0254	13.9	145	-65.2	85.2
31	:57	14.8	126	-65.3	80.2
32	0300	15.2	118	-65.2	70.5
33	0302	15.6	111	-66.4	48.2
34	0305	16.3	99.0	-65.8	BB
35	0308	16.9	90.0	-67.1	48.2
36	0310	17.0	89.0	-67.1	70.5
37	0313	17.7	80.0	-58.4	80.2
38	0316	18.0	76.5	-58.6	85.2
39	0318	18.1	74.5	-59.2	90.0
40	0321	19.0	64.5	-64.0	93.6
41	0324	19.7	59.0	-60.8	90.0
42	0326	20.0	56.0	-60.2	85.2
43	0329	20.1	54.5	-60.5	80.2
44	0332	20.3	53.5	-61.2	70.5
45	0334	20.9	48.5	-60.4	48.2
46	0336	21.5	44.0	-56.2	BB
47	0339	21.8	42.0	-56.4	48.2
48	0342	21.9	41.0	-57.0	70.5
49	0344	22.7	36.5	-60.8	80.2
50	0347	23.2	34.0	-59.0	85.2
51	0350	23.5	32.5	-57.7	90.0
52	0352	24.0	30.0	-57.0	93.6
53	0355	24.4	28.0	-56.4	90.0
54	0358	24.6	27.0	-56.2	85.2

Table V. Cont'd.

Record	Time (MST)	Alt. (km)	Press. (mb)	Air Temp. (°C)	Source Angle (deg)
55	0400	25.1	25.5	-55.6	80.2
56	0403	25.3	24.4	-55.3	70.5
57	0406	25.6	23.3	-54.9	48.2
58	0408	26.1	21.7	-54.3	BB
60	0414	26.7	19.7	-53.9	48.2
61	0416	27.0	18.8	-53.9	70.5
62	0419	27.4	17.5	-53.6	80.2
63	0422	27.9	16.3	-52.2	85.2
64	0424	28.7	14.5	-49.8	90.0
65	0427	29.0	13.8	-49.0	93.6
66	0430	29.3	13.2	-48.1	90.0
67	0432	29.4	12.9	-47.8	85.2
68	0435	29.7	12.3	-47.0	80.2
69	0438	29.9	12.0	-46.4	70.5
70	0440	30.0	11.7	-46.1	48.2
74	0451	30.4	11.0	-44.9	48.2
76	0456	30.4	11.0	-44.9	30.2
77	0459	30.4	11.0	-44.9	85.2
78	0502	30.4	11.0	-44.9	90.0
79	0504	30.4	11.0	-44.9	93.6
80	0507	30.4	11.0	-44.9	90.0
81	0510	30.4	11.0	-44.9	85.2
82	0512	30.4	11.0	-44.9	80.2
83	0515	30.4	11.0	-44.9	70.5
84	0518	30.4	11.0	-44.9	48.2
86	0523	30.4	11.0	-44.9	BB
89	0530	30.4	11.0	-44.9	70.5
90	0533	30.4	11.0	-44.9	80.2
91	0536	30.4	11.0	-44.9	85.2
92	0538	30.4	11.0	-44.9	90.0
93	0541	30.4	11.0	-44.9	93.6

TABLE VI. Percentage of Absorbers in Atmospheric Layers

This Table gives the percentage of the total quantity of the indicated absorbers in each of the 16 layers into which the atmosphere was divided.

Layer	Uniformly Mixed Absorbers	CH_4	O_3	H_2O
1	21.54	22.46	2.0	47.90
2	17.40	18.36	1.60	39.12
3	14.24	14.86	1.30	10.82
4	11.42	11.90	1.28	1.64
5	9.02	9.40	1.50	0.44
6	7.00	7.30	2.40	0.054
7	5.16	5.38	4.30	0.0060
8	3.76	3.92	5.72	0.0044
9	2.74	2.86	6.30	0.0032
10	2.0	2.04	7.76	0.0024
11	1.46	0.36	10.24	0.00176
12	1.06	0.26	11.64	0.00128
13	0.78	0.18	11.00	0.00092
14	0.56	0.14	8.94	0.00068
15	0.42	0.10	6.76	0.00052
16	1.18	0.30	17.18	0.00140

Unclassified

Security Classification

DOCUMENT CONTROL DATA – R & D

(Security classification of title, body of abstract and indexing annotation must be entered when the overall report is classified)

1. ORIGINATING ACTIVITY (Corporate author)
University of Denver
Department of Physics
Denver, Colorado 80210

2a. REPORT SECURITY CLASSIFICATION
Unclassified

2b. GROUP

3. REPORT TITLE
FLOW OF RADIATION IN THE EARTH'S ATMOSPHERE

4. DESCRIPTIVE NOTES (Type of report and inclusive dates)
Scientific. Final. 1 December 1965 - 31 May 1969 Approved: 14 Sept. 1970.

5. AUTHOR(S) (First name, middle initial, last name)
Walter J. Williams David G. Murcray
Frank H. Murcray Thomas G. Kyle

6. REPORT DATE	7a. TOTAL NO. OF PAGES	7b. NO. OF REFS
January 1970	258	8

8a. CONTRACT OR GRANT NO.	9a. ORIGINATOR'S REPORT NUMBER(S)
AF 19(628)-5706	
b. PROJECT NO., Task, Work Unit Nos. 4076-04-01, LIRF-54-01	
c. Dod Element 6240527F, 61101F	9b. OTHER REPORT NO(S) (Any other numbers that may be assigned this report)
d. Dod Subelement 634076, 680100	AFCRL 70-0415

10. DISTRIBUTION STATEMENT
1. This document has been approved for public release and sale; its distribution is unlimited.

11. SUPPLEMENTARY NOTES	12. SPONSORING MILITARY ACTIVITY
This research was partially supported by the Air Force in-House Laboratory Independent Research Fund	Air Force Cambridge Research Laboratories (CRO) L. G. Hanscom Field Bedford, Massachusetts 01730

13. ABSTRACT

Four grating spectral radiometers and a filter radiometer were designed, constructed and flown on a balloon vehicle five times to measure atmospheric radiance from 5 to 20 microns. Measurements were made at twelve different angles between zenith and nadir and at altitudes up to 100,000 feet. The equipment and calibration procedures are described. Numerous sample spectra are presented showing the change in radiance with both angle and altitude.

A program is developed for theoretically calculating atmospheric radiance. This program combines a line by line calculation of atmospheric transmittance with a sixteen layer model of the atmosphere to calculate emission at various angles and altitudes.

DD FORM 1473

Unclassified

Security Classification

14. KEY WORDS	LINK A		LINK B		LINK C	
	ROLE	WT	ROLE	WT	ROLE	WT
Atmospheric Emission						
Infrared						
Spectrometer						
Balloon Instrumentation						
Radiometer						